UNIVERSITY OF BIRMINGHAM

HYDROPHOBINS AND AIR FILLED EMULSIONS

by

FIDELINE LAURE TCHUENBOU-MAGAIA

A thesis submitted to
The University of Birmingham
for the degree of
DOCTOR OF PHILOSOPHY

School of Chemical Engineering
College of Engineering Physical sciences
The University of Birmingham
January 2012

To the people who have inspired me, shaped my future and given me their invaluable and endless support.

- My life-coach my late grandmother Lydie
- My Parents Jeannette and Michel
- My lifetime soul mother and guide aunt Martine
- My daughter Rose
- My other self Manuel

ABSTRACT

Suspensions of micron sized air cells, Air Filled Emulsions (AFEs), represent a new colloidal material with outstanding physical properties. They have the potential for technological applications in very different fields such as biomedical, environmental sciences and the food industry. This thesis focuses on the construction of AFEs and their use as ingredients to construct reduced fat and calorie emulsion-based products. These microstructurally complex materials have been termed triphasic A/O/W emulsions.

A sonochemical templating process has allowed for the construction of air cells (the majority around 0.5-10 μm) in the size range of oil droplets found in emulsion based foods. Air cells were stabilised with either hydrophobins, obtained from submerged fermentation and extraction, or other cysteine rich but more common proteins such as bovine serum albumin (BSA) and egg albumen (EWP). The air cells were stable against disproportionation and ripening for substantial periods of time. They resisted destabilisation effect of oil droplets and could survive unit operations involving mild vacuum treatment and centrifugal forces, relatively high shear forces, temperatures and pressures.

Triphasic A/O/W emulsions were created with up to 60% included phase of air and oil in an aqueous continuous phase. This gave a greater than 50% reduction in lipid content. Comparative rheology and tribology showed that the triphasic A/O/W emulsions could have similar if not better lubrication properties than a full O/W version. The molecular properties of the protein used for the AFEs played a crucial role in the determination of lubrication properties (mouth-feel). Moreover, AFEs and triphasic emulsions offer the potential for new structures and textures for the food industry due to their self interaction to give a weak gel

behaviour. Hydrophobins were also able to form a complex with lipid oxidation products and may be used to reduce or prevent flavour deterioration from oxidation.

ACKNOWLEDGEMENTS

I would like to express my deepest gratitude to my supervisor, Dr. Philip Cox, for being a true and exceptional mentor in the etymological sense of the term, that is to say: “advisor, guide, companion in risk and uncertainty; the one who consistently encouraged me in identifying my inner reserves and capabilities to achieve the best possible results in our scientific quest”. THANK YOU.

My gratitude is also extended to the academic staff at the School of Chemical Engineering, in particular to Professor Ian Norton, Professor Owen Thomas, Dr. Tim Overton, Dr. Richard Greenwood, Dr. Gary Leeke and Mrs Madeleine Smith whose kindness, guidance and support helped me to complete this thesis.

A special and warm thank you also goes to all the support staff, Mrs Elaine Mitchell, Mrs Lynn Draper, Mrs Hazel Jennings, Mrs Liz Kent, Mr Jason Mahoney, Mr John Hooper and Mr Dave French for all the help and for making my experience as a PhD student so pleasant.

I am equally thankful to Dr. James Bowen for characterising the tribo-pair; my undergraduate students Miss Noor Al-Rifai and Miss Nor E Mohamed Ishak who carried out work on pre-heated proteins; Ms Karen Littlejohn for helping in the reconstruction of the secondary structure of hydrophobins; and to Mrs Theresa Morris, for helping with the SEM measurements.

I would also like to thank all my colleagues in the chemical and biochemical buildings, especially Dr. Roman Pichot and Dr. Tom Willet for their support.

I would like to acknowledge the financial support of the BBSRC and BASF for supplying the modified Class I hydrophobins.

The LTQ Orbitrap Velos ETD used in this research was obtained, through the Birmingham Science City Translational Medicine: Experimental Medicine Network of Excellence project, with support from Advantage West Midlands (AWM), which is acknowledged here.

Thank you to my family and friends for their long distance but genuine support and encouragement. Plus particulièrement, MERCI INFINIMENT à mes parents, à mes tantes et mamams: Martine, Sylvienne, Régine.

Rose, ma fille adorée, pour ta seule présence et ton autonomie, tu m'as été d'un soutien sans conteste: MERCI.

Manu, Merci pour ton amour, soutien et ta patience sans limite.

NOMENCLATURE AND ABBREVIATIONS

AFEs	Air Filled Emulsions
A/W	Air-in-water
C_p	Heat capacity
BSA	Bovine serum albumin
EWP	Egg whites, albumen
BSA-AFEs	Air filled emulsions stabilised by BSA
EWP-AFEs	Air filled emulsions stabilised by EWP
HFBII-AFEs	Air filled emulsions stabilised by hydrophobins, HFBII
O/W	Oil-in-water
PAGE	Polyacrylamide gel electrophoresis
SDS	Sodium dodecyl sulfate
SPG	Shirasu Porous Glass (material used for membranes)
spp.	Species
TFA	Trifluoroacetic acid
γ	Interfacial tension
W	Water (aqueous phase of an emulsion)
MW	Molecular Weight (kDa)

TABLE OF CONTENTS

LIST OF FIGURES

LIST OF TABLES

CHAPTER 1

INTRODUCTION

1.1. Context of the study

Obesity has reached epidemic proportions globally and contributes substantially to the global burden of chronic diseases and disability (WHO, 2010). These diseases include cardiovascular diseases, type 2 diabetes and certain forms of cancer. Obesity is generally the result of an imbalance between intake of energy and expenditure of energy over a prolonged period of time. A sedentary modern lifestyle combined with resistance within the public to change their eating habits makes it difficult to tackle. Therefore, the food industry is seeking novel ingredients that are familiar to the consumer but can allow for cost effective production of palatable low calorie, low fat foods. It is believed that suspensions of small stable air cells, designed to resemble oil droplets in terms of their size and physical properties can perform this task. These suspensions, named air filled emulsions in Tchuenbou-Magaia *et al.* (2009a) (see Figure 1-1), could be used to construct a wide range of reduced fat and calorie emulsion-based food products (Triphasisic A/O/W emulsion, Figure 1-2). For example, it would be an advantage if the typical fat content of a given mayonnaise or salad dressing - generally ranging from 70% to 84% or 30 to 60% (Pourkomailian, 2000) - could be reduced to at least half that value and filled with oil droplet-like air cells. This is possibly a sound approach as air cells are non- fattening and are already present both in non-processed foods (e.g. apples) and processed foods such as ice cream and whipped cream. However, such stable air cell based fat replacers do not currently exist. Moreover incorporating microbubbles in food may

deliver novelty of texture and appearance, facilitate mastication, enzyme accessibility to substrate and enhance flavour delivering (Campbell *et al.*, 1999; Wildmoser *et al.*, 2004; Lau and Dickinson, 2005; Zuniga and Aguilera, 2008). Also the remaining dispersed oil droplets may be used to incorporate fat soluble nutrients and flavouring compounds, and to reinforce the product mouth feel. However such systems, where air cells and oils droplets are dispersed in the same water continuous phase, imply that air cells must be robust enough to resist the destabilisation effect of oil. Potential air cells must be capable of surviving various mechanical forces and stresses generated by the processing conditions such as pumping and mixing to be incorporated into such formulations. They must also resist disproportionation and have similar physical properties to fat.

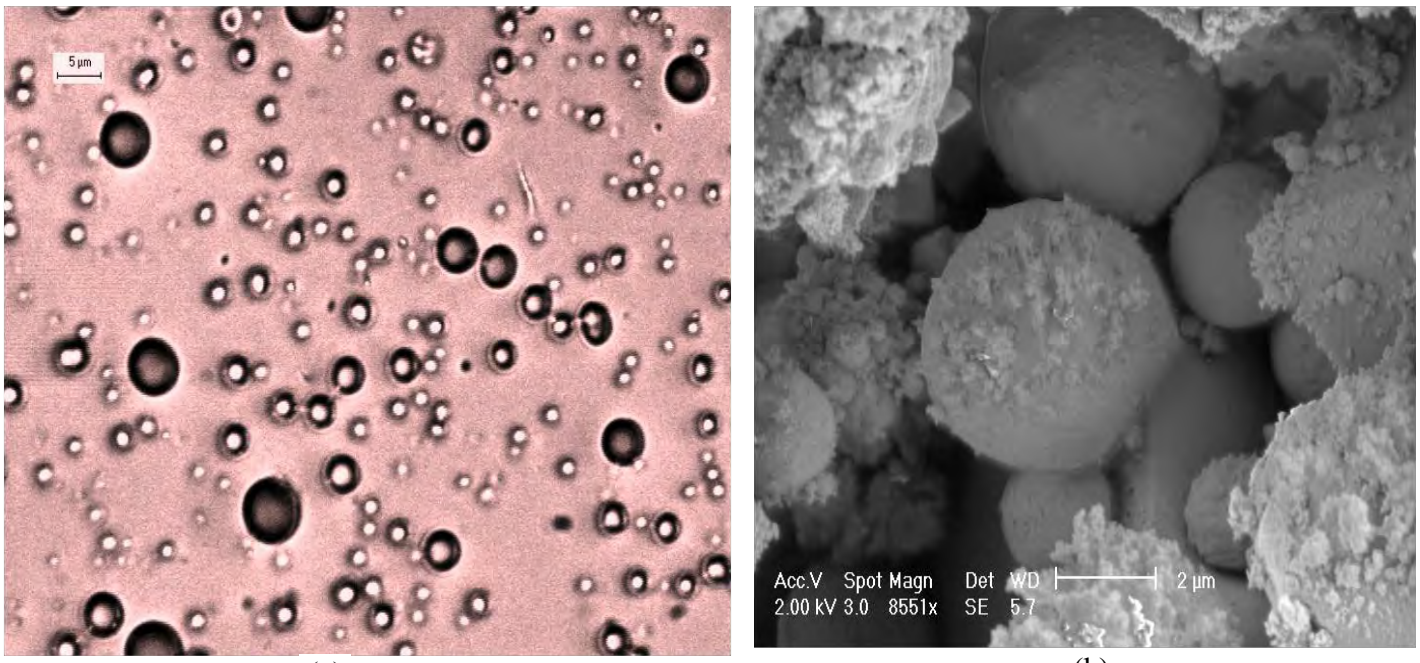

(a) (b)

Figure 1-1. Typical micrograph of suspension of air cells with protein coat: air filled emulsion (AFE with air volume fraction of 40 % ± 5 by volume).
(a) and (b) are brightfield image and etched Cryo-SEM micrograph, respectively.

Central to this work is that the size of air cells matches that of oil droplets. Oil droplets commonly found in emulsion-based food lie somewhere between 0.1 and 100 µm in size

(McClements, 2005). Air cells in the size range similar to those droplets are inherently unstable because of their high Laplace pressures and the solubility of air in water. Also, oil droplet-like air cells, microbubles, should be spherical and different from interlinked polyhedral foams (Exerowa and Kruglyakov, 1998) to allow for a desirable flowable opaque air based emulsified systems. Please note that the word "microbubble(s)" and "air cell(s)" are interchangeable throughout this thesis. It is believed that the stability of droplet-like air cells can be significantly improved if the adsorbed film surrounding them has an elastic component and exhibits a high viscoelasticity as observed with hydrophobin proteins (Cox *et al.*, 2007) or if the air/liquid interface is coated either with ordered nanoparticles (Dickinson *et al.*, 2004; Murray *et al.*, 2009; Dickinson, 2010) or with gelled lipid (Talu *et al.*, 2008).

Hydrophobins are a group of small, amphiphilic cysteine-rich proteins found exclusively in filamentous fungi. They can self-assemble at hydrophilic/hydrophobic interfaces (e.g., water/air, water/oil, and water/solid-hydrophobic-surface). Hydrophobins are divided into Class I and Class II according to the pattern of hydrophobic and hydrophilic amino acid residues within the protein sequence and by how easily the assembled amphiphilic layers are dissociated (Wessels, 1994). To some extent, these properties may account for the variability in surface and interfacial activity between the Classes of hydrophobins. In addition to their ability to stabilise air cells, hydrophobins can also stabilise O/W emulsions (Lumsdon *et al.*, 2005). These properties might make hydrophobins suitable for the production of air-based triphasic A/O/W emulsions. However researchers are still looking into ways of producing hydrophobins in large scale. This current limited hydrophobins availability constitutes a substantial obstacle to its utilisation for any mass production. Part of the work presented in this thesis deals with an attempt to circumvent these limitations.

Suspension of air cells stabilised by bulk food grade cysteine rich proteins such as egg white proteins and bovine serum albumin were made through a sonochemical method, initially developed by Suslick and co-workers for non food system (Grinstaff and Suslick, 1991; Suslick *et al.*, 1994). These authors suggested that microspheres are formed by chemically cross-linking cysteine residues of the protein with the sonochemical regenerated superoxide radicals. It is worth noting that, because Avivi and Gedanken (2002) were able to construct microspheres with streptavidin, a protein devoids of any sulphur residues (produced by *Streptomyces avidinii*), and attributed their stability to either the hydrophobic interaction between protein chains or thermal denaturation of the protein after the initial ultrasonic emulsification, it is possible that sonochemical production of proteinaceous microspheres involves a more complex mechanism than it first appears.

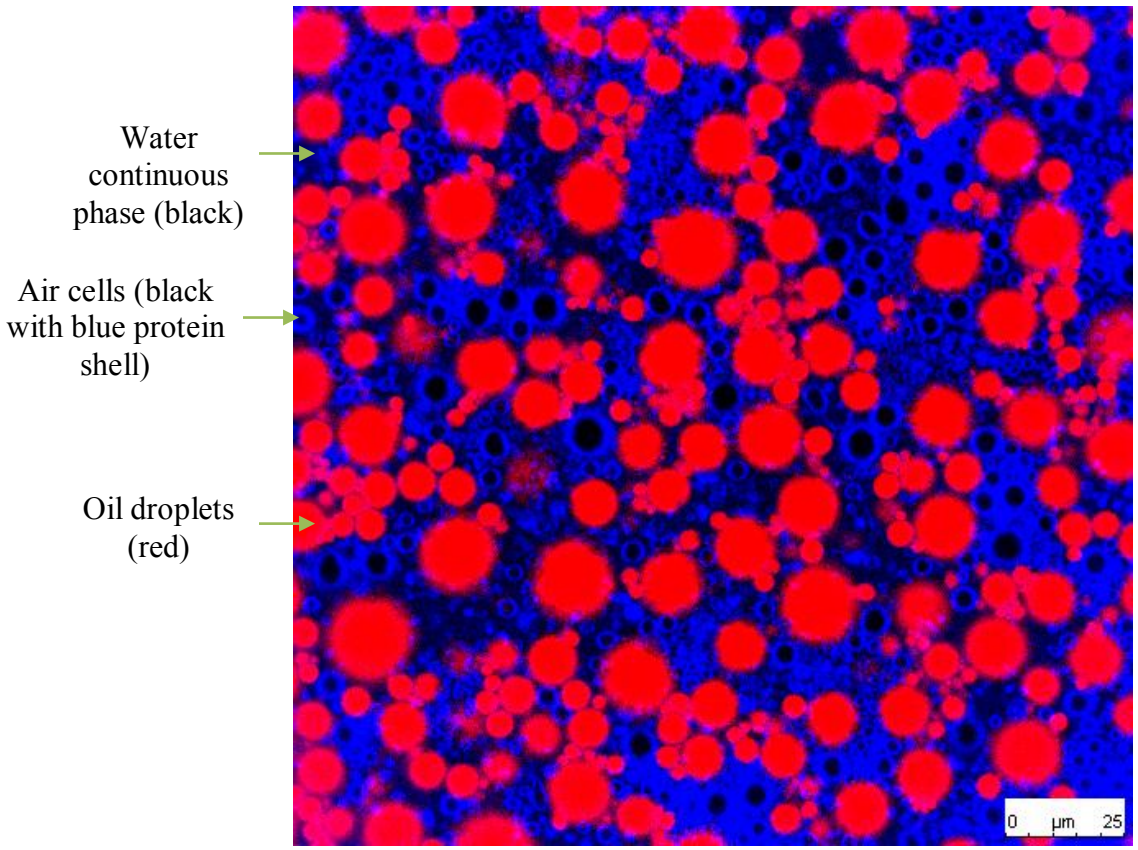

Figure 1-2.Typical CLSM micrograph of a triphasic A/O/W emulsion (air cells and oil droplets dispersed in water continuous phase; 20 % air, 10% oil and 70 % water).

1.2. Aims and Objectives

The aims and objectives of this thesis can be summarised around 4 core questions.

1. Could hydrophobins be extracted from edible mushrooms at an economic fashion and in a reasonable quantity that allows for further uses? Would it be possible to produce hydrophobin rich extracts from submerged culture of *Trichoderma reesei* with, a surface activity comparable to that reported for relatively pure ones (Chapter 4)?

2. Could Class II hydrophobins obtained in (1) be used to produce oil-droplets-like air cells? Could these be used as an effective ingredient for the reduction of the fat content of high fat emulsion-based products? For example to construct air-based triphasic A/O/W emulsion with comparable mouth-feel to that of the standard O/W emulsion (Chapter 5).

3. What are the surface activity and emulsifying capability of recombinantly produced Class I hydrophobins (produced at large scale)? How different are they from common proteins and other hydrophobins for emulsion production? Could they be used to provide some understanding of the behaviour of hydrophobins within formulations, for example triphasic A/O/W emulsion (Chapter 6)?

4. Could bulk food grade proteins be functionalised to give hydrophobins-like feature in terms of air cells stability (Chapter 7)?

1.3. Thesis structure

After the introductory part of this thesis, the next chapter (Chapter 2) presents some basic understanding and previous studies the work presented here lies on. This includes published works on hydrophobins that seem especially relevant to this thesis; general features that underlie protein adsorption at interfaces; emulsions and microbubbles formation, stabilisation and destabilisation; some fundamental differences between triphasic A/O/W emulsion and whipped system; and finally an insight into the relationship between microstructure, rheology, tribology and the mouth-feel as applicable to the development of new food product.

Chapter 3 gives details of materials and experimental techniques used in this thesis. Methods developed in the course of this work are also presented in this chapter.

In chapter 4 hydrophobin containing extracts for further study are obtained from edible mushrooms and from *Trichoderma reesei.* The extraction method was based on the solubility properties of Class I and Class II hydrophobins, as presented is chapter 2. The extract was then characterised, and surface and interfacial tension evaluated in order to assess the different extracts' ability to stabilised emulsion and air cells.

Chapter 5 deals with the sonochemical production of suspension of air cells (AFE) using the hydrophobin extracts obtained in chapter 4. The stability of these air cells coated by hydrophobin and their effectiveness as fat mimic are discussed.

Chapter 6 discusses the surface and interface properties of large scale recombinantly produced Class I hydrophobins using hydrophobin extract produced in chapter 3 as reference. A similar exercise is performed with other common bulk proteins. These proteins are also used to

provide a mechanism for proof of principle about the interaction of hydrophobin with lipid oxidation products and possible exploitation to reduced oxidation deterioration of emulsions.

Chapter 7 presents a feasibility study of the use of bulk cysteine rich proteins for sonochemical production of AFE. The effect of different parameters such as pH, protein concentration are discussed as well as the stability of air cells to different environmental stresses, especially, those encountered in the food industry such as high temperature/pressure treatment and mixing. In addition BSA is used as a model protein to valid some hypothesises made in chapter 5 and to confirm the microstructure of the triphasic A/O/W emulsion.

The main findings and some ideas for future works are summarised in chapter 8.

1.4. Publications- (see CD included with this work at the back of this thesis).

Patent

Norton, I. T., Cox, P. W. & Tchuenbou-Magaia, F. L. 2011. Low fat food containing gas bubbles. US patent application 20110287150.

Journal (Peer-Reviewed)

1. Tchuenbou-Magaia, F. L. & Cox, P. W. 2011. Tribological study of cysteine rich proteins stabilised air filled emulsions. Journal of Texture Studies, 42, 185-196.

2. Tchuenbou-Magaia, F. L., Al-Rifai, N., Ishak, N. E. M., Norton, I. T. and Cox, P. W. 2011. Suspensions of air cells with cysteine rich protein coats: air filled emulsions. Journal of Cellular Plastics, 47, 217-232.

3. Tchuenbou-Magaia, F. L. and Cox, P. W. 2010. Air-based ingredients for healthy food: Air filled emulsions. Journal of the Institute of Food Science and Technology, 24, 40-42.

4. Tchuenbou-Magaia, F. L., Norton, I. T. and Cox, P. W. 2009. Hydrophobins stabilised air-filled emulsions for the food industry. Food Hydrocolloids, 23, 1877-1885.

Two papers are in preparation for publication:

- Tchuenbou-Magaia, F. L. and Cox, P. W., Adsorption behaviour of H*proteins at interfaces and a kinetic analysis, to be submitted to the Journal of Colloid and Interface Sciences.
- Tchuenbou-Magaia, F. L. and Cox, P. W., Investigation into the potential oxidative damage from the presence of air filled emulsions and novel emulsification processes, to be submitted to the Journal of Food Hydrocolloid.

Book Chapter

Tchuenbou-Magaia, F. L., Norton, I. T. & Cox, P. W. 2010. Microbubbles with protein coats for healthy food: Air filled emulsions. In: WILLIAMS, P. A. & PHILLIPS, G. O. (eds.) Gums and Stabilisers for the Food Industry 15. Cambridge: RSC. PP. 113-125.

Conferences/meetings/awards

This section also present a nomination for an Award (1) for a mouth mimicking machine I developed within the context of inreach and outreach activities, taking inspiration on my PhD work. Also some of my PhD data was used for the development of this inspirational tool.

1. Tchuenbou-Magaia, F.L., Lee, L., Turner, A. & Leeke, G. An inspirational tool to engage, educate and excite young people about chemical engineering. IChemE innovation & excellence awards 2011, category Education and Training. Shortlisted.

2. Tchuenbou-Magaia, F.L. Suspensions of air cells with cysteine rich protein coats: air filled emulsions. IChemE innovation & excellence awards 2010, category Food and Drinks. Shortlisted.

3. Tchuenbou-Magaia, F.L. & Cox, P. W. Suspensions of microbubbles as base for novel formulations: case study of emulsion based food products. IChemE Subject Group meeting - Scale up of formulated products, September 2010, Birmingham, UK (Poster presentation, awarded the poster competition prize).

4. Tchuenbou-Magaia, F.L. & Cox, P. W. Suspensions of microbubbles as base for novel formulations: case study of emulsion based food products. British Science Festival posters showcase, September 2010, University of Birmingham, UK.

5. Tchuenbou-Magaia, F.L. & Cox, P. W. Novel air based ingredients for healthy food: Air filled emulsions EFFoST annual meeting, November 2010, Dublin, Ireland (Poster presentation).

6. Tchuenbou-Magaia, F. L., Norton, I. T. & Cox, P. W. Oral behaviour of cysteine rich Proteins stabilised air filled emulsions. International conference on Food Oral Processing -Physics, Physiology and Psychology of Eating, July 2010, Leeds (Oral presentation).

7. Tchuenbou-Magaia, F. L., Norton, I. T. & Cox, P. W. Investigations into the potential oxidative damage from novel emulsification processes and the presence of air filled emulsions. 10th International Hydrocolloids Conference, June 2010, Shanghai, China (Oral presentation).

8. Tchuenbou-Magaia, F. L., Norton, I. T., & Cox, P. W. Novel air based ingredient for the food industry. In: Biofoams 2009 (on CDROM). October 2009, Niagara Falls, Canada (Refereed conference paper plus an oral presentation).

9. Cox, P. W., Tchuenbou-Magaia, F. L. & Norton, I. T. Air filled emulsions. Gums and Stabilisers for the Food Industry Conference, June 2009, Wrexham, UK (Plenary).

10. Tchuenbou-Magaia, F. L., Norton, I. T., & Cox, P. W. Air filled emulsions for the food industry. In: P. Fischer, M. Polard, & E. Windhab, eds. 5th International Symposium on Food Rheology and Structure (ISFRS). June 2009, ETH Zurich, Switzerland: pp. 134-137 (Non-refereed conference paper plus an oral presentation).

11. Tchuenbou-Magaia, F. L., Norton, I. T., & Cox, P. W. Microstructure of novel low fat salad dressing. University of Birmingham Postgraduate Poster competition event, May 2008, Birmingham, UK.

12. Cox, P. W., Tchuenbou-Magaia, F. L. & Norton, I. T. Application of hydrophobins to novel low fat foods. 10th International Conference on Engineering in Food, April 2008, Vina del Mar, Chile (Poster presentation).

CHAPTER 2

LITERATURE REVIEW

2.1. Hydrophobins: from discovery to production and purification

2.1.1. Hydrophobins origin and particularity

Hydrophobins are a class of surface active small proteins, unique to and ubiquitous in filamentous fungi that mediate interactions between the fungus and its environment, and play diverse roles in fungal growth and development (van Wetter *et al.*, 2000; Wosten, 2001; Cox and Hooley, 2009). Hydrophobins were first discovered as the products of genes that were abundantly expressed during the emergence of aerial hyphae in the wood-rotting mushroom like, *Schizophyllum commune*. They were named by Wessels "Hydrophobins", a name originally used for hydrophobic substances present in the walls of many prokaryotic and eukaryotic microorganisms, because of their relatively high hydrophobicity (Wessels *et al.*, 1991). Many hydrophobins have since been discovered. They are generally classified into two groups, Class I and Class II, and contain eight cysteine residues at a conserved position that are involved in forming four protein stabilising disulfide bridges (Sunde *et al.*, 2008; Figure 2-1). However, it is becoming evident that some hydrophobins may hold more cysteines than hitherto thought: such as HFBIII with one extra cysteine residue (Kisko *et al.*, 2007), new bioinformatically identified hydrophobin with 16 cysteine residues (Littlejohn *et al.*, 2011). Moreover, recent published works suggested the existence of intermediate class of

hydrophobins with partial characteristics of Class I and Class II hydrophobins (Jensen *et al.*, 2010; Littlejohn *et al.*, 2011).

Class I and Class II differ in their hydropathy patterns and the solubility of the assembled structures they form (Wessels, 1994). Class I hydrophobins form highly insoluble membranes in water, organic solvents and 2% SDS, but soluble in strong acids. In contrast, the membranes formed by class II hydrophobins can be easily dissolved in aqueous ethanol (60%) or 2% SDS. These properties of hydrophobins are genenerally used for their extraction (see below).

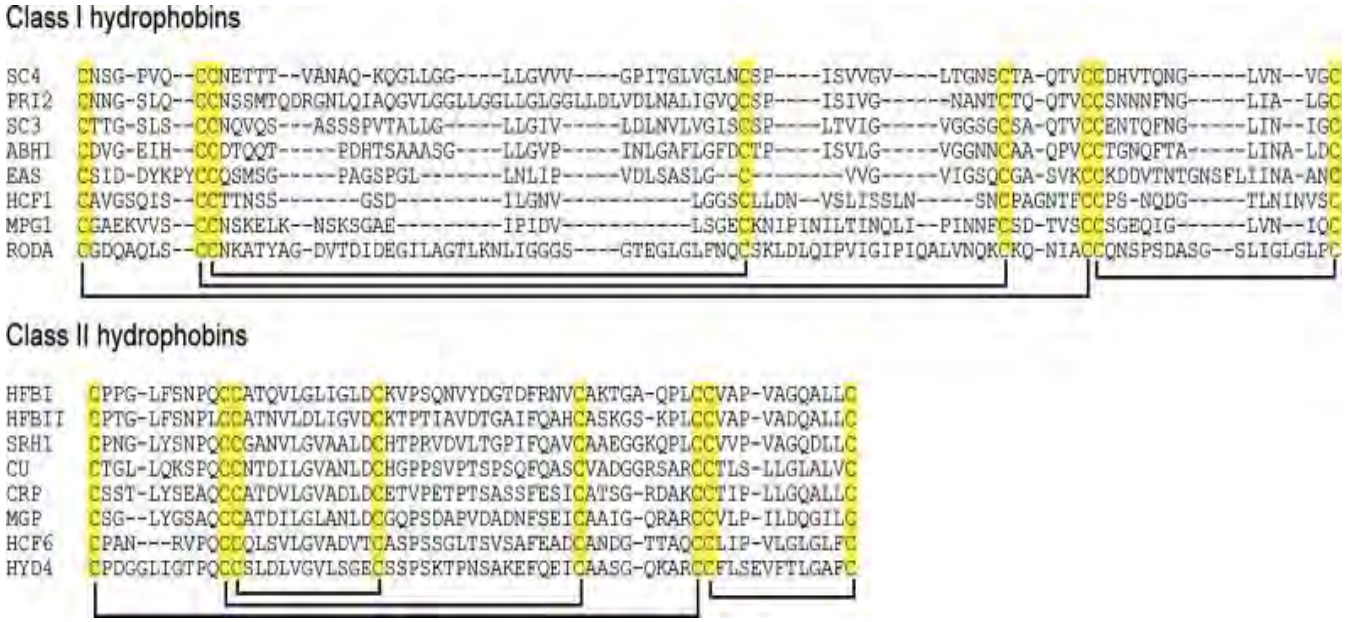

Figure 2-1. Consensus of amino acid sequences for class I and II hydrophobins (Sunde *et al.*, 2008). Only amino acids between the first and last Cys residues are shown due to high sequence variations at the termini. The conserved Cys residues are highlighted in yellow with the conserved disulphide bonding pattern indicated with brackets. The relatively low degree of sequence conservation is apparent. The abbreviations used are: SC3, *S. commune*; SC4, *S. commune*; EAS, *N. crassa*; MPG1, *M. grisea*; HCF1, C.; ABH1, *Agaricus bisporus*; PRI2, *A. aegerite*; RODA, *A. fumigatus*; HFBI, *T. reesei*; HFBII, *T. reesei*; CU, *O. ulmi*; CRP, *C. parasitica*; HCF6, *C. fulvum*; MGP, *M. grisea*; HYD4, *G. moniliformis* and SRH1, *T. harzianum*).

As a protein, the amphiphilic properties of hydrophobins may change in response to change of solvent properties such as pH, ionic strength or temperature (see later discussion) but hydrophobins present other properties beyond those of common surface active proteins. Hydrophobins can be compared to Gemini surfactants in the sense that they can form "submicellar aggregates" with low aggregation numbers (e.g. dimmers, tetramers) and are effective as surface active molecule at relatively low concentration as compared to conventional proteins. Gemini or dimeric surfactants are a class of surfactants that consist of two identical surface active molecules connected at the level of, or very close to, the head groups by a spacer group. They are characterised by critical micellisation concentration that are one to two orders of magnitude lower than for the corresponding conventional ones (monomeric) and are more efficient in lowering the surface tension (Zana, 1996; Castro *et al.*, 2002; Zana, 2002; Yoshimura *et al.*, 2005; Klijn *et al.*, 2007). The unique self-association behaviour and surface activity property of hydrophobins, explained by their molecular structure with non-centrosymmetric arrangement of the hydrophilic and hydrophobic patches make them be similar to Janus particles (Cox *et al.*, 2007; Walther and Muller, 2008). Janus particles are versatile small particles with two sides or at least two surfaces of different chemistry and/or polarity (Walther and Muller, 2008). Therefore hydrophobins combine, to some extent the Pickering stabilisation effect, known for particles and the amphiphilicity of classical surfactants.

Hydrophobins are highly stable when compared to other common cysteine rich proteins (see Table 9-1, Appendix 2). For instance, SC3 (from *Schizophyllum commune*), HFBI and FHBII (from *Trichoderma reesei*) are stable over a temperature range of 25-90◦C and to most chemicals (Askolin, 2006). Because of the long history consumption of mushroom, naturally containing hydrophobins, it is likely that hydrophobins can be accepted as food grade proteins

(Aldred *et al.*, 2007). All these properties of hydrophobins make them attractive not only for bubbles, foam and emulsion stabilisation but also in other fields, ranging from medical and technical coating to separation technologies (Wosten and de Vocht, 2000; Wosten, 2001; Hektor and Scholtmeijer, 2005; Cox and Hooley, 2009; Haas Jimoh Akanbi *et al.*, 2010; Valo *et al.*, 2010).

2.1.2. Production and purification of hydrophobins

Hydrophobins are naturally occurring proteins but have also been genetically engineered in order to improve their production yield, solubility and extend their applications (Bilewicz *et al.*, 2001; Wohlleben *et al.*, 2010). They can be secreted out in the growth medium or retained in the fungal structures (fruiting bodies, mycelium, and spores) where they form protective layers, structural components of the cell wall and mediate attachment of the fungus to surfaces as well as reduce the surface tension of the fungus environnment to allow aerial growth (De Vries *et al.*, 1993; Askolin, 2006). However, it is known that the expression of hydrophobins is regulated by environmental conditions and several hydrophobin genes can be found in one organism. Also different hydrophobins are expressed at different stage of fungal development and one fungus species can produce more than one class of hydrophobin of hydrophobins (Mikus *et al.*, 2009a; Stajich *et al.*, 2010; Littlejohn *et al.*, 2011).

Trichoderma reesei produces HFBI and HFBII depending on the type of carbon source used for fermentation; but HFB3, HFB4, HFB5 and HFB6 have been identified in certain strains (Neuhof *et al.*, 2007; Mikus *et al.*, 2009b). HFBI is mainly produced when fermentation is performed with glucose and sorbitol as carbon source and HFBI gene (hfb1) seems not to express in media containing polysaccharides (cellulose, xylan, cellobiose or lactose) whereas

the HFBII gene (hfb2) highly expressed in vegetative cultures on these media as well as by nitrogen, carbon starvation and light (Nakari-Setälä *et al.*, 1996, 1997).

Hydrophobins was first extracted from mushroom-forming fungus, *Schizophyllum commune* by Wessels *et al*. (1991). The authors could extract hydrophobin from the cell wall of *Schizophyllum commune* with cold formic acid after hot SDS treatment. However, because the resulting hydrophobin resisted common reducing agents like mercaptoethanol and dithiothreitol, they used performic acid which oxidises all disulfide bridges and converts cystine and cysteine into cysteic acid. This allowed them to identify hydrophobins Sc3 and Sc4. In 1993, De Vries *et al.* (1993) investigated the insoluble hydrophobin complexes in several filamentous fungi including *Schizophyllum commune, Pleurotus ostreatus, Agaricus bisporus, Apergillus nidulans, and Penicillium chrysogenum* discovered that, not only trifluoroacetic acid (TFA) was as effective as formic acid in extracting hydrophobin from the hot-SDS treated walls but also transformed hydrophobin complexes into monomers. For example SC3 can only be dissociated by agents such as TFA, after which the monomers are soluble in water, aqueous ethanol, and detergents. After dissolution of the monomer in water, the interfacial assembly can be repeated, but it is prevented by the presence of lipid solvent or detergent (Wosten *et al.*, 1993).

It should be noted that, in contrast to formic acid that dissociates hydrophobins aggregates into monomeric form by oxidising disulfide bonds with formation of cysteic acid, the mechanism by which TFA transforms hydrophobin aggregates into monomer is still unclear. Nevertheless their findings laid the foundation for the extraction and purification of hydrophobins, especially class I present in mycelium and fruiting body of fungi. For instance, Yu *et al.* (2008) isolated and purified HGFI a class I hydrophobin from edible mushroom

(*Grifola frondosa*) by means of TFA extraction followed by a polishing step using reverse-phase HPLC. Similarly, Cryparin, a class II hydrophobin was extracted directly from dried spore of *Cryphonectria parasitica* with TFA (Kazmierczak *et al.*, 2005). HFBI and HFBII, class II hydrophobins from *Trichoderma reesei* mycelium are comonly purified via SDS extraction followed by hydrophobic interaction chromatography (HIC) and anion exchange chromatography (Askolin *et al.*, 2001) or by reverse-phase chromatography (Collén *et al.*, 2002) .

Hydrophobins present in culture medium are generally extracted by exposing them to an air/water interface, either by mechanical agitation or by bubbling a clarified fungal culture media, followed by a TFA (trifluoroacetic acid) treatment of hydrophobin assemblages after separation (Takai and Richards, 1978; Wosten *et al.*, 1993; Lugones *et al.*, 1998; Tchuenbou-Magaia *et al.*, 2009a). Although gracefully simple, this method relies on the use of TFA, which is for environmental and safety reasons not desirable. Alternative methods have been developed based to some extent on the standard proteins purification processes. Class I hydrophobin, Sc3 has been isolated by means of hydrophobic interaction chromatography and gel filtration (Martin *et al.*, 2000; Wang *et al.*, 2004). Another method consists in taking up a hydrophobins containing solution in contact with a hydrophobic surface, Teflon, to allow their absorption into it, follows by the release of the adsorbed hydrophobin with a solution of non-ionic surfactant, Tween 20 or Tween 80, has been developed and patented (de Vocht *et al.*, 2005). However these methods are only applicable for purification of hydrophobin once in solution and could not be used for separation of hydrophobins from organisms such as mushrooms. Thus methods used in this thesis are based upon the biophysical properties and solubility of hydrophobins themselves i.e. by foam fractionation followed by TFA extraction or by direct SDS extraction.

2.2. Surface properties of proteins and kinetics of adsorption at interfaces

Knowledge about protein adsorption and the kinetics of adsorption is important for controlling processes, especially in foams, bubbles and emulsion formation and stabilisation. The adsorption kinetics of the emulsifier determine the time needed to stabilise the newly form droplets, bubbles against coalescence in all stages of formation, therefore determine the final droplet/bubble size. Moreover, the adsorption of the emulsifier at the interfaces lowers the interfacial or surface tension which is central for both the optimisation of the energy input involved in the emulsification and the achievement of small size of droplet and bubble, which is one of the most crucial parameters that determine the stability of the dispersed system. Time-dependent surface/interfacial tension known as dynamic surface tension/interface tension (DST), as illustrated by Figure 2-2, generally provides information about the adsorption behaviour of surface active molecules at the solution/air or solution/oil interfaces. DST of aqueous protein can be characterised by 3 to 4 regimes, referred in Figure 2-2 by numbers 1, 2, 3 and 4 (Tripp *et al.*, 1995; Beverung *et al.*, 1999). As the protein molecules diffuse and adsorb at the interface, the surface/interface tension ($\gamma(t)$) decreases from the pure solvent until lower equilibrium value is attained (regime 4). This steady state regime is reached when protein molecules have achieved both the equilibrium surface concentration and conformation. It is interesting to note that, although the equilibrium surface tensions of concentrated protein solutions are often around 45 mN/m, it seems that it is more important to consider the capacity of the protein to rapidly decrease surface tension (Foegeding *et al.*, 2006).

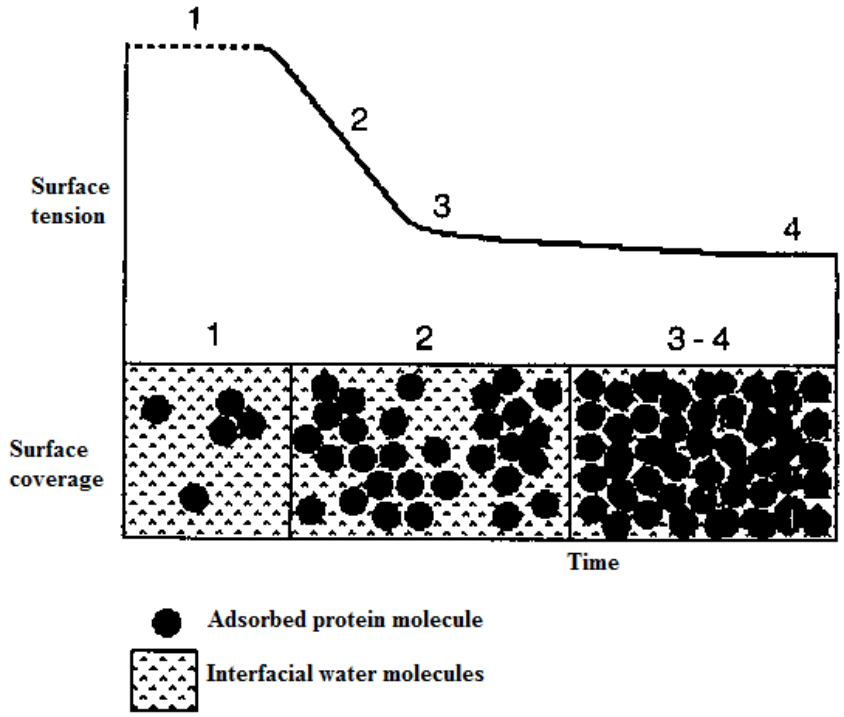

Figure 2-2. Schematic of dynamic surface tension-surface coverage relationship, illustrating the three possible dynamic surface tension kinetic regimes (Tripp *et al.*, 1995).
1, induction time and low to half monolayer surface coverage (generally observed for lower concentration and/or slowly adsorbing surfactants; this regime is often absent for highly concentrated or rapidly adsorbing surface active molecules such as hydrophobin HFBII (see Chapter 4)) ; 2, rapid decrease in surface tension corresponing to half to full monolayer surface coverage; 3, mesoequilibrium surface tension, slow further decrease in surface tension due to coformational changes and packing rearangements; 4, the equilibrium surface tension.
Note that the surface tension is not directly proportional to the surface coverage for all possible values of surface concentration.

The conditions during the adsorption process such as the protein concentration, pH, temperature and the presence of mixed species, either different oligomers of the same protein or contaminants influence the adsorption rate and the composition of the adsorbed film. These factors are not independent and exercise their effect through direct influence on the main driving forces for protein adsorption which are hydrophobic and electrostatic interactions (Vermeer, 2006). The control of these driving forces for the optimisation of protein adsorption process is discussed below.

2.2.1. Electrostatic effects in protein assembly

The aim of controlling protein surface charge is to reduce or eliminate the repulsive electrostatic forces between proteins so that the attractive van der Walls forces and/or hydrophobic interaction dominate in the system. This can be achieved by means of charge screening by adding electrolyte to neutralise charge or charge patch on the protein surface, and/or by controlling the pH.

Proteins carry an electric charge depending on the pH of the medium in which they are dissolved. When a protein takes on a net electrical charge, an electrical potential barrier appears. In order to adsorb at the interface, charged protein must overcome this barrier which can be quantified as $\int_0^{\varphi} q d\varphi$, where q is the charge on the protein and φ is the electrical potential in the plane of the charge groups at the interface (Macritchie, 1978). Conversely, when a protein adsorbs from a solution with the pH close to its isoelectric point (PI), this additional barrier is minimised or eliminated and this is reflected by the maximum in the adsorbed amount of protein that is commonly found around the protein PI. In a similar light the adsorption rate also increases (Wierenga *et al.*, 2005). However, it is worth mentioning that the PI of the protein in an adsorbed state may be different from that of the protein in the solution and it is the former that determines the electrical potential. For instance, a shift from 6.5 to 7.5 has been reported for the PI of HFBII aggregates in solution and at the surface of bubbles (Basheva *et al.*, 2011a) and PIs of 5.2 and 4.0 for β-lactoglobulin in the bulk and in the O/W interface, respectively (Basheva *et al.*, 2006). The authors pointed out different explanations to this shift: a conformational change for β-lactoglobulin and an insertion of part of the ionised groups of hydrophobin in the close packed protein layer. Moreover in some cases the adsorption behaviour of the protein is more affected by the position of a particular

charged group rather than the net charge as suggested for two mutant lysozymes (Podhipleux *et al.*, 1996) or for H*protein A and H*protein B hydrophobins (see Chapter 6). Other complex factors intrinsic to the protein are also in play; for example, a higher flexibility in the protein structure enables a more efficient coverage at the interface (Vermeer, 2006).

2.2.2. Hydrophobic effects in protein assembly

The adsorption of proteins from solution to the air/aqueous or oil/aqueous interface is a thermodynamically driven process due to the simultaneous dehydration of the hydrophobic interface and hydrophobic portions of the protein. Hydrophobic patches on a protein surface initiate this process and once contacts are made with the interface, natural flexibility within the molecules can expose previously buried hydrophobic portions to the interface, potentially leading to interfacial denaturation of the molecules (Graham and Phillips, 1979; Dickinson, 1986; Foegeding *et al.*, 2006). Furthermore, a strong relationship has been demonstrated between surface hydrophobicity and lowering of interfacial/surface tension, and between surface hydrophobicity and the emulsifying and foaming capacity of a wide range of proteins, both native and denatured (Kato and Nakai, 1980; Kato *et al.*, 1981; Moro *et al.*, 2001). Proteins are therefore, sometimes partially denatured in mild conditions such low pH, moderate concentration of denaturant (e.g., urea) and relatively high temperature or pressure in order to increase their surface hydrophobicity. In some cases, proteins are enzymatically modified or chemically treated to remove some hydrophilic segment, for example by deamidation (Matsudomi *et al.*, 1982). Treatment that leads to partial denaturation of protein usually converts globular proteins into their “molten globule” state, a protein configurational state with a native-like secondary structure and a disordered (unfolded) tertiary structure. It

has been postulated that the adsorbed globular protein is closed to this state and that adsorption and interfacial conformational rearrangements might well occur more rapidly when the protein adsorbs from the molten globule state than when it adsorbs from the native (Dickinson and Matsumura, 1994). This concept was behind the thermal treatment of proteins prior the production of AFEs, especially for AFEs made with common cysteine rich proteins (see Chapter 7).

However it is pertinent to point out that protein in the molten globular state can expose a number of its nonpolar groups, thus increasing its hydrophobic surface, but it can also screen its non-polar groups even more than the native state (Vermeer, 2006). For instance heat-treatment increased the surface hydrophobicity of whey protein isolate and decreased the surface hydrophobicity of sodium caseinate and bovine serum albumin (Hiller and Lorenzen, 2007). The effect of the temperature on protein is even more complex, especially for proteins such as hydrophobins which behave like surfactant, in the sense that they can form dynamic aggregates in aqueous solution (Figure 2-3), in the same manner as surfactants will undergo micellisation/demicellisation. The main factors determining the extent to which micelles influence the adsorption kinetics are the rate of formation and disintegration of micelles (Noskov, 2002) which in turn is also concentration-dependent.

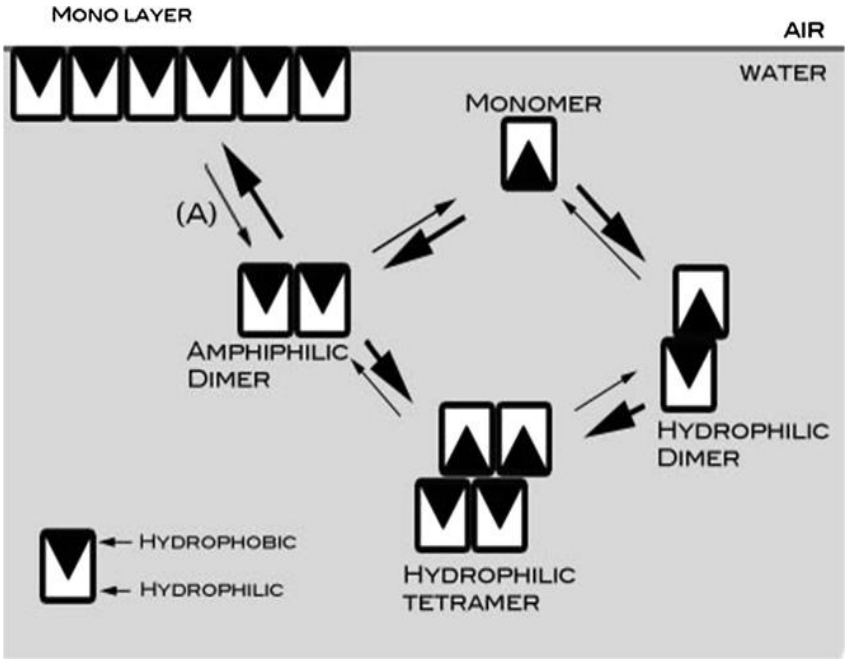

Figure 2-3. The formation and kinetics of oligomerisation of hydrophobins as redrawn from Kallio *et al.* (2007) by Cox and Hooley (2009). The kinetics of film formation are marked as (A). Predominantly formed oligomers are dimers or tetramers, which arrange themselves so that the hydrophobic regions of the proteins are inaccessible to the aqueous solvent. The formation and inter-conversion between oligomeric forms is a concentration-driven process, as is the rate of formation of the final layer if an interface is available; but HFBII undergoes less oligomerisation than other forms of hydrophobins, which may explain its higher rate of adsorption (Wang *et al.*, 2004; Cox and Hooley, 2009).

On the other hand, there is controversy about the influence of hydrophobic interaction on the adsorption kinetic (Tripp *et al.*, 1995) but this is understandable given that the proteins tested by these authors differed in other structural properties (e.g., electrostatic charge and size) that also matter for protein adsorption into interfaces. However, other works involving protein modification with small hydrophobic molecule, for example, by attaching small acyl chains (RCO-, where R is an organic group) such as capryloyl ($CH_3(CH_2)_6CO$-) to it, in order to change their exposed hydrophobicity while retaining the other functional characteristics evidently showed, as aforementioned, that increasing the number of non-polar patches on the protein surface leads to more rapid adsorption kinectics (Baszkin *et al.*, 2001; Wierenga *et al.*,

2003). Similar analogy may be put forward for hydrophobin HFBII and that their small size and the exposure of hydrophobic patches on its surface account for its rapid adsorption into interfaces (see Chapter 4). As mentioned previously, the kinetics of adsorption of a surface active molecule have a direct implication on the formation and stabilisation of emulsions and bubbles, which are the concern of the next section.

2.3. Emulsions and bubbles

An emulsion consists of two immiscible fluids one of which forms a dispersed (droplets) phase within a continuous (outer) phase. Emulsions can be classified either as water-in-oil emulsions such as margarine and butter or as oil-in-water emulsions such as mayonnaise, sauces, dressings and beverages. The latter category was considered throughout this work. The construction of Oil-in-water (O/W) or water-in-oil (W/O) emulsion depends mainly on the choice of emulsifier and volume fraction of oil to water. Microbubbles can be considered as gas emulsions in a sense that they consist of a dispersed gas (e.g. air) in a continuous aqueous phase. They are spherical, possess some fluidity and are different from interlinked polyhedral foams (Exerowa and Kruglyakov, 1998).

2.3.1. Method and mechanism of emulsions and microbubbles formation

Emulsions and microbubble suspensions are by nature thermodynamically unstable because the contact between dispersed phase (oil or gas) and the aqueous phase is thermodynamically unfavourable. As a result energy is required to create the dispersed state and generated

interface needs to be stabilised against recoalescence. The energy is provided by means of different types of apparatus such as a rotor-stator device, an ultrasonic probe, a high-pressure homogeniser and a porous membrane (Figure 2-4). Although the nature of the forces that are responsible for droplet deformation and break up depend on the type of the apparatus used, it is generally believed that, for a production of a spherical droplet of radius, r, an external stress far larger than the Laplace pressure ($\Delta P = \frac{2\gamma}{r}$) which act across the O/W interface towards the centre of the droplet must be applied (Walstra, 1993). This implies that the pressure required to form a droplet increases as its size decreases and/or as the interfacial tension (γ) increases. A study comparing ultrasonic emulsification with rotor–stator dispersing has led to the conclusion that ultrasound is more energy efficient, required less surface active molecules, generated smaller droplet size with monodispersed particle size distribution (Abismaïl *et al.*, 1999). The last claim is arguable as emulsions (AFE and O/W emulsions) made via ultrasound typically showed a broad particle size distribution (see Chapters 5 and 6). The discrepancy could easily be explained by different experimental conditions and system used because many factors such as acoustic power and frequency, ultrasonic irradiation time, the type and amount of gas dissolved in the sonication medium, the pH, temperature, viscosity and vapour pressure of the liquid medium control the efficiency of sonochemical process (Table 2-1). These factors are often interdependent of each other (Behrend *et al.*, 2000; Behrend and Schubert, 2001; Vijayalakshmi and Madras, 2004; Ashokkumar, 2006; Dolatowski *et al.*, 2007). For example ultrasound emulsification can generate nanoemulsions if the optimum ultrasonic energy intensity input for the system is used, but excess energy input may lead to an increase in droplet size (Kentish *et al.*, 2008). Also, it has been shown that after three minutes of production of emulsion by ultrasound, irrespective of the

ultrasound power, the size of droplets did not significantly change (Cucheval and Chow, 2008).

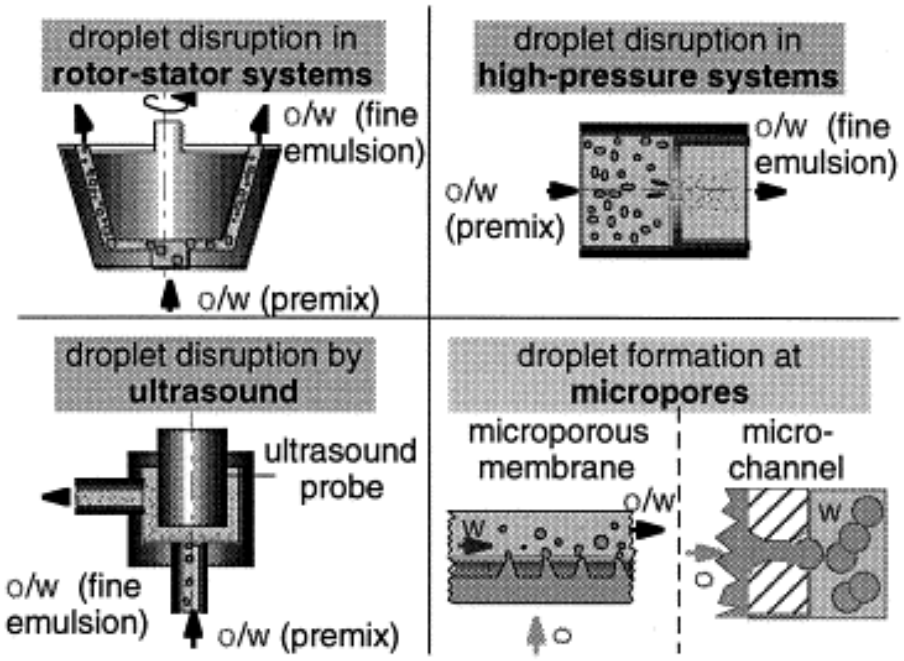

Figure 2-4. Conventional means of producing emulsions (Behrend and Schubert, 2001).
Note that the dispersed phase can also be applied where a premix is used. The same device could be used to produce micro-bubbles.

Most applications of ultrasound (the sound waves above human hearing which is above a frequency of 18 kHz, see Figure 2-5) in the preparation of colloids make use of the physical or mechanical effects of the sound as it is reflected, adsorbed or transmitted through the medium, giving rise to cavitation. Cavitation refers to the rapid formation, growth and violent collapse (sometimes followed by fragmentation) of bubbles in a liquid medium and the consequences of these physical perturbations (Ashokkumar, 2006). As illustrated by Figure 2-6, cavitation events result in the near adiabatic heating (because the process happens in extremely short time) of the gas and vapour inside the bubbles, creating a local high temperature and pressure, “hot spot”, with generation free radicals. These mechanical and

chemical effects of cavitation were exploited for the construction of AFEs, especially AFEs made with alternative proteins (see section 3, Chapter 3 for details).

Rotor-stator device, ultrasound probe and high-pressure homogenisation use relatively high energy input, and great stresses are applied to droplets or bubbles during their formation, making it hardly applicable for processing very shear sensitive material. A typical example is aggregation of proteins and reduction of their surface activity due to an excessive coagulation of proteins at the air/water interface as a result of a long whipping time. Alternatively, in membrane processes, droplets or bubbles are directly formed at the surface of a microporous membrane (e.g. by forcing the dispersed (oil or gas) through the membrane into the continuous). Therefore, energy consumption in membrane process is lower, and the stresses on the system at the membrane surface and inside the pores are relatively smaller. It also makes possible the formation of monodisperse systems, which generally are more stable when compared to polydisperse ones (Schröder *et al.*, 1998; Yuyama *et al.*, 2000). However membrane emulsification has some disadvantages because the membrane pores can be easily obstructed during the emulsification, especially when readily self-associated proteins such as hydrophobins are used (see Chapter 6).

Table 2-1. Experimental parameters affecting cavitation and the efficiency of sonochemical processes (Cravotto and Cintas, 2012)

Parameters	**Influence on cavitation**
Frequency	At higher frequency, the rarefaction phase is shortened. More power is required to make a liquid cavitates as the frequency increases
Solvent viscosity	Collapse produces shear forces in the bulk; viscosity increases the resistance to shear
Surface tension	No simple relationship. Cavitation generates liquid-gas interfaces; addition of a surfactant facilitates cavitation
Vapour pressure	Cavitation is difficult in solvents of low vapour pressure. A more volatile solvent supports cavitation at lower acoustic energy
Temperature	Any increase in temperature will raise the vapour pressure and cavitation will be easier, though a less violent collapse.
Intensity	In general, an increase in intensity will also increase the sonochemical effects. A minimum intensity is required to reach the cavitation threshold.
External pressure	Raising the external pressure will produce a larger intensity of cavitational collapse.
Bubbled gases	The energy on collapse increases for gases with a large polytropic ratio (Cp/Cv); monatomic gases (i.e., argon) are preferred

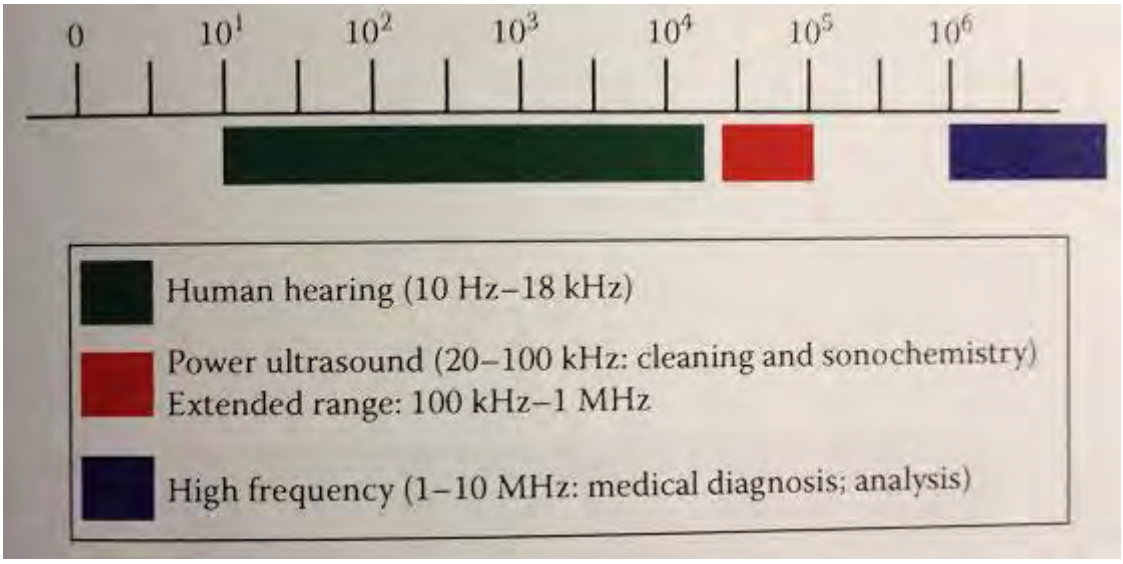

Figure 2-5. Sound frequencies (scale in Hz) from Ozcan *et al.* (2012)

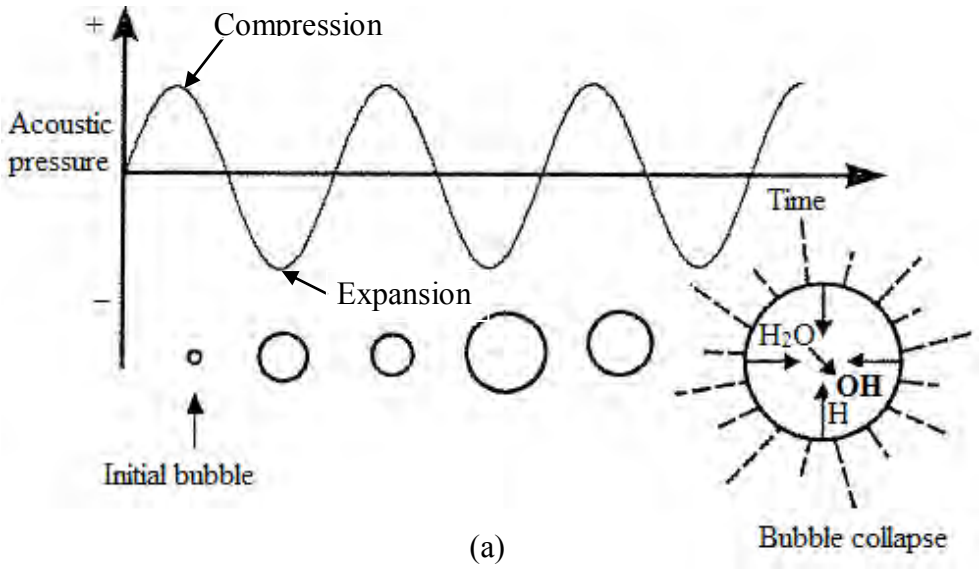

(a)

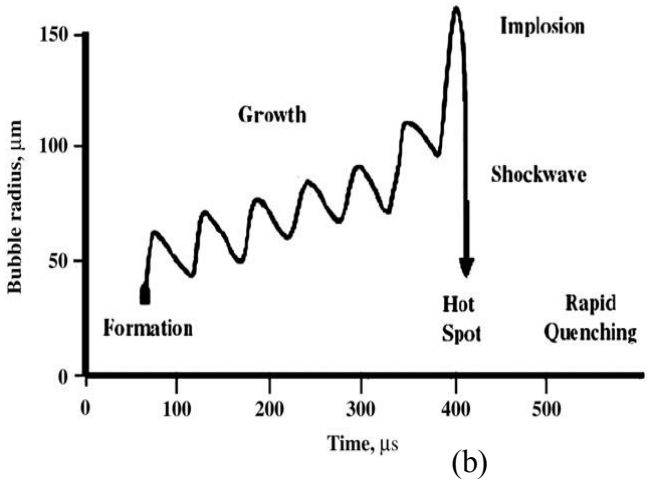

(b)

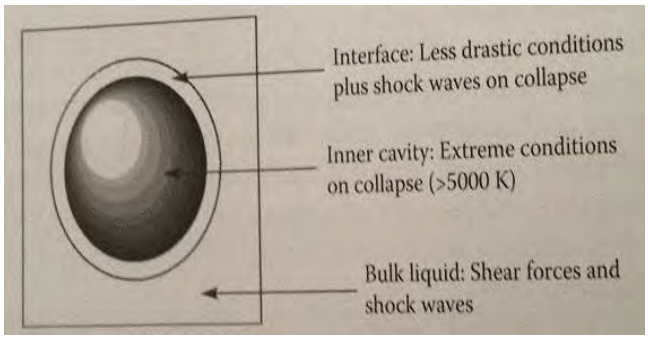

(c)

Figure 2-6. Schematic depiction of ultrasonic cavitation.
(a) and (c) depict bubble growth and collapse with the generation of a hot spot in which radical formation takes place by decomposition of solvent molecules (from Ashokkumar (2006); Chowdhury and Viraraghavan (2009)). When an ultrasound wave passes through a liquid medium, positive and negative pressures are exerted on a liquid by compression and expansion, creating bubbles during expansion (rarefaction) stage. These bubbles survive repeat cycles of compression and expansion until a critical size (typically, tens microns, Dadras *et al.,* 2012) is reached and collapse. The growth of cavitation bubbles is mainly sound intensity dependent whereas the critical size depends on the ultrasound frequency. The compression of gas and vapours inside the cavity generates heat with temperatures of approximately 5200 K in the inner gas-phase and 1900 K at the interface shell (see (c)). On collapse this concentrated energy is released and rapidly quenched by the surrounding liquid (heating and cooling rate of > 10^{10} K s^{-1}).
(c) is a simplified shell model for a cavitation bubble in a homogenous medium highlighting three different temperature domains (Cravotto and Cintas, 2012).

As mentioned previously, it is possible to make emulsions or bubbles that are kinetically stable for a reasonable period of time (weeks or years) with the aid of stabilisers. A stabiliser is defined as any ingredient that can be used to enhance the stability of an emulsion and are classified as either an emulsifier or a texture modifier, depending upon its mode of action (McClements, 2005). Emulsifiers lower the interface tension (facilitating droplet break up) and prevent the recoalescence by adsorbing at the interface and forming a protective membrane at the surface of droplets or bubbles. In contrast, texture modifiers act by either increasing the viscosity of the continuous phase (thickening agents) or by forming a gel in the continuous phase (gelling agents). Various proteins, a non-ionic surfactant (polyoxyethylene sorbitan monostearate, Tween 60), and two texture modifiers (Iota carrageenan and Xanthan gum) were used in the work presented in this thesis.

Tween 60 is a water-soluble emulsifier for cosmetic, pharmaceutical and food applications. In food products such as salad dressings, it is an efficient surfactant which maintains the stability of the emulsion. However, Tween 60 is often used in conjunction with other emulsifiers to impart certain advantageous qualities to the food; for instance, to give a uniform grain, improved texture, larger cake volume and increased moistness in cake or to improve fat aggregation and the meltdown resistance of reduced fat ice cream (Smullin *et al.*, 1971; Golding and Pelan, 2008; Orthoefer, 2008).

Carrageenan is a high-molecular-weight linear hydrophilic polysaccharide comprising repeating disaccharide units of galactose and 3,6-anhydrogalactose both sulphated and non-sulphated, joined by alternating α-(1,3) and β-(1,4) glycosidic links (Blakemore and Harpell, 2010). The positively charged groups on a protein ($–NH_3^+$) strongly interact with $–OSO_3^-$ groups, thus sulphated hydrocolloid such Carrageenan will react with protein at acidic pH.

However, this interaction may occur, even at neutral or alkaline pH (i.e. well above PI) via positive charge patches carried by some proteins at those pHs (Hattori *et al.*, 2001; Dickinson, 2003). Protein-carrageenan interaction may be fairly more important in system with Lambda carrageenan than that containing Iota carrageenan or Kappa carrageenan since it carries more sulphate groups (37% ester sulphate for Lambda, 32% for Iota and 22% for Kappa carrageenan). However, Iota carrageenan acts synergically with starch, the most widely used food stabilisers and this synergy is not observed with other types of carrageenans (Blakemore and Harpell, 2010).

Xanthan gum consists of a cellulosic backbone of β-(1,4) linked D-glucose units substituted on alternate glucose residues with a trisaccharide side chain composed of two mannose units separated by a glucuronic acid. Xanthan is a preferable thickener with widespread applications when compared to Iota carrageenan because of its unique rheological behaviour, which seems to be not or only marginally affected by the pH, temperature and the presence of salts (Phillips and Williams, 2000). However, ι-carrageenan has one advantage over xanthan as it interacts with proteins whereas xanthan does not (Table 2-2). This property of Iota carrageenan may be particularly interesting for a triphasic A/O/W formulation because its interaction with air cells via their protein coats may help improving the physical stability of such system (see section 5.3.3, Chapter 5). Xanthan solution can withstand up to 50% ethanol and, it is believed to be more stable than other commonly used thickeners (Sworn, 2010). It forms highly viscous solutions at very low concentration, which prevent particles sedimentation, droplets creaming and, in the meantime its high shear thinning behaviour allows product to readily flow from the bottle after shaking. The combination of these properties and its stability to acid and salt (Table 2-2) make Xanthan the ideal stabiliser for non-oil, low-oil and regular salad dressings (Monsanto, 2000). Furthermore Iota carrageenan

and xanthan are often used in combination in formulation, though they were used separately in formulations presented in this thesis.

Table 2-2. Comparison between the properties of Iota carrageenan and xanthan gum (Imeson, 2010)

Proprerties/application	**Iota carrageenan**	**Xanthan**
Water solubility	Dissolve in hot water (40-60 °C)	Dissolve in water at room temperature
pH range of stability	Autohydrolysis at pH <4.3	pH 10- 4 and with extreme pH conditions (pH 11–12, pH 1–2) only have minor effect
Temperature range of stability	Up to 70 °C; increase in temperature (75-80°C) lead to the decrease in viscosity	Up to 130 °C
Gelation	Strongest gels with Ca++	-
Protein reactivity	Strong protein interaction in acid	-

2.3.2. Mechanism of emulsions and bubbles destabilisation and means for enhancing their stability

From the previous sections is apparent that emulsion or bubble systems are metastable systems. The crucial question is how to enhance the relative stability of such systems? In order to answer this question is important to understand the destabilisation mechanism. A stable emulsion or bubbles system is one with no noticeable changes in its physicochemical properties such as oil droplets or bubbles size and size distribution, their spatial arrangement within the sample container and alteration of some molecules present (for example, due to lipid oxidation), over the time-scale of observation. Figure 2-7 summarises the main destabilisation phenomena of an emulsion of microbubbles system. More than one of these phenomena may occur at the same time or one can constitute a trigger for others (e.g. creaming promotes coalescence). It is therefore important to identify the predominant

destabilisation mechanism(s) in a particular system in order to effectively develop means to control and improve the stability of emulsion-based system. In triphasic A/O/W emulsion, the dominant mechanisms of instability is likely to be gravity creaming, Ostwald ripening, lipid oxidation and the destabilisation of air cells by oil droplets. A brief literature about the main destabilisation phenomena of emulsion and bubbles system along with their control means is considered below. The destabilisation of bubbles in the presence oil droplets is discussed in section 2.3.4.2. of this chapter. Note that, if not directly specified, a dispersed phase refers to the droplets, whether oil or air.

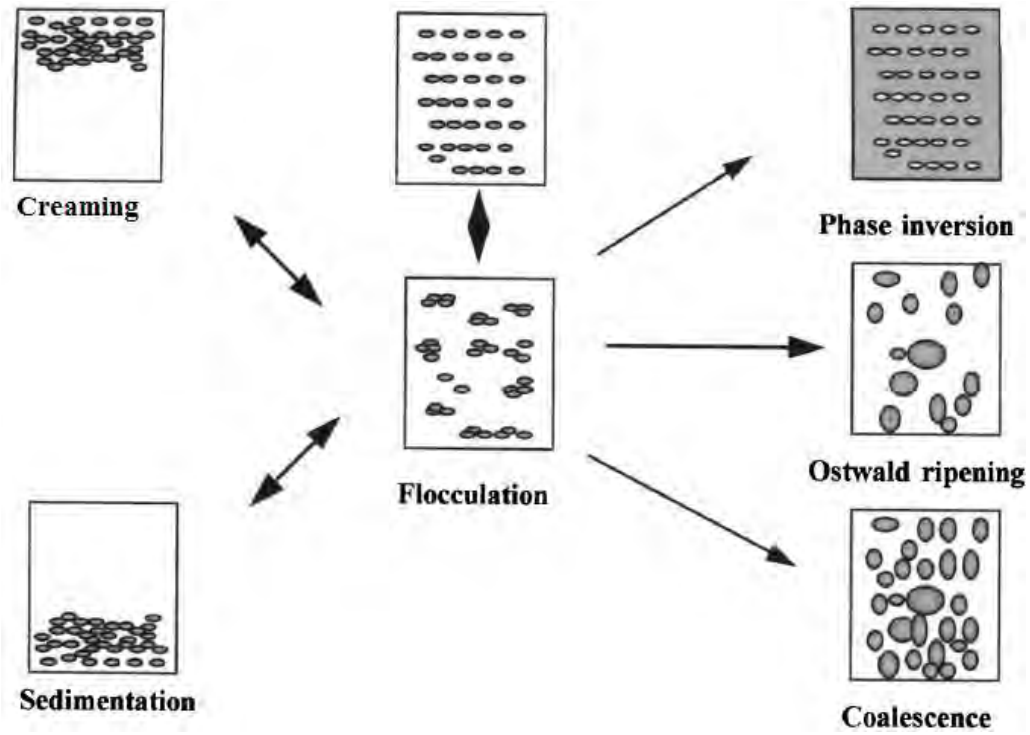

Figure 2-7. Destabilisation phenomena of emulsion (Abismaïl *et al.*, 1999)

2.3.2.1. Creaming/Sedimentation

The physical appearance of a product is of paramount important for the consumer and for emulsion-based products, any phase separation or non-homogeneity may be considered as poor quality or reduced shelf-life, even though the product may be rehomogenised to its initial state by shaking or inverting of the container. When the dispersed phase and the continuous phase are of different densities, gravitation will cause droplets to migrate and form more or less packed layer at the top (**creaming**) or at the bottom (**sedimentation**) depending on whether the dispersed phase is less or more dense than the continuous phase. Because creaming is more encounter in O/W emulsion whereas sedimentation is more likely in W/O emulsion as the density of oil is lower than that of water, only creaming will be discussed below. Moreover, bubbles are typically less dense than oil droplets, and thus gravity creaming is more rapid for bubbles system than for the corresponding O/W emulsion.

The creaming rate can be predicted using the Stokes equation (Eq.2-1), by considering that it is the limiting speed at which the force of gravity is balanced by frictional forces of the fluid suspension

$$mg = 6\pi\eta RV \qquad \text{Eq. 2-1}$$

Implying that $V = \frac{mg}{9\eta\pi R} = \frac{2R^2(\rho_1-\rho_2)g}{9\eta}$ Eq. 2-2

Where $m = \frac{4}{3}\pi R^3(\rho_1 - \rho_2)$ is the effective mass of each droplet, V is is the velocity of a droplet or bubble of radius R, ρ_1 and ρ_2 are the density of the continuous and the dispersed phases, respectively; g is the acceleration due to gravity and η is the viscosity of the continuous phase.

It is assumed that Eq.2-2 is true only for dilute monodispersed emulsions and Eq. 2-3 should be considered for dilute polydispersed emulsions (Damodaran, 2005).

$$V = \frac{(d^2+\sigma^2).(\rho_1-\rho_2)g}{18\eta} \quad \text{Eq. 2-3}$$

Where, d and σ are weight average particle diameter and standard deviation, respectively.

Although these equations cannot hold for concentrated emulsions such as mayonnaise and dressings, they suggest that creaming of the emulsion can be prevented or reduced by (1) minimising the density difference between the dispersed and the continuous phase; (2) reducing the size of droplets or bubbles; (3) increasing the viscosity of the continuous phase.

Minimising the density difference between droplets and the continuous phase: this approach is rarely used except for beverage emulsions where weighting agents such as sucrose acetate isobutyrate and brominated oil are used to increase density of the oil phase (Chanamai and McClements, 2000b); but the latter present potential health problem (Horowitz, 1997). The density of the oil droplets can also be increased by means of emulsifiers that form thick and dense interfacial layers around the oil droplets.

Reduction of droplet size: this can be achieved by increasing the energy input and the density of the continuous phase and by decreasing the interfacial/surface tension (see the empirical equation (Eq.2-4) of Walstra, 1988 from Damodaran (2005)).

$$d \approx \frac{\gamma^{3/5}}{E^{2/5}\rho^{1/5}} \quad \text{Eq. 2-4}$$

Where d is the average size of droplets produced during the homogenization, E is the energy input per unit volume per unit time, γ is the interfacial tension between the dispersed and continuous phases.

Creaming is significantly reduced or even prevented if droplets are small enough (sub-micron range so that their Brownian motion is almost equal to creaming rate (Robins, 2000). Moreover, if recall Eq.2-2, creaming will be 100 times slower for an emulsion with an average droplet size of one micron when compare to a similar emulsion with an average droplet radius of 10 μm. It is also evident that any phenomenon that increases the apparent droplets size, as observed with **flocculation,** will tend to increase the creaming rate.

Increase of the continuous phase viscosity: this generally achieved by incorporating gelling/stabilising agents (as discussed in section 2.3.1) and as a result the motion of droplets may be reduced. Increasing the concentration of the dispersed phase also has similar effect (i.e. as the dispersed phase volume increases, creaming rate decreases).

2.3.2.2. Flocculation

Flocculation is a process whereby two or more droplets form aggregates while maintaining their individual integrities. Droplet flocculation has a direct implication on the apparent droplet size, thus influences product viscosity, gravitational separation, microstructure (as it may lead to the formation of a weak gel-like network (Dickinson, 1989)) and sensory attributes. Therefore, whether flocculation is advantageous or detrimental to emulsion properties depends on the degree of the flocculation and the product type.

Flocculation largely depends on the adsorbed molecules surrounding the droplets whose physicochemical properties, along with the composition of the continuous phase, determine the net attractive interactions between droplets. Different types of interactions between droplets are summarised in Table 2-3; but the most frequent types encountered in food emulsions are electrostatic and hydrophobic (Dickinson, 2003). Details of these factors and their influence on these forces can be found in section 2.2. Droplets can also flocculate because of the adsorption of one molecule polymer on the surface of more than on droplets (**bridging flocculation**); for instance, the adsorption of unfolded protein molecules on different droplets via noncovalent interactions (Monahan *et al.*, 1996). In similar fashion, biopolymer in the continuous phase may trigger bridging flocculation if carrying opposite electrical charge to the droplets charge. Also micelles or nonadsorbed protein aggregates (e.g. sodium caseinate sub-micelles) and polysaccharide in the continuous phase at certain concentration may create an osmotic pressure gradient resulting in the depletion of these polymers between the neighbouring droplets (Dickinson and Golding, 1997). This phenomenon is called **depletion flocculation.** Depletion and bridging flocculation may coexist in the same system; for example, when large numbers of small spherical particles interpose themselves between some larger ones, thus enhancing their attractive interactions to form a dense phase. This leaves behind a less dense phase richer in larger spherical particles (Dickinson, 1989).

Droplets flocculation is controlled by manipulating the concentration of the biopolymers and by controlling the net attractive interactions between droplets (controlling droplets surface charge) by varying, for example, the pH and ionic strength of the system. Some emulsifiers may also prevent flocculation via steric repulsion if the latter is sufficiently strong to overcome any attractive forces in the system. However, steric interaction is difficult to

predict because its strength varies from system to system as it depends on the molecular characteristics of the interfacial layer such as packing (thickness), flexibility, molecular interactions (McClements, 2005).

Table 2-3. Characteristics of different types of colloidal interactions between emulsion droplets (McClements, 2005)*

Type of interaction	Sign	Strength	Range	Major factors affecting
Electrostatic static	R	W→ S	SR→ LR	σ, pH, I, Ψ_δ
Hydrophobic	A	S	LR	$\emptyset_H$, T
Van der walls	A	S	LR	ε, n, I
Steric				
Elastic	R	S	SR	δ, E
Mixing	A or R	W→ S	SR	ω, δ
Depletion	A	W→ S	SR	$\emptyset_c$, r_c
hydration	R	S	SR→ MR	T
Thermal fluctuation	R	S	SR→ MR	T

* The interactions are classified as follows: A= attractive, R= repulsive, S= strong, W weak, SR= short range (< 10 nm), MR= medium range (10-20 nm), and LR= long range (> 20 nm). The major factors affecting interaction are surface potential (Ψ_δ), Surface charge density (σ), Ionic strength (I), surface hydrophobicity ($\emptyset_H$), temeprature (T), dielectric constant (ε), refractive index (n), thickness of the interfacial layer (δ), elastic modulus of the interfacial layer (E), effective interaction parametre for emulsifier-solvent interactions (ω), colloidal particle volume fraction ($\emptyset_c$) and particle radius (r_c).

2.3.2.3. Coalescence

Coalescence is a thermodynamically driven process involving the decrease in the contact area between the dispersed phase and the continuous phase. This occurs by the fusion of two or more droplets into a single large one. The process may lead to a complete loss of gas in bubble systems or the formation of single layer of oil sitting on top of an aqueous phase. Droplets can only merge if they are in very close proximity and the thin film (any interfacial membrane and the continuous phase surrounding droplets) between them ruptured (Aveyard

and Clint, 1996; McClements, 2005). Therefore, droplet coalescence is influence by (1) any physical mechanism that would increase the probability of droplets to meet with each other such as Brownian motion, turbulence and gravity; (2) the interplay of intermolecular forces of attractive and repulsive interactions (Table 2-3) between two droplets which may result in **droplets flocculation** if the intermolecular repulsive forces are sufficiently strong to hold the droplets separated at a small equilibrium distance or **droplets coalescence** if the film ruptures; (3) the resistance of the thin film to rupture.

Moreover, the size of the droplets dictates whether the two approaching droplets, under the forces mentioned above, kept their spherical shape (small droplets, Figure 2-8a) or deformed, flattened with formation of a planar film droplet (more likely to occur for relatively big droplets, Figure 2-8b) until the moment of flocculation or coalescence (Ivanov *et al.*, 1999). The contact area between the two approaching droplets increases, when droplets are flattened, and thus, increase the susceptibility of droplets to coalescence. The tendency of droplets to deformation can be described by a Weber number (We, Eq.2-5) with propensity for droplets to become deformed if We < 1 or droplet tend to remain spherical for We > 1. For example, considering this equation, McClements (2005) postulated that droplets in food emulsions with droplet radius < 1μm tend to remain spherical unless they are centrifuged at relatively high speed whereas those with droplets larger than 10 μm or with low interfacial tension will be easily deformed.

$$We = \frac{\sigma_{Ext} r^2}{2\gamma h} \qquad \text{Eq. 2-5}$$

Where σ_{Ext} is the external force (colloidal, hydrodynamic and mechanical forces), r is the droplet radius, γ is the surface tension and h is the surface-to surface separation or the thin liquid film (pseudoemulsion film as discussed below).

The net effect of these external forces often referred to as the disjoining pressure (⊓), which is defined as the net force per unit area acting normal to the film surfaces (Figure 2-8b), opposes the internal forces which are the consequence of the Laplace pressure and the resistance of the interfacial membrane to deformation. A positive ⊓, tends to thicken the film (favouring bubble system or emulsion stability) whereas negative values cause spontaneous thinning and possibly leading to film rupture.

From the above, coalescence can be prevented mainly by a careful choice of emulsifiers as the latter determine the property of the film surrounding the droplets (e.g. emulsifier with high surface shear elastic and viscous moduli), reducing the net attraction force between droplet as discussed above and by increasing the viscosity and the stability of the thin liquid film separating two approaching droplets (Aveyard and Clint, 1996; Ivanov *et al.*, 1999; Zuniga and Aguilera, 2008). The stability of this thin film is control by the presence of miscelles, particles, protein aggregates which in turn influence Ostwald ripening process.

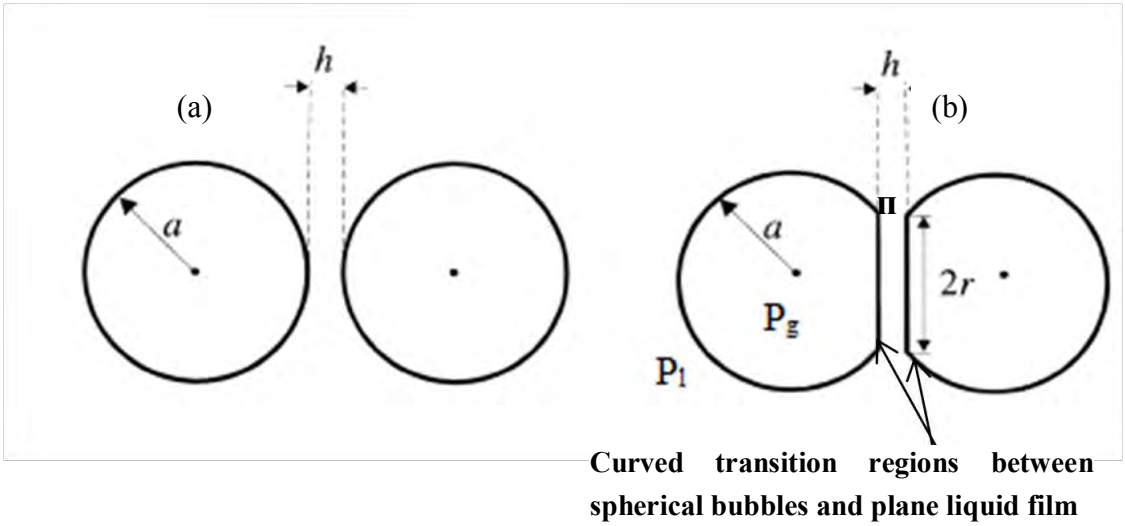

Figure 2-8. Schematic of two approching emusion oil droplets (or air cells) of radius, a, separated by surface to-surface distance, h, as redrawn from (Aveyard and Clint, 1996; Ivanov *et al.*, 1999).
(a), the two approaching droplets kept their spherical shape and show larger h when compare to (b) where, droplets have flattened surface and forming a thin planar film (smaller h) and radius, r.
The Laplace pressure (P_g-P_l) tends to suck liquid from the film and is just opposed by the positive disjoining pressure Π.

2.3.2.4. Ostwald ripening/ disproportionation

The transport of gas or liquid dispersed phase between bubbles or droplets of different sizes is known as disproportionation or Ostwald Ripening. This phenomenon occurs because the solubility of the dispersed phase increases as the droplet size decreases according to Eq. 2-6 (Heinmenz and Rajagopalan, 1997).

$$S(r) = S(\infty)\exp\left(\frac{2\gamma V_m}{RTr}\right) = S(\infty)\exp\left(\frac{2\gamma}{r}.\frac{V_m}{RT}\right) \qquad \text{Eq. 2-6}$$

Where S(r) and $S(\infty)$ are the solubility of the dispersed phase in the continuous phase for a droplet of radius r and with infinite curvature, respectively; γ is the surface/interfacial tension, V_m is the molar volume of the dispersed phase, R is the gas constant and T the thermodynamic temperature, $\frac{2\gamma}{r}$ is the Laplace pressure.

This equation suggests that, there will be a high concentration of the dispersed phase around smaller droplets than around the larger ones and, because of this concentration gradient, the dispersed phase diffuses from smaller to the larger droplets. As a result, small droplets shrink whereas larger droplets grow, leading to an overall net increase in the average droplet size with time. Ostwald ripening is a self-accelerating process because, as small droplets shrink, their internal pressure increases and, thus, the increase in the solubility of the encapsulated oil or gas (e.g. air). This process is generally less pronounced for O/W emulsion than for bubbles system, which may be partially explained by the difficulty in controlling or stopping gas diffusion. This may also elucidate why long-term stability is believed to be much more difficult to achieve for aerated systems than it is for emulsions (Dickinson, 2010).

Gas may also diffuse to the atmosphere but it is the exchange of gas between bubbles that generally dominates. Moreover, disproportionation does not only result in bubbles disappearing but also could serve to accelerate gravitational separation, and coalescence (see Eq. 2-2 and 2-5).

Returning to Eq. 2- 6, it can be seen that Ostwald ripening could be retarded when the temperature of the system is lowered, the solubility of the dispersed phase in the continuous phase is reduced, surface active agent that is highly effective at lowering surface/interfacial tension is used and when produce a monodispersed system. However, the property of adsorbing membrane around the droplet also controls the diffusion and should be taken into consideration. A thick tightly packed protein membrane could be less permeable even to air, and may considerably retard Ostwald ripening in the same manner as nanoparticles. For example, hydrophobin HFBII is able to adsorb in a multilayer (Figure 2-9) and to form elastic and cohesive film (Figure 2-10). Figure 2-9 shows a FHBII bilayer (S-bilayer) with the two

molecules connected via their hydrophilic patch. However, Basheva *et al.* (2011b) has demonstrated that the major interation between between them is hydrophobic. The fact that one of the hydrophobic patches is exposed to the aqueous phase indicated the possibility of adsorption of other hydrophobin molecules (monomers or aggregates) on the S-bilayer as detailed in chapter 4.

It is worth highlighting several attempts made to increase the stability of emulsions and bubbles via protein modification by heat, pressure or chemical treatment which resulted, in some cases, in the increase of protein surface hydropbicity and formation of viscoelastic protein aggregates film at the interface, i.e. the works of Dickinson *et al.* (1999) and Kim *et al.* (2005). However, as discussed in section 2.2., the outcome of this process is fundamentally unpredictable (especially for physical modification) and involves a trial and error approach because of the interplay of many parameters (pH, concentration, shear and heating rate, temperature, and so on). Moreover proteins may loss flexibility and/or solubility which are important for protein adsorption and formation of a viscoelastic film at interfaces.

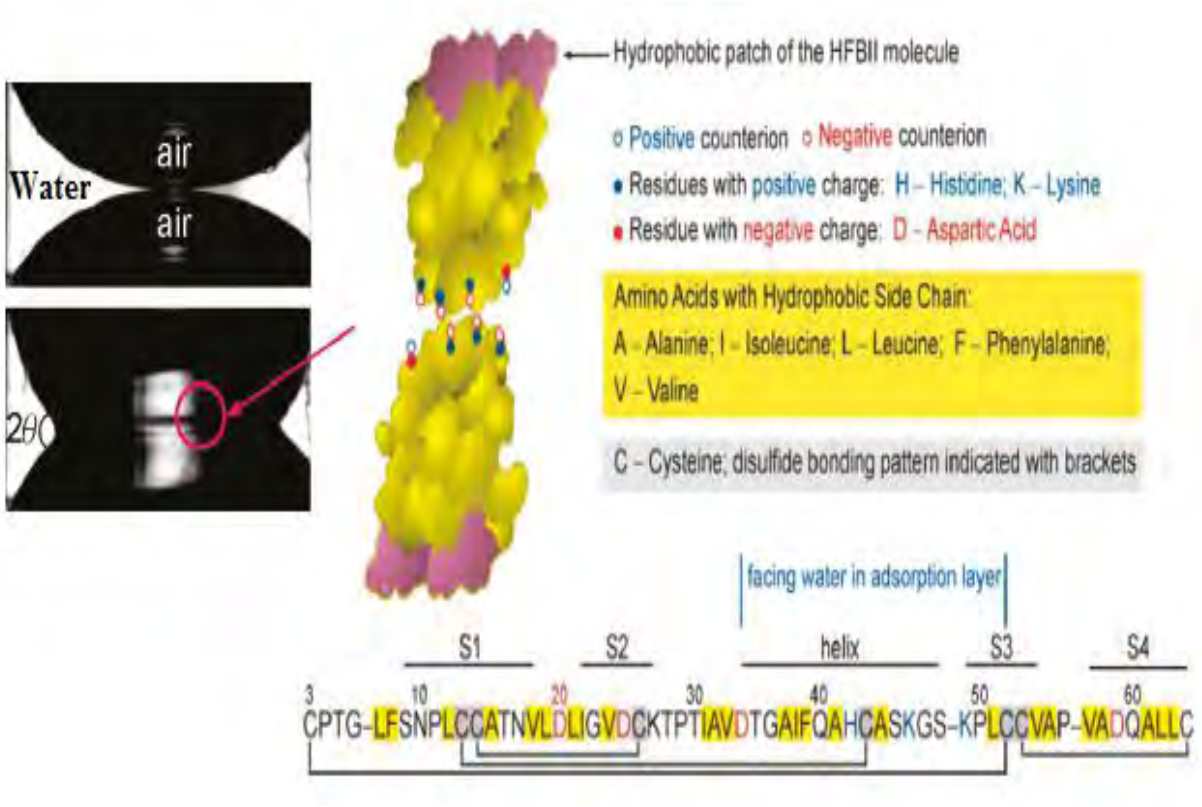

Figure 2-9. Hydrophobin HFBII bilayer at the A/W interface showing the portion of the sequence that faces the water phase (Basheva *et al.*, 2011b).

The authors postulated that the ionisable groups in the zone of contact of the two molecules are neutralised by condense conterions whereas the hydrophobic groups are able to serve as adhesive force.

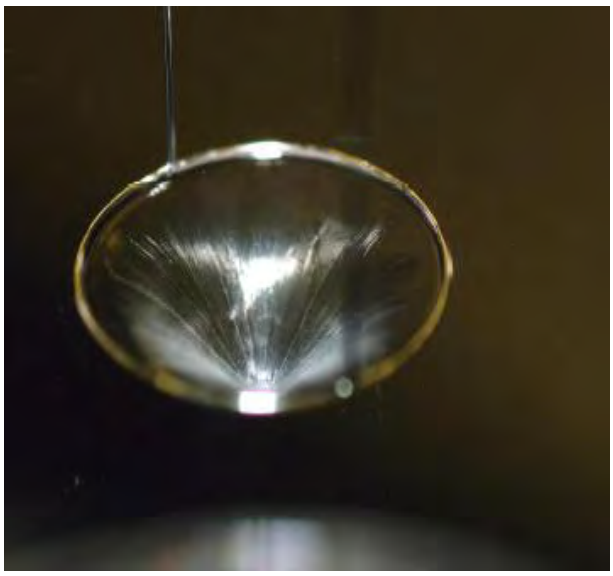

(a)

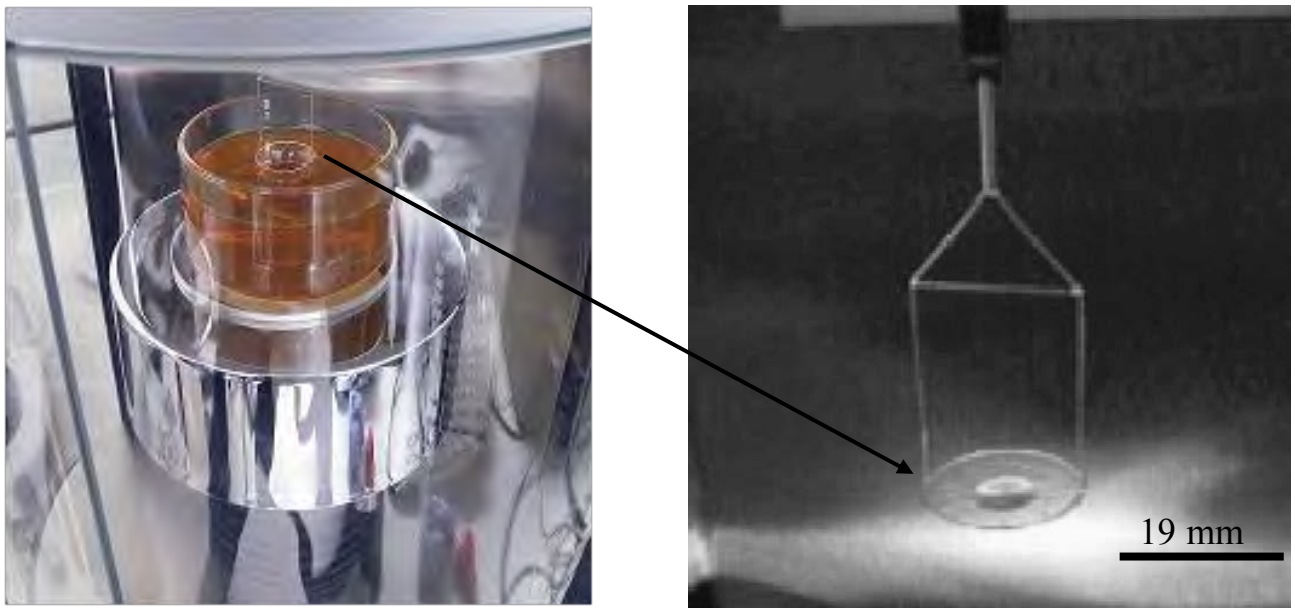

(b1) (b2)

Figure 2-10. Photograph illustrating the robustness of hydrophobin HFBII film adsorbed onto a Du Noüy ring (diameter 19 mm) which has been raised from an air/water.
(a) from Cox *et al.* (2007) and (b) from Tchuenbou-Magaia *et al.* (2009a). The film is vertically stretched as the Du Noüy to which hydrophobin is raised from the air/hydrophobin containing solution interface, but part of the film still in the solution interface (b1). The Du Noüy ring is then raised further and the protein film completely out of the solution, resulting in a horizontally stretched hydrophobin film; during this process hydrophobin film carries a big water droplet (b2).

2.3.2.5. Lipid oxidation

Oxidation of polyunsaturated acid present in an emulsion generates peroxides, aldehydes and other compounds that can not only alter food organoleptic properties (taste, texture, physical appearance) but also may result in loss of nutritional quality (essential fatty acids and vitamins) (McClements and Decker, 2000; Choe and Min, 2006) and form a health risk by the formation of potentially toxic and carcinogenic compounds (Kubow, 1992; Shahidi, 1998). In addition, absorption of lipid oxidation products may cause an increase in oxidative stress and deleterious changes in lipoprotein and platelet metabolism which, leads to an increase of risk of cardiovascular diseases (Kubow, 1992, 1993; Nielsen *et al.*, 2006).

Lipid oxidation is generally promoted by heat, light, available oxygen or air and transition metals (e.g. Fe^{2+}). Other factors that influence the oxidative stability of emulsion based food include the type of emulsifier, oil phase volume and droplets size, pH and processing conditions (Hu *et al.*, 2003; Osborn and Akoh, 2004; Nakaya *et al.*, 2005; Dimakou *et al.*, 2007; Sorensen *et al.*, 2007; Haahr and Jacobsen, 2008; Kargar *et al.*, 2011). Moreover, oxidation in emulsions is very complex because of the presence of droplet membrane, the interaction between the ingredient, the partitioning of ingredients or electron transfer events in all the different phases of the systems (Coupland and McClements, 1996; Jacobsen *et al.*, 2008; Waraho *et al.*, 2011). This may be especially true in a triphasic emulsion system where air cells and oil droplet are dispersed in water continuous phase.

Oxidation stability of an emulsion can be improved by means of anti-oxidants such as EDTA that can scavenge pro-oxidants (metal ions) from the aqueous phase (Jacobsen *et al.*, 2008; Waraho *et al.*, 2011) or by structuring the interfaces of droplets with emulsifier/stabiliser carrying charges and/or to form less permeable or thick interface membranes. This will repel

and reduce pro-oxidant diffusion or provide steric hindrance of interactions between water- and oil-soluble components (Guzey and McClements, 2006; Kargar *et al.*, 2011; Waraho *et al.*, 2011). Also, the ampholyte nature of proteins and their ability to interact with lipid oxidation products can be used to control and prevent the oxidation or the propagation of the oxidation, and the particularity of hydropbin in this regard is discussed in chapters 5 and 7.

2.3.3. Methods to characterise destabilisation phenomena of emulsions and bubbles

The previous section shows that emulsion and bubbles destabilisation phenomena involve, to some extent, changes in droplet or bubble sizes. Therefore monitoring the droplet sizes and size distribution over a given time will give a good picture of the kinetic stability of an emulsion. Microscopy and light scattering techniques are most commonly means of measuring droplets size, and was used in this thesis. However electrical pulse counting, ultrasonics and NMR are also used (McClements and Coupland, 1996; Kiokias *et al.*, 2004; Smyth *et al.*, 2004; Johns, 2009). Because coalescence, Ostwald Ripening and, sometimes, flocculation lead to the increase in droplets size, it may be difficult to distinguish between those phenomena. The combination of microscopic observation and other particle sizing methods, the measurement of changes in droplets size distribution over time and the examination of factors that influence the rate of droplet growth help to overcome this problem. Flocculation may also be assessed by measuring the viscosity of the emulsion as the viscosity will increase if gel particles are formed or by breaking down flocs, for example, using solvent such as SDS, followed by particle size measurement (Tadros, 1996; Dickinson and Golding, 1997; Manoj *et al.*, 1998).

Gravitational separation is characterised by placing an emulsion in a transparent container and measuring the height of the interface between different layers formed. More sophisticated techniques such as ultrasound velocity scanning, light scattering and NMR are available (Dickinson and Golding, 1997; McClements, 2005).

2.3.4. Triphasic A/O/W emulsions versus standard aerated emulsions: a definition of the structure

Triphasic A/O/W emulsion is relatively a new concept and its absolute definition along with its microstructure, in comparison with a well know aerated system is presented below.

2.3.4.1. Microstructure

Triphasic A/O/W emulsions as defined within this study are emulsions with two distinct dispersed phases, air cells and oil droplets and both dispersed phases are intimately mixed in a single aqueous continuous phase. Conversely, whipped emulsions are, generally emulsions containing air cells predominantly stabilised by either partially-coalesced fat globules network (Boode *et al.*, 1993) or aggregations of the protein-coating surrounding the droplets (Allen *et al.*, 2006). Although ingredients might be, to some extent, similar especially for non dairy based-emulsions, the processing methods as well as the microstructure and bubble stabilisation mechanisms of these two kinds of emulsions containing bubbles differ (Figure 2-11). The creation of whipped emulsions and triphasic emulsions are both two-step processes in a sense that O/W emulsions are made first. However, in the former products, air is directly incorporated into the emulsion through whipping. The advantage of non direct incorporation

of air is not only the long term stability of the resulting triphasic emulsion but also the possibility to "tune" the microstructure of this system and control its texture. This might be achieved by separately engineering or manipulating the size of oil droplets (O/W) and of the air cells (AFE) (Tchuenbou-Magaia and Cox, 2011). Furthermore the A/O/W formulations showed interesting properties with possible interactions between the air cells via their protein shells, and possibly other components in the product matrix, resulting, in a weak gel like behaviour, which contributes to better resistance to creaming (Tchuenbou-Magaia *et al.*, 2009a, 2010) (see Chapter 4).

Although whipped emulsions containing liquid oil where air cells stabilised by protein aggregates have been made (Allen *et al.*, 2006; Heuer, 2009), whipped emulsion-based products generally required a high fat content in order to provide a sufficient number of fat crystals at the whipping temperature, 4-10ºC (Jakubczyk and Niranjan, 2006; Goff and Vega, 2007). This implies using a high content of saturated fatty acids, which are known undesirable for health reasons. However, the overrun may by higher in whipped emulsions than triphasic A/O/W emulsion as there seems to exist a critical air phase volume (around 50%), below which the air does not affect the stability of triphasic emulsion (see Chapter 5).

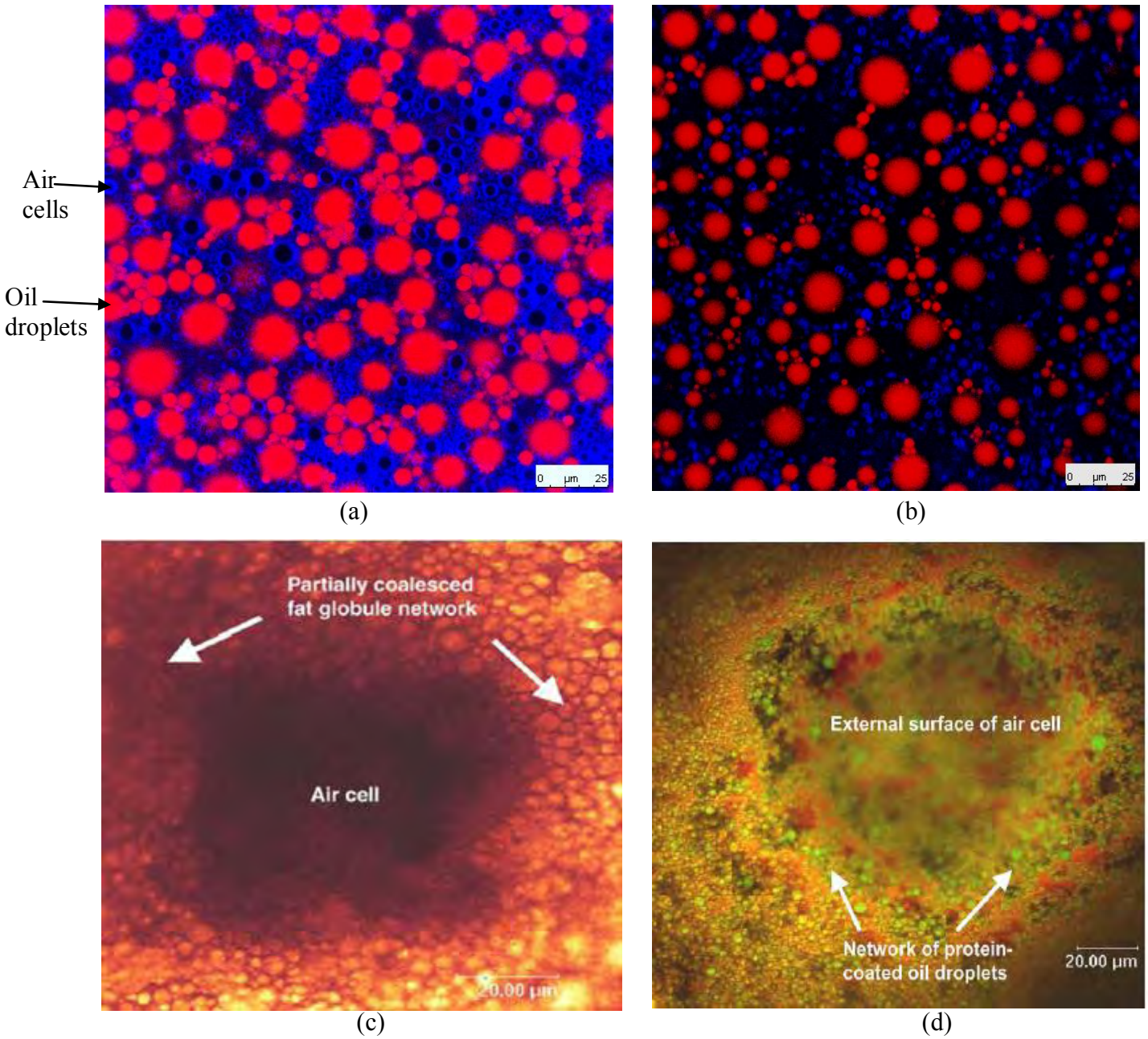

Figure 2-11. Comparison of microstructure of triphasic A/O/W emulsion and whipped emulsions
(a) and (b) are confocal micrographs of the triphasic A/O/W made with AFE stabilised with BSA and O/W emulsion with Tween 60 (ratio AFE:O/W, 1:1). AFE was concentrated and fractionated by gravity overnight at room temperature in a separating funnel. Larger air cells migrated to the upper layer (due to their relative greater buoyancy) but entrained with them substantial amount of smaller ones. This upper layer (1/5 of the suspension) was used to construct sample (a, 20 % air, 10% oil and 70 % water) whereas the middle layer containing almost monodispersed smaller air cells was used for the production of sample (b, 5 % air, 10% oil and 85 % water) and the bottom layer (3/5 of the dispersion) was discarded. No polysaccharide was used in the formulation. Air cells are black with blue protein shell; oil droplets are coloured red.

(c) is a confocal image of a whipped cream and (d) is that of a whipped emulsion where air cells are stabilised by acidified sodium caseinate. Oil is coloured red and protein green. These two images are reproduced from Allen *et al.* (2006).

2.3.4.2. Destabilisation/stabilisation mechanism of bubbles in the presence of oil droplets

In addition to emulsions and bubbles breakup mechanism described in section 2.3.2, oil droplets may also contribute to the destabilisation of the triphasic O/A/W emulsions by acting as a bubble breaker. This phenomenon is schematically illustrated by Figure 2-12. The most generally accepted mechanism of destabilisation of bubbles in the presence of oil is that oil droplets enter and spread at the air/water interface, and cause film rupture through a Marangoni mechanism (surface tension gradient)(Aveyard *et al.*, 1994). Entry is the precursor to spreading and for entry to occur, the entry coefficient (E) must be positive. E corresponds to the decrease in the free energy that occurs when an oil droplet in the aqueous phase enter or form a lens at the A/W interface. This is defined in terms of macroscopic interfacial tension as

$$E = \gamma_{A/W} + (\gamma_{O/W} - \gamma_{O/A}) \quad \text{Eq. 2-7}$$

Where $\gamma_{A/W}$, $\gamma_{O/A}$ are the surface tensions of the aqueous and the oil phase, respectively, and $\gamma_{O/W}$ are the oil/water interfacial tension. Once a droplet has entered the A/W, whether spreading occurs depend on the value of the spreading coefficient interface (S), defined as:

$$S = \gamma_{A/W} - (\gamma_{O/W} + \gamma_{O/A}) \quad \text{Eq. 2-8}$$

A microscopic spreading will occur if $S \geq 0$; otherwise ($S < 0$) the droplet remains as a lens on the A/W interface. According to Aveyard *et al.* (1994), if the oil remains as a lens on one surface of the film, as the film thins (due to the Marangoni effect) the droplet will eventually enter the opposite surface, forming a bridge across the film. Whether this oil bridges rupture the bubble films or not, generally depends on the value of the bridging coefficient (B).

$$B = \gamma 2_{A/W} + \gamma 2_{O/W} + \gamma 2_{O/A}$$ Eq.2-9

Positive values of B correspond to unstable bridges, while negative values of B correspond to mechanically stable bridges (Denkov, 1999). However, the formation of the oil bridge may be sufficient to cause the rupture of foam film (Lobo and Wasan, 1993). Alternatively, oil spreading may not occur when an oil droplet enter the A/W interface but rather an extraction into the oil phase (for example by diffusion) of the surface active agent that stabilised bubbles, thereby contribute to their destabilisation (Princen and Goddard, 1972).

When oil droplets and air cells approach each other, there may be a stable liquid film or pseudoemulsion film separating them that prevent oil droplets from entering the air/water interface even when E > 0 (see Figure 2-12, scenario (a)). In this situation, oil droplets may instead contribute to the stability of the bubbles system (Wasan *et al.*, 1995). The stability of this film is governed by the drainage, which in turn is controlled by many other factors, either singly or in combination, such as the tension gradients at the interfaces, interfacial viscosity and the presence of aggregates or micellar structuring the pseudoemulsion film as discussed in section 2.3.2.4.

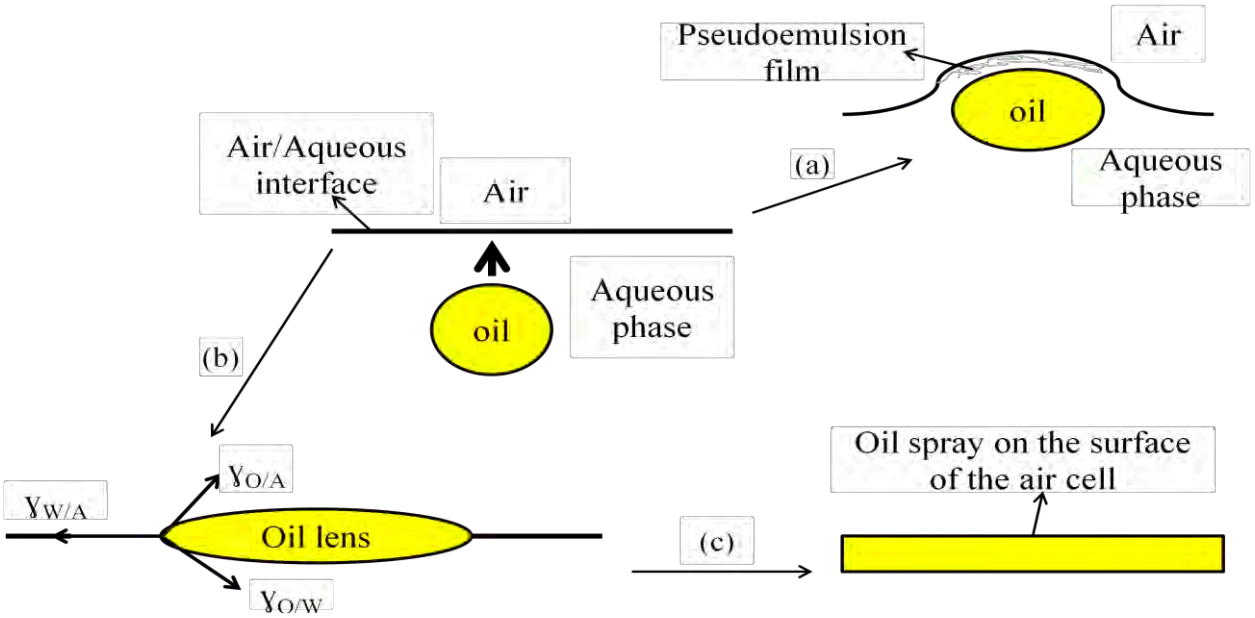

Figure 2-12. Schematic of possible mechanisms of stabilisation or destablisation of bubbles in the presence of oil as drawn from Lobo and Wasan (1993), Aveyard *et al.* (1994) and Hotrum *et al.*, (2003).
There are two possible scenarios when an oil droplet approaches an air/aqueous interface, as indicated by the arrow: (a), there is a pseudoemulsion film or thin aqueous film separating the approaching oil droplet and the bubble surface which prevents oil to enter the A/W interface; (b) the oil droplet may enter the A/W interface and trigger the bubble film rupture via spreading (c).

2.4. Microstructure, rheology, tribology and mouth-feel

The majority of elements that critically participate in transport properties, physical and rheological behaviour, textural and sensorial properties of foods are below the 100 μm range (Aguilera, 2005). These microstructural elements include protein assemblies, food polymer networks, oil droplets and gas bubbles. The spatial organisation of these microstructural elements defined as **microstructure** determines the texture of food which in turn dictates the rheological, tribological and other food attributes included mouth-feel. **Mouth-feel** is a term used to describe a variety of tactile sensations that are experienced within the mouth during food mastication, such as creamy, thick, rich and watery (McClements, 2005).

Rheology can be defined in a simplest way as a study of deformations and flow of matter or a study of materials in which structure changes under the influence of applied forces. It is postulated that forces sensed by mechanoreceptors (responsible for tactile sensory attributes) of soft epithelial surfaces that cover the mouth are produced by the viscous forces of the food flowing on the tongue surface, the friction of tongue and palate in contact and particles grinding between tongue and palate (van Aken, 2010a). The latter two sources of forces can be better emulated by thin film rheology or tribology, whereas the former is linked to the bulk rheology.

The rheological regime applied in the mouth (chewing and swallowing of foods) correspond to a shear rate of 10 to 100 s^{-1} (Braun and Rosen, 2000) or 5 to 50 s^{-1} (McClements, 2005) and this may fluctuate even more because of the type of food-dependent motion of the tongue and jaws. The ratio of shear stress (force per unit of the surface area) to the shear rate (velocity/distance between the geometries where the product is confined as in the rheometer) corresponds to the coefficient of viscosity or viscosity. Since many emulsion-based products are non-Newtonian fluids, their viscosity will vary with applied shear. Small-deformation oscillatory shear at a single frequency (50 rad/s) is also thought to give a reasonable representation of the food oral processing conditions (McClements, 2005). Several studies reported a strong correlation between product viscosity and sensory attributes such as creaminess, smoothness, and stickiness, sliminess (Richardson *et al.*, 1989; Frøst and Janhøj, 2007; Ciron *et al.*, 2012). The viscosity of an emulsion-based food is influenced by many factors included droplet size and any attraction between droplets in the dispersed phase. This is largely dependent on the type of material present at the interface between the dispersed phase and the liquid phase, and the size of droplets.

Tribology is concerned with the friction, lubrication and wear of surfaces in relative motion. In the context of food, the friction coefficient is used to retrieve information about lubricational properties, thus generally the fat related attributes of the product. This friction coefficient is derived from the friction generated when two surfaces sliding/rolling over one another at a given entrainment speed, and in the presence of a product which acting as lubricant. The study of the tribological behaviour of food is based on the fact that a tribometer can be designed or set up to emulate a mouth and the motion of the tongue around the oral mucosa, for example, by choosing the tribo-pair that can best possible mimic the tongue and the palate, the normal force and the entrainment speed relevant for food oral processing (Malone *et al.*, 2003; de Hoog *et al.*, 2006; Ranc *et al.*, 2006; Dresselhuis *et al.*, 2007a). Moreover, sensory attributes such as smoothness, thickness, fattiness and creaminess have been shown to correlate with the friction between surfaces lubricated with semi-solid foods (Malone *et al.*, 2003; de Wijk and Prinz, 2005; de Hoog *et al.*, 2006; de Wijk and Prinz, 2006).

In a tribology study, three regimes can be distinguished and each of the regimes might be related to one or more phases of food oral processing. The boundary regime, where the friction depends mainly on the tribo-pair surface asperities and the presence of any adsorbed layer of lubricant. This regime may correspond to the clearance phase of oral processing where the tongue rubs against the palate and any coated material on both surfaces sensed. Here again food microstructural elements play a crucial role. Surfactant, protein, or polysaccharides that are able to adsorbed to the surface and lower the boundary friction may contribute to the improvement of the sensory attribute of low fat products (van Aken and de Hoog, 2009; Tchuenbou-Magaia and Cox, 2011). Furthermore, the behaviour of food product when initially in the mouth may be described by bulk rheology, i.e. when the film between

surfaces is relatively thick (Zinoviadou *et al.*, 2008). This corresponds to the hydrodynamic lubrication regime where a thick layer of lubricant has separated the surfaces. Between the boundary and the hydrodynamic regime lies the mixed regime of lubrication where the tribo-pair is partially separated by the lubricant film. Again this regime is influenced by the size and shape of the microstructural elements as well as their ability to interact between each other (Kilcast and Clegg, 2002; Tchuenbou-Magaia and Cox, 2011; Garrec and Norton, 2012) as these will determine whether or not, and to which extent, they will be entrained into the tribo-pair contact zone at relatively low entrainment; and thus how they will be felt in the mouth.

It is pertinent to acknowledge the difficulty in making a direct link between the mouth-feel to the microstructure and the composition of food, as the mouth-feel is the consequence of diverse and complex phenomena, not limited only to the interaction between the content of the mouth during the eating process (food and saliva) and mechanoreceptors present in the mouth but also depends on the visual appearance of the food. Nonetheless, because good correlation exists between the microstructure, tribological and rheological behaviour of food and its mouth-feel or sensory (de Wijk and Prinz, 2005) this approach has become an integrated part of the process of the development of low fat products. For instance, low fat stirred yogurts with creaminess and desirable texture properties similar to, or better than, full-fat conventional yogurt have been recently made by manipulating the microstructure, especially the size of fat globules by microfluidisation of milk (Ciron *et al.*, 2012). According to the authors, microfluidised nano-sized fat globules strongly interacted with proteins and embedded within the protein networks. Whereas larger, micron sized, fat globules were not able to enter into protein networks but were rather located at network junctions (either attached or adsorbed). This difference in microstructure resulted in significant changes in sensory profile and rheological behaviour with a concomitant increase in the gel strength by

171–195% and viscosity by 98–103%. Also, spherical particles made with proteins and/or polysaccharides aggregates and having a size ranging between 0.1 and 20 μm have been reported to provide oil droplet mimics for fat reduction in emulsion-based products (McClements, 2005). These highlight the importance of both the microstructure and the physical properties matching for the design of a fat substitute if aiming to provide a mouth-feel similar to that of the conventional full fat product. This concept, as stated in the introduction, is the cornerstone of this thesis.

2.5. Conclusion

This review has covered the production/purification, classification and colloidal behaviour of hydrophobins. The physical properties and solubility of Class I and Class II hydrophobin were exploited for the extraction of hydrophobins (see Chapters 3 and 4). Methods of formation, stabilisation and destabilisation of emulsions, microbubbles and emulsions containing bubbles have also been described. Particular emphasis has been given to the use of ultrasound technology for the contruction of emulsions and bubble systems. In addition, this chapter highlights fundamental differences between well known aerated emulsions (whipped cream) and the novel triphasic A/O/W emulsion (air cells and oil droplets dispersed in water continuous phase) presented in this thesis.

CHAPTER 3

MATERIAL, METHODS AND METHOD DEVELOPMENT

3.1. Introduction

This chapter introduces the materials, techniques and the experimental procedures used throughout this work. Firstly, the main ingredients used for the different emulsion formulations are presented and a special focus on the production and extraction of hydrophobins is given. This is followed by details of the methods used for the construction of emulsions, their characterisation and some of the more general analyses used.

3.2. Material

3.2.1. Surfactants/emulsifiers

Several proteins and Tween 60 were used as surface active agents in this study. The proteins used were: hydrophobin rich extracts obtained either from edible mushrooms or *Trichoderma reesei* through submerged fermentation (see section 3.2.1.1 for details about the extraction method). Two genetically modified hydrophobins supplied by BASF (Germany) were also used. These are fusion proteins obtained by expressing a combination of a DNA sequence from *Bacilus subtilis,* yaaD and a DNA sequence from *Aspergillus nidulan* with a gene coding for a Class I hydrophobins, DewA. The combined gene is then expressed and to give H*proteins. These consist of the entire protein generated from *Bacillus subtilis* gene, YaaD

and hydrophobin, DewA (H*Protein A, ≈ 47 kDa) with exception that H*Protein B (≈ 19 kDa) has a truncated form of protein yaaD of Bacilus subtilus (Wohlleben *et al.*, 2010).

Other proteins used were lyophilised Bovine serum albumin (BSA), dried chicken egg white protein powder (EWP) and Zein corn protein (all from Sigma, UK), whey protein isolate (bipro), 98 wt% protein (donated by Davisco Foods International, US)

3.2.1.1. Production and extraction of hydrophobins

3.2.1.1.1. Class I hydrophobins

- *Sample preparation*

Four different edible mushrooms (Figure 3-1): closed cup white mushrooms, closed cup brown chestnut mushrooms and flat open brown Portabella (all Agaricus Spp) and Oyster mushrooms (*Pleurotus ostreatus*) were bought from a local market. They were washed, sliced and freeze-dried. The water content (as determined by oven drying) ranged from 87 % (Potabella) to 92 % (White mushroom) for freshly bought and from 6 % (Oyster) to 8% (chestnut) after freeze drying (Table 3-1). Samples were then packaged hermetically and stored at -18^{o}C, ready for hydrophobin extraction.

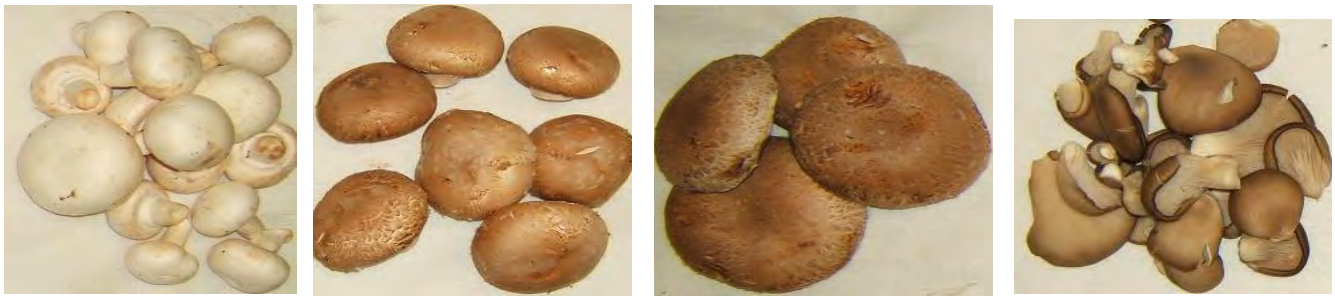

Figure 3-1. Photographs of the different mushrooms used.

Table 3-1. Different varieties of mushrooms used for the extraction of Class I hydrophobins

Mushrooms	**Water content Freshly bought g/100g**	**Water content After freeze-drying g/100g**
White	92.52 ± 0.3	7.91 ± 0.21
Chestnut	89.8 ± 0.5	8.15 ± 21
Portabella	86.76 ± 1.7	7.76 ± 24
Oyster	90.37 ± 0.6	6.03 ± 0.21

- *Hydrophobin extraction*

The method of extraction of hydrophobin from mushroom is based on the solubility properties of hydrophobins and was inspired by the published works discussed in chapter 2 (De Vries *et al., 1993*; Wosten *et al., 1993*; Trembley *et al., 2002*).

The procedure was as follows:

Removal of soluble proteins: freeze-drying mushrooms were ground to a very fine powder using mortar and pestle and 5g of powder were dissolved in Tris buffer (0.1 M Tris–

HCl, pH 8.0, 10 mM MgSO) for 30 min at 4°C followed a centrifugation step at 20,000g for 10 min and the pellet was washed in this way 3 times.

Removal of hot 2% SDS soluble material: the pellet from the above step was resuspended in a buffered SDS solution (0.05 M Tris, pH 6.8, 2% SDS) at 85 °C for 15 min, followed by a centrifugation. This step was carried out twice and the supernatant was discarded.

Removal of lipids: Hydrophobins are associated with cell wall proteins but membrane proteins will tend to co purify with lipid compounds as they link together via van der Waals forces and perhaps by ionic bonds. Therefore the insoluble fraction obtained from the previous step was subject to lipid extraction according to the method of Folch et *al.* (1957). Samples were mixed with chloroform/methanol (2:1) at 60°C for 10 min then centrifugation at 20,000g for 10 min. This was done 4 times. The SDS insoluble and lipid free material (hydrophobin containing fraction) was then freeze-dried overnight. The extraction yield at this stage was calculated as:

$$Yield = \frac{\text{weight of dried hydrophobin rich fraction}}{\text{weight of mushroom powder}} \times 100 \qquad \text{Eq. 3-1}$$

Transformation of assemblage hydrophobins into soluble monomer: the dried hydrophobin rich fraction was resuspended in ice cold 100% trifluoroacetic acid (TFA) for 90 min. The slurry was sonicated in an ice-cold water bath for 2 min (three times each 30 min apart). Undissolved fragments were removed by centrifugation and the TFA supernatant was evaporated under a stream of nitrogen. TFA residues were resuspended overnight in 10 mM Tris, pH 8.0 or in water. In some cases the residues were resuspended in 60 % ethanol. Again insoluble material was removed by centrifugation and the quantity of hydrophobin in the supernatant was estimated using a Bradford assay (Bradford, 1976). Fourier Transform

Infrared Spectrometry (FTIR) was used as a qualitative method to identify the presence of hydrophobins by identifying the presence of disulfide bonds. In addition the protein rich supernatant was freeze dried and weighted for the extraction yield estimation. FTIR and Bradford methods are described in more detail in section 3.6.

3.2.1.1.2. Class II hydrophobins from submerged culture

- *Preparation of Trichoderma reesei spore suspensions*

Trichoderma reesei strain IMI 192656ii, (QM 9414, ATCC 26921, CABI Europe, UK) was used in this study. Three solid media were tested for mycelium growth and spores production. These were Malt extract (Oxoid CM59), Potato dextrose (Oxoid CM39) and YM agars (Difco,). Cultures were grown on plates or slants and were examined visually or microscopically for the presence of spores (Figure 3-2). It was observed that *Trichoderma reesei* grew slightly faster with shorter time for the onset of sporulation on Malt extract agar when compared to others, and so, it was used for the production of spore stocks for the rest of the study. The fungus was grown at 25 °C for a month in 1 L medical flat bottles containing 250 mL of malt extract agar. This was prepared by dispersing in distilled water malt extract powder agar (5%). The solution was then autoclaved (121°C /15 min), poured into sterile medical flats bottles, allowed to cool and set at room temperature before inoculation. Spores were harvested by the rolling action of glass beads and sterile 0.01% (w/v) Tween 80 (prepared with distilled water). The mixture was centrifuged at 4000 rpm (3255g) for 10 min. The pellet of spores was resuspended in a preservation broth containing 20% (w/v) glycerol as cryoprotector. Other components of the preservation broth (g L^{-1}) were: peptone (4.0), yeast extract (1.0), KH_2PO_4 (4.0), $(NH4)_2SO_4$ (2.8), $MgSO_4 \cdot 7H_2O$ (0.6), $CaCl_2 \cdot 2H_2O$ (0.8). The

concentration of the suspension was serially diluted to ≈10^7 spores/mL before testing for germination. The spore suspensions obtained were transferred into ependolf tubes (1 mL) and stored at -80 °C until required.

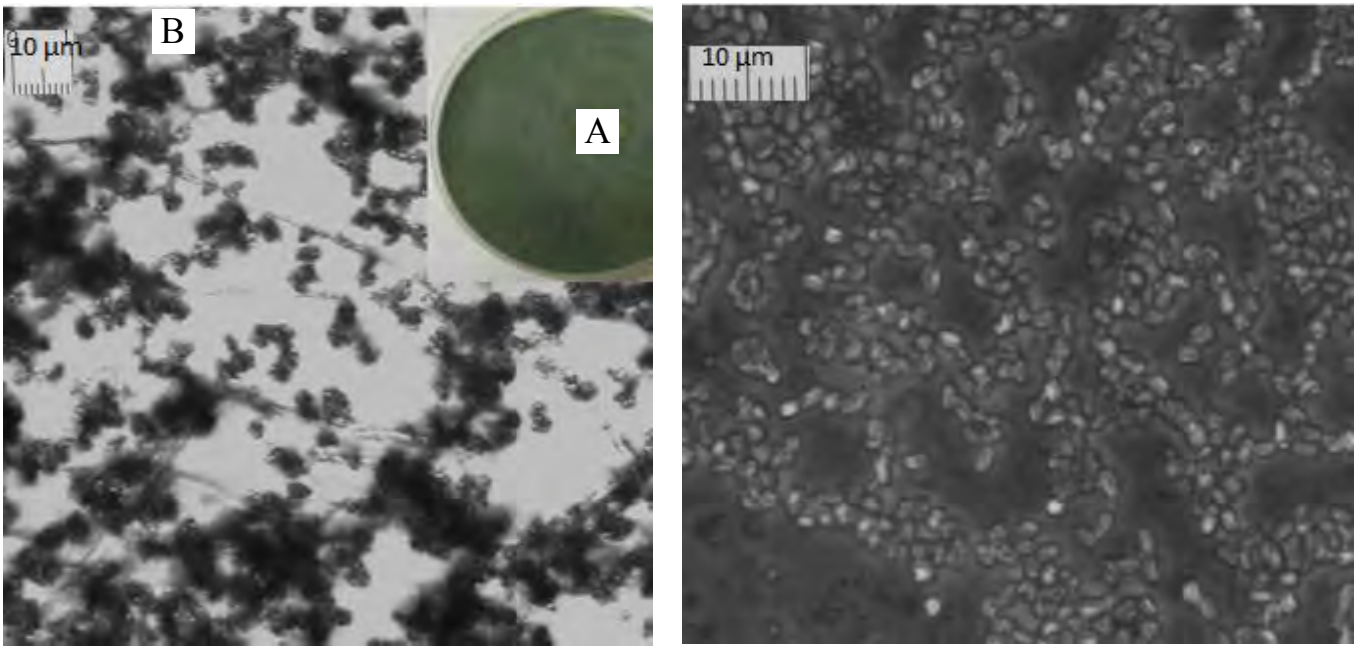

(a) (b)

Figure 3-2. *Trychoderma reesei*. (a) is a micrograph showing mycelium and spores of a week culture (B); a sellotape was pressed on the Petri dish (A) and stick over a microscope slide and observed with a 20x objective. (b) is a micrograph of a suspension of spores imaged with a 40x objective.

- *Cultivation*

Trichoderma reesei was cultivated in a 2L shake flask in a rotary shaker at 200 rpm at 29 °C. This was carried out in two steps: (1) inoculation of 50-mL of medium into 250-ml flask using one mL of 10^7 spores/mL samples; (2) Transferral of the inoculum, after three days of fermentation, into shake flasks containing 200 mL of medium for a further six day growth.

The cultivation media used contained ($g.L^{-1}$): peptone (4.0), yeast extract (1.0), KH_2PO4 (4.0), $(NH4)_2SO4$ (2.8), $MgSO4 \cdot 7H_2O$ (0.6), $CaCl_2 \cdot 2H_2O$ (0.8), trace elements (2 mL): $FeSO4\ 7H_2O$ (5.0mg), $MnSO4 \cdot H_2O$ (1.6), $ZnSO4 \cdot 7H2O$ (1.4) $CoCl_2 \cdot 7H_2O$ (3.7 mg) in 1L of

distilled water (Askolin et al. 2001). This medium was supplemented with the appropriate carbon source, either glucose or lactose at level of 20.0 $g.L^{-1}$. A solution of H_3PO_4 (10% v/v) was used to adjust the starting pH to 4.5. All chemicals were purchased from Sigma, UK.

Lactose or glucose consumption and pH changes were monitored but not adjusted. Sugar consumption rates were quantified by off line high performance chromatography (HPLC) and total soluble protein in culture media by Bradford (1976) (see section 3.6 for details). The culture medium and biomass were separated by centrifugation (17.000g, 45 min, 2^{o}C; Beckman UK).

- *Extraction/separation of hydrophobins from Trichoderma reesei culture broth and their characterisation*

A hydrophobin rich extract was obtained by foam fractionation by bubbling the culture medium supernatant with air. The resulting foam was dried and treated with TFA. The method was adapted from Takai and Richards (1978) and Calonje *et al.* (2002). The procedure was as follows: culture supernatant (500 mL) was poured into a 2L separating funnel and bubbled with sterile compressed air (Figure 3-3). Foam was allowed to accumulate on the liquid surface until it nearly filled the remaining space in the funnel. The liquid layer was then drained away through the bottom of the funnel so only the foam layer remained. The foam was allowed to collapse by washing with 80% aqueous ethanol, followed by evaporation of ethanol and freeze-drying. In some simpler experiments the culture supernatant was bubbled in 5L beaker and the foam was scooped out and dried. About 400 mg of dried foam were obtained from 1L of culture broth. The dried, hydrophobin rich, foam was re-suspended in cold 100 % TFA on ice for 90 min (1 mL solution/100 mg dry material). The slurry was sonicated in an ice-cold water bath three times (2 mins duration, 30 mins apart). Undissolved

fragments were removed by centrifugation (20,000g, 20 min at 4 ^{o}C) and the TFA was evaporated off under a stream of nitrogen. The resulting TFA free solution was re-suspended overnight in water (4 mL/g of foam initially used for the extraction). Insoluble material was removed by centrifugation and the pH of Hydrophobin Rich Extract (HRE) adjusted to 5.0 with 10% aqueous NH_4.

Hydrophobin was also extracted from the fungal cells (mycelia pellet from the centrifugation with 0.2 M acetate buffer, pH 5 containing 1% SDS (Collen *et al.*, 2002). The volume of SDS solution corresponded to about 5–7 times the mycelium mass. The suspension was then continuously mixed for 3 h with a laboratory shaker (100 rpm), and centrifuged as previously described. SDS in the supernatant was precipitated as water-insoluble potassium dodecyl sulfate by adding to it 2 M KCl (ratio volume KCl solution/sample volume, 2:5) and discarded after centrifugation (Askolin *et al.*, 2001). However, SDS is also surface active, and unfortunately can be persistent throughout the remainder of the processing steps. To avoid this contamination, the cell free extract was used for the majority of the work.

Total proteins in the extracts were estimated using a Bradford assay (Bradford, 1976). The presence of possible hydrophobins was checked at different stages by running sodium dodecyl sulphate-polyacrylamide gel electrophoresis (SDS PAGE). This was performed on a gradient gel 5 -20% according to the method of Laemmli (1970), the protein bands were stained with coomassie brilliant blue R-250. Surface tension and interfacial tension of hydrophobin rich extract were measured using a tensiometer K100 (Kruss, Germany) according to the manufacturer's instructions (see section 3.6 for details). All chemicals used for electrophoresis were supplied by Bio-Rad Laboratories Ltd (UK) except for the protein marker (Invitrogen, UK).

Figure 3-3. Separation of hydrophobin from the culture broth of *Trichoderma reesei* by foam fractionation

3.2.2. Thickening/stabilising agents and chemicals

Iota carrageenan and Xanthan gum powder were used as thickening/stabilising agents (Fluka, Biochemical, UK). Sunflower oil was bought freshly from a local market.

Chemicals used for preparation and characterisation of samples are presented together with their corresponding methods.

3.3. Experimental apparatus and methods

3.3.1. Productions of emulsions

3.3.2. Productions of air-filled emulsions (AFEs)

Air filled emulsions were constructed by ultrasonic irradiation protein solutions at an appropriate pH, concentration and temperature. A high-intensity ultrasonic probe (VCX 750, 20 kHz, Sonic and Materials Inc, US) was used. Solutions were sparged with air or oxygen. The protein solution was either the hydrophobin rich extract (as describe above) or egg white proteins (EWP) and bovine serum albumin (BSA).

BSA and EWP were used as supplied (native) or heat treated in a dry state or after being dispersed in water. For thermal treatment of protein powders, 70 g of samples were placed in a sealed glass bottle (250 ml) which was wrapped with aluminium foil to prevent light oxidation and incubated in a laboratory oven at 50°C (EWP) for either 1 or 3 days. BSA was incubated at 40°C. Native or dry heated samples were weighed and dissolved in distilled water by stirring at room temperature for at least 2h; 1M HCl or 1 M NaOH solution was used to adjust the pH of the protein solutions to the desired pHs (pH3- 8 ±0.05).

Insoluble particles were present in EWP solution and were removed by centrifugation (17,000g, 40 min, 4°C; Beckman UK). An initial concentration 5% of egg albumin powder corresponds to a final concentration of 4.75% egg albumin in the supernatant post centrifugation (MS). This calculation was based on the dry matter of the supernatant and that of the initial protein powder mass, both obtained by heating sample in the laboratory oven at 105°C for 24h.

$$MS = \frac{5\ g\ of\ egg\ albumen\ \ as\ \ purshased \times dry\ matter\ of\ the\ supernatant}{Dry\ matter\ of\ 5\ g\ of\ egg\ albumen\ powder} \quad \text{Eq. 3-2}$$

The protein solution (50 mL) was placed in a jacketed vessel (250 mL) and the ultrasound horn was positioned at the air–solution interface. The solution was sonicated at 20 kHz, 50% amplitude for 3 min whilst sparging with oxygen or air. The air (laboratory compressed air) was supplied at a flow rate between 30 and 60 cm^3/min. Oxygen was used only for the initial work on testing the suitability of alternative proteins (with reference to hydrophobins) for the production of AFEs. The production of AFEs stabilised by these proteins was based on method developed by Grinstaff and Suslick (1991) for imaging contrast agents. They postulated that gas filled microspheres were formed by a combination of two acoustic phenomena (emulsification and cavitation) followed by cross-linking. Firstly, ultrasonic emulsification creates the microscopic dispersion of air into the protein solution necessary to form the shape of the microsphere shell and secondly, a superoxide (generated by sonolysis of water in the presence of oxygen) creates inter-protein disulphide bond that cross-link the protein shell (Figure 3-4). It is also worth mentioning that the position of the ultrasound horn is very important, and the horn had to be placed precisely at the interface between the air and the protein solution (see Chapter 7). The quantity of energy transferred into the system was estimated according to the equation:

$$P = m \times C_P \times \frac{d(T)}{d(t)}\ (t = 0) \quad \text{Eq. 3-3}$$

Where P is the power (Watt), m is mass of water (50 g), C_P is the specific heat of water (4.184 J/K/g) and $\frac{d(T)}{d(t)}\ (t = 0)$ is the derivative of the equation of the polynomial regression of the curve of temperature versus sonication time (t), for t equal zero second.

The acoustic intensity (I) was calculated as follows:

$$I = \frac{P}{S} = \frac{P}{r^2\pi} \quad \text{Eq. 3-4}$$

Where P, from Eq.3-3, is the power (Watt); S and r are the surface area and the radius of the tip of the probe, respectively.

The initial temperature of the protein solution was selected to be below but close to the denaturation temperature of the protein. However, because HFBII is stable to temperature for up to 80-90°C and its self-association is temperature dependent (Torkkeli *et al.*, 2002; Askolin, 2006), the protein extract was sonicated at a test series of 25, 45, 55 and 70°C. Likewise EWP-AFE was prepared at 50°C, 60°C and 70°C. The initial temperatures rose by 5 °C during sonication. The air volume fraction (Φ) was measured after 2.5 hours, to allow all the larger unstable bubbles and foam to disappear, and was approximately 25- 40% for all trials. This was calculated using the following equation:

$$\Phi = \frac{Vt - Vi}{Vt} \times 100 \quad \text{Eq. 3-5}$$

Where Vt is the total volume of the suspension after sonication and Vi the volume of the protein solution before sonication.

(a)

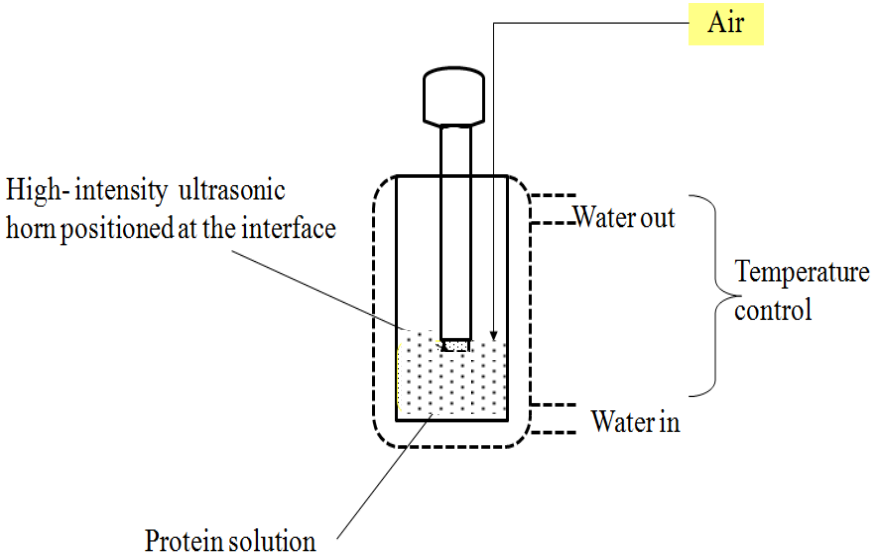

(b)

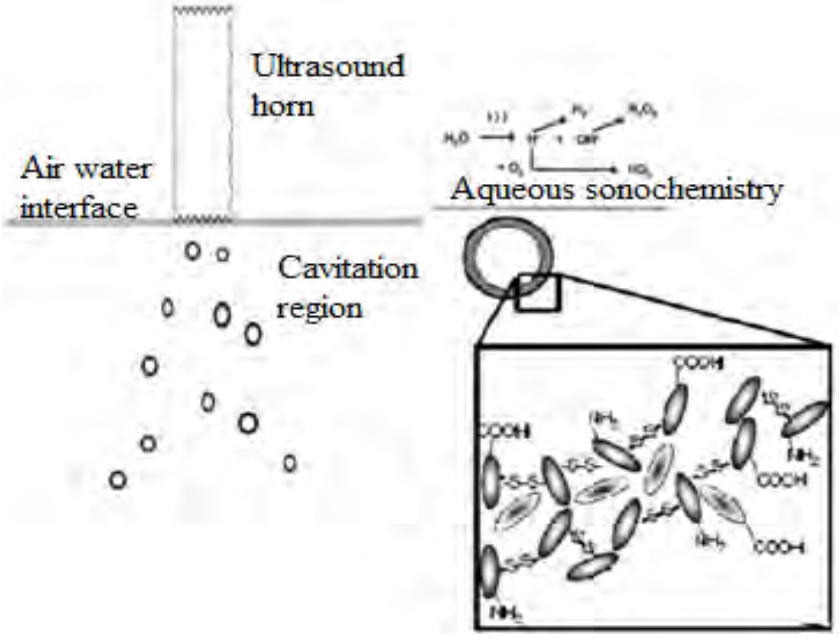

(c)

Figure 3-4. (a), high intensity ultrasonic probe used for the production of AFEs; (b), schematic of the AFEs production system. Air is emulsified as a micrometre-sized dispersion into the aqueous protein solution. The vortex created by the radiation force maintains the probe at the air/protein solution interface; the exact sequence of events could be obtained from the observation of the air-protein solution interface using, for example, a high-speed camera. Proteins adsorbed at the surface of air cells are held together by inter-protein disulphide bonds from cysteine oxidation. Cysteines are oxidised by superoxides generated by the sonolysis of water in the presence of oxygen (see (c)).
(c), mechanism underpinned AFEs formation. The schematic representation of the chemical effect of cavitation is reproduced from Suslick *et al.* (1999).

3.3.3. Productions of oil/water emulsions (O/W)

O/W emulsions were constructed either for the production of triphasic A/O/W emulsions (see Chapter 5) or for testing the emulsification efficiency or behaviour of the genetically modified hydrophobins H*proteins (see Chapter 6).

- *O/W emulsions used for the construction of triphasic A/O/W emulsions*

O/W emulsions were stabilised with 0.5% Tween 60 (emulsion A) or 1 % whey proteins isolate (WPI) (emulsion B).

Emulsion A was formulated with 20 wt % sunflower oil (bought at a local market) and 0.2 wt % Iota carrageenan. Carrageenan powder was added to the water phase and stirred continuously at 60 °C until totally dispersed. The solution was then cooled to room temperature before adding the Tween 60. The resulting solution was mixed with the oil phase using a Silverson high shear mixer fitted with a workhead with fine perforation at 6000 rpm for 4 min. This mixture was passed through a high-pressure homogeniser at 70 bar (FT9 homogeniser, Armfield, UK, Figure 3-5a) four times.

Emulsion B contained 0.2 % xanthan gum as a stabiliser/ thickening agent and 40% sunflower oil. The emulsion was prepared by slowly mixing oil into a WPI solution using a Silverson high shear mixer at 6000 rpm for 30 s followed by addition of xanthan solution and blending for 2 min. This mixture was passed through a high-pressure homogeniser at 35 bar four times. The stock solutions of xanthan (2 % w/v) and WPI (4 % w/v) were prepared by dissolving the weighed quantities of WPI or xanthan powders into distilled water at room temperature. This was achieved by stiring the mixture (overnight) using a mechanical mixer for xanthan or with a magnetic stirrer (four hours) for WPI. WPI stock solution was diluted with a given volume

of distilled water then added to the sunflower oil to obtain an emulsion with 40 % v/v sunflower oil, 1 wt % WPI and 0.2 wt% xanthan. It is important to note that emulsions made in these conditions but at 70 bar resulting in W/O emulsion instead, presumably due to the exposure of more hydrophobic amino acids.

- *O/W emulsions constructed for assessing the contribution of air cells to the perception of fat related sensory attributes.*

A 28% O/W was constructed to have a similar phase volume to the 28% triphasic emulsion and was intended to exhibit a poly-dispersed size range similar to the combined air and oil phases in the 28% triphasic emulsion. The O/W emulsion was constructed as follows: 28 wt% sunflower oil, 0.2 wt% carrageenan and 0.5 wt% Tween 60 was prepared using a Silverson mixer fitted with a large mesh head (6000 rpm for 7 min); 90 ml of this was mixed with 10ml of a similar emulsion that had passed through the homogeniser four times, the mixed system was then blended in the Silverson at 3000 rpm for 7 min.

- *Preparation of O/W emulsions for assessing the emulsification efficiency and behaviour of H*proteins*

Several emulsions with 10, 15 and 20% sunflower oil phase volumes were made with a high intensity ultrasound, high pressure homogeniser, high shear mixer and cross-flow membrane filtration. Hydrophobins H*Protein A or H*Protein B solutions (0.4% w/v) were prepared by dispersing the necessary quantity of protein in water distilled at room temperature using a laboratory magnetic stirrer. Emulsions were constructed by mixing the oil phase and the protein solution using Silverson mixer at 6000 rpm for 7 minutes. Ultrasound emulsification was performed by positioning the ultrasound horn (VCX 750, Sonic and Materials Inc, US) at the oil/water interface and by sonicating the two phase system in a beaker for three minutes.

Emulsions made with the high pressure homogeniser were obtained by passing the mixture of oil and the water phase through the valve of the homogeniser 35 bar four times as in the case of emulsion made with WPI. For membrane emulsification, a Shirasu-porous-glass (SPG) membrane (SPG Technologies, Japan) with a mean pore size of 2.8 µm was mounted on a cross-flow system (Figure 3-5). The continuous phase was flowed outside the membrane by means of a gear pump while the dispersed phase circulated inside the membrane and was forced out the membrane pores by a compressed air. Pressures were 20 kP and 15kP for dispersed and continuous phases, respectively, giving a transmembrane pressure of 5kP. Other membrane emulsification conditions such as high transmenbrane pressure and lower pore membrane pore size were tested before choosing the above conditions.

(a) (b)

Figure 3-5. High pressure homogeniser (a) and cross-flow membrane emulsification set up (b).

3.3.4. Productions of tri-phasic air/oil/water (A/O/W) emulsions

Triphasic A/O/W emulsions with up to 65 % phase volume of air were constructed by diluting either the O/W emulsion A or emulsion B (as described above) with a given volume of a concentrated AFE. The mixture was then blended with the Silverson mixer at 3000 rpm for seven minutes to make well-mixed tri-phasic emulsions.

3.4. Characterisation of emulsions

3.4.1. Microstructure of emulsions

The microstructure of AFE, O/W and A/O/W emulsions was examined using: light microscopy (Polyvar 2, Reichert-Jung, Germany), confocal scanning microscopy (Leica TCS SPE mounted on a Leica Model DM 2500 microscope base), standard high vacuum SEM (Jeol, JSM/6060LV), environmental scanning electron microscopy in cryo and wet modes (ESEM) (XL30FEG Cryo-SEM, Philips, UK) and transmission electronic microscopy (TEM, JEOL JEM-2100 LaB6). A drop (≈100 µl) of the emulsion neat or diluted was placed on the microscope slide and a cover slip applied. The structures of emulsions were then observed using either brightfield or phase contrast modes of illumination.

For confocal imaging Nile blue and Rhodamine B were used to stain proteins and Nile red to stain the oil phase. A stock solution of 0.01% (wt/wt) of each dye was prepared at room temperature by mixing a given quantity of Rhodamine B in distilled water or Nile blue and Nile red in ethanol. The solution was stored in the dark until used. 4 ml of AFE were thoroughly mixed with a 20 µl of the Rhodamine B or Nile blue and 100 µl (approximately) of the mixture was then placed on a microscope slide. The slide was covered with a welled

cover slip (CoverWell™ Imaging Chamber, PCI-A-1.0, GRACE, BIO-LABS) and observed with a 63X oil immersion objective lens. The triphasic A/O/W emulsion was observed using the same conditions as above except that the sample (four mL) was mixed with 10 µL of Nile blue and 10 µl of Nile Red stock solutions. All mixtures were prepared just before the microscopic observations. The samples were excited at 488 nm (Rhodamine B and Nile blue) and the 635 nm for Nile red. The emission was recorded at 10 nm above the excitation wavelength. Images were recorded at a resolution of 512× 512 pixels and processed using the built in Leica image analysis software.

Samples for standard high vacuum SEM were air-dried by leaving them overnight or by leaving them for two days in a fume cupboard. Samples were then coated with gold and examined at 10 or 20kV. Some samples were fractured before coating. Cryo-SEM samples were placed on a sample holder and plunged into nitrogen slush. The frozen samples were fractured, etched for two minutes and coated with gold for one minute. Examination was at two kVacceleration. Measurements were made on both fractured and unfractured samples. Non fractured samples were etched in the SEM chamber for four minutes. For ESEM, the samples were placed on a sample holder inside the microscope and examined at 20kV. The pressure and the temperature inside the microscope were 3 Torr and 2°C, respectively.

TEM images of air cells cross-sections were obtained as follows: samples were fixed with 2.5% gluteraldehyde for 12 h in order to cross-link protein coats prior to embedding in acrylic resin. It was found that air cells were destroyed if 50% ethanol was added to the AFE for dehydration. Embedded samples were cut in ultra thin sections (50-150 nm) and stained with uranyl acetate and lead citrate.

3.4.2. Particle size analysis

A particle size analyser (Mastersizer Hydro 2000SM, Malvern Instrument Ltd, UK) was used to determine the size and size distribution of air cells and oil droplets. However, because optical properties of AFEs were not known, different measurement conditions (optical properties and pum/stirrer speeds) were tested and results were then calibrated against the size distributions from light microscopy. This screening allowed the selection of the following optical properties: refractive index 1.450, 1.469 and 1.456 absorption; 0.01, 0 and 0 for AFE, O/W and A/O/W emulsions respectively.

The mechanism of measurement for the Mastersizer 2000 is based on Mie scattering theory (Malvern Instrument's technical paper), which assumes that particle is spherical and that the refractive indices of the material, the medium and the absorption function of the refractive index are known or can be estimated accurately. It measures particle size in the range of 0.02 to 2000 μm. The sample was diluted with distilled water in the dispersion unit with its stirrer and pump. The variable pump/stirrer speed available allows a wide range of particle sizes and densities to be suspended and circulated around the cell where particles are illuminated by the laser. The light diffracted by particles is detected and transformed in size based on the Mie theory. Also the measurement was carried out at pump/stirrer speed varying 500 to 3000 rpm in order to find out if bubbles were destroyed during the measurement. Some air cells were not pump through the measurement cell but remained dispersed inside the sample presentation chamber at pump/stirrer speed below 1000 rpm. However, higher speeds led to the destruction of air cells. The particle size decreased with the increased speed and reached a first plateau around 1500- 2000 rpm. This resulted in the selection of 1500 rpm which was used for all measurements.

AFEs were also characterised with a Coulter Multisizer II to obtain a particle size distribution. The Coulter Multisizer II analyzer is a particle size analyzer which employs the Coulter electrical impedance method to provide a particle size distribution analysis within the overall range 0.4 um to 1200 μm depending on the diameter of the aperture used. Results are displayed graphically as a percentage of channel content, which can be selected to represent volume (weight), number (population) or surface area, in either differential or cumulative form. However the one available to this project was set with a 75 microns aperture for a sisze range of 1 to 100 μm. Only this population data could be obtained but give a rough idea of size distributions. The turbidity was determined at 450 nm against water as a blank for protein solution before sonication and after sonication. Any solution was always diluted to the absorbance below one unit. The net turbidity was compared to the data obtained with coulter Multisizer II. The optical density or turbidity (τ), of an emulsion containing monodispersed particles is a function of particle concentration and size and can be given by the relationship shown in Eq. 3-4 (Reddy and Fogler, 1981):

$$\tau = \frac{\ln(\frac{I_0}{I})}{l} = \kappa \pi a^2 N \qquad \text{Eq. 3-6}$$

Where I_0 and I are the intensity of the incident and transmitted light respectively; a is the particle radius; l is the scattering path length; N is the concentration of particles; *K* is the total scattering coefficient.

3.4.3. Evaluation of emulsions stability

3.4.3.1. Total air phase volume as a function of time

Seven mL of AFE or A/O/W emulsions were transferred into tubes and the emulsion height and total volume were measured against time according the method of Cox *et al.* (2009).

3.4.3.2. Measurement of size and size distribution as a function of time

The stability of emulsions was evaluated over time, by measuring the change in size distribution with time using the Mastersizer and microscope as described above. Emulsions were gently mixed before sampling as they are very heterogenic systems, and care was taken to ensure that AFE emulsions, which can separate into two phases within a short period of time (upper layer rich in air cells with larger particle size and the lower layer, poor in air cells) and contains smaller air cells) were sampled correctly.

3.4.3.3. Stability of AFEs to high temperature/pressure and mild vacuum

In order to assess the stability of AFEs to processing conditions such as high temperature/pressure and pumping, AFEs were subjected to a sterilisation test using an autoclave (Denley Model Majestic, BA 853), at 121°C/1 bar for 15 min and to conditions of mild vacuum test. For the latter test, 20 mL of AFEs were placed in a Büchner flask which and closed with a rubber bung. The vacuum inside the flask was created by a water aspirator connected to an empty Büchner flask, before that containing the sample, in order to prevent the sucking back of water from the aspirator into the sample (see Figure 3-6).

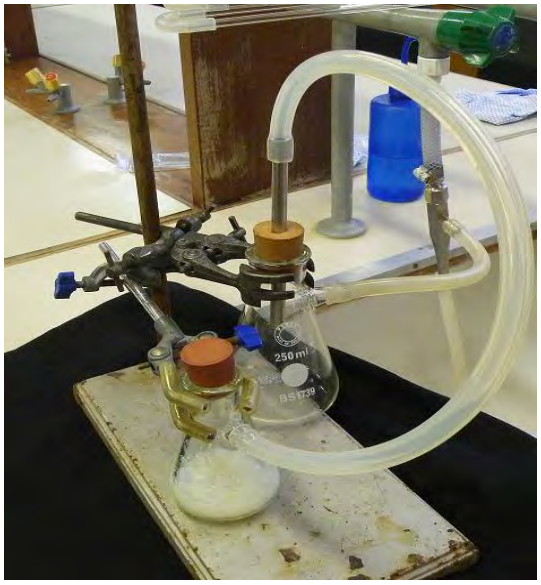

Figure 3-6. Equipment used to assess the effect of vacuum treatment upon AFEs. The size of air cells within the AFE was measured before and after treatment.

3.4.3.4. Evaluation of oxidation stability of emulsions

The oxidative deterioration of emulsions was assessed by measuring the concentration of primary (hydroperoxides) and secondary (carbonyl) oxidation products formed during storage at 40°C for up to 8 days in a laboratory oven. In emulsion based food products, such as mayonnaise, hydroperoxides concentration expressed as peroxide value (PV) is a useful means for predicting the onset of the rancidity (lipid oxidation) and the secondary oxidation products also provide information about the degree of rancidity (Depree and Savage, 2001). Freshly made emulsions (5 mL) were stored in 15 mL glass containers. The containers were then sealed, covered with aluminium foil and allowed to potentially oxidise at 40°C. Samples were removed periodically for hydroperoxides, p-anasidine value and pH determination.

Hydroperoxide concentrations were determined from triplicate samples using a method based on hydroperoxides oxidation of ferrous ions (Fe^{2+}) to ferric ions (Fe^{3+}), which are then complexed by thiocyanate. Lipid hydroperoxides in emulsions were extracted by mixing 0.3

mL of an emulsion with 1.5 mL of isooctane/2-propanol (3:1 v/v) in a 2 mL ependolf for 10 second. This was followed by benchtop centrifugation for 5 min at 1000 rpm. 0.20 mL of the clear upper layer was collected and mixed with 2.8 mL of methanol/1-butanol (2:1 v/v), 30 µL of thiocyanate/Fe^{2+} solution. The reaction was allowed to take place for 20 min and the absorbance was measured at 510 nm against a blank that contained all reagents and isooctane/2-propanol in lieu of the sample, using a spectrophotometer (Scientific Laboratory Supplies Ltd, UK). The thiocyanate/ Fe^{2+} solution was prepared in two steps as follows: (1) a solution of 30% of ammonium thiocyanate dissolved in water was prepared; (2) Barium chloride dihydrate was dissolved in 0.4M HCl to form a 0.8% wt/v solution; a given volume of this solution was then mixed with an equal volume of 1% ferrous sulphate heptahydrate dissolved in distilled water followed by centrifugation for 10 min at 4000rpm; a given volume of the clear upper layer, a solution of Fe (II) Chloride ($FeCl_2$) was mixed with an equal volume of solution (1) to form a solution of thiocyanate/Fe^{2+} (Katsuda *et al.*, 2008). The concentration of hydroperoxides was calculated from a cumene hydroperoxide standard curve (Figure 3-7a). Standard cumene hydroperoxide was weighed in a volumetric flask and dissolved in mixture of isooctane/2-propanol (3:1 v/v) to reach a concentration of 1mg/ml. A series of dilution was then made from this stock and the concentration of hydroperoxide was determined as above. Standard hydroperoxide, aldehyde, and P-anasidine were purchased from Sigma-Aldrich Company, UK. All other reagents and solvents used for assessing the oxidation stability were provided by Fisher Scientific, UK.

Secondary products of oxidation were measured according to the AOCS method (AOCS 1997). This method based on the reactivity of aldehydes with p-anisidine in acetic acid, resulting in a complex that absorbs at 350 nm. One mL of emulsion was mixed with 24 mL isoactane by means of a vortex mixer followed by centrifugation 20 min at 4000 rpm. 5 mL

of the top layer were pipeted into glass tubes. One mL of p-anisidine reagent (0.25g dissolved in 100 mL of glacial acetic) was added to each tube, and the sample was mixed for three seconds. After 10 min incubation the absorbance of the sample was measured at 350 nm. The absorbance of the extract without p-anisidine reagent was also measured. Results were express in terms of P-Anisidine value (P-AnV), calculated using the following:

$$P - AnV = 25 \times \left(\frac{1.2 \times As - Ab}{m}\right) \quad \text{Eq. 3-7}$$

Where As is the absorbance of the extract after reaction with p-anisidine reagent; Ab is the absorbance of the extract without p-anisidine reagent; m is the mass of the emulsion used for carbonyl extraction (g).

Standard aldehydes, trans, trans-2, 4-decadienal and trans-2-Decenal were used to confirm the accuracy of the method. These aldehydes are decomposition products of oxidised linoleic (C18:2) and oleic (C18:1) acids which constitute 59.1 and 30.4 % of total fatty acid of sunflower oil respectively (Muik *et al.*, 2005). Standard aldehydes were weighed in a volumetric flask and dissolved in isooctane to attain concentration of one mg/mL. A series of dilution was then made from this stock and the P-AnV was determined as previously described. A strong correlation between the concentration of these aldehydes and the obtained AnV for a calibration curve was obtained (R^2 = 0.9960, Figure 3-7b).

The total oxidation was calculated using the formula: $TOTOX = 2\,(PV) + AnV$ (Osborn and Akoh, 2004; Maduko *et al.*, 2008).

In order to eliminate the potential effect of the droplet size on oxidation stability of emulsion, PV and AnV were also normalised to the total surface area of the emulsion by dividing by the latter.

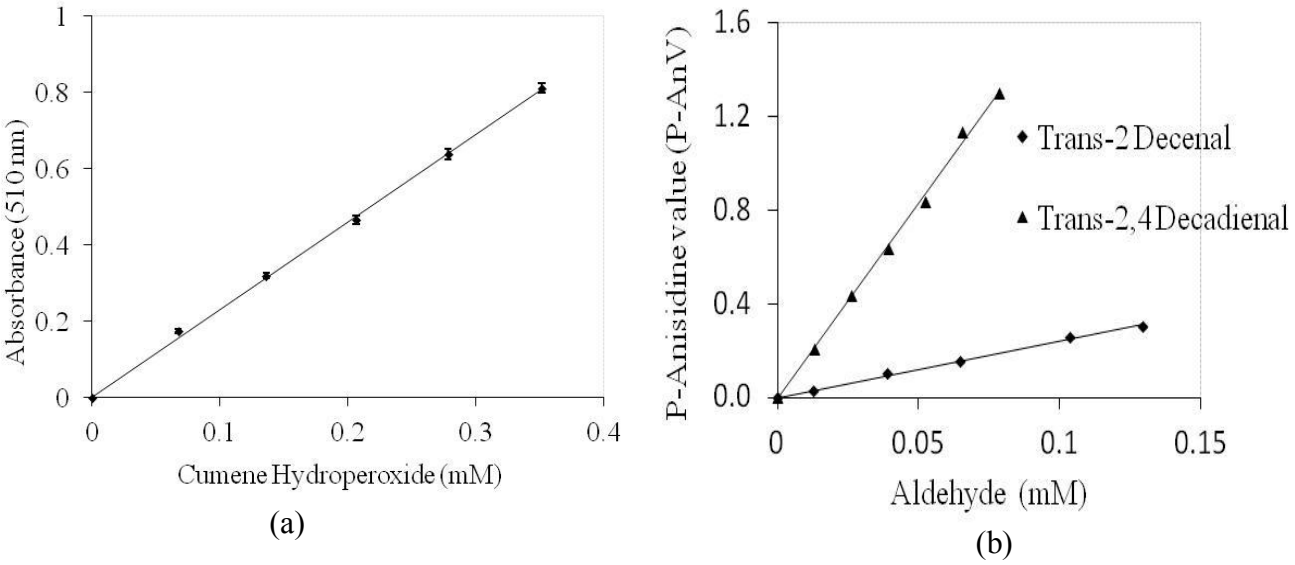

Figure 3-7. Example of standard curve of lipid oxidation products.
(a) is Cumene Hydroperoxide and (b) is aldehydes. R^2 value is at least 0.996 for each curve.

3.4.3.5. Investigation of the formation of hydrophobin-lipid oxidations products complexes

Two genetically modified hydrophobins supplied by BASF (Germany), were used in this study. H*proteins were incubated, at 40°C for 45 h, with lipid oxidation products used for as standards for lipid oxidation analysis (Cumene hydroperoxide, Trans, trans-2, 4-decadienal and Trans-2-decenal) and any modifications of the protein were ascertained using a combination of fluorescence spectroscopy and liquid chromatography-electrospray tandem mass coupled with mass spectrometry (LC-MS/MS). Details about the experimental set up can be found in Appendix 9-5.

3.5. Instrumental probing of the mouth-feel

The mouth-feel of samples was assessed by measuring their viscosity and tribolological or lubrication behaviour.

3.5.1. Viscosity measurement

The viscosity of samples was measured with a Bohlin Gemini HR nano stress-controlled rheometer (Malvern Instrument Ltd, UK) under control strain mode using stainless steel cone and plates. The cone diameter was 40 mm and the cone angle 4°. Samples were sheared from 0.1-200 s^{-1}. Some samples were sheared only from 0.1-100 s^{-1}.

3.5.2. Tribological study

The lubrication behaviour of samples was evaluated by measuring the friction between a stainless steel ball (3/4 inch, AISI 440, PCS Instruments Ltd., UK) and a silicone disk (46 mm diameter, Samco, UK) in relative motion with the sample acting as lubricant. The tribo-pair was mounted on a mini traction machine (MTM; PCS Instruments Ltd., UK) with the ball loaded against the face of the disc and. Both geometries are independently driven by separate motors to produce a sliding/rolling contact, according to the test profile defined by the user (Figure 3-8). The MTM is a computer controlled instrument that provides a fully automated traction mapping of lubricants under boundary, mixed and hydrodynamic lubrication regime The ratio of the sliding speed to the mean rolling speed at the contact (SRR) expressed as a percentage was set at 50%. This is calculated as follows:

$$SRR = \frac{U_1 - U_2}{U}$$ Eq. 3-8

Where U_1 and U_2 are the disc and ball speeds respectively. U is the average speed of the disc and the ball (the entrainment speed). The mixed rolling–sliding contact was used to emulate the contact tongue-palate as the latter is believed to be a mixed rolling-sliding one (de Vicente *et al.*, 2005). The frictional or tangential force (F) between the ball and disc measured by a force transducer is converted into a friction coefficient (μ) based on the applied load (W). The chosen load was 3 N as it yielded frictional data with correlations to sensory attributes generated by a panel (Malone *et al.*, 2003).

$$\mu = \frac{F}{W}$$ Eq. 3-9

The roughness of the tribo-pair was characterised by interferometric measurements of samples using a MicroXAM interferometer (Scantron, UK), operating using a white light source. Samples were imaged using a 20X objective lens. Scanning Probe Image Processor software (Image Metrology, Denmark) was employed for the analysis of acquired images, yielding an average roughness (S_a) and root-mean-square roughness values for surface roughness. The disk was rough with S_a and S_q or 598 ± 67 nm and 804 ± 115 nm respectively. The smooth surface of the ball had a S_a of 7 nm and S_q of 12 nm.

All tests were carried out at 20°C (±1°C) with entrainment speeds of 1 to 1000 mm/s and 30 data points chosen logarithmically. In order to study the time dependency properties of each sample, tribological tests were performed under the above-mentioned conditions three times, and each cycle was started without unloading the ball. The idle speed of ball was set at 1mm/s. At least three measurements per sample were carried out. After each test the ball was

cleaned with detergent, followed by rinsing with distilled water and finally cleaned with ethanol, rinsed with distilled water and air dried before being reused. A new silicon disc was used for each test experiment. Discs were cut freshly from a silicon sheet then gently cleaned following the same cleaning procedure as for the ball.

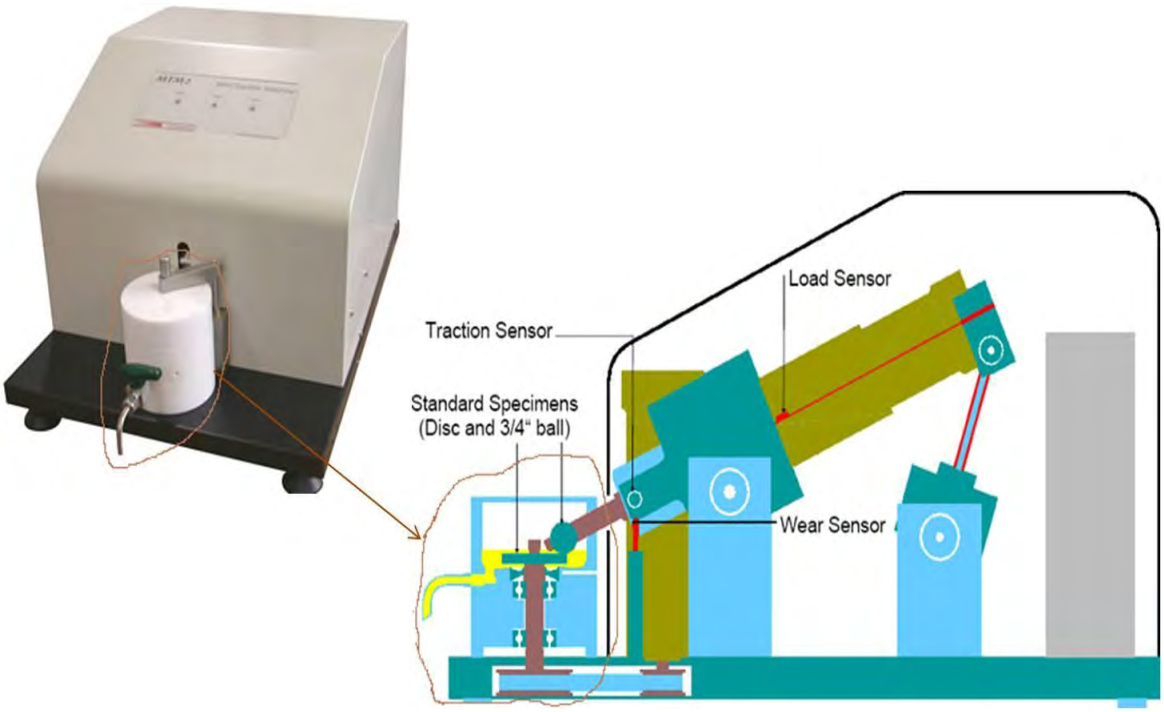

Figure 3-8. Schematic of the MTM Tribometer (PCS Instruments Ltd., UK).

3.6. Other analyses

3.6.1. FT-IR spectroscopy

Fourier Transform Infrared spectrometry (FTIR) was used as a qualitative method to identify the presence of hydrophobins (via the presence of disulfide bonds). 2 mg of freeze dried hydrophobin rich extract were ground with 300 mg of KBr until a fine, homogenous powder was produced. These mixtures were then pressed between pellets at 10 tons, and the resulting discs were tested with a Nicolet 380 FT-IR spectrometer (Thermo Fisher Scientific, USA). All spectra

were recorded from the accumulation of 16 scans in 4000–400 cm^{-1} range with a 4 cm^{-1} resolution. A measurement without any sample in the beam was used as a background. The FT-IR spectrum of each sample was obtained by subtracting its spectrum from the background.

3.6.2. Quantification of proteins by Bradford method

Total protein concentration in samples including the culture medium was determined by the Bradford method, based upon the binding of a dye (Coomassie Brilliant Blue G250) to basic and acid groups of proteins. The formation of the protein-dye complex causes a change in the light absorption spectrum of the dye, which is used to determine the protein concentration by a spectrophotometer at 595 nm. A calibration curve was prepared with dry bovine serum albumin dissolved in water. Figure 3-9 is an example of the standard curve obtained.

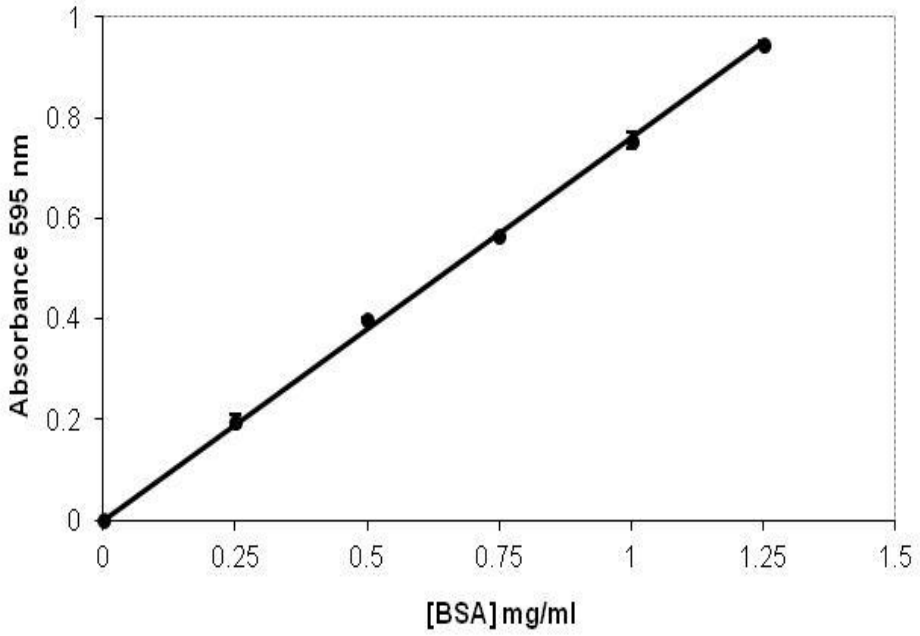

Figure 3-9. Example of calibration curve obtained from the measurement of different concentrations of BSA using the Bradford method. R^2 value is 0.999.

3.6.3. Glucose and lactose analysis

Glucose and lactose consumption during fermentation were determined by high performance chromatography (HPLC) with Aminex column HPX-87H (Bio-Rad, UK) and refractive index (RI) detection.

Culture media from 1, 2, 3 4, 5 and 6 days cultures were filtered through a 0.22 µm filter. The filtrate was injected (20 µL) into the HPLC system and eluted with an isocratic mobile phase of 0.05 M sulfuric acid at 0.6mL/min. Column temperature was maintained at 50°C. Sugar concentrations were calculated from the integrated peaks using a calibration curve. Calibration curves (Figure 3-10) were obtained by injecting pure glucose or lactose dissolved in water.

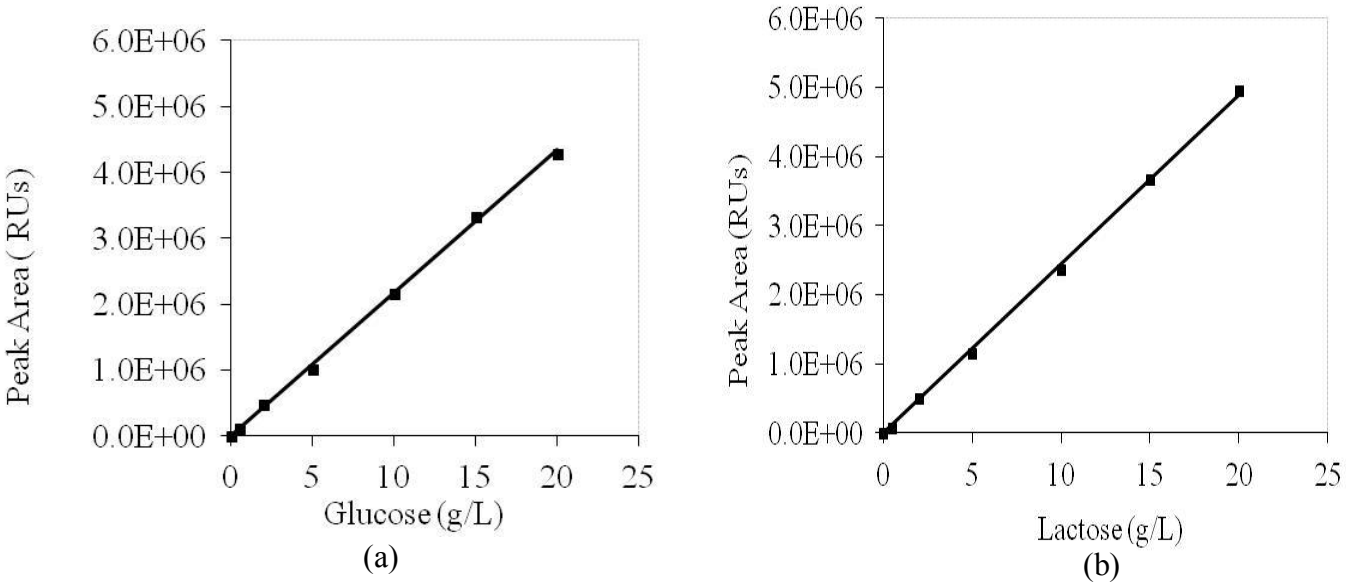

Figure 3-10. Example of calibration curve showing the peak Area (RUs) as a function of glucose (a) and lactose (b) concentration. R^2 value is at least 0.998 for each curve.

3.6.4. Electrophoretic mobility and estimation of protein's isoelectric point

The electrophoretic mobility (the velocity of a particle in an electric field) of H*proteins in solution was measured using a Zetamaster (Malvern Instruments, UK). The technique measures the mobility of particles by Laser Doppler Electrophoresis. The general theoretical background is that, charged particles exposed to a constant electric field migrate with constant velocity if the electrostatic force and hydrodynamic friction cancel each other. The resulting electrophoretic mobility (U_E) is:

$$U_E = \frac{z}{6\pi R_H \eta} \quad \text{Eq. 3-10}$$

Where Z is the elementary charges per particle, R_H is the hydrodynamic radius and η is the viscosity of the solvent.

0.1 wt % protein solution was prepared and the pH adjusted with 0.5M of hydrochloric acid or sodium hydroxide HCl in order to form a range of protein solutions from pH 3 to pH 9. Each solution was injected into the electrophoresis cell and measurements were performed at 25 °C. The zeta potential (z) can be calculated from the electrophoretic mobility U_E using the Henry equation.

$$U_E = \frac{2\varepsilon z f(ka)}{3\eta} \quad \text{Eq. 3-11}$$

Where ε, the dielectric is constant; $f(ka)$, the Henry's function which is generally considered as equal to 1.5 for moderate concentrated electrolyte in aqueous media (Kaszuba *et al.* 2010); η, the viscosity.

3.6.5. Surface and interfacial measurement

Surface and interface tension were measured with a tensiometer K100 or a goniometer EasyDrop (Kruss, Germany). Although initial experiments were carried out with the tensiometer using a Wilhelmy plate or the Du Noüy Ring, it was found that hydrophonbins rapidly migrate to the air/protein solution interface, coated the plate or the ring which made it difficult the measurement and provide less reproducible data. The very beginning of the adsorption kinetics could not be recorded due to the time needed to set up the measurement (see Chapter 4). Moreover, it has been reported a difference in values of surface tension measured by the ring method, about 10 mN/m higher than those obtained with the pendent drop (Wüstneck *et al.*, 1996). This was thought to be caused by the surface stretching as the ring is pulling out from the solution and was advised not to consider data from ring method for further calculations (Wüstneck *et al.*, 1996). The pendent drop technique proved better and was used to characterise the adsorption behaviour of new fusion hydrophobins. This technique is based on the determination and analysis of the drop profile of a liquid suspended in air (e.g., solution/air) or another liquid (e.g. solution/oil) at hydromechanical equilibrium. The interfacial tension is inferred from the analysis of a video image of a liquid drop and compared with the theoretical profiles calculated from the Laplace equation using Drop Shape Analysis (DSA) software (Kruss). The aqueous solution containing the surface active molecules were held in the syringe forming a drop at the tip whereas the oil phase was kept in a glass cuvette and the interface tension was automatic recorded over time using a Tracker mode. The droplet volume was set at 20 mL and the syringe needle (Hamilton Bonaduz AG, Switzerland) diameter was 1.820 mm.

The dynamic surface tension or interfacial tension versus time $\gamma(t)$ was described by the empirical equation of Hua-Rosen (Hua and Rosen, 1991).

$$\gamma(t) = \gamma_m + \frac{\gamma_0 - \gamma_m}{1 + (t/t^*)^n} \quad \text{Eq. 3-12}$$

Where $\gamma(t)$, γ_0 and γ_m are the surface tensions at any time, at liquid phase interface without surfactant and at mesoequilibrium (where the surface tension shows only a minor change with time), respectively. t* is a time constant equal to 50% of the time to attain the initial mesoequilibrum value (γ_m) and n the dimensionless exponent.

n, t*, γ_m were derived from the time-dependent surface/interfacial tension curve by fitting experimental data with the Hua-Rosen's equation using Sigma-plot software. The maximum reduction rate (V_{max}) of γ was obtained by differentiating equation (Eq.3.12) with respect to t and substituting t for t*:

$$V_{max} = \frac{n(\gamma_0 - \gamma_m)}{4t^*} = -\left(d\gamma_t/dt\right)_{max} \quad \text{Eq. 3-13}$$

3.7. Conclusion

Materials, techniques and the experimental procedures used throughout this work have been presented. Methods used for the extraction of hydrophobins from mushrooms seem tedious whereas the foam fractionation method used for the extraction of Class II hydrophobin is simple and could be used for industrial separation of hydrophobins present in the culture medium. Air filled emulsions were made using an ultrasonic processor devise with the horn positioned at the air/protein solution interface. It is postulated (in this work) that the vortex

created by the radiation force maintains the probe at the air/protein solution interface during AFE production. However, the exact sequence of events would have to be confirmed by observation of the air-protein solution interface using, for example, a high-speed camera.

CHAPTER 4

PRODUCTION AND EXTRACTION OF HYDROPHOBINS

4.1. Introduction

Hydrophobins are a family of low molecular weight surface active proteins (ca. 7-24 kDa) with a conserved spacing of eight cysteine residues that form four disulfide bonds. They are ubiquitous in the fungal kingdom and are present as assembled forms in various biosurfaces of fungus (e.g. spores and fruiting bodies) or are excreted in an aqueous medium during different stages of fungus growth. This chapter deals with the extraction of hydrophobins, based on their solubility properties, as described in section 2.1.2, Chapter 2.

The first part of the chapter investigates whether hydrophobins (generally class I) could be obtained in a reasonable quantity (to allow further uses) from commercially available mushrooms. The second part deals with the production and the extraction of hydrophobins (Class II) from *Trichoderma reisee*.

4.2. From mushrooms to hydrophobins rich extract

Class I hydrophobins were extracted from four different edible mushrooms (White mushroom, Chestnut, Portabella (all three Agaricus spp) and Oyster mushroom (*Pleurotus ostreatus*)) using two steps extraction method. Because it is believed that hydrophobins are present in mushrooms as assembled forms insoluble in most organic solvent and in even 2% hot SDS, but are only soluble in strong acid such as formic acid and TFA, the first step consisted in obtaining SDS insoluble material after the removal of soluble proteins and lipid.

Hydrophobins were then extracted from this dried SDS insoluble and lipid free fraction with a cold TFA. Fourier Transform Infrared Spectrometry (FTIR) was used as a qualitative method to identify the presence of hydrophobins (e.g. presence of disulfide bond). Figure 4-1 shows the FTIR spectra of dried, lipid free SDS insoluble fraction of the four types of mushrooms. Each mushroom extract showed weak bands at 520-540 cm^{-1} which is characteristic of the disulfide bond (Li and Li, 1991;1994).

From examining the relative intensity of the bands, Chestnut mushrooms seem to contain more hydrophobins than the other varieties, whereas the least concentration was found in the white mushrooms. Oyster mushrooms showed slightly higher amount of lipid free, SDS insoluble matter than white mushrooms but both mushrooms yielded similar amount of TFA extract. This may be due to the presence of more insoluble compounds, such as insoluble fibres, in *Pleurotus Ostrearus* mushrooms than in *Agaricus bisporus* variety (Manzi *et al.*, 2001). Although Chestnut and Portabella yielded slightly more hydrophobins rich matter (0.2 g per Kg of fresh mushroom), the overall yield was very low (Table 4-1). Yu *et al.* (2008) had also reported a very low abundance of HGFI (hydrophobin from edible mushroom, *Grifola frondosa*) as the protein could be observed using a Silver staining and hardly seen when using Coomassie brilliant staining.

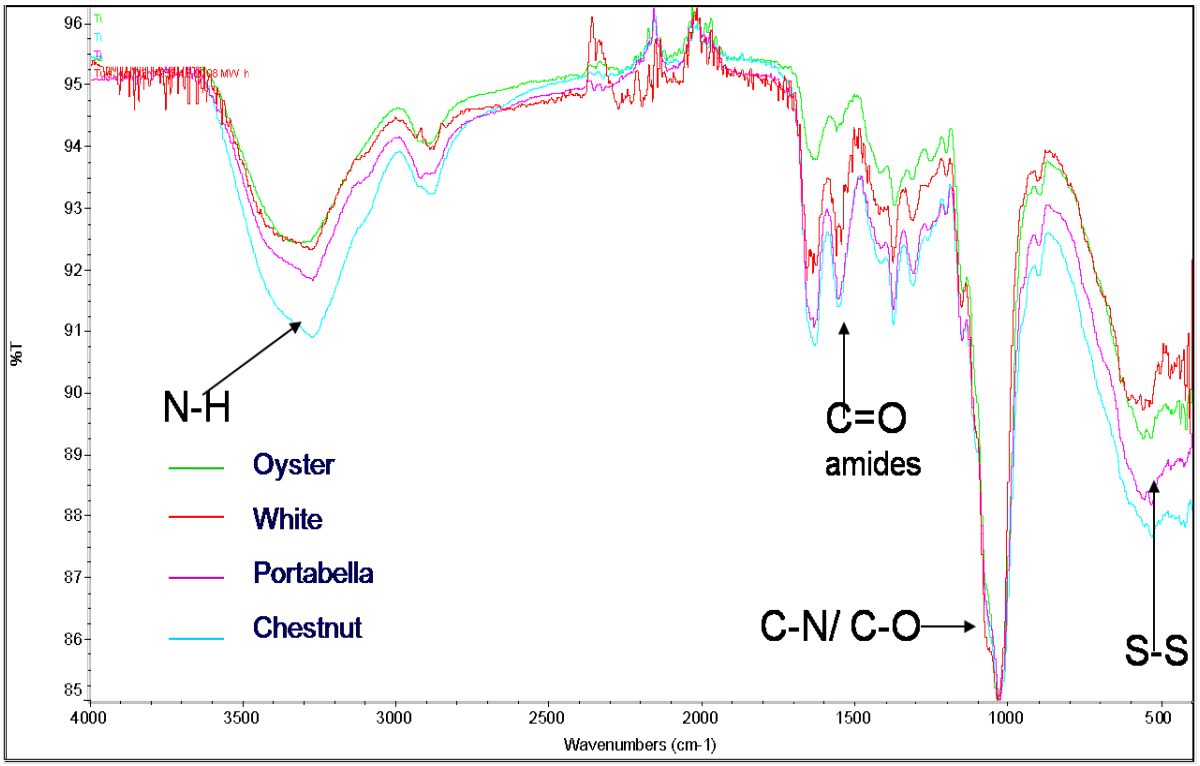

Figure 4-1. FT IR spectra of dried lipid free hot SDS insoluble material from 4 edible mushrooms

Table 4-1. Hydrophobins extraction yield

Mushrooms	Freeze dried Mushrooms (g)	Fresh Mushrooms (g)	Lipid free, SDS insoluble material Yield (%)	Hydrophobin rich material after TFA extraction Yield (%)	Hydrophobin rich material, g/ kg of fresh mushrooms
White	5	61.6	20 ±3	0.11	0.09
Oyster	5	48.8	26 ±2	0.12	0.12
Chestnut	5	45.0	20 ±3	0.17	0.18
Portabella	5	34.8	24 ±2	0.12	0.17

However, it is worth noting that the repeatability of the TFA extraction step was not satisfactory. Indeed, after TFA extraction and its evaporation, the dried extract was not always soluble in water and a highly hydrophobic film could be formed as illustrated by Figure 4-2. It is known that 100% TFA dissolves aggregates of Class I hydrophobins (e.g. Sc3) and that after removal of TFA by evaporation using a stream of gas the hydrophobin monomers are soluble in water, in 0.1 M Tris-HCl, pH 8.0, in 2% SDS buffered with 0.1M Tris, pH 8.0, in 0 to 60% ethanol, in 0 to 50% acetone, and in 0 to 60% acetonitrile (Wosten *et al.*, 1993). The same authors pointed out an instantaneous aggregation of the TFA-treated Sc3 (monomers) into an SDS-insoluble complex when presented at a water-gas interface (e.g. by shaking the protein solution). Therefore, the dried TFA treated monomers in a glass beaker exposed to air, thus, air/ hydrophilic glass interface, may account for the formation of the insoluble film after evaporation of TFA.

The build up of hydrophobic film after the removal of TFA was observed only when attempts were made to extract hydrophobins from hot-SDS insoluble fraction greater than a gram. On the basis of these results, this hydrophobic film formation may be driven by high hydrophobin concentration. It has been demonstrated that the self-association of hydrophobin Sc3 into

rodlets at water-hydrophobic solid interface was promoted by increasing its concentration (300 µg/ml) and by prolonging the incubation time (Scholtmeijer *et al.*, 2009). It was then crucial to carefully control the TFA evaporation step in order to overcome this problem. Moreover, when TFA treated residue was taken up in water without appropriately removing TFA, crystals of TFA were formed in solution and a more basic solution (Ammonia) was required to neutralise the TFA and return the protein solution to the working pH of pH 5.

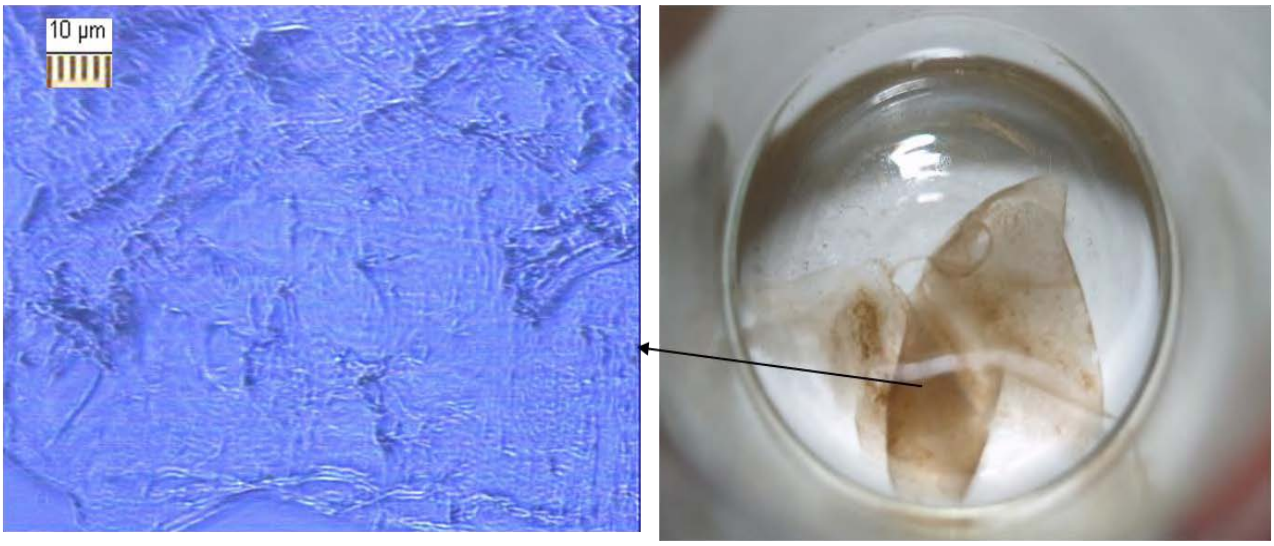

Figure 4-2. Typical hydrophobin film formed after evaporation of TFA. Left, light micrograph of the film; right, photograph of the film.

The surface activity of the hydrophobin extract was determined by making an oil/water emulsion with 20% oil and 80 % water with 0.08 mg/mL of hydrophobins. The protein concentration was determined by Bradford method. The emulsion was made using a Silverson blender (see Chapte 3). Figure 4-3 shows oil droplets (3 µm) stabilised by hydrophobin with an obvious spherical shape. It could be noted that not all the oil droplets were coated, due to a small quantity of protein and a high oil volume fraction in this initial screenning. The properly emulsified phase was stable for the tested period (2 weeks) and this helps provide evidence of the ability of hydrophobins to not only stabilise emulsion but also enable formation of small

droplets 10 ± 7 µm oil droplets have previously been reported for olive oil emulsions made with a pure SC3 using a sonication method (Askolin, 2006; Askolin *et al.*, 2006). However, because of the tediousness of the extraction method, the building up of the protein film after TFA evaporation and the very low extraction yield it was decided to investigate other source of hydrophobins. Hydrophobins produced by submerged fermentation are discussed in the next subsection.

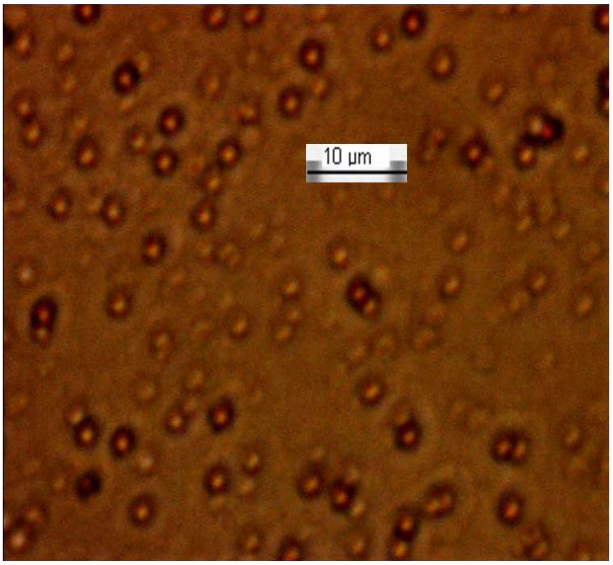

Figure 4-3. Light microscopy of 24 h old oil in water emulsion made with 0.08 mg/mL of TFA-extracted potential hydrophobins.

4.3. *Trichoderma reesei* growth hydrophobins rich extracts

4.3.1. Fungal growth

Trichoderma reesei is known to produce two major hydrophobins (HFBI and HFBII) when grown under different physiological and fermentation conditions. HFBI gene (hfb1) has been

shown to be expressed on glucose and sorbitol based media but not on media containing lactose or polysaccharides such as cellulose, xylan and cellobiose. In contrast the HFBII gene (hfb2) is highly expressed on all these carbon sources but its expression on glucose containing medium is very low. The synthesis of HFBII is also induced by light and by nitrogen and carbon starvation (Nakari-Setälä et al., 1996, 1997). Based on this background, *Trichoderma reesei* QM9414 was cultivated in a series of shake-flask fermentation containing either lactose or glucose based medium. Because it is known that the expression of hydrophobins is regulated by environmental conditions/stresses, lactose or glucose consumption and pH of the growth medium were monitored over time but not adjusted. In the meantime soluble protein formation was evaluated. The biomass was measured only on the last three days of the fermentation.

Figure 4-4a shows that the consumption of glucose was slower than that of lactose during the studied period with an apparent lag phase for the first two days of fermentation. Conversely, lactose was consumed rapidly during the first four days. After this time, the concentration of lactose ($\approx$ 2 g L^{-1}) was relatively constant for the rest of the fermentation (day 4 to day 6) whereas glucose declined to this level on day six of cultivation.

The biomass on 4^{th} day for the lactose-based medium culture was almost the double of that obtained for the glucose-based medium (12.8 g L^{-1} and 6.2 g L^{-1}). But this biomass decreased, and reached a comparable value (4.4 g L^{-1}) to that of glucose containing medium (4.9 g L^{-1}) on 6^{th} day of fermentation. This decrease in biomass may be explained by the loss of matter through respiration of assimilated carbohydrate, hyphal autolysis and changing morphologies from mycelium to spores predominant culture (Ibba *et al.*, 1987).

There was a linear increase in the soluble protein concentration in both glucose and lactose based media (Figure 4-4b). However the lactose containing medium showed a slightly greater protein production rate, which increased after day five to reach 0.12 g L^{-1} by day six as compared to 0.08 g L^{-1} in the glucose based medium at the same time. Also, the colour of the lactose containing media changed and became green at day six probably due to intense sporulation (see agar plate of a week culture in chapter 3, Figure 3-3a) triggered by nutrients depletion. This phenomenon has already been reported by Bailey *et al.* (2002) and would presumably correspond to more synthesis of hydrophobin HFBII as it is involved in sporulation and hydrophobicisation of spores (Askolin, 2006). No change in colour was found in the glucose containing medium, it remained a yellowish colour. The results obtained for glucose containing medium were in accordance with those observed by Askolin (2006).

The pH of both culture media increased at the beginning of the cultivation from pH 4.5 to pH 6.5 at day 1 and day 2 for lactose and glucose based media, respectively. After this time, there was only a minor decrease in pH during the rest of the cultivation period for glucose based medium whereas the lactose containing media showed a considerable decrease in pH, which reached pH 3.4 on day four, before increasing again for the rest of fermentation. This may be due to the production of organic acid during the fungal growth (Ferreira *et al.*, 2009) followed by the utilisation of these organic acids for carbon sources by the fungal due to nutrients depletion. Also, because more proteins were excreted in the medium during the last two days of cultivation the neutralisation effect of proteins might also play a role. The same trend in lactose consumption and pH changes has been previously observed (Bailey *et al.*, 2002) during the cultivation of *Trichoderma reesei,* and again for the production of HFBII. However Bailey *et al.* (2002) reported higher yield in soluble proteins and biomass (almost 7 times and three fold the data here) for a four day fermentation. This discrepancy might be explained by

the difference in cultivation conditions as they used larger scale fermentation with higher agitation speed (500-800 rpm) and oxygen enrichment. However, it is important to stress that it was not the purpose of this thesis to study the fermentation of *Trichodermer reesei*, but rather, fermentation was a means to obtain the protein for the production of AFEs and triphasic low fat emulsions.

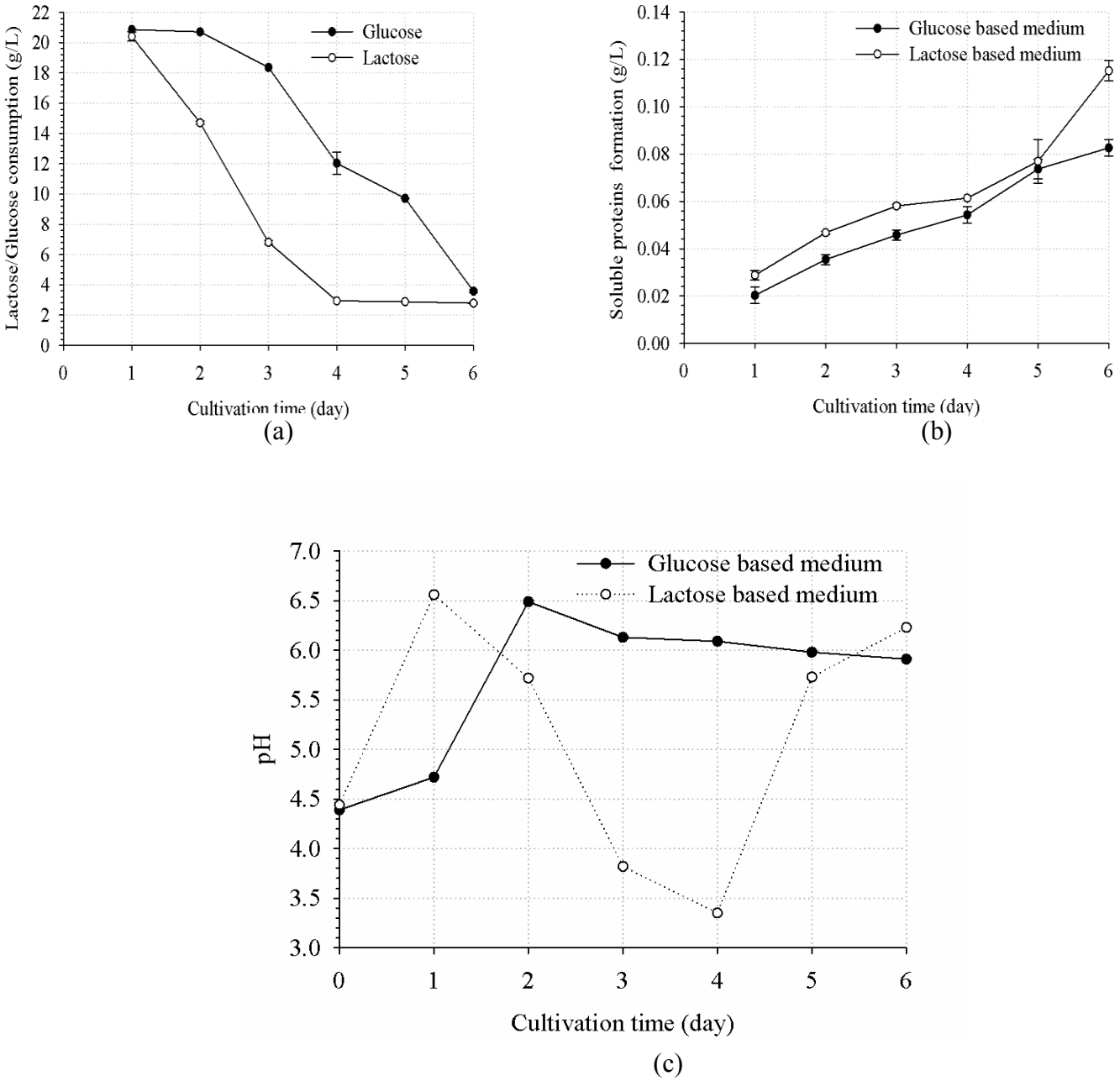

Figure 4-4. Changes in carbon source nutrients as function of the cultivation time of *Trichoderma reesei* in glucose and lactose based media. (a), Glucose and lactose consumption; (b), Soluble proteins formation; (c), pH changes over fermentation time (error bars are smaller than the symbols). Glucose and lactose measurements show an offset at ≈ 3 g/L. Data corresponds to the average of three replicates.

In summary, cultivation of *Trichoderma reesei* QM9414 on lactose containing medium yielded slightly more biomass and soluble proteins when compared to a glucose-based

medium. In contrast, lactose was rapidly consumed and, after nutrients depletion, intense sporulation was observed. This is thought to match with the production of Hydrophobin HFBII by the fungus since it is involved with sporulation and spore hydrophobisation (Askolin, 2006). This onset of intense sporulation was observed on 6th day of fermentation. Interestingly, Askolin et al. (2001), found a minor degradation of HFBI by *Trichoderma reesei* proteases and suggested short cultivation and storage time as one means to overcome this problem. In view of this onset of sporulation, generally associated with the synthesis of hydrophobin, especially HFBII, six days fermentation was chosen as the most suitable duration for the present experimental conditions. Furthermore, although the objective of this thesis was not to study the fermentation, information gained by monitoring pH, lactose, glucose and soluble proteins concentration during the fungal growth, not only guided the decision of the cultivation duration but also could be exploited to enhance natural production of hydrophobins via fermentation.

4.3.2. Intentional Partial purification and characterisation of hydrophobins

Hydrophobins were extracted from mycelium of six days culture of *Trichoderma reesei* with 1% SDS (wt/wt). Any hydrophobins excreted into the culture medium was extracted by foam fractionation. The SDS-PAGE (Figure 4-5) showed similar concentration of hydrophobins in the culture medium and in the mycelium. Proteins of approximately 7 kDa mass believed to be hydrophobins can be seen in lanes 2 and 4. These lanes correspond to the proteins isolated from the lactose- based culture medium and mycelium. Conversely, only a very faint band in the hydrophobins mass range was observed for extract obtained from the culture in glucose

containing medium. Similar results were obtained when the extraction method was changed to 60% ethanol or a mixture of 20% acetonitrile and 0.1% TFA. The visualisation of this band might have been improved by Silver staining because of its lower protein detection limit (1 - 10 ng) as compared to the Coomassie brilliant blue used (50 -100 ng) (Shevchenko *et al.*, 1996). This was unnecessary as the main objective here was to select a culture medium that favours the production of hydrophobins.

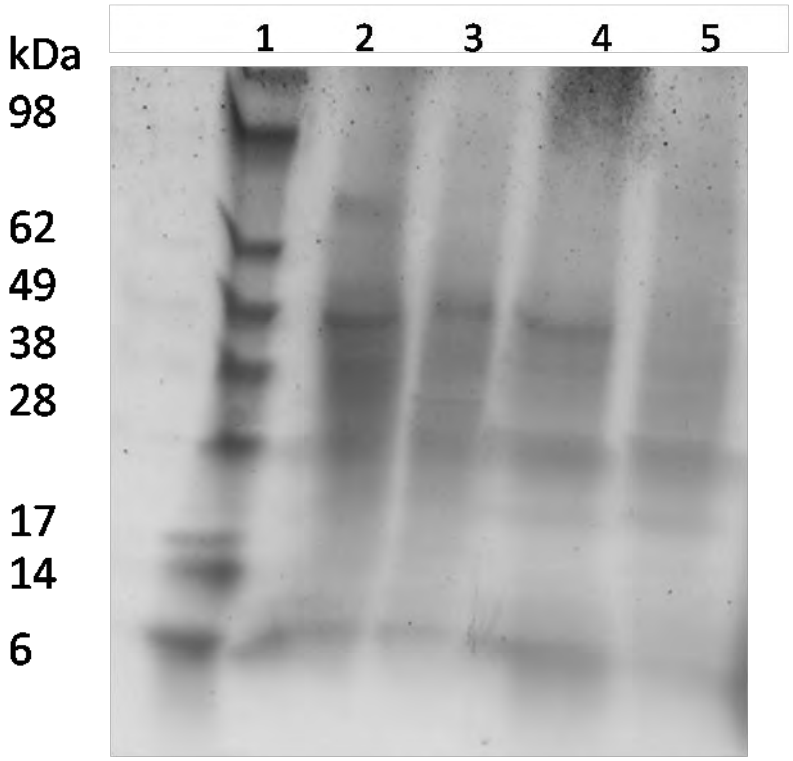

Figure 4-5. Coomassie-stained SDS/PAGE (5-20%) analysis of proteins extracted from mycelium and culture medium of *Trichoderma reesei* cultivated for 6 days in shake flasks.
Lane 1, ladder; lane 2 and 3, proteins isolated from the lactose and glucose-based culture medium respectively by bubbling; lane 4 and 5, 1% SDS protein extracts from mycelium of the lactose and glucose-based culture, respectively.

In order to confirm if the 7 kDa proteins present in the extract are hydrophobins or at least act like hydrophobins, and therefore available for use to stabilise air cells, the potential

hydrophobin rich extract was irradiated with ultrasound, whilst sparging with air to generate an air cell suspension (see Chapter 3). This suspension was then allowed to separate into foam-like, top phase and liquid, bottom phase. Both phases were dried and treated again with TFA to release protein monomer. Proteins recovered from air cells and liquid phases were characterised by SDS-PAGE.

Figure 4-6 shows the SDS-PAGE gel of the bubbles phase and liquid phase of the hydrophobin rich extract after sonication. As already stated, the original protein extract (lane 2) is relatively rich in 7 kDa proteins, which are most likely to be the HFBII monomers, as in the extract from the cells (Lane 3). HFBII concentration in the extract was about 0.01% w/v as estimated from the electrophoresis gel and the total proteins content of the extract was 0.02% w/v. A working solution was prepared by diluting the parent material shown in lane 2 to produce the material shown in lane 4. After processing, a considerable amount of the contaminating proteins remained in the liquid phase as it still appears rich in ≈ 49 kDa proteins (lane 5). The hydrophobins were then concentrated into the air cells rich phase (lane 6). The contaminating protein are possibly the 50 kDa endoglucanase III as *Trichoderma reesei* QM9414 also produces extracellular cellulolytic and hemicellulotic enzymes when grown on lactose (Macarron *et al.*, 1993) and these proteins have been shown to foam fractionate (Zhang *et al.*, 2006). However, these proteins appear be surface active when foam fractionated but their surface activity and absorption kinetics are low, thus they are absent in the air cells surface; as illustrated by lanes 5 and 6 (Ilmen *et al.*, 1997; Bailey *et al.*, 2002). The discussion of the presence of these proteins is made later in section 4-2.3 and in Chapter 5.

The low concentration of hydrophobin monomers in lane 4 is concentrated into the material found in lane 6 (i.e. air cell wall). Although the concentration of hydrophobin in lane 6 is low, image analysis based estimates from the gel give an approximate concentration of 0.1 mg/mL (lane 6) and this was formed from a starting concentration of approximately 35 μg/ml (lane 4).

It is worth noting that a sequence analysis of the protein bands on SDS–PAGE gels carried out by excising the protein bands from the SDS–PAGE gel that corresponds to the putative of hydrophobins HFBII followed by a trypsin-digestion and proteomic analysis of the resulting peptides was inconclusive. The obtained peptide mass maps did not correspond to any relevant protein in the *Trichoderma reesei* protein data bases. Because the proteins were highly surface active and showed HFBII-like features (see next section) it was postulated that the absence of identification of hydrophobin by peptide mass fingerprinting could have been due to an occurrence of partial enzymatic protein cleavage, resulting in peptides with internal missed cleavage sites, as proteases frequently fail to digest proteins to their limit peptides (Siepen *et al.*, 2006), brought about by the following phenomena: (1) an insufficient Coomassie brilliant blue removal, which is known to hamper the enzymatic cleavage of the protein (Shevchenko *et al.*, 1996); (2) presence of trace of SDS which has been shown to either greatly reduce the proteolysis rate or completely inhibit proteolysis, including trypsin digestion of hydrophobin HFBII (Askolin *et al.*, 2001).

Another possible explanation for this inconclusive result from the putative hydrophin sequencing could be some form of post-translational modification of the protein or the presence of a trace of interfering compounds such as carbohydrate. This is somewhat disappointing but, again does not detract from the main thought of this thesis. SDS-PAGEs

showed streaks and strong background, which are often attributed to an insufficient protein cleanup before analysis (Kniemeyer *et al.*, 2006). This might be improved in the future work by introducing a protein cleanup stage after the foam fractionation. For example, the foam fraction (hydrophobin containing fraction) could be treated with a cold acetone or a mixture of acetone/trichloroacetic acid/betamercaptoethanol in order to extract only proteins (by pricipiation) before performing SDS-PAGE.

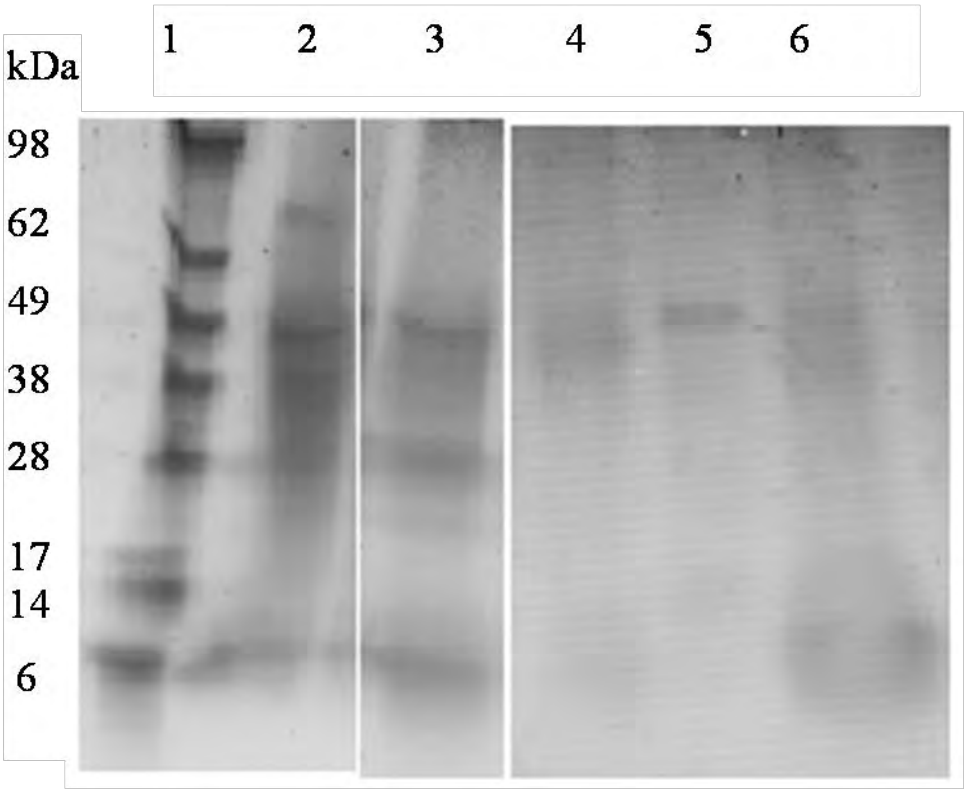

Figure 4-6. Coomassie-stained SDS/PAGE (5-20%) analysis of the protein recovered from the culture medium and mycelium of a 6-day-shake flask cultivation of *Trichoderma reesei* on lactose-containing medium.
Lane 1 is a molecular weight ladder; lane 2, proteins isolated from the culture medium by bubbling; lane 3, 1% SDS extract from mycelium; lane 4, TFA extract of dry foam obtained by bubbling the supernatant of the culture medium; lane 5 and 6, serum and bubble phases of TFA extract after sonication.

4.3.3. Surface and interfacial tension of HFBII containing extract

Figure 4-7 depicts the surface tension and interfacial tension for sunflower oil-aqueous system containing 0.08 mg/mL of total proteins and 35 μg/ml of (lane 4, Figure 4-6) putative hydrophobins. It is worth noting that this material will now be referred to a just hydrophobin for the remainder of the thesis. It appears that the hydrophobin material becomes concentrated when exposed to an air interface and it is capable of rapidly reducing the surface and interfacial tensions to 31 mN/m and 6 mN/m, respectively. These dynamic surface and interfacial tension curves did not show any induction time when compared to that typically found for protein (see Figure 2-2, Chapter 2). Although the contaminating proteins in the extract may have contributed to some of the surface activity of the extract, the final values are in a range that has been previously reported for experiments with pure hydrophobins (Lumsdon *et al.*, 2005; Cox *et al.*, 2007). Furthermore the minimum water tension was reached after 10 to 50 seconds. These results are in agreement with the work of Askolin *et al.* (2006), who measured a surface tension of 28 mN/m using 0.02 mg/mL of pure HFBII solution; but the rate of change was much higher than here and, again may be due to the remaining other proteins.

The remaining contaminating proteins could easily have been removed by a polishing step such as gel filtration or reverse-phase HPLC. However, they were retained intentionally, in order to exploit contaminant proteins for the control of the assembly process of hydrophobin at ai/water interface. The idea was based on the work of Askolin *et al.*(2006) who found a decrease in the kinetics of the reduction of the water surface tension of Class II hydrophobins in the presence of CIass I hydrophobins. If used alone, the maximal lowering of the water surface tension can be almost instantly reached with 100 μg mL^{-1} of HFBII (Askolin *et al.*,

2006). But they found that in a mixture of HFBI, HFBII and SC3, those proteins interact with each other and compete for the available interface, but do not co-assemble. Therefore it was speculated that the presence of contaminant proteins may produce a controllable rate of association, and thus a rate of assembly which can be tailored to match industrial processes.

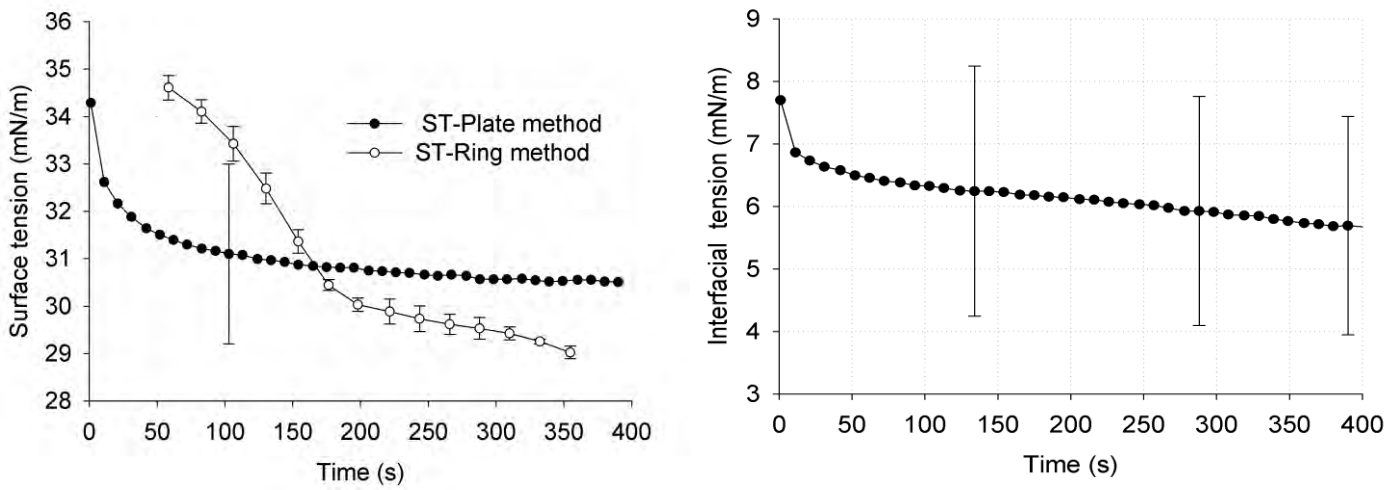

Figure 4-7. Time evolution of surface tensions of hydrophobin rich extract measured with a Noüy ring and a plate (left); (Right) interfacial tension for a sunflower oil water- HFBII containing extract. Error bars denote standard deviations of four measurements.

The characteristic properties of hydrophobins are also seen during the surface tension experiments when using the Du Noüy Ring. HFBII containing extract could rapidly form a stable film across the ring used as measurement geometry (Figure 4.8), which made measurements difficult. For example, at a return distance of 10% (the percentage of force retrieved from the balance before the next measurement) the ring remains outside the solution as the elastic film creates a substantial additional force to confuse the measurement. For this reason further surface tension analysis was performed using the Wilhelmy Plate technique (Figure 4-7). Results were comparable to the ring method, but with poor repeatability. According to the manufacturer of the tensiometer (Kruss) two explanations may be given to

that: (1) the wetted length of the ring that is about 3 fold that of the plate, leading to higher force on balance and better accuracy; (2) the line between the ring and liquid which is more even than that of the plate for surfactants (e.g. cationic surfactants) with poor wetting properties on platinum. Because only minor improvement was observed when an attempt was made to correct (1) by reasonably increasing the penetration distance of the plate, it was concluded that hydrophobin solution may have poor wetting properties for platinum. Furthermore other authors have reported low accuracy and repeatability of the dynamic surface tension measurements of protein solution when using a Wilhelmy plate and attributed that to the adsorption of proteins onto the plate (Tripp *et al.*, 1995). It is recognised that these problems can be overcome by using the pendent drop technique instead, and subsequent experiments were carried out using this technique (see Chapter 6).

The formation of a stable film at the air water interface is one of the most important features of hydrophobins (Szilvay *et al.*, 2007). Although the production of a hydrophobin film across an interfacial tension measuring geometry is not novel, as Cox *et al.*(2007) have also shown a Du Noüy Ring coated with HFBII hydrophobin when using pure proteins (see Figure 2-10, Chapter 2), it is worth reiterating the outstanding physical properties that these protein films offer. The image in Figure 4-8b shows the protein film across the measuring geometry, the ring diameter is 19 mm, at the centre of the ring is a water droplet. This drop is a significant fraction of a gram in mass and is suspended on a film of self assembled hydrophobin.

A protein film was also observed at the sunflower oil/aqueous interface but to a lesser extent than that formed at air/liquid interface. Once again, this could be explained by the rapid migration of the protein to the interface followed by extensive aggregation. Indeed, during the time required to add the oil to the protein extract for the measurement, a film already started

to form, despite the oil phase being loaded as rapidly and carefully as possible in order to obtain reproducible data. It is also worth mentioning that, although it was possible to measure the surface tension with the ring method, it was hard and almost impossible to measure the interfacial tension with that method. This may possibly be explained by the readily formation of the protein film at the interface and its disruption by the movement of the ring resulting in the mixing of the two phases. With the plate method, the plate does not move after the interface has been detected. The interfacial tension of sunflower oil/water measured was 6 mN/m, which is in close agreement to data from pure systems (Cox *et al.*, 2007). Although the ionic strength and the pH of these systems may have been different, and might have affected the results, the interfacial tension of oil/extract is far lower than that of the initial conditions (6 mN/m as opposed to 26 mN/m). Again, although the protein sequencing was unsuccessful, the overall observations illustrate the presence of highly surface active molecules in the fugal extract, and reinforce the proposed mechanism for the presence and localisation of HFBII.

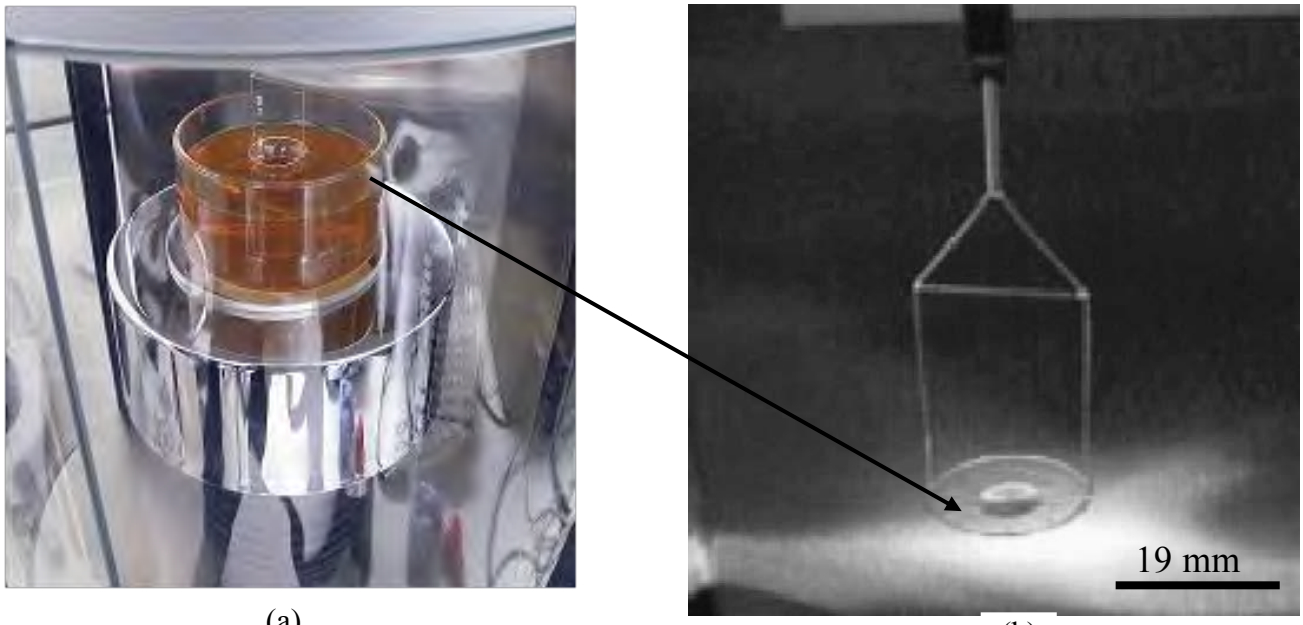

(a) (b)

Figure 4-8. A robust visco-elastic film of hydrophobin formed during the surface tension measurements. The film is vertically stretched as the Du Noüy ring (diameter 19 mm) to which hydrophobin has adsorbed is raised from the air/hydrophobin containing solution interface, but part of the film still in the solution (a). The Du Noüy ring is then raised further and the protein film completely out of the solution, resulting in a horizontally stretched hydrophobin film; during this process hydrophobin film carries a large water droplet (b).

4.4. Conclusion

An attempt to extract Class I and Class II hydrophobins has been carried out. It was found that hydrophobins could be extracted from edible mushrooms but the yield was very low and the separation method technologically tedious.

In contrast, Class II hydrophobin rich extracts were easily obtained from submerged cultures of mycelium and broth of *Trichoderma reesei*. However the extraction solvent used for separating hydrophobins from mycelium contains SDS, which is also surface active and, process improvements are required for its complete removal. To avoid this contamination, the foam fraction from the culture medium was used for the evaluation of the surface and interfacial properties of the extract. It was found that this hydrophobin extract could

significantly lower the water surface tension and spontanously form a robust elastic membrane at an interface in the same way as pure HFBII (Figure 2-10, Chapter 2). These results indicate that this extract could be used to stabilise air cells and this is investigated in the next chapter.

CHAPTER 5

HYDROPHOBIN STABILISED AIR FILLED EMULSIONS AND TRIPHASIC A/O/W EMULSIONS

5.1. Introduction

Chapter 4 deals with the production and characterisation of a hydrophobin rich extract. It was observed that hydrophobin present in the extract could self-assemble at the air/water interface to form a robust film similar to that already reported for pure HFBII hydrophobin from *Trichoderma reesei*. This chapter examines the use of this hydrophobin rich extract to construct micron sized air cell suspensions in water. These suspensions of microbubbles were termed Air Filled Emulsions (AFEs) in Tchuenbou-Magaia (2009a). The central concept in the experimental design was the engineering of air cells to ensure they resembled oil droplets in terms of their shape, size and surface rheology (i.e required physical properties), as proof of a fat replacement technology.

This chapter is divided in two parts. The first part deals with the construction of AFEs, their microstructure and stability under environmental stresses commonly encountered in the food industry. In addition, the oxidative stability of the tri-phasic A/O/W emulsion is examined.

The second part builds upon the development of these structures and assesses the effectiveness of AFEs as ingredient for the reduction of fat and calories content of emulsion based products such as mayonnaise and dressings. Particular emphasis will be given to the rheological and tribological behaviour of the triphasic A/O/W formulations in comparison to full fat versions.

5.2. Construction and characterisation of hydrophobin stabilised air-filled emulsions

Air filled emulsions stabilised by hydrophobins (HFBII-AFEs, see section nomenclature) were produced by irradiating a protein solution with a high-intensity ultrasonic probe whilst sparging with air. As mentioned in the previous chapter, hydrophobin, HFBII was partially purified from a *Trichoderma reesei culture* broth. The ultrasonication process was chosen for making air cells with hydrophobin coats mainly because of the very short time scale at which cavitations occurred (i.e. millisecond timescales, (Margulis, 1995). HFBII is known to aggregate very rapidly and irreversibly at the air/water interfaces thus offering little possibility for process control. However, it has been reported that mixed hydrophobin systems resulted in the reduction of this assembly rate at the interface (Askolin *et al.*, 2006). Ultrasonic emulsification combined with the presence of contaminant proteins (marginally surface active) and probably the appropriate processing temperature enabled to circumvent the HFBII interfacial accumulation rate problem and to construct the structures that characterise the air filled emulsions (see Figure 5-1 and later discussion). In essence, the use of cavitation presents a fixed time and length scale over which bubbles could act as template form. This section will examine mechanism by which a disconnection between interface generation and diffusion of hydrophobins takes place.

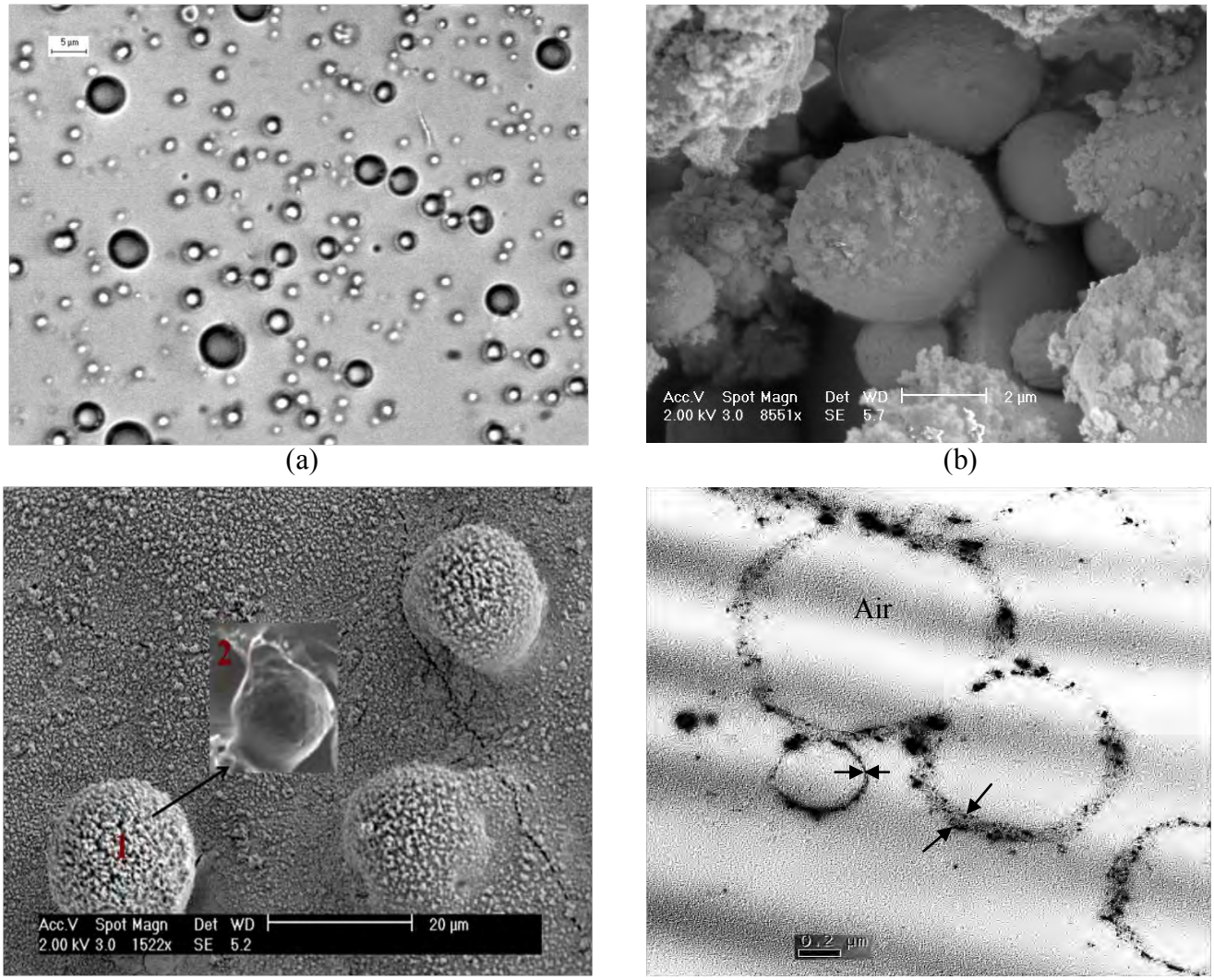

Figure 5-1. Micrographs of HFBII-AFE showing air cells size. (a) is a brightfield image of a one day old sample of AFE (air volume fraction, 40 ± 5 %) ; (b) and (c) are etched and non-etched Cryo-SEM micrographs of a 5 days old sample at high and low magnification, respectively; (d) a TEM section of a 5 days old sample (the shell thickeness, as indicated by the two small arrows, is about 20 nm; the apparent larger shell thickeness (about 75 nm) may be due to the adhesion of non adsorbed proteins to the microbubbles' shell).

5.2.1. Effect of the protein concentration upon AFE formation

Figure 5-2 shows the effect of the protein concentration for AFE-HFBII produced at 55°C. For a total protein concentration of 0.2 mg/mL, the size of air cells varied between 1 and about 100 µm with a small proportion of air cells larger than 100 µm. The majority of air cells were around 10 µm. When the protein concentration was increased to 0.5 mg/mL, smaller air

cells were formed with the majority falling between 0.5 and 10 μm, and no air cells above 100 μm were seen. This range of air cells sizes is within that of oil droplets found in emulsion based food products like mayonnaise and salad dressings (McClements, 2005), and therefore, on this criteria, it would be possible to use them as droplets mimics in such products. Interestingly, the air cells produced here are far smaller than the 114 μm reported by Cox *et al.* (2009) for pure HFBII. This could be explained by the differences in the techniques used for their production. Here sonication provides a short-lived air/water interface that acts as a template for hydrophobin layer formation; this is not the case in conventional whipping or sparging. Moreover, this short-lived interface, millisecond timescales, is in the same order of magnitude as the migration rate of HFBII to the interfaces as shown chapter 4. In conventional whipping method, the protein layer may form irreversibly before a suitable size distribution of air cells can be established or possibly proteins knock off from the interfaces because of the continued shear (Cox and Hooley, 2009). Moreover, the efficiency of ultrasound, when compared to mechanical agitation, for generating microbubbles, has also been demonstrated using two surfactants, SDS (sodium dodecyl sulphate) and L-150A (containing 38% sucrose laurate ester, 10% ethanol, and 52% water). Higher numbers of microbubbles (19-fold) and a lower bubbles size distribution, with mean diameter of 26 μm (L-150A) and 46 μm (SDS) were found for sonicated samples whereas the mechanically agitation produced samples showed a mean diameter of 68 μm (L-150A) and 72 μm (SDS) (Xu *et al.*, 2008). Similar results were found for oil/water emulsion stabilised by genetically modified hydrophobins (see Chapter 6).

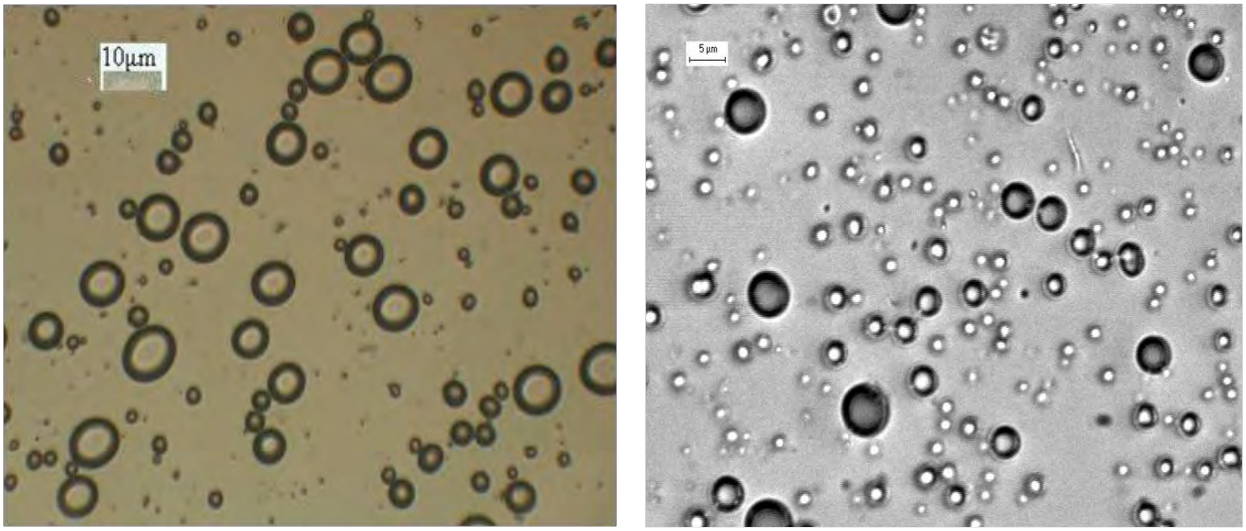

(a) (b)

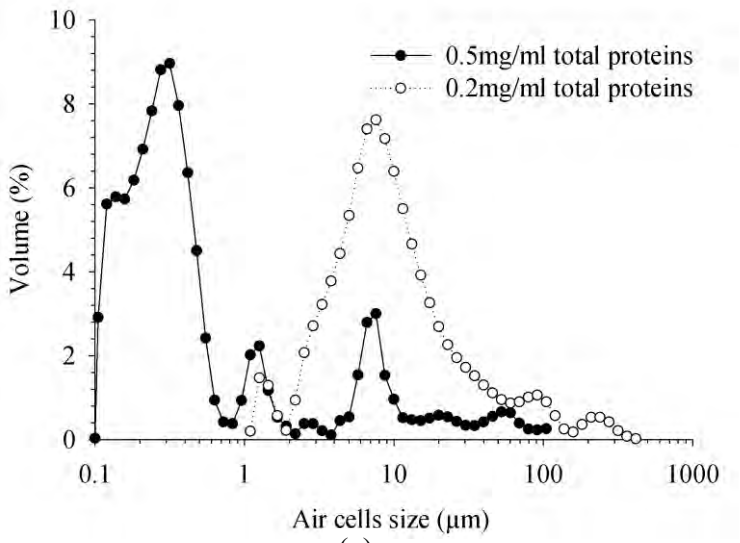

(c)

Figure 5-2. Effect of total proteins concentration upon air cells size and size distribution. (a) and (b), light micrograph of AFE constructed with HFBII rich extract that contained 0.2 mg/ml and 0.5 mg/mL of total protein ,respectively. (c), comparison of air cells size and volume distribution of AFEs (a) and (b). The air volume fraction was 40 % ± 5.

5.2.2. Effect of the temperature upon AFE formation

Hydrophobin rich extract with relatively high protein concentration solution (containing 0.25 mg/mL of hydrophobin and 0.5 mg/mL of total proteins) was sonicated at 25ºC, 40 ºC, 55 ºC and 70 ºC, with other required conditions that generate AFEs kept constant. Figure 5-3 shows

that the initial air phase volume decreases with the increased temperature whereas the average particle size follows the opposite trend. However, microscope observations showed the production of protein aggregates with partially entrapped air, and very few spherical air cells at 25ºC. The amount of protein aggregates decreases as the temperature increases. Although the effect of the protein concentration upon HFBII- AFE formation was expected (as the rate of formation of accumulation of protein at the interfaces is concentration dependent), that of the temperature is rather complex. These results may be discussed in terms of the interplay of simultaneous factors: the effects of the temperature on the aggregation and adsorption kinetics for the hydrophobins and the effects of the cavitation which also depends on the temperature. However, these factors are separately discussed below.

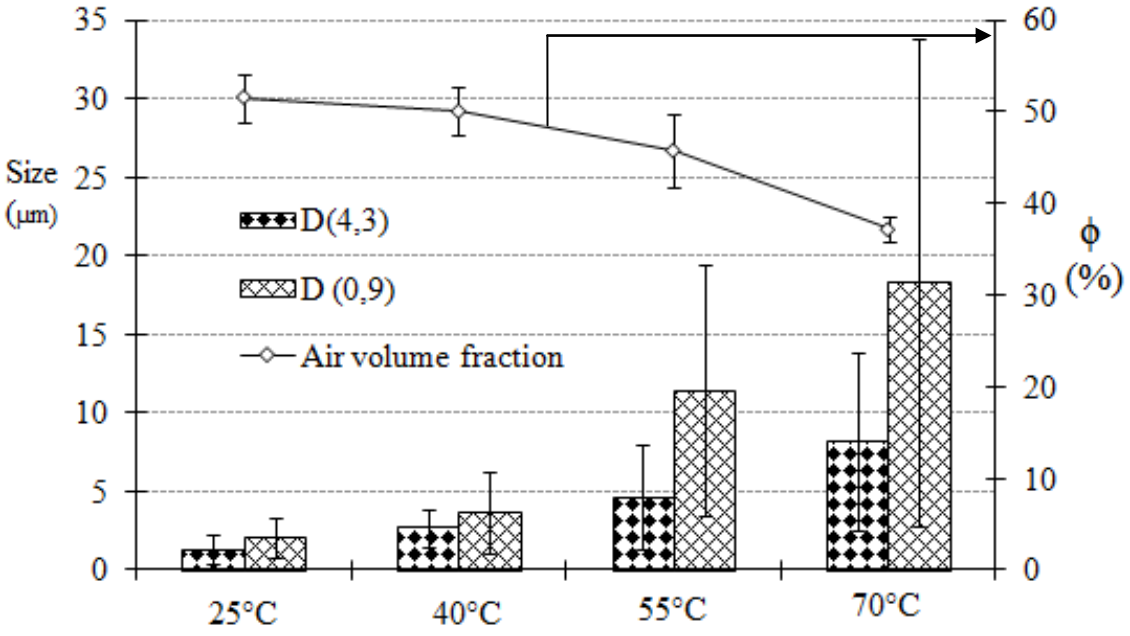

Figure 5-3. Effect of the production temperature upon air cells' size and air volume fraction (Φ). D (4,3) denotes diameter of volume-weighted mean and d (0,9) indicates the 90th percentile of the volume-size distribution. Error bars denote standard deviations. Data corresponds to the average of three replicates.

- *Effect of the temperature upon the aggregation and adsorption kinetics of hydrophobin*

The self-association process of hydrophobin HFBII is predominantly driven by hydrophobic interactions (Kallio *et al.*, 2007; Basheva *et al.*, 2011b). Therefore, factors that enhance these interactions will favour HFBII self-assembly process. At low concentrations in the order of a few μg/ml, hydrophobins will exist in solution, primarily as monomers, and will aggregate into dimers initially, and with increasing concentration (above 10 mg/mL) relatively stable tetramers (able to withstand heating to 80°C) are capable of being formed (Torkkeli *et al.*, 2002). Here, despite the low hydrophobin concentration (0.25 mg/mL), increase the temperature may trigger the formation of dimers and/or tetramers in solution, which then migrate at the A/W interface at a reasonable rate.

Another mechanism as discussed by Kallio *et al.* (2007) and Cox and Hooley (2009) is the possible existence of an equilibrium between protein monomer, dimers and tetramers in solution and this controls the adsorption rate of HFBII. This hypothesis is supported by the work of Kisko et al. (2008), who studied the behaviour of HFBII in aqueous solution at temperatures varying from 6°C to 60°C and observed not only gradual structural changes as function of the temperature of HFBII assemblies but also noticed that the positions of the individual monomers with respect to other also change, and the tetramer prevails at high temperature. This may also help in the formation of a multi-layer proteins at the A/W interface (see Figure 5-1d) and discussion below. It has been seen during this work that together low temperature and low bulk hydrophobin concentration resulted in only partial air cell coverage and not complete spheres.

- *Effect of cavitation*

The mechanical effect of cavitation is temperature dependent (see Table 2-1, Chapter 2). Interestingly, it has been shown that the rate of ultrasonically induced polymer degradation decreases with increasing temperature. This was explained by the reduction of the mechanical force due to the increase in vapour entering the cavitation bubbles as the temperature increases, thus cushioning its collapse (Madras and Chattopadhyay, 2001; Vijayalakshmi and Madras, 2004). Therefore, high shear (high mechanical force) at low temperature may account for the observed increase in protein aggregates as the temperature decreased. But when temperature is relatively high, such 50°C, the absorption of proteins at A/W interface is predominant. Furthermore the localised increase in temperature, known as the "hot spot" effect of acoustic cavitation, may trigger the formation of multi-layer proteins at the air cells surface. Indeed, TEM micrographs of HFBII-AFEs (Figure 5.1d) shows air cells with a shell thickness of approximately 20 nm. This corresponds to roughly 6-8 molecules forming the wall thickness (each hydrophobin unit correspond to 2-3 nm (Kallio *et al.*, 2007)).

It is usually assumed that HFBII forms monolayer interfaces but it is clearly evident that this is not the case here. Wang *et al* (2010) have demonstrated that other proteins such as bovine serum albumin and chicken egg avidin can adsorb on the top of a monolayer of HFBI once absorbed on a hydrophobic 1-hexanethiol surface. They suggested that interactions between the hydrophobin and the second layer were due to electrostatic interactions, involving charged residues that are close to the hydrophobic patch of the molecules. The same authors postulated that these charged residues may be involved in lateral protein-proteins interaction. Since the amino acid sequence of HFBII is 69% similar to HFBI (Nakari-Setala *et al.*, 1997) and both proteins have similarly folded structures (Hakanpaa *et al.*, 2004; Hakanpää *et al.*, 2006) it is reasonable to assume that other factors are common and that HFBII molecules may strongly

interact with a primary adsorbed layer, resulting in the apparent observed multilayer of proteins. Once again concentration and temperature will undoubtedly have an effect here. Recent works by Basheva *et al*. (2011a; 2011b) have confirmed the existence of two layers, a self-assembled bilayer, of HFBII at an air water interface. Interestingly, they also demonstrated the possible incorporation HFBII dimers and tertramers into this bilayer of proteins. Moreover, it has been pointed out that the Langmuir−Blodgett films of a class I hydrophobin from *Pleurotus ostreatus* at an A/W interface consist of bilayer hydrophobins or if a monolayer is present, it coexists with protein aggregates (Houmadi *et al.*, 2008). Thus, the formation of multi-layer protein coats may reinforce the stability of air cells and partially explain the high stability of hydrophobin stabilised air filled emulsion. The kinetics and the final morphology of the hydrophobin layers still require much work. However it should be noted that all these factors can be easily manipulated in such that the interesting structures seen in Figure 5-1 can be formed.

5.3. Stability of hydrophobin stabilised air filled emulsions (HFBII-AFEs) and their subsequent tri-phasic A/O/W emulsions

5.3.1. Stability of hydrophobin stabilised air filled emulsions (HFBII-AFEs)

The stability of HFBII-AFEs was inferred from changes in size and size distribution of air cells with time. These changes were measured using a light scattering method and verified by microscopical observation (Figure 5-4a-d). The importance of this second method is discussed in section 7-2, Chapter 7. Figure 5-4d shows the volume percent of air cells in the AFE as

function of size for fresh material (two hours old), and after 20 and 48 days storage at room temperature. A slight shift in the air cell size distribution was apparent but indicated only a minor change in air cell size volume over a 20 day period. The change in air cell number per size class showed even less change. The air cell size distribution was tri-modal, when expressed as a volume, with the majority of air cells around seven μm in size; but with a small number having a diameter at the two extremes of either of approximately 1 or 100 μm. After 20 days there was a slight shift of the main peak from seven to 10 μm. However, after 48-days storage, there was a decrease in the bubble size accompanied by an increase in proportion of smaller air cells (0.5 μm). The existence of a critical bubble diameter below which bubbles will shrink and above which bubbles will grow has been reported (Dutta *et al., 2004;* Xu *et al.,* 2008). Xu *et al.* (2008) monitored (over three minutes) the changes in size of SDS-stabilised microbubbles produced by ultrasound and found that bubbles with a diameter smaller than 100 μm experienced a comparatively slow reduction in diameter with time; whereas microbubbles equal to or larger than 100 μm were stable. They observed microbubbles shrinkage for a diameter for around 40 μm, and again observed an increased rate of shrinkage at a diameter less than 20 μm, which shrank rapidly and had disappeared within 30s. They obviously concluded that this was due to Oswald ripening. Although hydrophobin stabilised microbubbles are far more stable (two months presented here compared to three minutes by Xu *et al.* (2008)), there is a similar trend i.e. there was no modification of air cells of around 100 μm over the 48 days storage (Figure 5-4d). According to the Young–Laplace equation ($\Delta P=2\gamma/r$, where ΔP is the pressure difference, γ is the surface tension, and r is the radius of the bubble), the internal pressure of the bubble increases as the bubble size decreases. The reduction in bubble size increases its internal pressure which, in turn results in further shrinkage of the bubble population. Given the small size of air cells

shown here (as typified by Figure 5-4) plus the polydispersity of the air cells which induces a large pressure difference across the bubble population, one would expect the system to undergo rapid Ostwald ripening. Moreover there was no noticeable loss of volume during the study (low interfacial volume closed tubes). These results are in agreement with work by Cox *et al.* (2007) studying the stability of a single bubble with adsorbed HFBII where the bubble could disproportionate with the atmospheric air. They found no significant changes in bubbles stabilised with HFBII over the time periods studied (one hour), whereas, those stabilised with β-casein, β-lactoglobulin and sodium dodecyl sulphate shrank and vanished within about two minutes. The remarkable stability of HFBII stabilised bubbles has been shown to be due to its ability to pack together closely at an A/W interface and make a strong film with high surface shear viscosity and elasticity that are far beyond that of other proteins (Cox *et al.*, 2007; Blijdenstein *et al.*, 2010). This again is illustrated by Figure 5-4c which, when examined closely shows a wrinkled surface of the 27 days old bubbles after being left dry under a microscope slide for two hours. This suggests that HFBII once at A/W interface will not or hardly at all desorb back to the aqueous phase. Similar surface structures of HBII stabilised bubbles was observed by Cox *et al.* (2007), which led them to describing HBII as hydrophilic particles. However because of the changes in size of hydrophobin stabilised air cells after long term storage, one may speculate, as Kloek *et al.* (2001) did, that high interfacial rheology properties can retard bubble dissolution but will never completely stop the process. Another scenario might be that the presence of impurities may have somehow reduced the strength of the HFBII hydrophobin film.

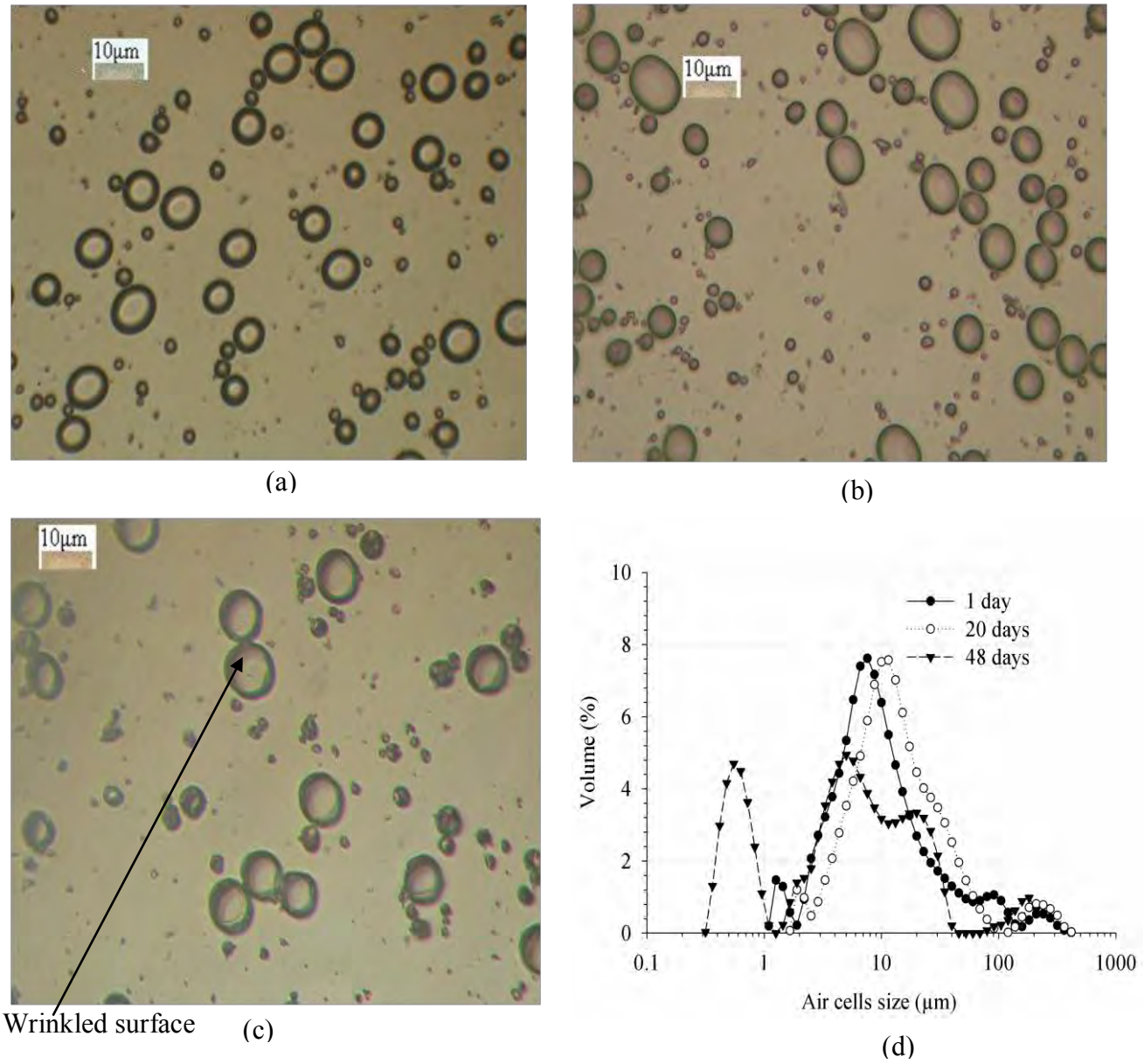

Figure 5-4. The stability of an HFBII-AFE during storage at room temperature: (a) and (b) are light micrographs of 1 day and 27 days old AFE (air volume fraction, 40 ± 5 and no noticeable change in the volume of AFE in graduated test tube was observed); (c) is sample (b) left dry for 2h under a microscope; (d) is the size and volume distribution of an AFE after 1, 20 and 48 days storage.

5.3.2. Stability of air cells in tri-phasic A/O/W emulsions

A range of tri-phasic emulsions (A/O/W) with up to 68 % total phase volume (air and oil) were prepared by diluting a 20% oil-in-water emulsion (O/W) with a concentrated AFE (≈ 80% air phase). Again, the Mastersizer and both light microscopy and SEM were used to

monitor the stability of emulsions (Table 5-1 and Figure 5-5). Table 5-1 shows the particle size of tri-phasic A/O/W emulsions with 28% (10% air, 18% oil), 36% (20% air and 16% oil) and 68% (60% air and 8% oil) phase volume over more than three months as monitored using the volume weighted diameter (d_{43}) and the size below which 90% of sample lies (d_{90}). The initial average air cells diameter of air filled emulsion used for A/O/W preparation was 4.6 µm and 11.4 µm for d_{43} and d_{90}, respectively (see Figure 5-2c, i.e. the AFE made with 0.5 mg/mL of proteins for the air cells size distribution). Overall, the triphasic emulsions showed only minor, if any changes in their size over the study period. Similar stability was observed with a triphasic emulsion (52% total dispersed phase, 40% air and 12% oil) made with AFE with a bigger mean air cell sizes (see Figure 5-2c (AFE made with 0.2mg/mL of proteins); and appendix 1, Tchuenbou-Magaia *et al.* 2009). However, a close scrutiny of Table 5-1 suggests a slight decrease in particle size during the storage, especially for sample with high total phase volume. Indeed, the d_{43} shifted from 3.8 µm, 6.5 µm and 6.6 µm (at day 1) to 3.5 µm, 5.7 µm and 5.6 µm (at day 57) for 28%, 36% and 68% tri-phasic A/O/W emulsions, respectively. The d_{90} remained practically unchanged for 28 % and 36% tri-phasic A/O/W emulsions, but did show a change of 8% after 100 days storage (from 12.5 µm to 11.5 µm) for the 68% sample. There was no noticeable change in the height of tri-phasic A/O/W emulsions stored into tubes, and visually monitored over the time. Together these results suggest that no bubble coalescence occurred and that the main destabilisation mechanism is Osward ripening, albeit at low rate.

At 100 days storage, all the triphasic A/O/W emulsions showed, to some extent, a slight decrease in their particle size. It should be borne in mind that when an emulsion is stabilised by surfactant at several times its critical micelle concentration (CMC), oil can exist in solubilised form (0.2-0.5wt%, of the total oil content) both within the micelles and as oil

droplets (Sherman, 1983; Lobo and Wasan, 1993; Christov *et al.*, 2002). This micellar system may affect the stability of the emulsion, by mediating the transport of oil between droplets (McClements *et al.*, 1993; Elwell *et al.*, 2004). The 20% O/W emulsion was made with 0.5% Tween 60 and it was estimated that it would take 0.03 g of Tween 60 for 100 ml of emulsion to achieve saturated coverage (see Appendex 3). The initial quantity of Tween 60 was more than 10 times higher than required and the excess Tween 60 in the aqueous phase is well above the CMC (0.03%, (Zhong *et al.*, 2008)). Although such excesses of surfactant are typical, the slight decrease in oil droplets size at long time storage may be explained by the accumulation of the oil into the micelles probably because, with aging, the rate of transport of oil from droplets to micelle becomes relatively higher compared to that of transport from micelle to oil droplets. This in turn might negatively affect the stability of the tri-phasic A/O/W as it has been reported that the presence of solubilised oil inhibits the formation of an ordered micellar structure (pseudo-emulsion) between oil droplets and the A/W interface (see Figure 2-12, Chapter 2), which, when it exists enhances the stability of bubbles (Nikolov and Wasan, 1989).

Table 5-1. Long-term stability results of triphasic A/O/W O/W emulsions. The initial mean air cells diameter of air filled emulsion used for A/O/W preparation was 4.63 and 11.42 for d_{43} and d_{90}, respectively.

Time (day)	**20%/O/W**		**28%-A/O/W**		**36%-A/O/W**		**68%-A/O/W**	
	d_{43}	**d_{90}**	**d_{43}**	**d_{90}**	**d_{43}**	**d_{90}**	**d_{43}**	**d_{90}**
1	0.9	1.6	3.8	8.3	6.5	12.4	6.6	12.5
	± 0.1	± 0.1	± 0.1	± 0.1	± 0.1	± 0.3	± 0.3	± 0.3
9	0.9	1.6	3.7	8.50	6.0	12.4	5.9	12.3
	± 0.1	± 0.1	± 0.1	± 0.1	± 0.2	± 0.3	± 0.2	± 0.3
27	0.9	1.6	3.7	8.4	5.7	12.2	5.2	11.6
	± 0.1	± 0.1	± 0.1	± 0.1	± 0.3	± 0.2	± 0.2	± 0.3
43	0.9	1.6	3.4	8.1	5.5	11.8	5.4	12.0
	± 0.1	± 0.2	± 0.1	± 0.2	± 0.3	± 0.3	± 0.3	± 0.3
57	0.1	1.6	3.5	8.3	5.7	12.1	5.6	12.0
	± 0.1	± 0.1	± 0.1	± 0.2	± 0.3	± 0.2	± 0.2	± 0.3
100	0.8	1.5	3.2	7.9	5.3	11.8	4.9	11.5
	± 0. 1	± 0.2	± 0.1	± 0.3	± 0.3	± 0.4	± 0.2	± 0.4

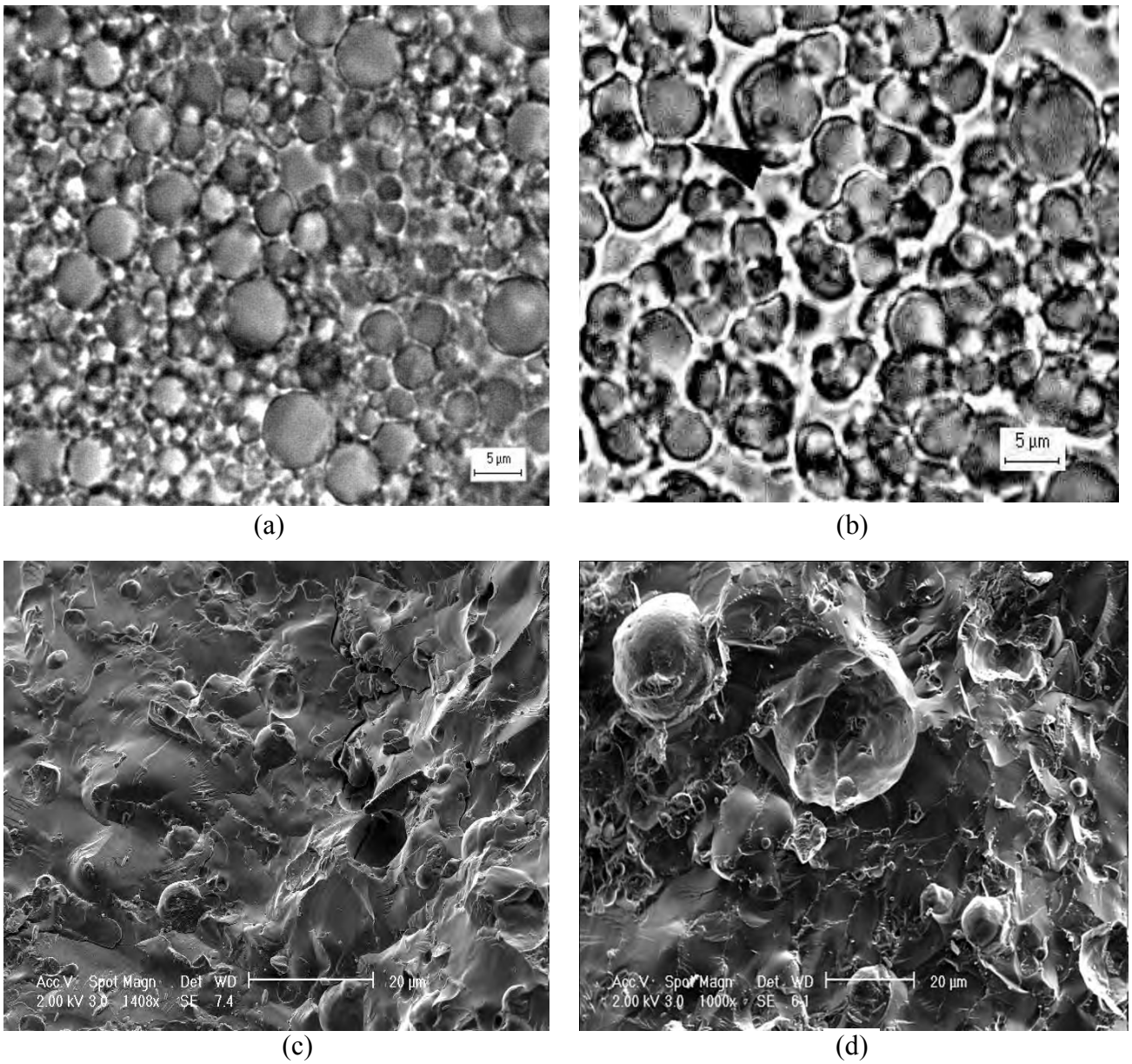

(a) (b)

(c) (d)

Figure 5-5. Typical micrographs of A/O/W emulsions showing air cells and oil droplet sizes (a) and (b): optical micrographs (1 day and 45 days old respectively); (c) and (d): Cryo-SEM micrographs (7 days and 40 days old respectively). The arrow in figure 5.4b indicates surface flattening but not coalescence between two adjacent air cells. This A/O/W emulsion contains 40% air and 12% oil by volume.

Air cells in the triphasic A/O/W emulsions showed greater stability when compared to the AFEs. To get some insight into the possible reasons for this, two approaches were explored. The first approach is based on the theory that the interaction of oil droplets with the bubbles' surface are characterised by the degree of oil spreading and the configuration of the oil

droplets at the A/W interface (Koczo *et al.*, 1992; Lobo and Wasan, 1993; Aveyard *et al.*, 1994; Denkov, 2004). First, the entry (E), bridging (B) and spreading (S) coefficients that theoretically dictate the probability of oil to enter and spread at an air/water interface were calculated. Please, refer to section 2.3.4.2 in Chapter 2 for the definition of these coefficients. They were estimated from the interfacial and surface tensions of the initial systems (see Table 5-2). It is important to note that, E and S depend on the state of the system (Aveyard *et al.*, 1994) and the estimated values may well be different from those of the triphasic system at equilibrium. Nevertheless, the initial coefficients corresponding to those of the pure interfaces have been successfully used in the literature to predict and control the entering and spreading of oil/fat droplets (Hotrum *et al.*, 2003) and may still provide some insight into the process taking place here. Also, there are theoretical constraints for possible values of E and S at equilibrium (Ee and Se). This is because any three-phase boundary between the oil (O), water (W) and air (A) interfaces (Figure 5-6b) disappears when $E < 0$, $S > 0$, and oil droplet will be expulsed into air when $\gamma_{O/W} + \gamma_{A/O} - \gamma_{A/W} < 0$; thus leading to $S_e \leq 0$ and $0 \leq E_e \leq 2\gamma_{O/W}$ (Aveyard *et al.*, 1994; Hotrum *et al.*, 2004).

Table 5-2. Surface (γA/W, γA/O) and interfacial (γO/W) tensions and the resulting Entry coefficient (E), Spreading (S) and bridging (B) coefficients.

$\gamma_{A/W}$ (mN/m)	$\gamma_{A/O}$ (mN/m)	$\gamma_{O/W}$ (mN/m)	E (mN/m)	S (mN/m)	B (mN/m)	$2\gamma_{O/W}$ (mN/m)	$\frac{\gamma_{O/W}}{\gamma_{A/W}}$
31	26	8.5	13	-3.5	357	17	0.27

Table 5-2 shows that the entry and bridging coefficient are positive whereas the spreading coefficient is negative. According to the initially proposed mechanism (Ross, 1950; Aveyard *et al.*, 1994), the oil droplet can enter the air water interface but the spreading cannot occur.

However, the oil droplet may remain as a lens on the bubbles surface or can form a mechanically unstable bridge between lamellae leading to the breakdown of air cells (as B> 0). The latter scenario is less likely as a microscopic observation of a 5 month old 28% A/O/W (after shearing under viscosity measurement) still showed conditions showed individual air cells (see Figure 5-7). Instead, Figure 5-7 shows flocculated oil droplets around air cells or oil droplets at the surface of larger air cells. Furthermore, it was observed that oil droplets tend to attach at the protein-covered air cells' surface, especially in older triphasic A/O/W emulsions (see Figure 5-5b and 5.7a). Since here the oil droplets are stabilised by a non-ionic surfactant this process may be driven by size difference between larger air cells and oil droplets; small particles have larger surface area than bigger ones and can easily sit at their surface.

Considering that most of the oil droplets were seen at the air cell surfaces during the aging process (Figure 5-5 and 5-7), it can be postulated that the presence of a thin film (pseudoemulsion) between an approaching oil droplet and air cell (A/W) exists. Such pseudoemulsion will act as a kinetic barrier to droplet entering, though $E > 0$ (Lobo and Wasan, 1993). As previously mentioned, this pseudoemulsion may become unstable with time, allowing the oil droplets to reach the A/W interface (see Figure 2-12, Chapter 2, reproduced in this section as Figure 5-6). Once at the interface oil droplets (intact) attach to the hydrophobin film, but oil lens was hardly visible. However, it has been hypothesised that even when oil droplet entering is kinetically hampered, from time to time a single droplet may overcome this barrier and enter the air/water interface. At this stage, because $S < 0$ the transition from the oil lens to a spray layer that may occur and destabilise the system might happen if any stress or large deformation causes the fracture of the hydrophobin film coating

air cells (Hotrum *et al.*, 2003). This may have an important implication on the oral behaviour of the triphasic emulsion (see the last section of this Chapter).

Table 5-2 also shows that the ratio of the O/W interfacial tension $\gamma_{O/W}$ to the A/W surface tension $\gamma_{A/W}$ is relatively high (0.27) when compared to the values (0.001 – 0.24) reported in the literature (Aveyard *et al.*, 1993; Binks and Dong, 1998; Basheva *et al.*, 1999; Arnaudov *et al.*, 2001). In a foam system, the shape of the droplet in the Plateau border is controlled by both the size of the oil droplet relative to that of the Plateau border and this infacial tension ratio (Neethling *et al.*, 2011). It has been demonstrated that less droplet deformation occurs at high ($\gamma_{O/W}$ / $\gamma_{A/W}$) ratio (Neethling *et al.*, 2011), and this may be considered as one of the reasons behind the non observation of an oil lens here.

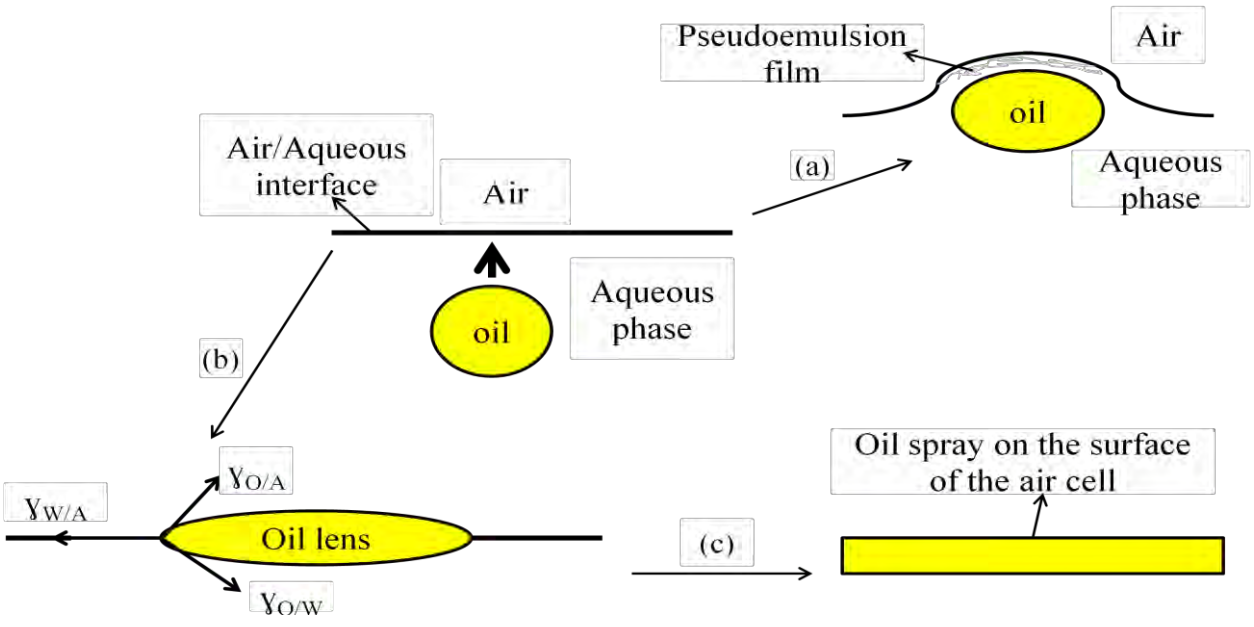

Figure 5-6. Schematic diagram of possible mechanisms of stabilisation or destabilisation of bubbles in the presence of oil droplets (this is a reproduction of Figure 2-12, Chapter 2 and more details can be found there).

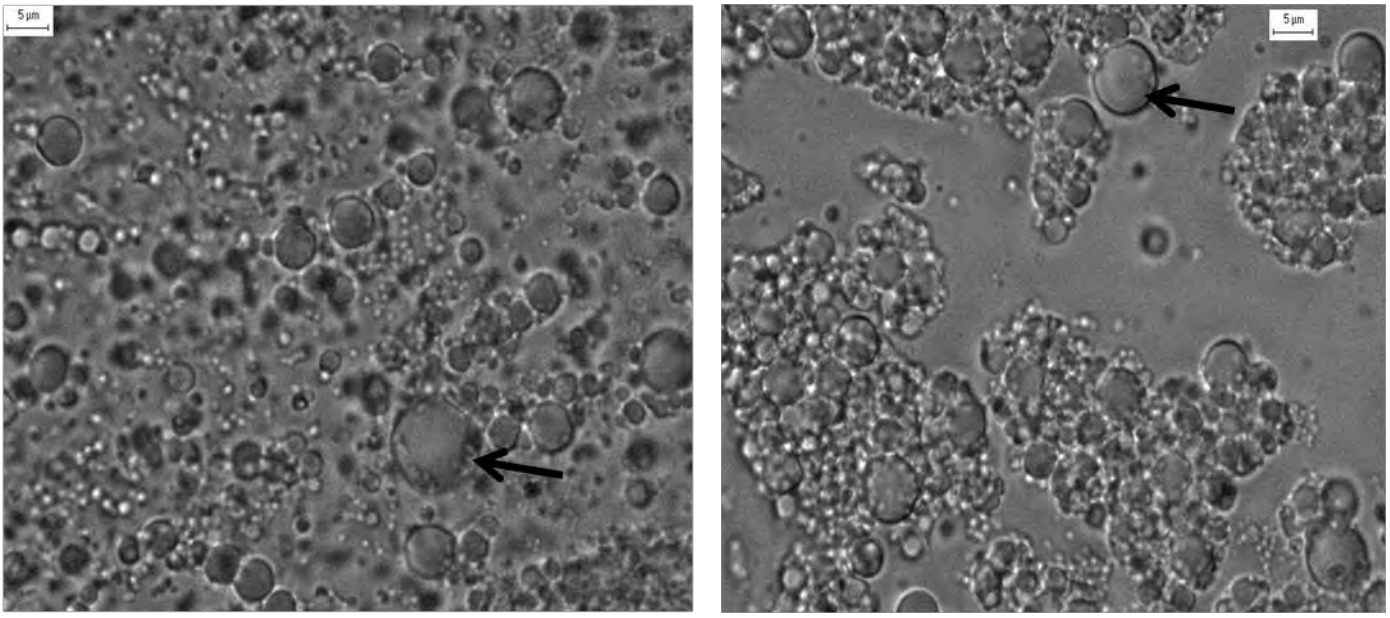

(a) (b)

Figure 5-7. Typical optical micrographs of A/O/W emulsions showing air cells and oil droplet sizes. 5 month old 28% A/O/W with 10 % air by volume (left hand) and 5 month old 28% A/O/W after being sheared from 0.1 to 100 s^{-1} followed by a 2nd shear from 0.1 to 500 s^{-1} under viscosity measurement conditions. The arrow in figure 5.5a indicates oil droplets attached at flattened air cells' surface.

Another possible explanation for the increased stability of air cells in the triphasic may be the apparent increase in the thickness of the air cells from the presence of oil droplets and thickener (e.g. carrageenan) (Koczo *et al.*, 1992). In this case the amount of oil droplets surrounding air cells would become a limiting factor to the stability of the triphasic emulsion. This may account for the reduction in the emulsion particle size over the storage for triphasic A/O/W emulsions, particulaly at high AFE volume fraction. Although more investigation is needed to help understanding the contribution of oil droplets to the stability of the triphasic emulsion, the rheology data indicated a possible existence of O/W and AFE ratio above which the triphasic emulsion becomes less stable to any stress (see next section, Figure 5.8).

5.3.3. Stability of A/O/W emulsion against creaming: possible weak gel formation

Figure 5-8 demonstrates the creaming stability of tri-phasic emulsions as compared to its parent O/W emulsion. With the A/O/W emulsions, the samples with the lowest total dispersed phase volume showed creaming when held at room temperature and this was apparent even after 24 h. However the creaming rate was observed to diminish with increasing air phase volumes until it was eliminated at a total phase volume of 68% (Figure 5-8a). Similar phenomena are known for O/W emulsion system where an emulsion does not exhibit any creaming at high oil droplets concentration due to complete close packing of oil droplets (Robins *et al.*, 2002). By analogy to O/W emulsions, the viscosity of the A/O/W emulsions should indeed, increase with an increase air phase volume (air cell concentration). Therefore, the viscosity of A/O/W emulsions with different air and oil phase volumes was measured, and as expected, the viscosity of the emulsions increases with the increasing total phase volume (Figure 5-9). However, the magnitude of the increase in viscosity did not match phase volume in a linear fashion. For example, the viscosity of the 28% tri-phasic emulsion (10% air and 18% oil) is slightly greater than that of the parent 20% O/W and, not unexpectedly, lower than the viscosity of 36% system (20% air and 16% oil). Thus, air cells and oil droplets contribute to the viscosity of the systems. However, the respective viscosities of 36% A/O/W and 68% A/O/W (60% air and 8% oil) systems are very similar despite the large increase in the phase volume. This similarity in viscosity might be attributable to their comparable size and size distribution (Table 5-1) or/and to the existence of a critical ratio of AFE and O/W emulsion above which adding more AFE to the system has a detrimental effect on the viscosity of the triphasic emulsion. As mentioned in the previous section, this plateau in viscosity is presumably an indication of either the fragility of or a peculiar behaviour from the

triphasic emulsion systems at high air phase volume. It should be noted that for such a polydispersed emulsion (Table 5-1 and Appendix 1, Tchuenbou-Magaia *et al.* (2009a)) the total phase volume (air and oil) is still below the threshold for creaming to occur (about 72%, Princen and Kiss (1989)).

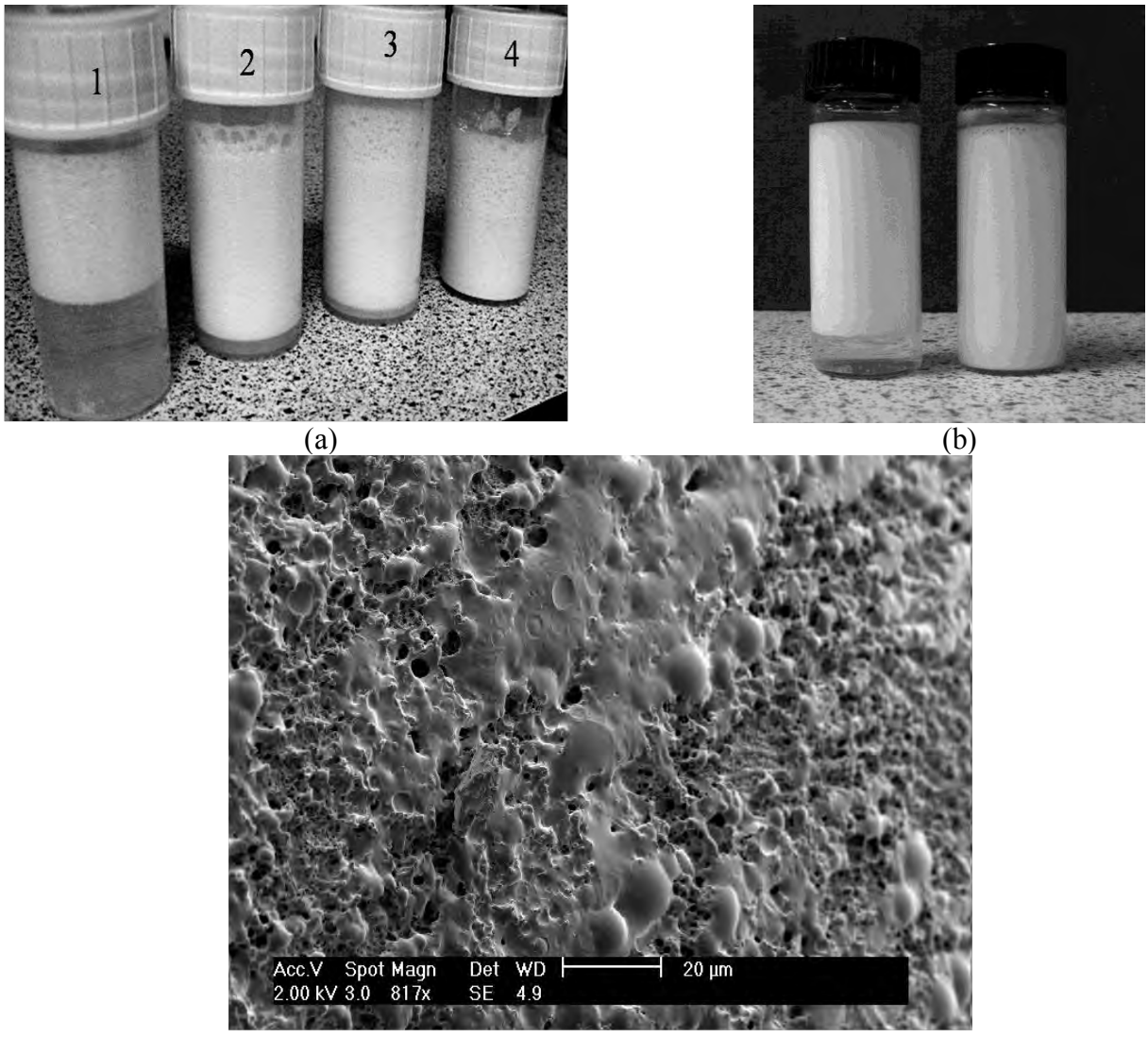

(a) (b)

(c)

Figure 5-8. Effect of air phase volume on creaming stability of triphasic emulsions. Triphasic emulsions were prepared by diluting O/W, 20/80 emulsion (a-1) stabilized with Tween 60 and containing 0.2% iota –Carrageenan. Samples numbered 2, 3 and 4 in Figure 5-9a are A/O/W emulsions with 10% (10/18/72 i.e. 10 % air/18 % oil/72% water), 20% (20/16/64) and 60% (60/8/32) air volume respectively. All these emulsions were stored 14 h at room temperature after being made. Some large bubbles are visible in some of the tubes (above the emulsion) and these are not to be confused with the AFE air cells; they may illustrate the presence of a Pickering foam. (b) is the parent O/W (left hand) and A/O/W emulsion (10/18/72 after 3 weeks storage at ca. 8°C. (c) is the cryo-SEM of A/O/W (10/18/72) showing a gel network.

Other work (referred later) leads to a reasonable hypothesis for the formation of the possible weak gels seen here. This is discussed below. Figure 5-8b shows a clear difference between A/O/W emulsions at very low air phase volume (20% air and 16% oil) and the parent O/W with regard to the creaming behaviour (here storage was at 8^{o}C). The parent O/W emulsion has separated into two phases despite the presence of carrageenan; with the concentrated emulsion occupying the upper seven-eighth of the tube and a clear serum layer filling the lower part. In contrast, the A/O/W emulsion remained uniform throughout the full height of the sample and no change in bubble size was observed (Table 5-1). This possibly indicates that the presence of hydrophobin-stabilised air cells in the system has induced a weak gel formation. The existence of a network is further supported by the cryo-SEM images of A/O/W (Figure 5-8c). The creaming of the O/W emulsion could have been due to depletion flocculation induced by the non gelling of the Iota carrageenan, originally included to prevent creaming by increasing the serum viscosity. According to Dickinson and Pawlowsky (1997), aqueous solutions of Iota carrageenan yield transparent thermoreversible gels upon cooling in the presence of cations (the effectivenesses of which follow lyotropic series $Ca^{+2} > K^{+} > Na^{+}$). However, no salt was added to these emulsions. Iota carrageenan is also believed to interact strongly with proteins in an acidic medium (Blakemore and Harpell, 1010); but it has been reported that a complex formation can occur between BSA and dextran sulphate, Iota carrageenan and Kappa carrageenan at pH > p*I* of the protein through a characterised patch of positive charge on the BSA molecule surface (Hattori *et al.*, 2001). In the case here of A/O/W emulsion, a possible interaction between hydrophobin and Iota carrageenan may account for its stability against creaming, despite the comparatively low phase volume. This hypothesis is again in line with the proposed attraction of Iota carrageenan to BSA (Dickinson and Pawlowsky, 1997) or sodium caseinate (Keogh *et al.*, 1996); once more due to interacting

patches of positively charged residues on the protein surface with the highly charged backbone on the anion polysaccharide. It may be also considered either an interaction between droplets that could lead to a more openly packed droplets thereby preventing creaming at lower droplet concentration (McClements, 2005) or more likely, a bridging of droplets by non absorbed hydrophobin giving rise to a weak network as illustrated by (Figure 5-8c and Figure 7-13, Chapter 7). The implication of these results is that air cells (via their protein shells) in the triphasic emulsion could also help in simplifying the formulation; i.e. the reduction of the amount of thickener for a standard O/W emulsion and still give a similar visual appearance and texture to a full fat original.

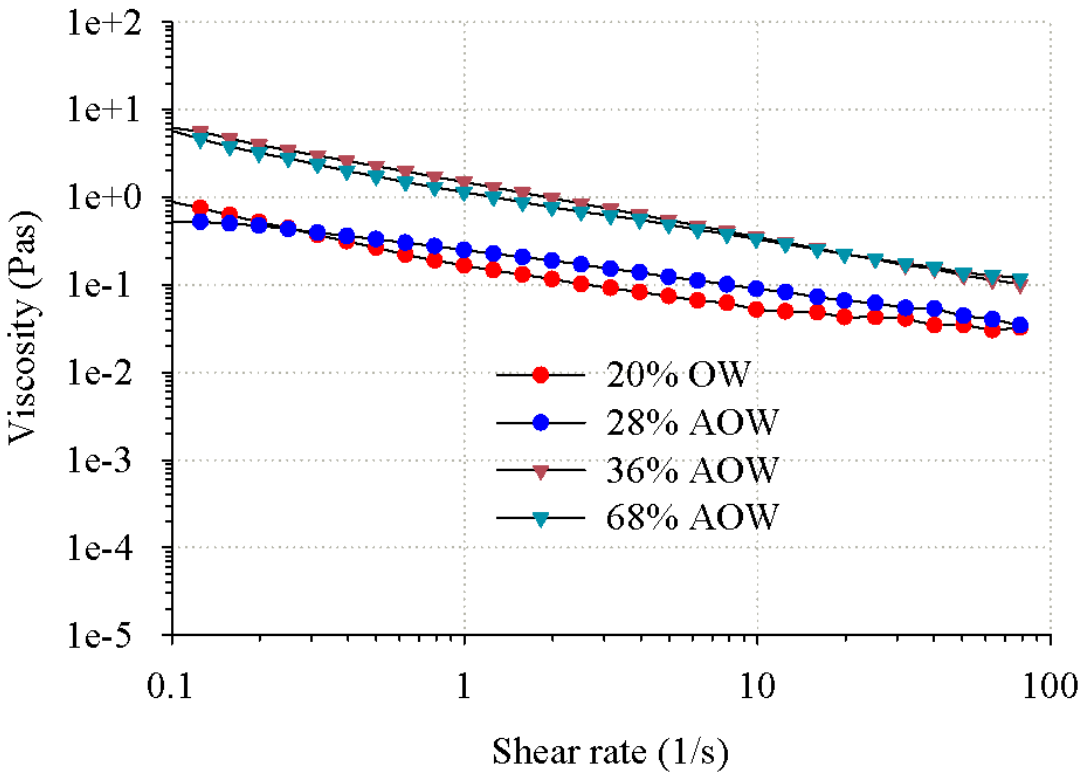

Figure 5-9. Log-log plot for viscosity against shear rate of the parent O/W emulsion and A/O/W emulsions with 28% (10% air and 18% oil), 36% (20% air and 16% oil) and 68% (60% air and 8% oil) phase volume.

5.3.4. Stability of the tri-phasic A/O/W emulsion: lipid oxidation

Micron sized air cells have a high surface area to volume ratio and, as consequence mass transfer between molecules will be enhanced in systems containing microbubbles. Moreover, air is strong lipid oxidation promoter. Therefore, oxidation reactions may be enhanced in a tri-phasic A/O/W emulsion. This would detrimentally affect unsaturated fatty acids, flavour, the overall food quality and shelf life. This section explores the influence of the presence of air filled emulsions upon the oxidation stability of the remaining oil in a triphasic A/O/W system. This was achieved by comparing the oxidation stability of a tri-phasic A/O/W emulsion and a comparable O/W emulsion. A 28% O/W, a mimic of the 28% A/O/W emulsion, was constructed to produce oil droplets with size and size distribution as close as possible to those of a 28% A/O/W emulsion with 10% air and 18 % oil. The 20% O/W emulsion is the parent to which air cells are added (Table 5-3).

It is worth noting that this section was submitted for publication with the title: “protection of delicate oils in triphasic gas-oil-water emulsions”. A full prior art patent search was performed. This patent application also prompted the work presented in Appendix 6 and summarised at the end of Chapter 6 concerning the interaction between lipid oxidation products and hydrophobins in O/W systems. However, although the prior art publications did not mention the oxidation stability of a triphasic gas-oil-water emulsions or the effect of hydrodrophobins/proteins upon the oxidative stability of such system, it did include the protective effect of hydrophobins and proteins against the oxidation deterioration of O/W emulsions. This was sufficient to prevent the progression of the second patent.

Table 5-3. Mean particle Size (Micrometers) of a triphasic emulsion (28% A/O/W, with 10% air by volume), its counterpart 28% O/W and the 20% O/W parent emulsion used for the preparation of the A/O/W emulsion.

Emulsions	d_{32}	d_{43}	d_{90}	Span
20% O/W	0.68 ± 0.01	0.89 ±0. 01	1.49 ± 0.02	1.35
28% O/W	0.88 ± 0.20	1.90 ± 0.12	3.82 ± 0.09	3.10
28% A/O/W	0.89± 0.01	2.76 ± 0.01	6.8 ± 0.08	4.63

- *Formation of hydroperoxide and secondary oxidation products*

Figure 5-10 shows the comparison between the oxidative stability of the 28% O/W emulsion, the 28% total phase volume tri-phasic emulsion and the 20% O/W emulsion used for the preparation of A/O/W systems after storage at 40°C for up to eight days. The 28% A/O/W initially showed a rapid increase in peroxide concentration (PV), which peaked by day three at 15 mM; after which the peroxides concentration decreased to a lower value of ≈ 7 mM by day seven and then remained constant for the rest of the study. In contrast, a more gradual increase in PV was found in both the 28% and 20% O/W emulsions over the period of test. From day four, peroxide concentration was greater in these emulsions than in the 28% A/O/W (Figure 5-10a). This might be explained by a combination of the decreased formation and an increased degradation rate of hydroperoxides after the initial three days storage.

Secondary oxidation products estimated in terms of anisidine value (AnV) were also higher in the 28% A/O/W as compared to its 28% O/W counterpart, especially over days four, five and six (Figure 5-10b). Because these secondary oxidation products are formed as a result of the degradation of primary oxidation products (peroxides), these results are expected as the rate of the formation of peroxides in 28% O/W was lower during the first three days of storage.

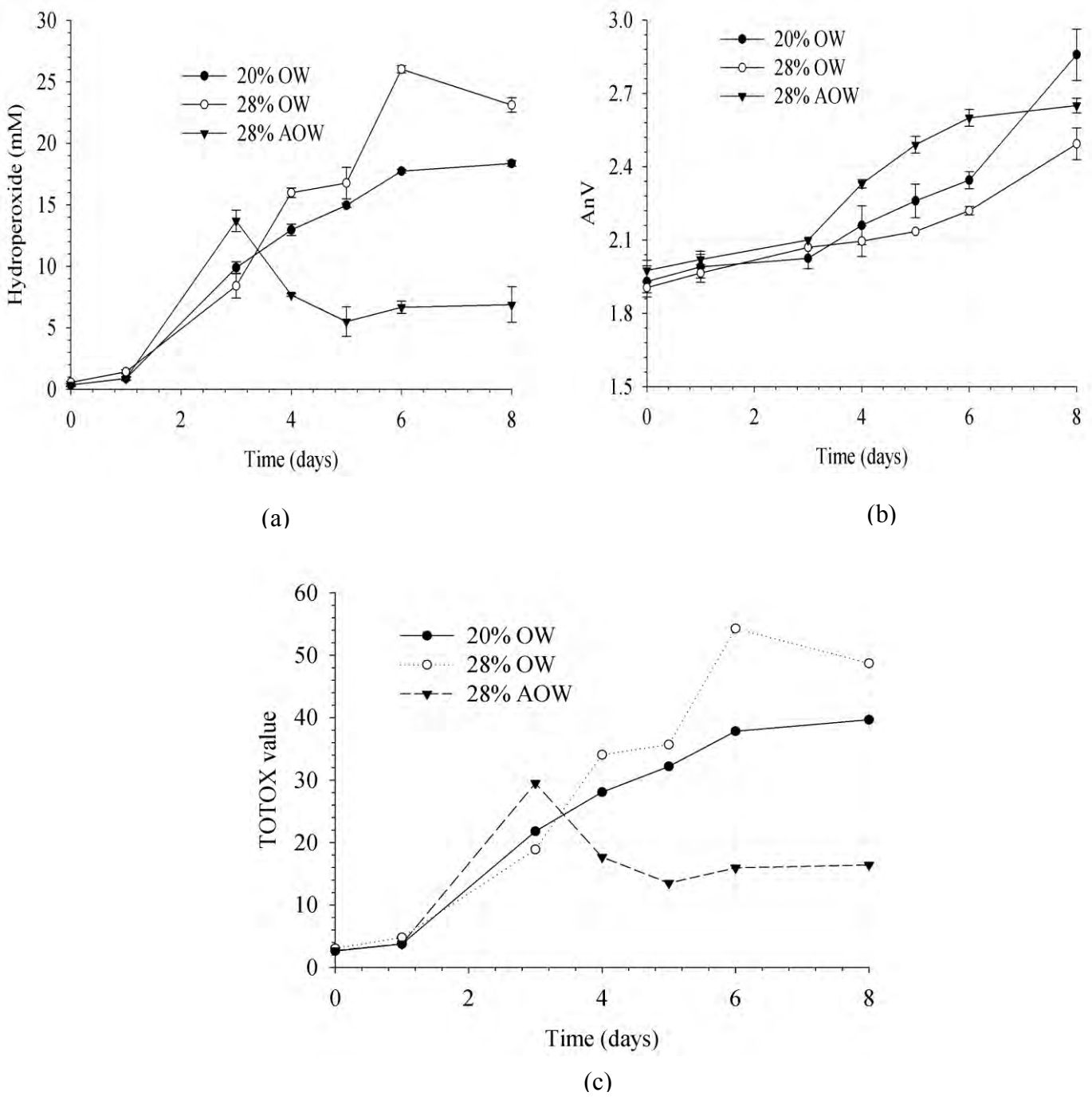

Figure 5-10. Comparison of oxidative stability of a 28% A/O/W (10% air, 18% oil) and 28% O/W emulsion. The 20 % O/W emulsion used for the preparation of the triphasic emulsion is presented as a reference. (a) Formation of hydroperoxides (PV); (b) Formation of secondary oxidation product (aldehydes) express as anisidine value (AnV); (c) Totox Value which is 2PV + AnV, calculated using the average value of PV and AnV. Emulsions were held at 40°C and the oxidative stability monitored over 8 days.

Importantly, the TOTOX value (Figure 5-10c) which is a combination of the PV and AnV, normally used to determine the total oxidative stability of an oil, indicated that the triphasic emulsion prematurely oxidised. However the higher TOTOX value for the A/O/W only persisted for the first three days of storage whereas its O/W emulsion counterpart showed far greater TOTOX value for the remaining time (from four to seven days). This latter period is well correlated to the concomitant change in the pH of the A/O/W emulsions. This serves to lower the pH below the p*I* of the hydrophobin HFBII (4.8) used for the preparation of the AFE. Therefore, it is postulated that, in addition to the possibility of increasing mass transfer (thus detrimentally affect the oxidation rate) the presence of air filled emulsions may also help buffer the oxidation of the triphasic emulsion through oil droplets and pH dependent mechanism suggested below (illustrated by Figure 5-11).

At pH value above the PI of the protein, air cells will be negatively charged and will attract oppositely charged ions from the surrounding aqueous phase. These ions could be the commonly found Fe^{2+}, F^{3+}, Cu^{+} and Cu^{2+} which are all recognised as lipid oxidation promoters (McClements and Decker, 2000). This will then accelerate the oxidation of any oil droplet within the immediate vicinity of air cells. The previous section shows that if the size of droplets is small enough, they will tend to attach to the cell surface. Thus, this may, in part, account for the fact that the initial rate of peroxide formation was high for the triphasic emulsion (first three days, where air cells are negatively charged). Moreover, if the pH value is below the PI of the protein, then the air cell surfaces would carry a positive charge and would thus, repel these metals from the interface towards the aqueous phase. This would reduce the susceptibility of their neighbouring oil droplets to the oxidation. Consequently, the oxidative stability of the A/O/W emulsion could be enhanced by manipulating the pH of the system. Nevertheless, further studies are required to confirm this hypothesis. It should also be

considered amino acids present in the air cell coats and their assistance in inhibiting lipid oxidation in triphasic emulsion by scavenging free radicals (Hu *et al.*, 2003; Elias *et al.*, 2005).

Another mechanism that could also contribute to the sharp decline seen in hydroperoxide concentration between days three and five involves their reactivity with the non absorbed and absorbed protein forming the air cell coats. This possible interaction between hydrophobin and lipid oxidation products was investigated within hydrophobin stabilised O/W systems (see Appendix 6) and is further discussed below.

Hydroperoxide can be degraded as a result of an interaction with proteins or amino acids (McClements and Decker, 2000). The radical transfer takes place through temporary complexes between lipid hydroperoxide (ROOH) and the nitrogen or sulphure of reactive amino acid residues within the protein (PH). The following equation depicts such a reaction:

$$\mathrm{ROOH} + PH \rightarrow [ROOH \cdots HP] \begin{cases} \longrightarrow RO^{\cdot} + P^{\cdot} + HO_2 \\ \searrow RO^{\cdot} + HO^{\cdot} + PH \end{cases} \qquad \text{Eq. 5-1}$$

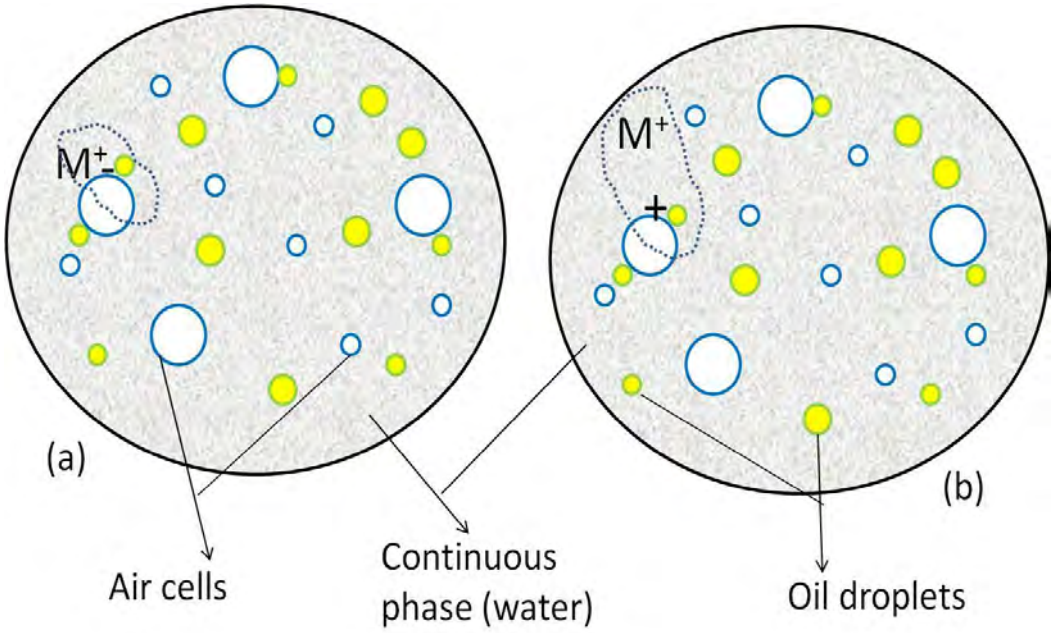

Figure 5-11. Schematic diagram of triphasic emulsion system with pH greater or lower than the p*I* of the protein forming the air cell coats. (a), refer to a negatively charged air cell shell; (b) is the scenario where the air cell coats carry a positive charge. M+ correspond to any transition metal for example, Fe2+ contaminately present.

- *Change in pH during oxidation*

The previous section examined the role of protein in protecting emulsion from oxidation with pH change. This section examines the mechanism behind such changes. The pH of a triphasic A/O/W emulsion decreased from 6.9 (freshly made sample) to 4.6 at day three during storage at 40°C. The pH then stabilised around this value for the rest of the study period, whereas the pH of similar O/W emulsions remained almost unchanged (Figure 5-12). Indeed, Van Ruth *et al.* (1999) did find a decrease for pH of sunflower O/W emulsion stabilised by Tween 60 (from 6.2 to 3.0) during 60 days oxidation and identified the following acids: acetic, propanoic, 2-methylpropanoic, butanoic, pentanoic, hexanoic, heptanoic, octanoic and nonanoic. In the case of the triphasic emulsion three reasons may be considered: (1) acidic compounds generated by lipid oxidation (van Ruth *et al.*, 1999); (2) interactions between lipid

oxidation products and basic amino acid within the protein coats or (3) a combination of (1) and (2).

Although it has been suggested that the progressive oxidation of sunflower oil produces a wide variety of aldehydes, alcohols and acids (Keszler *et al.*, 2000), here the pH of O/W emulsions did not change significantly. Thus, it is unlikely that the acidic compounds produced by oil oxidation are the major contributors to the pH change of the triphasic emulsions. The absolute fate of the oxidation products is unclear as a number of possible reactions they can partake is large. Lipid hydroperoxides and/or secondary products of oxidation are known to physically complex with proteins (see last section of Chapter 6); aldehydes and ketones interact with amino acids via condensation to form Schiff's bases or via typical nucleophilic substitutions. Aldehydes, ketones and alcohols have been shown to interact with soy protein and bovine serum albumin via electrostatic and hydrophobic attractions (Gardner, 1979); with β-lactoglobulin to form fluorescent condensation products and protein polymers (Stapelfeldt and Skibsted, 1994). As more background, it has been demonstrated that a hydrophobic interaction between lipid hydroperoxides and tubulin, a neuron protein, with modification of its methionine and interestingly its cysteine (Kawakami *et al.*, 2000), and the exposure of histidine cysteine and lysine to peroxidised lipid has led to the formation of imidazole lactic acid, imidazole acetic acid, cysteic acid, aspartic acid, α-aminoadipic acid and pipecolic acid.α-aminoadipic acid and pipecolic acid (Gardner, 1979). Therefore, the complex interactions from the incubation of the aldehydes and genetically modified hydrophobins are also in line with above quoted works and showed a decrease in pH of the protein solution with an increase in aldehydes concentration. Also all basic amino acids were modified by these compounds (see Chapter 6). As the hydrophobin HFBII used for the

construction of air filled emulsion contains 8 cysteines (4 cystines), 1 histidine, 1 methionine and 4 lysines it is reasonable to postulate that the same scenario may be occurring here.

To add another level of complexity, it should be noted that, hydroperoxide and most of the secondary product of lipid oxidation are amphiphilic molecules. For example, different peroxidised lipids (free fatty acid, methyl ester and triacyglicerol) will induce a lower surface tension than their nonoxidised counterparts (Nuchi *et al.*, 2002). The implication is that these molecules will orientate in oil/water or air/ water interfaces with their reactive carboxylic acid/carbonyl groups in the aqueous phase. The reactive function would then be adjacent to the adsorbed protein and may react with any basic amino acids and N-terminus amino acid residues, thereby further reducing the pH. It is a plausible conclusion that the predominant mechanism underpinning the decline in pH seen in the triphasic emulsion is the interaction between lipid oxidation products and proteins (unabsorbed and absorbed protein) at air cell surfaces. This is in addition to degradation of amino acids with generation of acid compounds albeit to a lower extent.

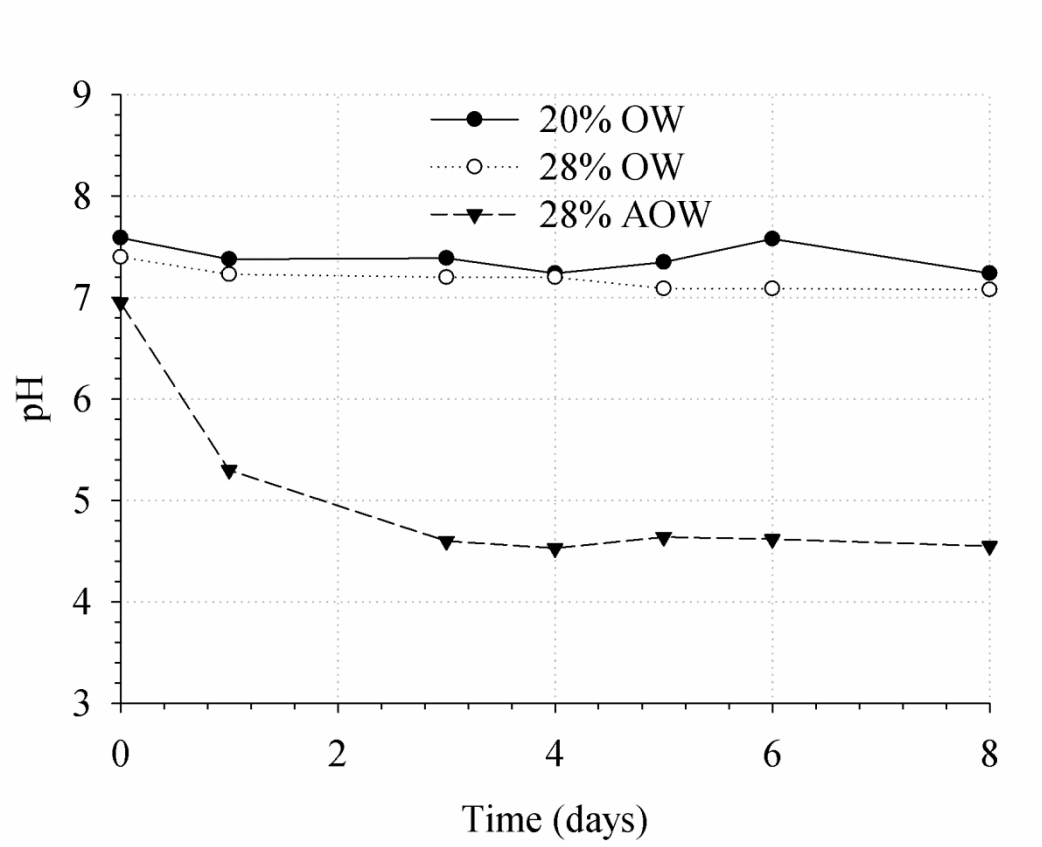

Figure 5-12. pH changes during the oxidation of a 28% A/O/W (10% air, 18% oil), a 28% O/W and the 20 % O/W emulsions used for the preparation of A/O/W. Emulsions were held at 40°C and the oxidative stability monitored over 8 days. The error bars are within points. Data correspond to the average from three replicates.

5.4. Probing the mouth-feel and the perceived indulgence of the triphasic emulsion

After the investigation of the various aspects of the stability of HFBII-AFEs and their tri-phasic emulsions the next question is: are tri-phasic A/O/W emulsions likely to have the same mouth-feel and perceived indulgence as a traditional O/W emulsion? In order to answer this question, the rheological and tribological behaviours of the A/O/W were compared to those of similar O/W emulsions. This study is based on the fact that sensory attributes such as smoothness, slipperiness, thickness, fattiness, and creaminess are inversely correlated with the

friction between surfaces lubricated by semi-solid foods (Malone *et al.*, 2003; de Wijk and Prinz, 2005; de Hoog *et al.*, 2006; de Wijk and Prinz, 2006). Most of those attributes have also been shown to be influenced by the bulk rheological properties (Akhtar *et al.*, 2006; de Wijk *et al.*, 2006; van Aken and de Hoog, 2009).

It should be noted that some of data presented and discussed in these section have been used in the publication by Tchuenbou-Magaia and Cox, (2011) and can be found in Appendix 1(CD).

In the first set of experiments, a 28 % O/W was constructed to produce oil droplets with a mean size and size distribution as close as possible to those of the A/O/W (10 % air and 18 % oil, see Table 5-3). Figure 5-13 shows the comparisons between the flow behaviour of the 28% O/W emulsions and the 28% tri-phasic emulsion (for three different storage times at ≈ 8°C). This figure demonstrates not only the close rheological match between the O/W emulsion and the tri-phasic emulsions, but also, confirms the long term textural stability of the tri-phasic system. Interestingly, according to Sherman (1983), the viscosity of an emulsion should decrease if there is droplet coalescence. Here there was no noticeable difference between the viscosity curves of three days, 48 days and 140 days old triphasic A/O/W emulsions.

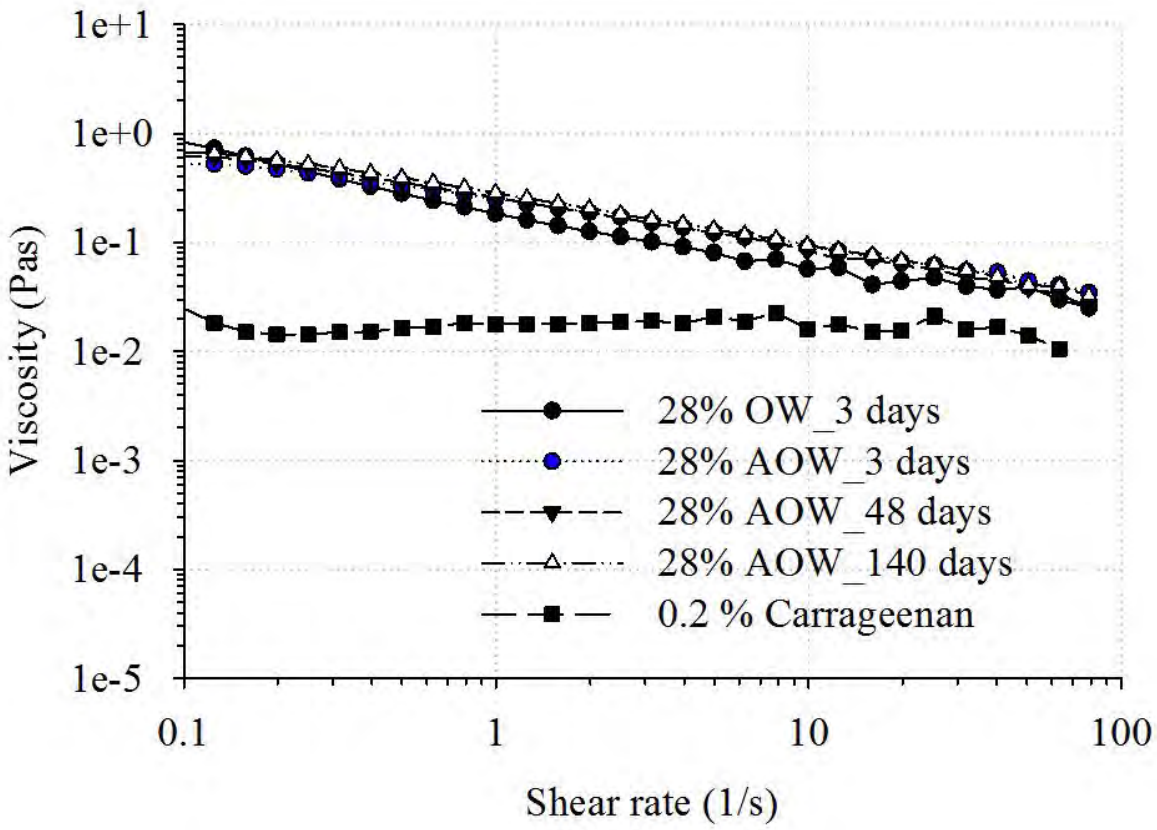

Figure 5-13. Comparison between the flow properties of 28% O/W and 28% A/O/W: a log-log plot of viscosity against shear rate.

The lubrication properties of O/W and A/O/W emulsions as measured via tribological analysis are presented in Figure 5-14. As mentioned in the material and methods chapter, the friction measurements were performed three times with an entrainment speed varying from 1 to 1000 mm/s without unloading the ball in order to mimic the dynamic process of continuous oral breakdown of food structure closely and, in the hope of providing an accurate picture of the dynamic lubrication properties of the product. Also it was assumed that, if oral processing starts from the first bite till after swallowing/clearing, the friction as function of speed curve of run "n" if it is equal to the following run "n+1", would indicate the in-mouth friction (in-mouth sensation) of a given product. It is evident from Figure 5-14 that there is a lower

friction coefficient for the 28 % A/O/W when compared to the standard 28 % O/W emulsion for the first run. The friction curve of both emulsions was similar for the second run of friction measurement. It is apparent that the AFE has contributed to lowering the friction coefficient and thus to the perceived creaminess and fattiness. These observations might be explained by one or more of the following:

(1) The presence of air cells in the triphasic emulsion induces more droplet coalescence upon shearing, in the same way as in-mouth aeration of emulsion has been described (Benjamins *et al.*, 2009). This results in more oil release and therefore, more lubrication. For example, an increased sensitivity to coalescence of oil droplets due to a partial break down of air cells upon shearing. Shear may also induce/increase the amount of attached oil droplets to the protein-covered air cell surface and interfacial floculation of oil droplets with partial coalesence of the flocs (Hotrum *et al.*, 2005). This extra coalescence may also be due to the smallest air cells physically acting as small robust particles and piercing the emulsifier film surrounding the larger oil droplets during shearing and allowing oil release. However, further shear may result in the re-emulsification of any adsorbed oil and its removal from the surfaces, thereby re-increasing the friction. This was seen for the A/O/W emulsion during the second ramp of the friction measurement.

(2) Shear has induced oil droplets spreading at the air cell surfaces and oil deposition at the contact zone. As mentioned earlier, it has been demonstrated that β-lactoglobulin and glycinin film at the air/water interface fracture when exposed to large deformation and shear. This promotes the simultaneous entry and spreading of oil droplets in the crack area (Hotrum *et al.*, 2003). Although the viscoelastic properties of HBII are far greater than those of these proteins, the same phenomena may happen.

(3) The AFEs, may fill the gap between the contact zones of the tribometer allowing extra lubrication (see Figure 7-20, Chapter 7). It has been reported that the perception of creaminess increases when small particles less than 4-7 μm were incorporated into the food system (Kilcast and Clegg, 2002) and most of the air cells used in this work were below this range of size.

(4) Situations (1) and (2) and (3) concurrently occur.

Whatever the mechanism involved, these results suggest that a triphasic A/O/W emulsion could have a similar or even better mouth-feel than the original full fat version, but with lower fat (calorific) content. Therefore AFEs may offer a reasonable approach for reducing the fat and calorie content of emulsion based food products such as mayonnaise, dressings, sandwich spreads, dips and sauces without compromising their sensory attributes.

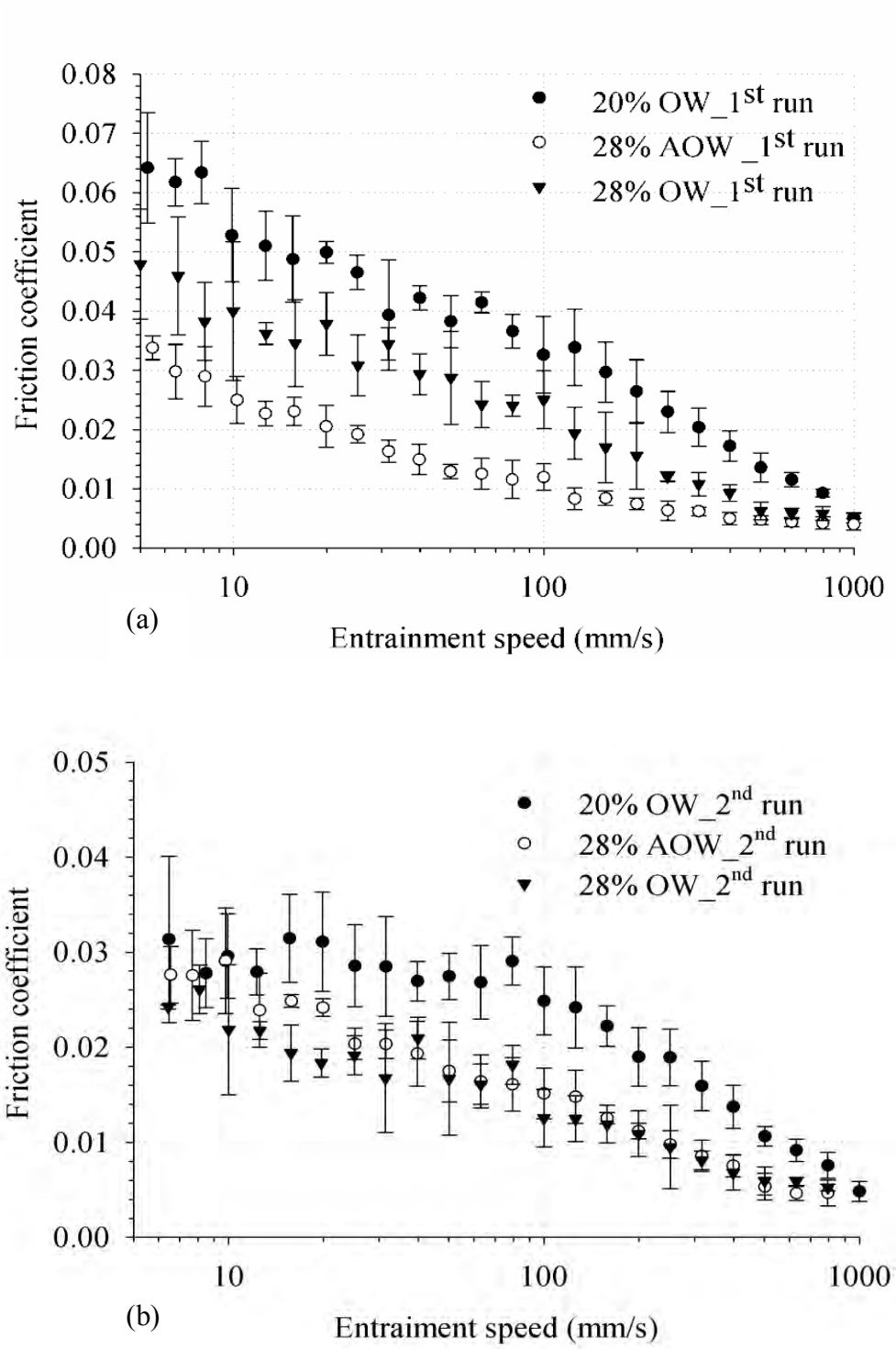

Figure 5-14. Comparison of tribological behaviour of air based triphasic emulsion (A/O/W) and O/W emulsions. (a) and (b) 28 % O/W and 28 % A/O/W emulsions formulated with 0.5% Tween 60 and containing 0.2% iota-Carrageenan for the first and second cycle of the friction measurement, respectively. The curve of the parent 20 % used for their production is shown as a reference. The error bars denote standard deviations from 4 repeats.

In order to further assess the possible use of AFE as an effective ingredient for fat reduction in traditional high fat emulsion based products such as dressings and mayonnaise, a second triphasic emulsion was constructed with ingredients commonly used in the industrial formulation of dressings and mayonnaise. A 46 % A/O/W emulsion (36 % oil and 10 % air by volume) was made from a 40 % O/W emulsion stabilised with 1% WPI and 0.2% xanthan gum as a thickener. Figure 5-15 shows a comparison between the flow curves of a triphasic A/O/W with 46 % total phase volume (10% Air and 36% by volume) and the 40% O/W emulsion. Here commercial mayonnaise and dressings were used as reference full fat products to the low fat air based versions. It must be admitted that the rheological and tribological properties of such complex food system depend not only on the oil content and oil droplet size but also on other components such as hydrocolloids and other particles. Commercial mayonnaise and dressings might contain different types and amounts of these different elements. Nevertheless their rheological and tribological properties served as a good comparison and might help direct the development of future air based versions, with comparable behaviour and indeed recognisable mouth-feel and consumer acceptance.

For the rheology data, there is disparity. The “up” and the “down” curves overlap for 40% O/W emulsion whilst the triphasic A/O/W showed a hysteresis loop similar to that of the dressing and mayonnaise; but to much more lesser extent (Figure 5-15). Although such a hysteresis loop could indicate an irreversible change in sample structure upon shearing, another possible and plausible explanation is the presence of weak attractive forces between particles giving a weak network. These possible interactions between air cell protein coats and the other components (xanthan and WPI) with formation of weak gel like behaviour have been discussed (Mewis and Wagner, 2009). More explicitly the A/O/W emulsions made with a 20% O/W emulsion stabilised with a non-ionic surfactant and Iota carageenan (as described

earlier) showed a similar behaviour. They were more stable against creaming due to the interactions between protein shell and other components.

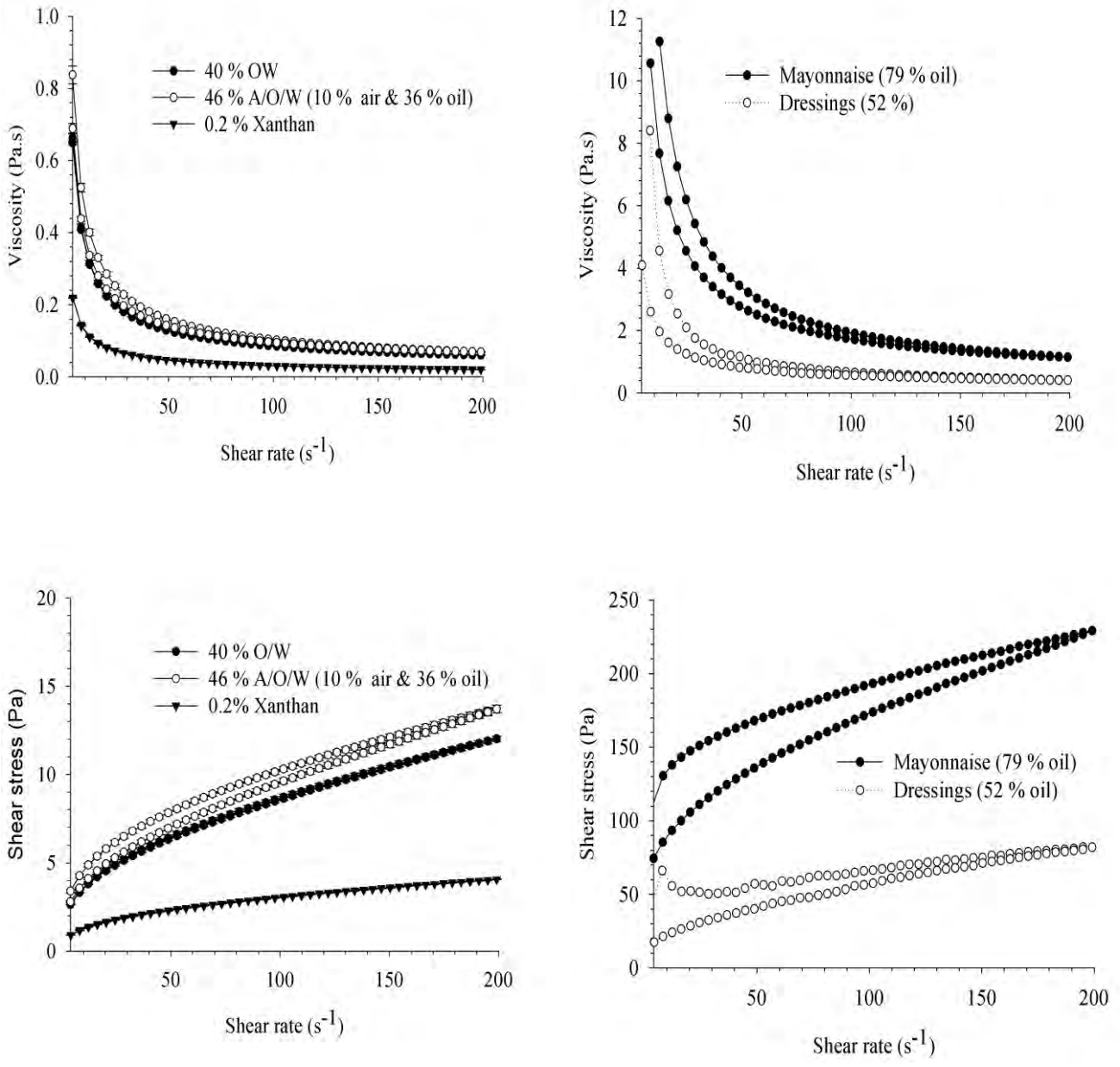

Figure 5-15. Comparison between the flow properties of 40% O/W and 46 % A/O/W: linear scale plots of viscosity or shear stress against shear rate ("up" and "down" curves). The supermarket mayonnaise and dressing curves are shown as a reference.

Furthermore, the tribological study of these emulsions suggested that the friction coefficient of the triphasic A/O/W emulsion was lower than that of its parent O/W emulsion (Figure 5-16). However, and unexpectedly, the friction coefficient of the 46 % A/O/W and its parent 40 % O/W emulsion were higher than that of the 28 % A/O/W and its parent 20 % O/W emulsion; the boundary friction of 46 % A/O/W was about three times that of 28 % A/O/W This triggered a further study of the lubrication properties of the emulsifiers and polysaccharides, at the concentrations used, in the formulation. 0.5 % Tween 60 showed lower boundary friction compared to 1% WPI (Figure 5-17a). Conversely, there was no apparent difference in the friction curve of 0.2 % xanthan gum and 0.2 % Iota carrageenan (Figure 5-17b), although the xanthan solution was far more viscous than that of the carrageenan (Figure 5-18). These findings suggest that the use of the different thickeners was not the absolute cause of the observed differences in friction behaviour, but that the emulsifier may still play a pivotal role in the differences. It is worth mentioning that the mixture of xanthan-WPI processed in the high pressure homogeniser in the same conditions as those used for the construction of emulsion showed a relatively higher friction coefficient than the mixture prepared with a laboratory magnetic stirrer, whereas no difference was observed in the case of a Tween 60-carrageenan mixture (Figure 5-17c-d). Similarly, the viscosity of the xanthan-WPI processed in the high pressure homogeniser was relatively lower than that of the non treated mixture.

Another factor that may account for the difference in the lubricative properties of these emulsions is the oil droplet size. The 40 % O/W emulsion had an average oil droplet size of 3 µm, whereas the droplet size of the 20 % emulsion was about 0.9 µm (see Appendex 1, Tchuenbou-Magaia *et al.* (2010); Tchuenbou-Magaia and Cox (2011)). The critical film thickness under the boundary lubrication regime is reported between 0.5 and 1 µm (Malone *et*

al., 2003). Therefore the 3 µm droplet must break up or at least deform before entering the contact zone of the tribometer. The low applied shear at low entrainment speeds may not be enough to allow for oil droplet break up or deformation. On the other hand a 0.9 µm droplet might freely enter the contact zone and physically stop the tribo-pair surfaces from contacting thereby efficiently reducing the friction. These findings are in agreement with the work of de Wijk and Prinz (2005) that showed an increase of the friction coefficient with the increase of the oil droplets size.

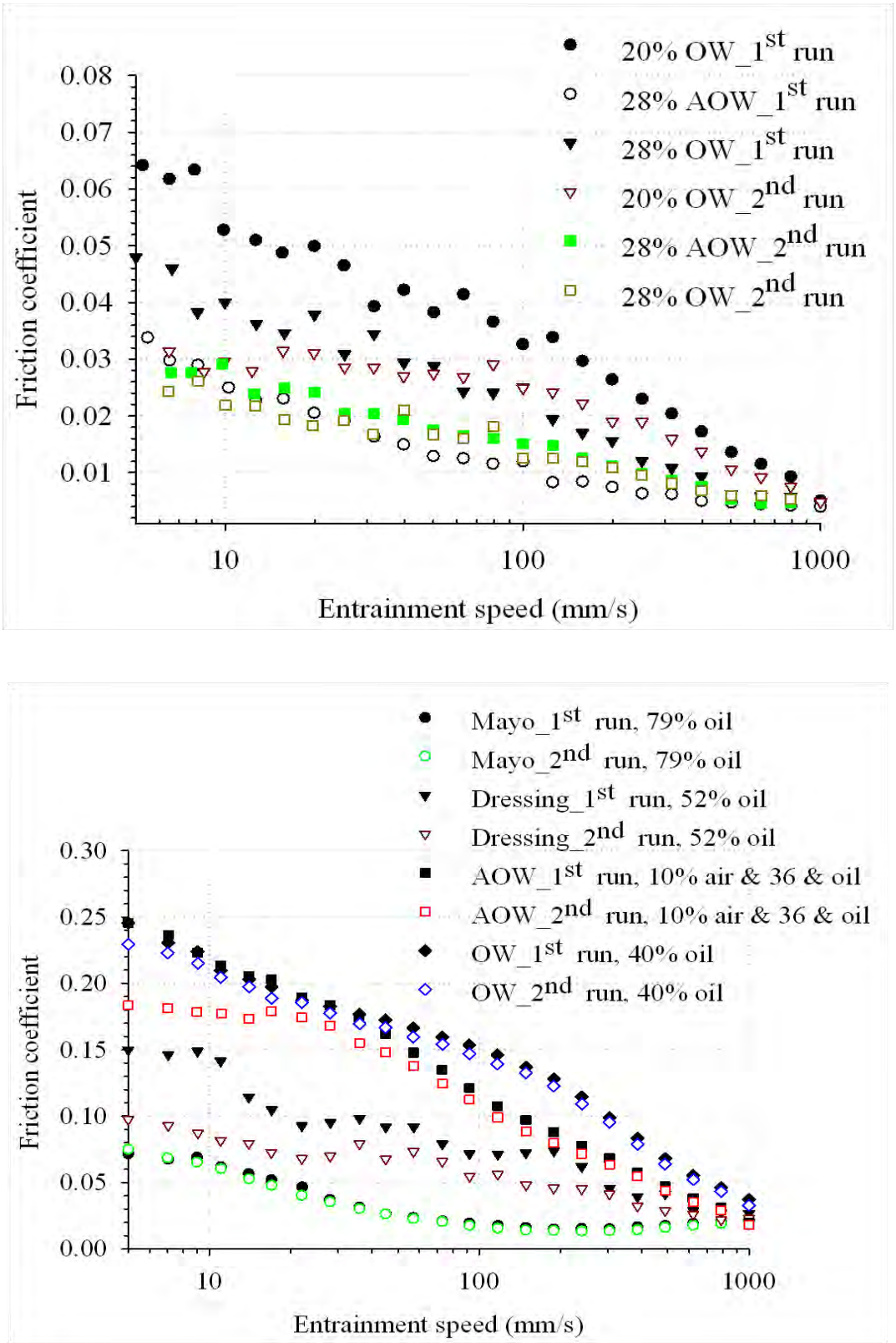

Figure 5-16. Comparison of tribological behaviour of different emulsions and the supermarket dressings and mayonnaise.

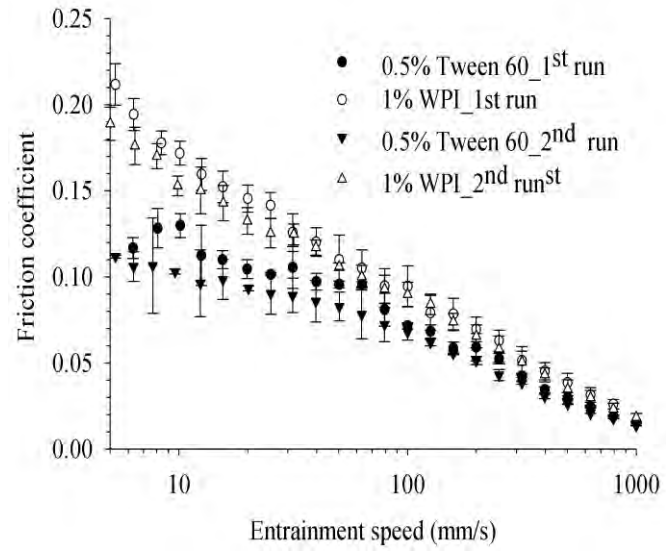

(a)

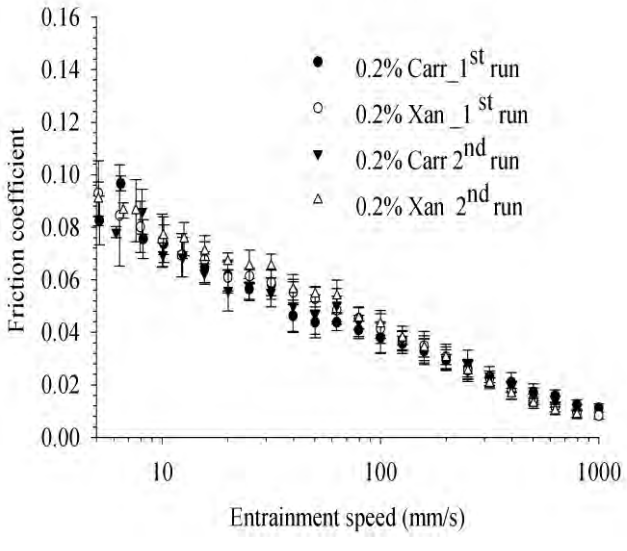

(b)

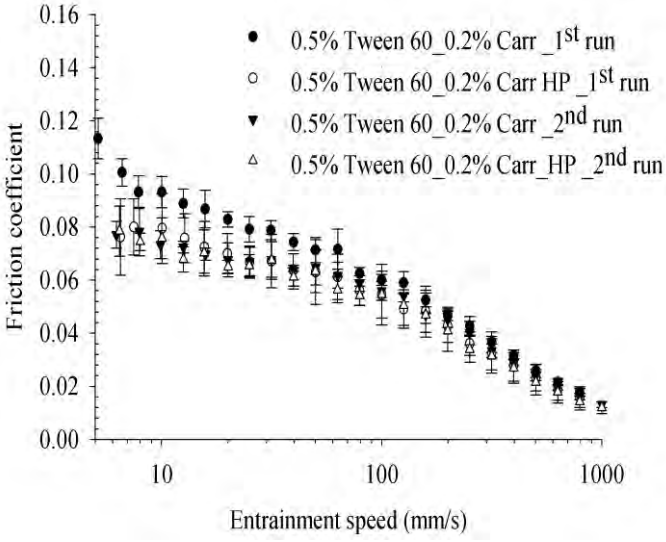

(c)

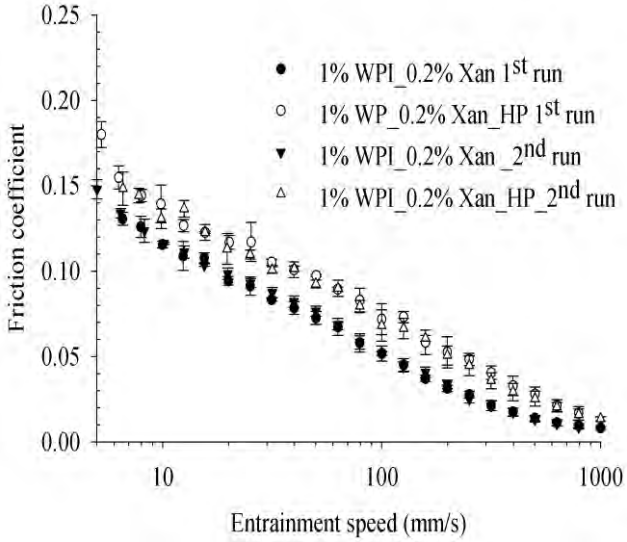

(d)

Figure 5-17. Comparison of tribological behaviour of emulsifiers and thickeners used in the formulation of the various emulsions. Tween 60_Carr and Tween 60_Carr_HP correspond to the mixture of Tween 60 and carrageenan prepared with a laboratory magnetic stirrer and processed in the high pressure homogeniser in the same conditions as those used for the construction of emulsion. WPI_Xan_HP and WPI_Xan are mixtures of Xanthan and whey protein isolate for treated and non treated under emulsification conditions, respectively.

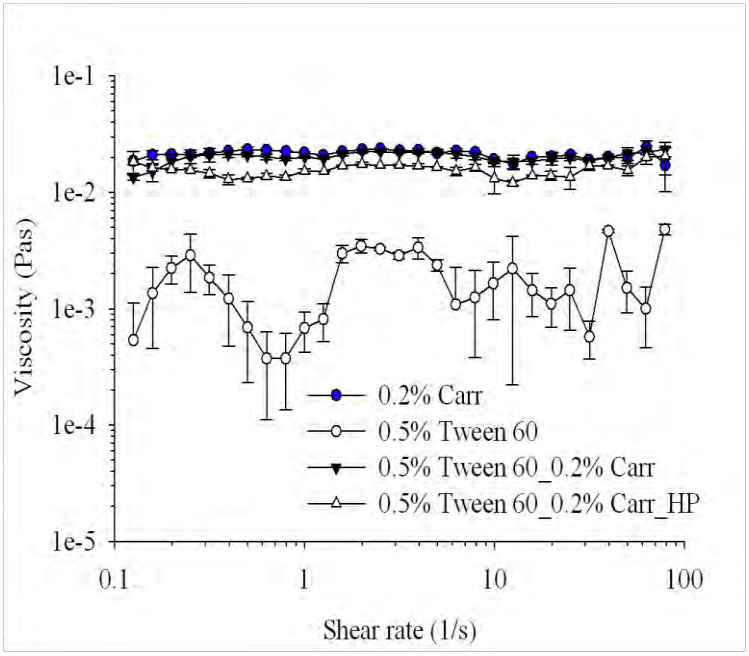

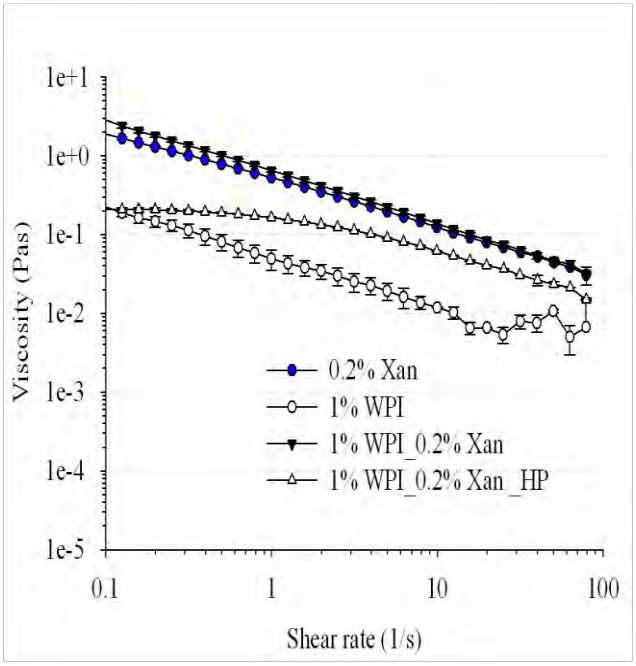

Figure 5-18. Comparison of flow curve (viscosity) of emulsifiers and tickeners used in the formulation of the emulsions. Tween 60_Carr and Tween 60_Carr_HP correspond to the mixture of Tween 60 and carrageenan prepared with a laboratory magnetic stirrer and processed in the high pressure homogeniser in the same conditions as those used for the construction of emulsion, respectively. WPI_Xan_HP and WPI_Xan are mixtures of Xanthan and whey protein isolate for treated and non treated under emulsification conditions.

5.5. Conclusion and remarks

A hydrophobin HFBII rich extract has been used to stabilise air inside a protein coat formed through a sonochemical process. The size distribution of air cells was broad with size ranging from 0.1 to 100 µm, but with the majority of the air cells falling within a 0.5- 10 µm size range. This was dependent, to some extent, on the protein concentration in the extract. These suspensions of air cells were termed “air filled emulsions” (AFEs). All indications are that AFEs could be successful for producing reduced fat food products. The reason for this is that the air cells in air filled emulsions have a robust surface structure, provided by the hydrophobin film, and this helps prevent disproportionation and ripening over a substantial periods of time. The air cells were capable of surviving high shear processing steps, e.g. for

up to seven minutes shearing in a Silverson high shear mixer. Air cells resisted oil destabilisation and, again show excellent stability in triphasic A/O/W systems (made by diluting an O/W emulsion with a concentrated AFE). Indeed, the triphasic emulsion was stable for months with regard to the particle size and, this was attributed to the combination of a strong hydrophobin film and a possible existence of a thin film (pseudoemulsion) between approaching oil droplet and air cell which act as a kinetic barrier to droplet entering the air/water interface. Also it was postulated that the presence of oil droplets and thickener may contribute to the increase in the apparent thickness of the air cell shells, leading to further decrease in Oswald ripening. However there seems to be a critical ratio of AFE/OW emulsion, for the formulation of the triphasic A/O/W emulsion above which the system becomes less stable. Likewise the size of oil droplets may also play a role. These last two hypothesises deserve a more systematic investigation which time did not permit here.

The triphasic A/O/W emulsions show good stability against creaming when compared to an O/W emulsion. This is due to an interaction between the air cells, via their protein shells and other components of the system; this results in a weak network structure. Such a finding suggests that less thickener may be needed for the formulation of the triphasic emulsion as compared to that of the O/W emulsion version for a similar visual appearance and texture. Unfortunately, the triphasic A/O/W emulsion shows premature lipid oxidation when compared to the standard O/W emulsion. However the ability of hydrophobin to complex lipid oxidation products leads to the eventual quenching of the propagation of free radical chain reactions and may prevent/reduce flavour deterioration. A schematic design showing how the triphasic A/O/W emulsion can be manipulated through adapting the pH and the oil droplets size in order to reduce oxidation rate of the system has been proposed (Figure 5-11). Again, this requires further systematic investigation.

Rheological and tribological results suggest that the triphasic A/O/W could be manipulated to be similar to the standard oil water emulsion in terms of lubrication behaviour and sensory perception. It is postulated that AFEs may contribute to lower the friction in several ways. Air cells may adsorb on the surfaces, via the protein shells or can be entrained into the narrow gap between the tribo-pair and so, by extension, the tongue and palate. But this is true, only if their size is below the critical boundary film thickness. Furthermore, air cells in the triphasic A/O/W emulsion might induce extra coalescence and droplets spreading at air surfaces. This leads to oil deposition and results in a further reduction of the friction.

CHAPTER 6

INTERFACIAL AND EMULSIFYING BEHAVIOUR OF RECOMBINANTLY PRODUCED HYDROPHOBINS AND THEIR EMULSION STABILITY

6.1. Introduction

This chapter focuses on the interfacial and emulsifying properties of commercially produced recombinant hydrophobins, H*protein A and H*protein B. These proteins consist of Class I hydrophobin DewA and a protein from *Bacillus subtilis* (protein YaaD). H*protein A is approximately 47 kDa and has attached the entire protein YaaD, whereas H*Protein B is approximately 19 kDa and has a truncated protein yaaD (Wohlleben *et al.*, 2010). H*proteins are commercially produced with a yield of thousand fold greater than that obtained from the native source presented in Chapter 4. But these recombinant proteins are not intended for food use but do provide a mechanism of proof of principle. However, due to their Class, they only favour the formation of O/W and not A/W emulsions.

In this chapter, four main specific points will be presented and discussed. These are:

- The adsorption behaviour at air/water and triglyceride oil/water interfaces of the modified Class I hydrophobins. A kinetic analysis at different concentration and pHs will also be given. The selection of the pHs studied was based upon the isolectric point of the protein, determined by electropheric mobility analysis.
- The effect of pH of the H*proteins upon the size and size distribution of a model oil/water emulsion.

- The effect of emulsification processes on the emulsion droplets size and stability. This includes physical and oxidative stability.
- Investigation into the possible formation of complexes between hydrophobins and lipid oxidation products, and the potential contribution of amino acids. This will use the H*proteins as a model system and aim for confirmation of the hypothesis stated in Chapter 5 (section 5.2.4).

6.2. Electrophoretic mobility

The electrophoretic mobility of H*proteins in aqueous solution as a function of pH is shown in Figure 6-1. The experimentally derived isoelectric point (PI) of both proteins is pH ≈ 4.9, and in neutral solutions the proteins are negatively charged. This PI is in the range of that of a number of naturally occurred hydrophobins, such as VMH1-1 (4.78), VMH1-2 (4.85) VMH3-2 (5.21) and Fbh1 (4.77) from *Pleurotus ostreatus* (Penas *et al.*, 1998; Penas *et al.*, 2002) and the HFBII from *Trichoderma resei*, 4.8 (Cox *et al.*, 2007). As stated previously, H*proteins are fusion proteins that consist of hydrophobin DewA (a class I hydrophobin) and a peptide from *Bacillus subtilis*. Hydrophobin DewA is located in the wall of *Aspergillus nidulans* conidiospores (Stringer and Timberlake, 1995). Interestingly, the analysis of the electrophoretic mobility of the *Aspergillus nidulans* conidiospores has shown that their PI is about 4.6 (Dynesen and Nielsen, 2003), which is comparable to that of H*proteins.

It was observed that both proteins readily form aggregates at pHs above pH3 and below pH 6.0, and as a result any protein solution becomes turbid between these values. There was a considerable increase in the size of the aggregates at pH around 4 and 5 (Figure 6-2). Although the formation of protein aggregates could be explained by the protein charge

neutralization at pHs close to the isoelectric point, the fact that the pH window at which the protein spontaneously aggregates is broad, is an indication of the propensity to self-assemble. This characteristic is known of both Class I and Class II hydrophobins (Stroud *et al.*, 2003; Cox *et al.*, 2007). For example SC3 in solution and in absence of any interface, slowly self associates in a time-dependent manner, into large irregularly shaped macromolecules (Stroud *et al.*, 2003). Moreover, the results reported here are consistent with previous works on H*proteins (Wohlleben *et al.*, 2010) and confirm that both fusion proteins possess the main feature of hydrophobin. Therefore it is interesting to investigate the adsorption behaviour of H*proteins at their natural pH, at pH 6 and pH 3.

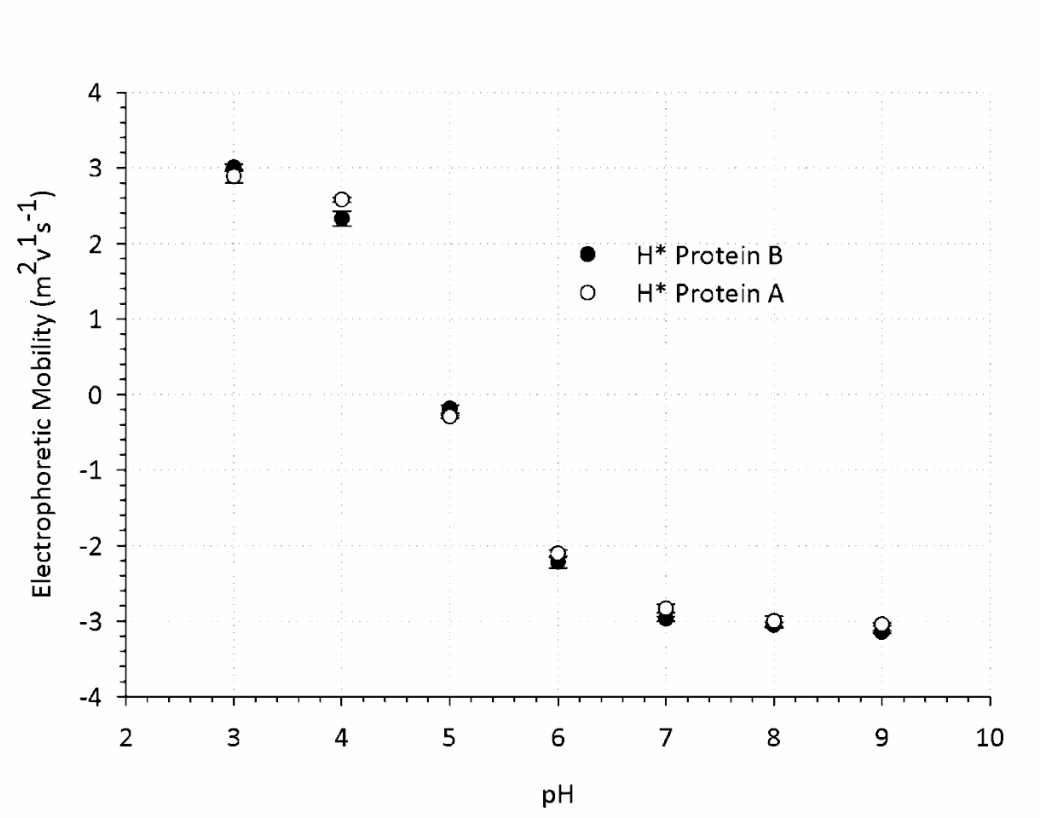

Figure 6-1. Electrophoretic mobility (Ue) as a function of pH for a solution of 0.1 wt % H*Protein A and H*Protein B showing the isoelectric point of both proteins to be at pH ≈4.9.

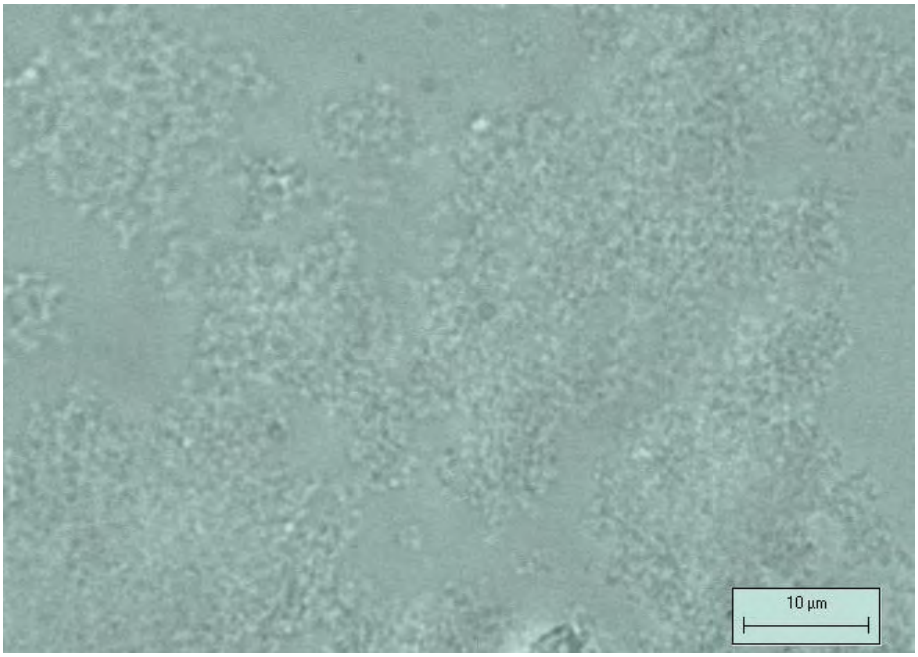

Figure 6-2. Typical micrograph of H* protein aggregates in solution (Both proteins form large aggregates at pH around 4-5).

6.3. Adsorption behaviour of H*proteins at interfaces and a kinetic analysis

6.3.1. Air/water interfaces

The dynamic surface tension measurements were performed at 25 ± 1°C for the H*proteins at the following concentrations: 0.005, 0.01, 0.05 and 0.1% (wt/wt); at their natural pH, pH 3 and pH 6. The natural pH is the final pH of the protein once dissolved in the distilled water, and was 7.73 for 0.1% H* protein A and 7.63 for H* protein B. Figure 6-3 Figure 6-4 depict the dynamic surface tension as function of time. As expected there is a decrease in surface tension with the increase in the protein concentration (Figure 6-3). The surface tension was lowered slightly more by H*protein A than by H*protein B, especially at lower concentrations. At concentrations 5x 10^{-3} and 10^{-2} % (wt/wt), the dynamic surface tension

curves of both the H*proteins show induction periods (see section 2.2, Chapter 2) where the surface tension, close to that of the water remains virtually constant prior to the onset of the decrease. These were about three minutes and six minutes at 5x 10^{-3} %, 1.3 minutes and three minutes at 10^{-2}%, for H*protein A and H*protein B, respectively. The induction period has been reported in several publications for proteins and long chain surfactants. For example, 80 minutes for 1.3 x 10^{-4} % SC3 and 10s for 10^{-3} % SC3 (Corvis *et al.*, 2006), 2.1 minutes for 10^{-3} % wt/wt sunflower protein isolate (Miñones Conde and Rodríguez Patino, 2007), one minute for 10^{-2} % wt/wt β-casein and 40 mins for 10^{-2} % wt/wt Lysozyme (Tripp *et al.*, 1995) have been reported. However, Rodríguez Niño *et al.* (2005) reported no induction time for 10^{-2} % wt/wt caseinate, 10^{-2} % wt/wt β-conglycin and 10^{-2} % wt/wt β-glycinin at pH 7, but did find an induction time for these system of about 1 min, 58 mins and 98 mins when at pH 5 i.e. close to their isoelectric point. Interestingly, these results show the differences in the absorption kinectic between the Class I and Class II Hydrophobins. And the values above should be contrasted against the data of HFBII at 10^{-3}% wt/wt where no induction time was observed (see Chapter 4 and Askolin *et al.* (2006)). These incredibly rapid kinetics of adsorption for the Class II hydrophobins, and especially HFBII show why they are capable of stabilising air cells and not the Class I hydrophobins and other common proteins.

From these literature data, it is also apparent that the induction period for H*proteins is in the same order of magnitude as that of random coil milk proteins (Caseinate and β-casein) but longer than that for the SC3 hydrophobin. SC3 and H*proteins have analogous self association behaviour in solution (Wohlleben *et al.*, 2010) and here it is not clear whether the longer induction period observed for H*protein is linked to the presence of impurities. Such impurities might constitute a barrier to a more rapid absorption (as exploited in Chapter 5) or is due to an intrinsic difference between SC3 and the H*proteins. The physics of induction

period are related to the protein flexibility, conformation changes and to strong intermolecular attractions (Lin *et al.*, 1991; Zangi *et al.*, 2002). This point is discussed at the end of this section. At higher concentrations (from 0.05 % w/w) no induction period was observed and the initial slopes of the surface tension curves are steeper but to a slightly lesser extent for H*protein B as compared to H*protein A. Further increases in protein concentration resulted in no apparent difference between the dynamic surface tension curve of H*protein A and H*protein B.

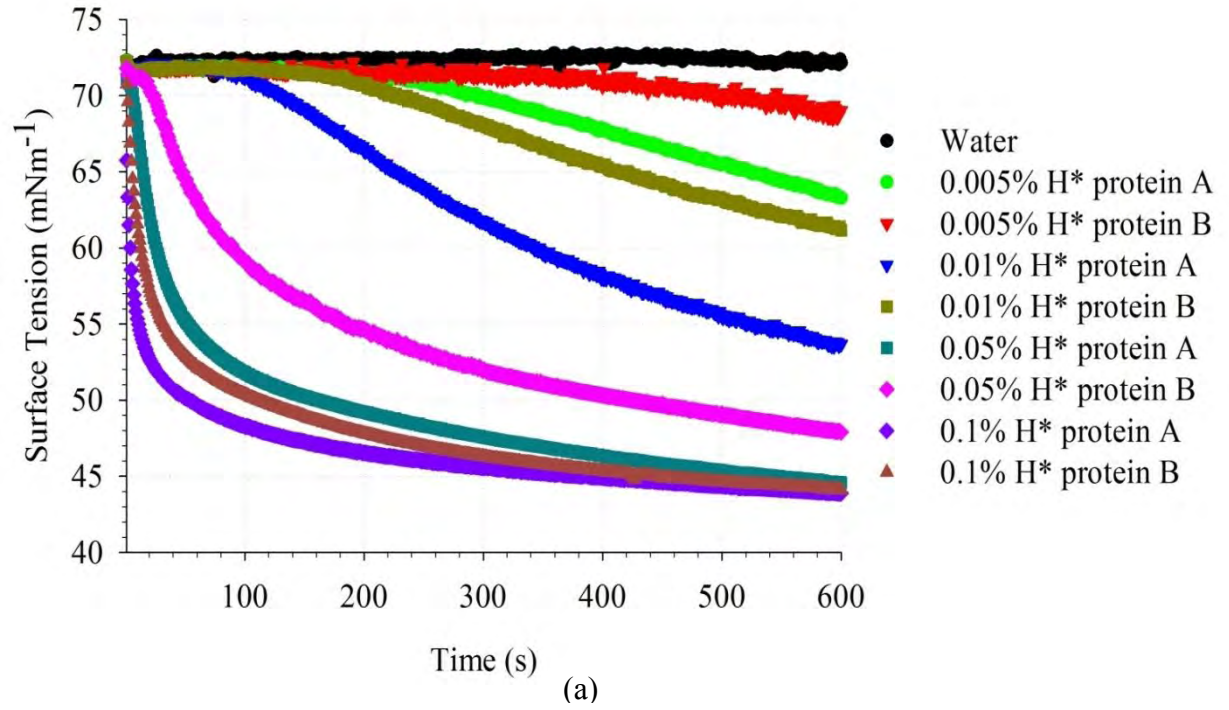

(a)

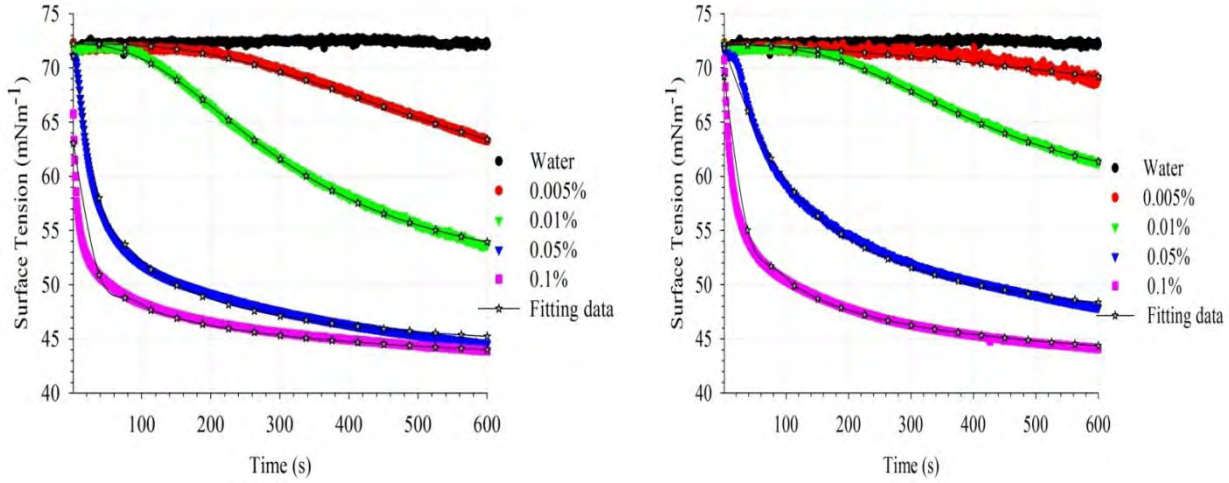

(b) (c)

Figure 6-3. Dynamic surface tension of different concentrations (% wt/wt) of H*proteins (a). (b), H*protein A; (c), H*protein B. The distilled water used for protein dispersion is showed as reference. The gray stars connected with line refer to the fitting and the parameters are given in Table 6-1.

Figure 6-4 shows the pH-dependence of surface tension of H*proteins at 0.05%. For each H*protein, the surface tension curve at pH 3 is similar to that obtained at their natural pH (pH about 7.7). The surface tension was lower at pH 6 when compared to other pHs. This pH effect seems to be more pronounced for H*protein B where the surface tension is significantly lower at pH 6 than at the other pHs studied. Returning to Figure 6-1, which is the electrophoretic mobility of H*proteins as a function of pH, and assuming that the mobility of a protein is directly proportional to the electrostatic force on its surface (i.e. net charge), it can be deduced that the net charge of H*protein at pH 3 and at their natural pH would be almost identical but opposite; i.e. the protein is positively charged at pH 3 and negatively charged at its natural pH. H*proteins are less charged at pH 6 when compared to pH 3 and pHs between 7 and 9. Therefore, the protein net charge may be playing a role here (see later on this matter).

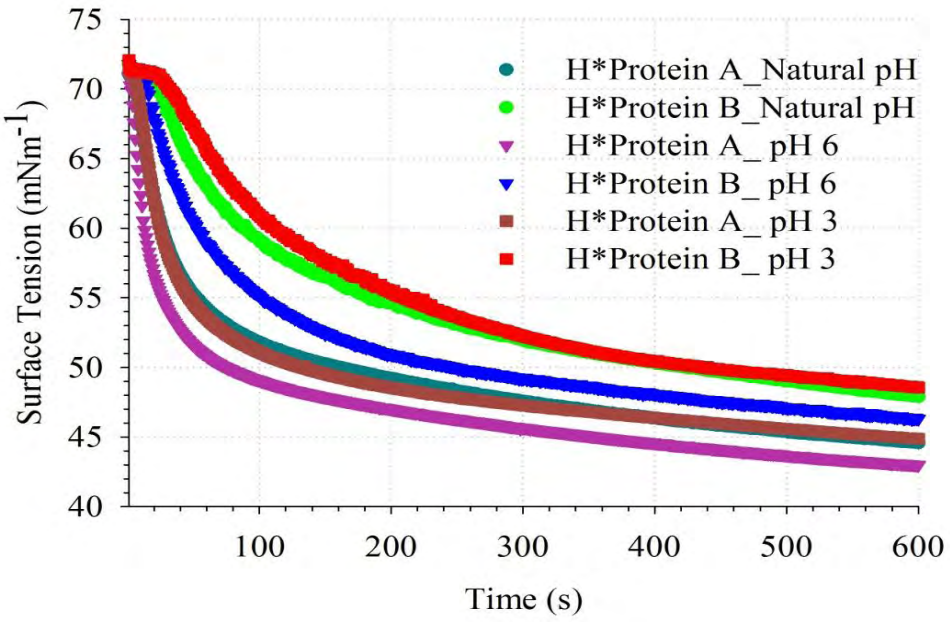

(a)

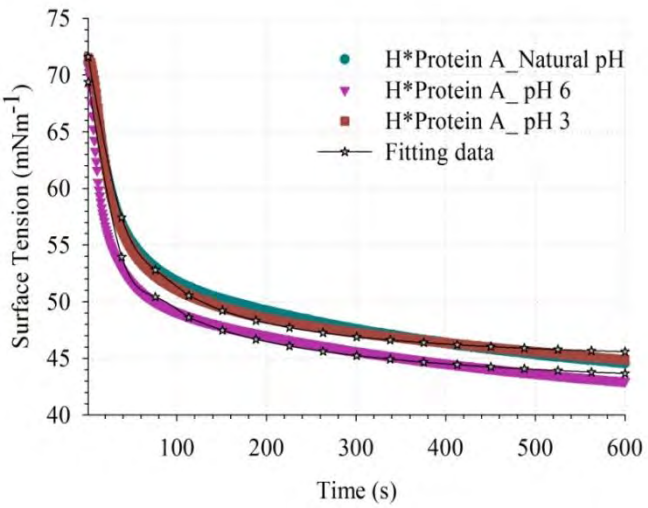

(b)

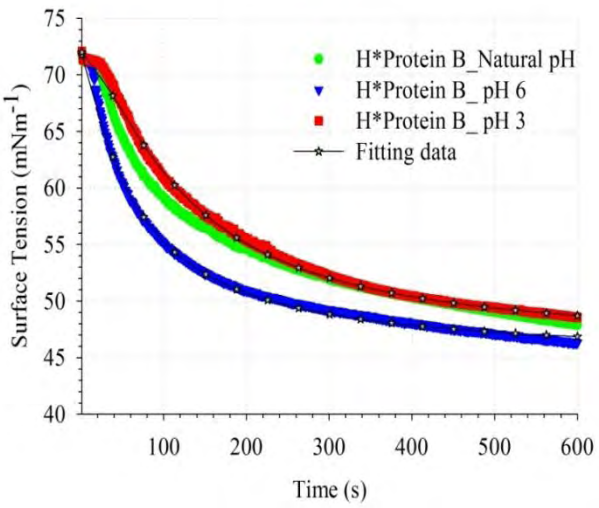

(c)

Figure 6-4. Dynamic surface tension of 0.05% H*protein A and H*protein B at different pHs (a). (b), protein A; (c), H*protein B. The natural pH is about 7.63 for H* protein B and 7.73 for H* protein A. The gray stars connected with line refer to the fitting and the parameters are given in table 6.1. For clarity reasons only the fitting data for samples at pH 6 and 3 are presented in this figure and for those at their natural pH one may refer to Figure 6.3.

In order to generate quantitative information about the adsorption kinetic of the H*proteins at an air/water interface the experimental data was fitted to the Hua-Rosen equation (Hua and

Rosen, 1991), as detailed in Chapter 3 section 5. The kinetic parameters γ_m, t*, n and V_{max} obtained from this are listed in Table 6-1. For comparison, the results of Tripp *et al.* (1995) for a range of proteins with different physical and structural properties and, the data of Deleu *et al.* (1999) for Surfactin, a lipopeptide from *Bacillus subtilus* are also presented. As observed from the dynamic surface tension curve (Figure 6-3), the fit to the Hua-Rosen equation failed for the concentration of 0.005% (w/w) H*protein B. This could presumably be due to the long induction time observed for this protein. Broadly, the γ_m (the surface tension at mesoequilibrium, where the surface tension shows only a minor change with time) and the half-time (t*) required for reaching γ_m decrease with an increase in the protein concentration. Similar trends were observed for anionic surfactants (polyoxyethylenated n-dodecyl alcohols) (Hua and Rosen, 1991). However, Hua and Rosen (1991) suggested no effect of the surfactant concentration upon the value of n (a dimensionless exponent of the Hua-Rosen equation). It is evident from Table 6-1 that there is a concentration dependency for n; i.e. n increases with a decrease in H*protein concentration. The findings here seem logical as n is related to the difference between the energies of adsorption and desorption and, the closer n is to zero, the more the adsorption rate approachs equilibrium (Deleu *et al.*, 1999). Furthermore results obtained here are more consistent with the typical concentration-dependence effect of surface tension. Therefore, the discrepancy between their data and that of the present study might be simply due to the narrow concentration range of the surfactants studied by Hua and Rosen (1991) (1.94 to 14.9 x10^7mol/cm^3).

At a given concentration, the values of n and t* were higher for H*protein B than for H*protein A. Since the parameters n and t* are known to increase with the increase in the hydrophobic character of a surfactant (Hua and Rosen, 1991; Rosen and Gao, 1995), it can be postulated that H*protein B is more hydrophobic than H*protein A. This hypothesis

corroborates with the findings of Rogalska *et al*. (2000) that the adsorption to an air/water interface from the bulk solution of the most hydrophobic molecules at low concentrations requires longer times to reach equilibrium as compared to the less hydrophobic ones. Also a previous study showed that H*protein B self-associates into larger structure than H*protein A in pure water with and without pH-control at any temperature (Wohlleben *et al.*, 2010). This is an indication of the higher hydrophobicity of H*protein B, given that self-association process is generally a hydrophobic interaction driven.

At higher concentrations, γ_m values for the H*proteins are almost identical (Table 6-1, 40 mN/m). This value is similar to that reported for β-Casein, but lower than that of BSA and Lysozyme (43 mN/m) (Tripp *et al.*, 1995). According to the values for Vmax (the maximum rate of reducing the surface tension at t*) these proteins can be ranked in the following order depending on how rapidly they migrate to an interface: β-casein (24.1 kDa) > H*protein A (47.0kDa) > H*protein B (19.0 kDa) > Recombinant human growth hormone (22.0 kDa) > BSA (67.0 kDa) > Lysozyme (14.4 kDa). As mentioned above, it is interesting to note that the pH has a significant effect on the adsorption rate of H*proteins with higher adsorption rate at pH 6 (0.232 $mNm^{-1}s^{-1}$ against 0.150 $mNm^{-1}s^{-1}$) for H*protein A and 0.122 $mNm^{-1}s^{-1}$ against 0.068 $mNm^{-1}s^{-1}$ for H*protein B at their natural pH. This suggests that H*proteins may adsorb at the air/water interface as faster as β-casein and Surfactin. The order of the protein also appears to be independent of the molecular weight. However, considering the value of γ_m for 0.1% H*proteins, as comparable to that of the equilibrium surface tension, given that the value of γ_m is affected by the same parameters that determine the value of the equilibrium surface tension and that n is close to zero, it becomes more obvious that H*proteins lower the air/water surface tension to a lesser degree than SC3 (29 mNs^{-1}, Corvis *et al.* (2006)) and HFBII (30-31 mNs^{-1}, Cox *et al.* (2007); Tchuenbou-Magaia *et al.* (2009a)). These values for

H*proteins are close to the 42 mNs^{-1} reported for the 13.7 kDa modified HYDPt-1 protein, a fusion hydrophobin similar to H* protein A and B, but made of HYDPt-1 hydrophobin from *Pisolithus tinctorius* and Histidine-tagged (Bilewicz *et al.*, 2001). These values are also in the surface tension range (45 mNs^{-1}) found for most commonly used food proteins (Foegeding *et al.*, 2006).

Table 6-1. Kinetic parameters of curves $\gamma = f(t)$ of H*proteins at air water interface. The surface tension data were fitted with the Hua-Rosen's equation, $\gamma(t) = \gamma_m + \frac{\gamma_0 - \gamma_m}{1 + \left(t/t^*\right)^n}$. γ_m, t*, and n are the surface tension at mesoequilibrium, the half-time required to reach γ_m and dimensionless exponent, respectively. $V_{max} = \frac{n(\gamma_0 - \gamma_m)}{4t^*}$

Proteins	γ_m **(mNm^{-1})**	**t* (s)**	**n**	V_{max} **x 10^{-2} (mNm^{-1} s^{-1})**
0.1% H*protein A-Natural pH	39.48	10.07	0.44	35.7
0.1% H*protein B-Natural pH	39.99	29.42	0.62	16.9
0.05% H*protein A-Natural pH	42.50	42.44	0.86	15.0
0.05% H*protein B-Natural pH	44.85	115.77	1.16	6.8
0.05% H*protein A -pH 6	40.82	24.06	0.72	23.2
0.05% H*protein B pH 6	45.08	66.22	1.20	12.2
0.05% H*protein A pH 3	44.20	34.31	1.03	20.9
0.05% H*protein B –pH 3	46.22	127.81	1.44	7.3
0.01% H*protein A-Natural pH	50.22	309.04	2.40	4.2
0.01% H*protein B-Natural pH	57.44	414.99	2.74	2.4
0.005% H*protein A-Natural pH	55.95	563.66	2.64	1.9
0.005% H*protein B-Natural pH	n.d.	n.d.	n.d.	n.d.
0.1% Recombinant Human growth hormone[T]	35.2	32.88	0.36	10.1
0.1% Beta-Casein[T]	40.5	0.44	0.17	301.5
0.1% Hen egg lysozyme[T]	43.4	1182	0.53	0.3
0.1% Bovine Serum Albumin[T]	43.6	409.8	0.15	0.3
0.1% bovine erithrocyte superoxide dismutase[T]	48.7	738.0	1.04	0.80
Surfactin C13[D]	47.24	48.58	1.73	22.0
Surfactin C15[D]	36.33	38.28	3.01	80.0

n.d.: not determined. It was impossible to obtain realistic kinetic parameters by fitting experimental data to empirical equation of Hua and Rosen (1991), [T]Data fromTripp *et al.*(1995); [D]Data from Deleu *et al.*(1999).

6.3.2. Oil/water interfaces

The time dependence of change in interfacial tension at sunflower oil/ aqueous H*proteins for a range of concentrations of H*protein A and H*protein B is shown in Figure 6-5. As for the air/water interface, the adsorption behaviour depends strongly on the H*proteins' bulk concentration with longer induction time for H*protein B than H*protein A, at low concentration. But the duration of the induction period appeared to be longer at oil/water interface when compared to that at the air/water interface. Furthermore the dynamic interfacial curve for the H*proteins at concentrations below 0.1% showed more than one inflection point. The observed variation with several stepwise changes in the interfacial or surface tension is best explained by the presence of impurities or the presence of more than one surface active species (Fainerman *et al.*, 2001; Alahverdjieva *et al.*, 2008). The mass spectroscopy and fluorescence spectroscopy analysis of H*proteins confirmed the presence of impurities (see section 6.4). Contaminants might also have been introduced by the oil. However, there was no significant decrease in the minimum interfacial tension over time for the triglyceride oil/distilled water system.

In addition to the impurities, another process could also operate. Different forms of H*proteins would be present in the solutions; i.e. monomers, dimers, tetramers or even small amount of more advanced protein aggregates, all with different affinities to the available interface. Also a dynamically dissociation as the bulk concentration of monomers or dimers is reduced due to the consumption at the interface may be considered. The critical aggregation concentration for H*proteins as reported by Wohlleben *et al* (2010) is 250 ppm ($2.5x10^{-2}$ %). Nevertheless, the above hypothesis is supported by the work of Corvis *et al.* (2006) with hydrophobin, SC3. They determined from adsorption isotherm a critical aggregation concentration of SC3 as 10^{-2} % (wt/v) but, did find at much lower SC3 concentration, $2.6x10^{-}$

^{3}% (wt/v), a mixture of monomeric and polymeric forms (the latter form is usually smaller than those formed at concentration above 10^{-2}% (wt/v). As a result Corvis *et al.* (2006) postulated that (1) the obtained critical aggregation concentration does not reflect the first stage of aggregation and may correspond more to the saturation of the interface with the protein; (2) SC3 aggregation in the bulk may occur in parallel with the adsorption to the interface and this may been apparent here. Furthermore, it has been pointed out that acidic pHs induce an effective stabilisation of dimer and tetramer of H*proteins (Wohlleben *et al.*, 2010). The effects are amplified at pH 3, and at concentration $5x10^{-2}$% (wt/v) to produce a more pronounced two steps variation.

In contrast to the air/water interface where a good fit was obtained for all the concentrations studied (except $5x10^{-3}$% for H*protein B), only data for H*protein concentrations of $5x10^{-2}$ and 0.1% gave a good fit to the equation of Huan and Rosen. Also, it was impossible to get an acceptable fit with the whole experimental data for $5x10^{-2}$ % H*protein B at its natural pH or at pH 3. This was presumably due to the more pronounced variation observed for the dynamic interfacial curve of this protein when compared to that of H*protein A. Satisfactory results were obtained when only data of part of the curve, starting from the beginning of the second step of decrease in the interfacial was considered Figure 6-6. The kinetic analysis revealed that γ_m tends to be considerably lower for H*protein B than for H*protein A, irrespective of their pH or concentration. However, the length of time required to reach a mesoequilibrium surface tension is substantially longer for H*protein B than that for H*protein A. Again suggesting the higher hydrophobicity of H*protein B. It is also possible that H*protein B packs more tightly or is more likely to form a multilayer at oil/water interface than H*protein A. Further experiments are needed to confirm this.

The lower value of γ_m (9.3 Nms^{-1}) at 5x 10^{-2} % for H*protein A was obtained at its natural pH whereas the highest value (15.3 Nms^{-1}) was observed at pH 3. However, the protein lowered the interfacial tension more quickly at pH 6 with $V_{max,}$ almost 4 to 8 fold than obtained at other pHs. Likewise the effect of pH upon the interfacial property of H*protein B was even more apparent with γ_m of 5.7, 1.7 and 16.4 Nms^{-1} at its natural pH, pH 6 and pH 3, respectively. The very low rate at which the mesoequilibrium was reached indicates that the pH affects the protein conformational change, rearrangement and/or reorientation at the oil/water interface most, rather than the initial adsorption. Also, because the apparent net charge of H*protein A and H*protein B seems to be similar and that the interfacial behaviour of H*protein B is more influenced by the pH as compared to H*protein A, may suggest that it is the location of specific charged residues that accounts for the pH effect rather than the protein net charge. The results presented here are consistent with other findings, i.e. electrostatic interactions play more significant role in the self-association process of H*protein B than that of H*protein A (Wohlleben *et al.*, 2010).

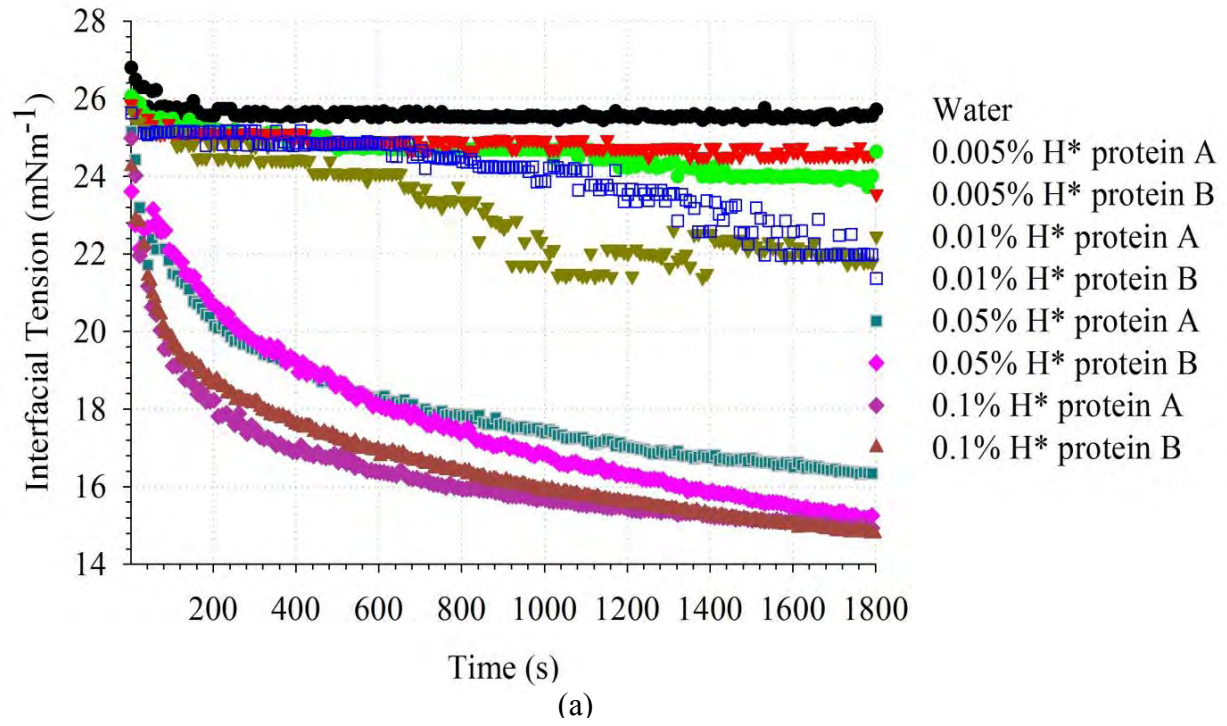

(a)

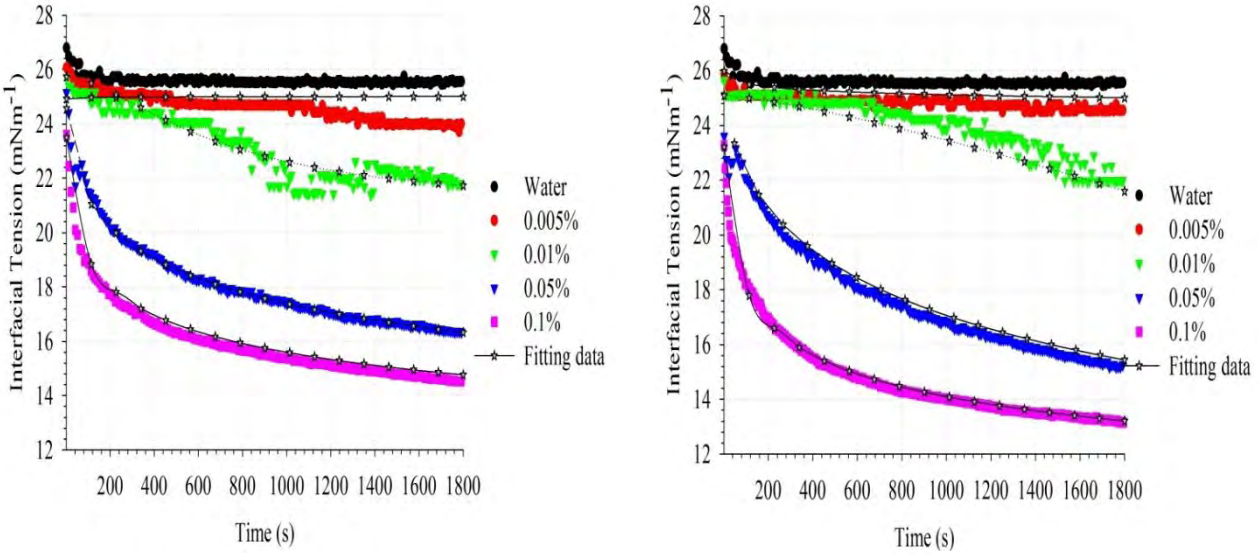

(b) (c)

Figure 6-5. Dynamic interfacial surface tension of different concentrations (% w/w) of H*proteins (a). (b), H*protein A; (c), H*protein B. The interfacial tension of sunflower oil-distilled water (used for protein dispersion) is showed as reference. The gray stars connected with line refer to the fitting and the parameters are given in table 6-2.

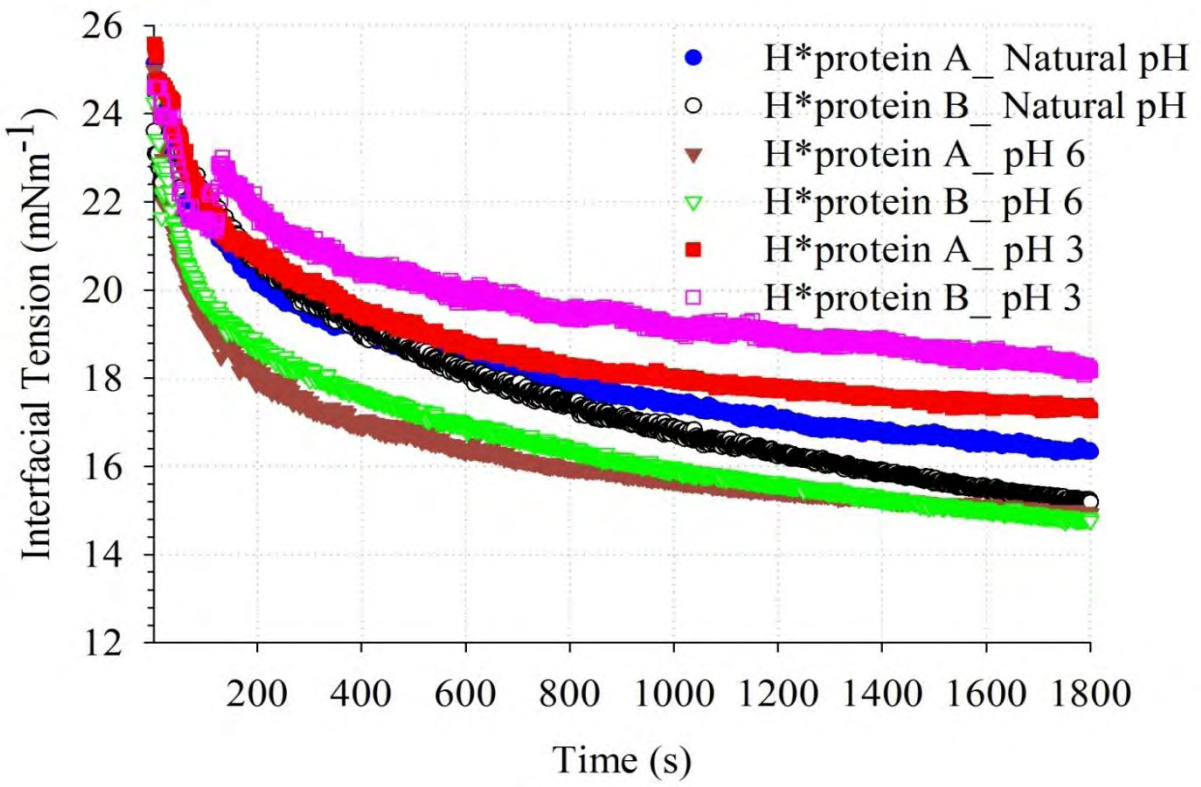

(a)

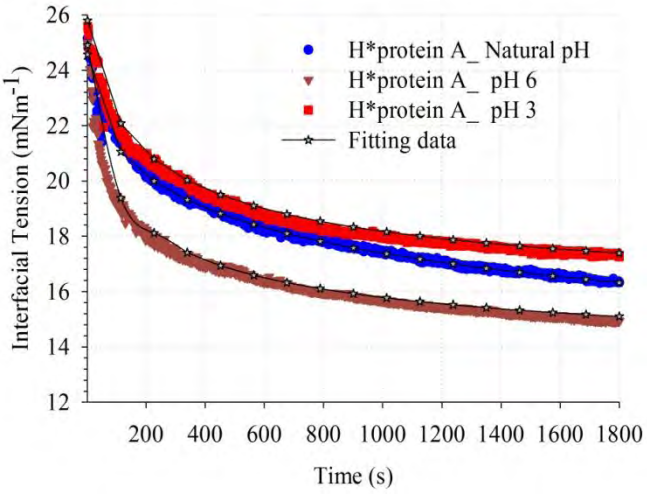

(b)

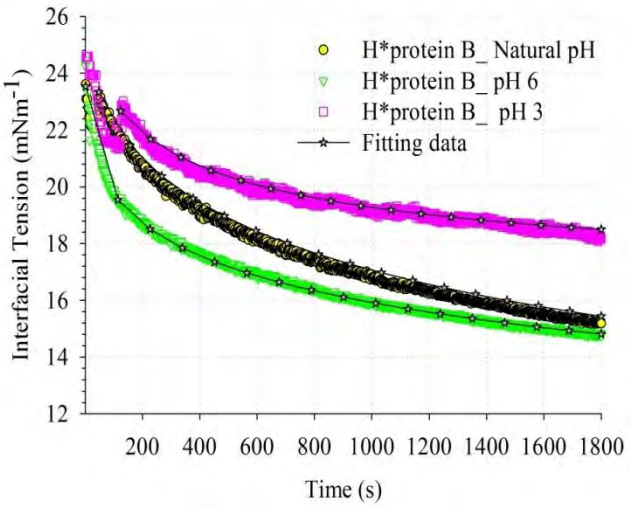

(c)

Figure 6-6. Dynamic interfacial tension of 0.05% H*protein A and H*protein B at different pHs (a). (b), H*protein A; (c), H*protein B. The natural pH is about 7.63 for H* protein B and 7.73 for H* protein A. The gray stars connected with line refer to the fitting and the parameters are given in table 6.2.

Table 6-2. Kinetic parameters of curves $\gamma = f(t)$ of H*proteins at the sunflower oil water interface. The surface tension data were fitted with the Hua-Rosen's equation. $\gamma(t) = \gamma_m + \frac{\gamma_0 - \gamma_m}{1 + (t/t^*)^n}$. γ_m, t*, and n are the surface tension at mesoequilibrium, the half-time required to reach γ_m and dimensionless exponent, respectively. $V_{max} = \frac{n(\gamma_0 - \gamma_m)}{4t^*}$

Protein	γ_m **(mNm^{-1} s^{-1})**	**t* (s^{-1})**	**n**	V_{max} **x 10^{-3} (mNm^{-1} s^{-1})**
0.1% H* protein A-Natural pH	8.59	302.83	0.34	4.9
0.1% H*protein B-Natural pH	2.65	1752.12	0.34	1.1
0.05% H* protein A-Natural pH	9.31	984.00	0.45	1.9
0.05% H*protein B-Natural pH	5.16	1694.90	0.531	1.6
0.05% H*protein A-pH 6	12.88	106.37	0.57	17.5
0.05% H*protein B-pH 6	1.37	3647.16	0.32	0.5
0.05% H*protein A-pH 3	15.34	232.01	0.71	8.1
0.05% H*protein B- H 3	16.36	318.73	0.72	5.4
0.01% H* protein A-Natural pH	n.d.	n.d.	n.d.	n.d.
0.01% H*protein B-Natural pH	n.d.	n.d.	n.d.	n.d.
0.005% H* protein A-Natural pH	n.d.	n.d.	n.d.	n.d.
0.005% H*protein B-Natural pH	n.d.	n.d.	n.d.	n.d.
Surfactin C13[D]	14.50	2.30	1.27	5180
Surfactin C15[D]	8.15	9.25	2.07	2450

n.d.: not determined. It was impossible to obtain realistic kinetic parameters by fitting experimental data to the empirical equation of Hua and Rosen, (1991); [D]Data from Deleu *et al.* (1999).

In summary and by comparing the two interfaces studied, considerable differences can be found for the two H*proteins. There were step variations in the O/W dynamic interfacial tension curve, whereas the A/W surface tension showed almost no apparent fluctuation. The adsorption rate of H*proteins at the A/W interface was greater than for the O/W interface. Moreover, although there was no significant difference between the calculated mesoequilibrium values for high concentration of both proteins at A/W, H*protein B shows slightly lower value of γ_m than H*protein A at O/W interface and this has been partially attributed to the higher hydrophobicity of H*protein B when compared to H*protein A. At minimum bulk concentrations, kinetic analysis showed systematically a much slower adsorption rate for H*protein B compared to H*protein A, irrespective of the interface. The molecular weight of H*protein B is smaller (19kDa) than that of H*protein A (45 kDa). Assuming that they have similar secondary and tertiary structure, it might be expected that the bulk Fickian diffusion and the mass transfer toward the interface is faster for H*protein B. However the opposite situation was observed, indicating that the adsorption rate of H*protein B is potentially limited by some energy barrier. Nevertheless, like other common proteins, the adsorption of H*proteins at both interfaces depends strongly on the bulk concentration.

The difference in behaviour of H*protein at the A/W and O/W interfaces may be interpreted in terms of the difference in the orientation of the protein at both interfaces as illustrated by Figure 6-7. This is presumably due to the difference in solvency of an oil phase for the hydrophobic amino acids side chains of the protein, resulting in longer time needs for molecules rearrangement at the O/W than at A/W interfaces as Murray (1997) pointed out when measured the interfacial pressure-area per molecule isotherms of spread films of β-lactoglobulin and bovine serum albumin at those interfaces. Furthermore, it has been reported that at the A/W interface the protein protrudes into the water phase more, whereas at a liquid-

liquid interface (e.g. O/W) the protein protrudes into both of the adjacent phases (Deleu *et al.*, 1999). This implies that H* proteins might be orientated more or less horizontally at the A/W interface whereas at the O/W interface they might be orientated more vertically. In the latter situation, H*proteins would occupy less area per molecule and this may account for the longer induction time observed for the O/W interface. The induction period is believed to terminate when about 2/3 of the maximum possible surface coverage is reached (Gao and Rosen, 1995). Thus more molecules within a unit time must diffuse to the O/W interface to initiate a rapid reduction in the interfacial tension. It may be postulated that H*proteins also adsorb at the oil/water interface in some form of aggregates in the same manner as the adsorption of amphiphilic helical peptides (high concentration) on lipid bilayer (Wu *et al.*, 1995). In contrast, it is possible that H*proteins may adsorb at the air/water interface mainly in the form of dimers which is supposed to be the starting building block for the oligomerisation of hydrophobins. This provides an explaination for the observed step variations for the O/W interfacial tension curve (Figure 6-6). There are similarities between SC3 and H*proteins in terms of self association mechanism in solution (Wohlleben *et al.*, 2010) and it has been pointed out that dimeric SC3 has an elongated shape (Wang *et al.*, 2004).

The surface and the interfacial tension of H*proteins vary with the pH (Figures 6-4 and 6-6) with H*protein B being more sensitive to changes in pH than H*protein A. The pH of H*proteins was thought to affect the protein conformational change, rearrangement and/or reorientation at interfaces rather than the initial adsorption rate. The process of rearrangement at the interface begins when the first few molecules of protein arrive at the interface and continues until an equilibrium is attained (Macritchie, 1978). This molecular rearrangement at the interface depends on the conformational stability of the protein and the specific chemical

forces acting on the proteins at the interface, which all are influenced by the pH (see section 2.2, Chapter 2).

When placed all together, the collected results raise the following questions: Is the pH-dependence interfacial tension reflected during the formation of emulsions (emulsion droplet sizes) and stability? Is the fact that the adsorption behaviour of H*proteins at the A/W and O/W interfaces resembles that of other commonly used emulsifying proteins implying that emulsions stabilised by H*proteins might be made using common processing conditions? The answers to these questions are explored in the following sections.

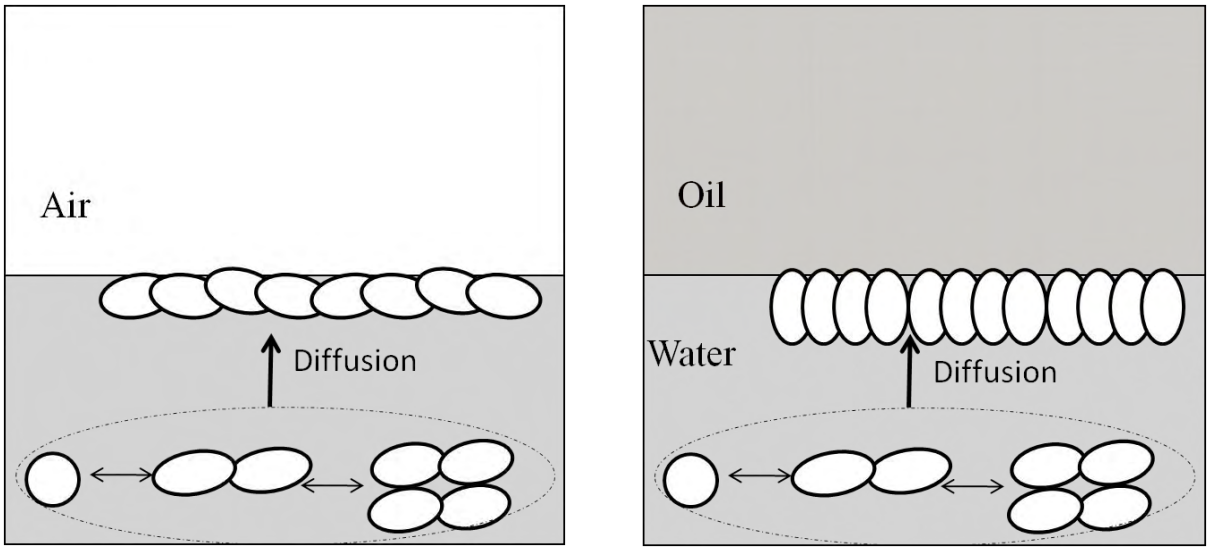

Figure 6-7. Proposed schematic representation of H*proteins adsorption at the air/water (a) and oil/water (b) interfaces. This schematic is based on the belief that H*proteins in solution at 25°C exist mainly in form of tetramer and that H*Proteins dimer and tetramer in solution have an elongated shape like SC3 (see the text). Monomer is assumed to be spherical. The exact form of hydrophobin that migrates to the interface is not known.

6.4. Influence of pH upon H*proteins stabilised emulsions: formation and stability

The effect of H*proteins pH upon their emulsification capacity and emulsion stability was investigated by producing a series of 15 % (wt/wt) sunflower oil emulsion from a fixed concentration of H*protein A and H*protein B (0.4%, w/w) at pH 6 and at their natural pH (pH 8) using a high pressure homogeniser. The size and size distribution of emulsions are shown in Figures 6-8 and 6-9. At their natural pH, H*protein A yielded slightly smaller oil droplets than H*protein B whereas there was no apparent difference in size and size distribution of the emulsions made at pH 6. Independently of the pH and H*protein types, the oil droplet sizes and distribution as measured with a Mastersizer and expressed in volume percentage (Figure 6-8) was bimodal with small number of oil droplets having a diameter around 1 μm. The majority of oil droplet sizes was around 6 μm for H*protein A at its natural pH, 12 μm for H*protein A at pH 6 and 17μm for emulsion stabilised with H*protein B at its natural pH or at pH 6. However it should be noted that the apparent droplet sizes obtained from the Mastersizer were bigger than those obtained from microscopy (most of the droplets were seen to be below 5 μm). This discrepancy is presumably due to droplet flocculation and bridging by non adsorbed or partially adsorbed (assuming multilayer adsorption, see chapter 5) H*proteins as illustrated by the confocal micrograph (Figure 6-9) (see later discussion). Nevertheless confocal images (Figure 6-9b and c).did confirm the general trend that droplets were slightly bigger when emulsion was stabilised with the protein at pH 6

Since high surface activity is associated with rapid adsorption of protein into an interfacial region and the formation of small emulsion droplets in the homogeniser this is an unexpected result as one would have thought of the opposite trend because the adsorption rate was higher

at pH 6 than at the natural pH (Dickinson *et al.*, 1985),. The time scale of adsorption and spreading out at the interface in order to protect the newly formed droplets during emulsification is supposed to be relatively long for very large macromolecules, or species that are strongly aggregated in the bulk aqueous phase (Dickinson, 2003). Therefore, it might be postulated, that the H*proteins self- assemble more rapidly upon pressure at pH 6 than at their natural pH and as a result larger molecules were formed with lower adsorption kinetic. Emulsion was made by pouring a protein solution into the homogeniser hopper followed by the oil phase and four passes through the homogeniser valve. During this process protein could well form large aggregates, also, emulsion droplets at pH 6 tended to aggregate more than those at pH 8.

Another intriguing result is that all the emulsions tended to decrease in size over the first month of storage, according to the Mastersizer measurement. However microscope observation revealed almost no noticeable change in droplet size (Figure 6-10). This point is discussed further in the section 6.5 as emulsions made with other emulsification methods also showed a similar trend.

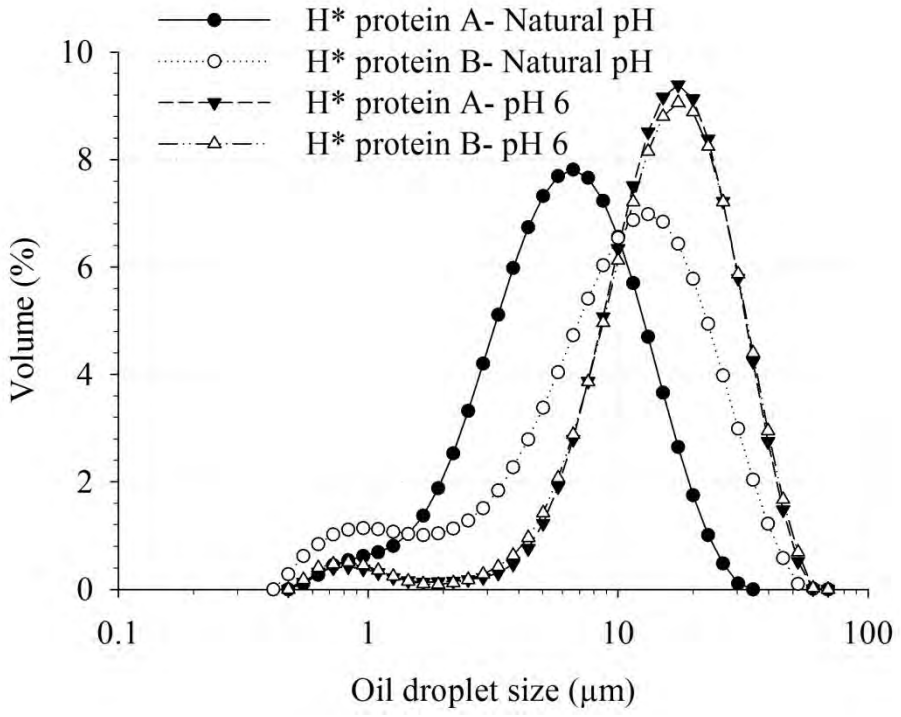

Figure 6-8. Droplet size distribution of freshly made emulsions (15 % sunflower oil) stabilised with 0.4% H*protein A or 0.4% H*protein B. Emulsions were made using high pressure homogeniser (4 passes at 500 psi).

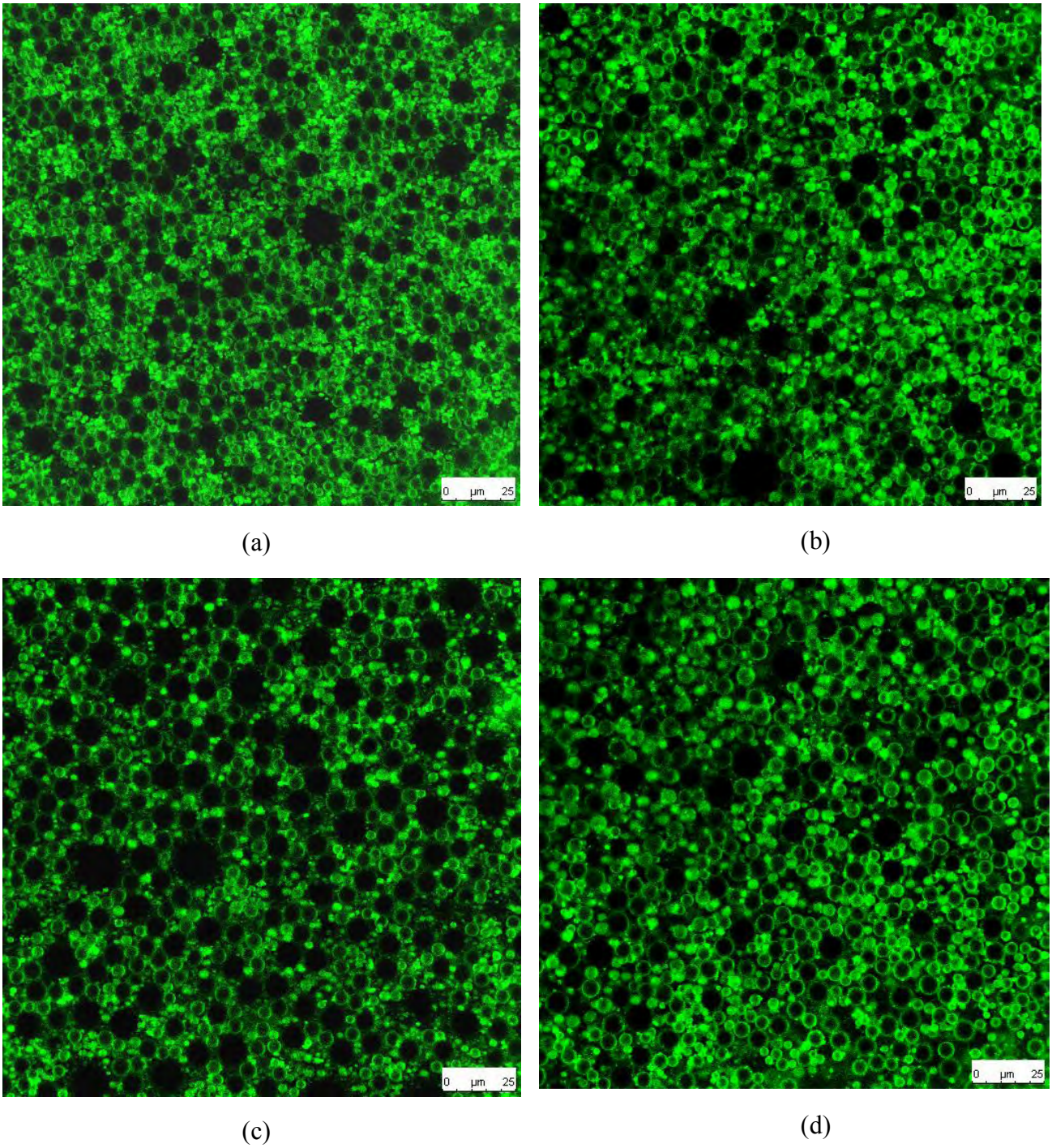

Figure 6-9. Micrographs of 0.4% H*proteins stabilised emulsions containing 15 % (w/w) sunflower oil. Emulsion stabilised with H*protein A at its natural pH (a), at pH 6 (b) or with H*protein B at its natural pH (c) and at pH 6 (d). Emulsions were made using a homogeniser (4 passes at 500 psi) and are 2 days old.

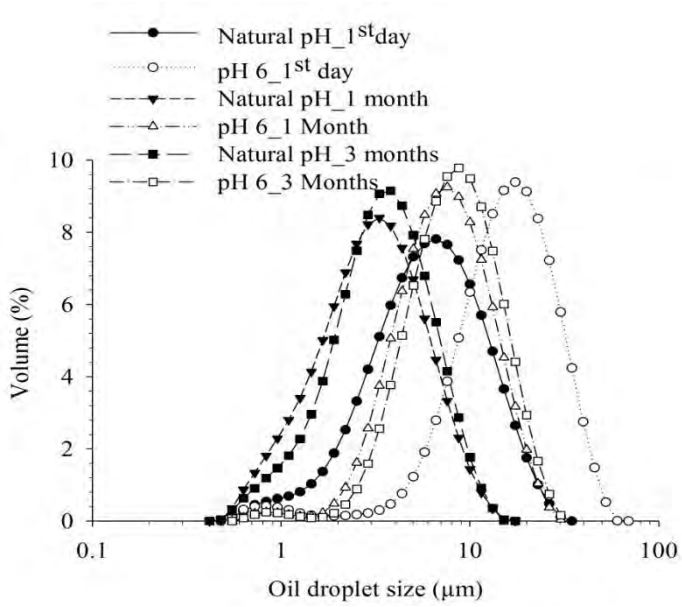

(a)

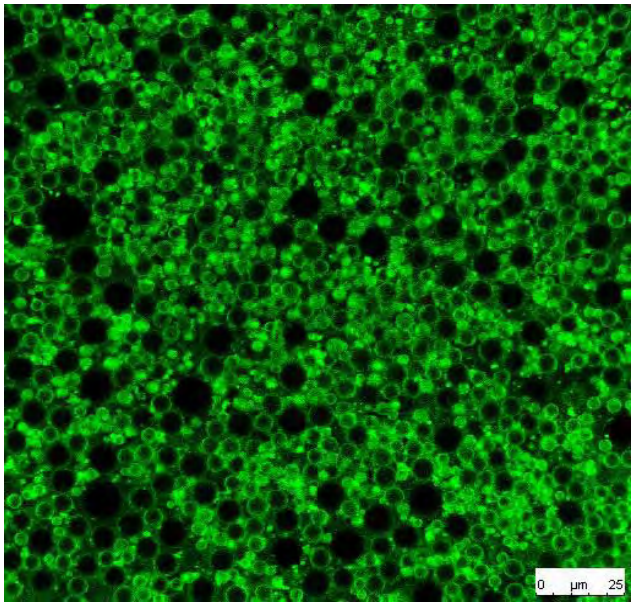

(b)

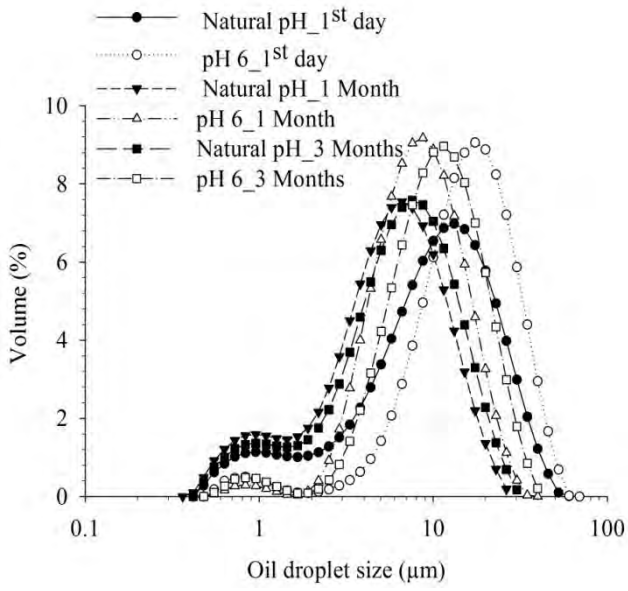

(c)

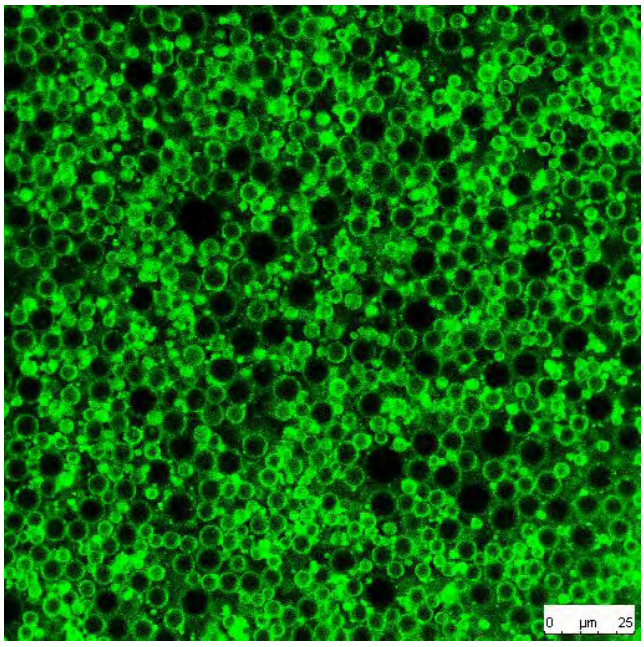

(d)

Figure 6-10. Evolution of droplet size and size distribution of 0.4% H*proteins stabilised emulsions containing 15 % (w/w) sunflower oil over three months storage at 8°C. (a) and (c), emulsion stabilised with H*protein A and H*protein B, respectively. Confocal images of 3 months old emulsions made with H*protein A (b) and with H*protein B at pH 6 (d).

6.5. Influence of emulsification processes upon H*proteins stabilised emulsion formation and stability

To progress from the previous section findings i.e. that the time scale of adsorption of H*protein A and H*protein B at the interface is in the same order of magnitude as that for common proteins such as caseins, the next step was to prepare emulsions stabilised by H*proteins using different but common emulsification methods. These were high pressure homogeniser, a rotor stator mixer, a cross flow membrane and ultrasound. The results from this sub-section should then allow selection of the most efficient method for the encapsulation of a hydrophobic bioactive molecule, but time did not permit this encapsulation here.

6.6. Influence of emulsification processes upon H*proteins emulsions: formation and physical stability

Emulsions stabilised by 0.4% H*proteins (15 % oil w/w) were made using the four different routes as described in Chapter 3: (1) by sonicating or blending sunflower oil and a solution of H*protein with an ultrasound probe or (2) rotor-stator device (Silverson); (3) emulsions were made with the high pressure as indicated above; (4) emulsions were made with a cross flow membrane system where a protein solution was flowed outside the membrane by means of a gear pump while the dispersed phase circulated inside the membrane and forced out trough the membrane pores. It should be noted that making emulsion stabilised with H*proteins using the current cross flow membrane configuration was not trivial. The pores of the membrane were easily blocked by H*proteins, especially by the vortex, created at the start up of the gear pump, which initiated the self-association process of H*proteins. These proteins aggregates physically blocked the pores of the membrane. This problem was tackled by

starting the emulsification with a protein at low temperature (8°C). After complete dissolution of proteins, samples were kept refrigerated for 24 h and removed from the cold store only just before the emulsification started. Previous study showed that H*protein oligomers disasociate into monomers when incubated at 5°C over 10 h to 20 h period (Wohlleben *et al.*, 2010). Wohlleben *et al.* (2010) also suggested that the presence of surfactants might disassociate large aggregates of H*proteins into tetramers.

However, neither making a previously stabilised (Tween 20) emulsion or by passing a solution of 1% Tween 20 (wt/wt) through the membrane prior adding the H*protein solution, nor soaking the membrane overnight in Tween 20 solution helped in preventing H*proteins from packing inside the membrane pores. It is worth also mentioning that the combination of a low temperature storage and incubation of emulsions stabilised by H*proteins with Tween 20 (up to surfactant-to-protein molar ratio of 16) showed no noticeable signs of emulsion deterioration (as examined using confocal microscopy and Mastersizer, see Figure 9-2 and Figure 9-3, Appendix 4). These results suggested that surfactant and low temperature storage may affect H*proteins assembles in solution but had no or negligible effects on absorbed assembles.

Emulsions made with ultrasound showed no significant creaming after one month storage at room temperature (Figure 6-11a). In contrast, the creaming was rapid in emulsions made via the membrane, Silverson or high pressure homogeniser. The creaming process was almost complete by 14 h after emulsion preparation. However, unlike the emulsions prepared with Tween 60, that creamed to leave a clear serum phase (see Chapter 5), the serum phase of the H* proteins emulsions was turbid throughout the storage period. Thus, the process may be treated as one of a phase separation into a droplet-rich phase (containing mainly larger droplets) and droplet-poor phase (with smaller droplets). Microscopic observations confirmed

that this droplets rich phase did only contain a small population of relatively small droplets. Also, any droplets present may have been weakly flocculated: this depended on the emulsification method (see later discussion) since droplets appear to have reorganised themselves in a network like structure (Figure 6-11b), presumably due to gravity and the Brownian motion. It is worth restating that no stabiliser was added to these emulsions and that the sole ingredients were: H*proteins dissolved in distilled water and sunflower oil. Moreover, H*proteins were at their natural pH (pH 8) and coated oil droplets should theoretically be negatively charged. Therefore, droplets would be expected to be stable to droplets-droplets attraction and flocculation because of the potentialy large electrostatic repulsion between them. However this seems not to be the case, as micrographs (Figure 6-9) showed individual droplets as well as flocculated clumps, and this may have an implication for the emulsion stability (see later discussion). The dissimilarity in creaming behaviour of different H*protein stabilised emulsions could be explained by their microstructural differences (Figure 5-11b-c). The emulsions typically showed a broad size distribution, with the emulsions made using ultrasound having the broadest but the smallest droplet size (Table 6-4; with substantial amount of droplet between 0.1 and 1µm, as illustrated by the micrograph, (Figure 5-11c). According to the Stokes equation (see section 2.3.2.2, Chapter 2), larger droplets cream faster than smaller ones. Moreover, the creaming rate reduces in polydispersed systems because of the presence of dissimilar neighbouring droplets and the consequent backflow of the continuous phase against the droplet. Creaming can be suppressed if the droplets are all in the sub-micron size range and their rapid diffusion via Brownian motion maintains them in suspension (Robins, 2000). This may account for the stability to creaming of emulsions made via ultrasound. Another factor that may be considered is the viscosity. It has been demonstrated that an emulsion with a limiting low-stress shear viscosity

of 10^3 Pa s or above will give good stability against creaming (Dickinson *et al.*, 1993). Although there is no rheological data for this system, it has been shown that at the same oil volume fraction, the emulsion with smallest droplets will have the greatest low shear viscosity as compared to ones with larger droplets (Chanamai and McClements, 2000a).

(a)

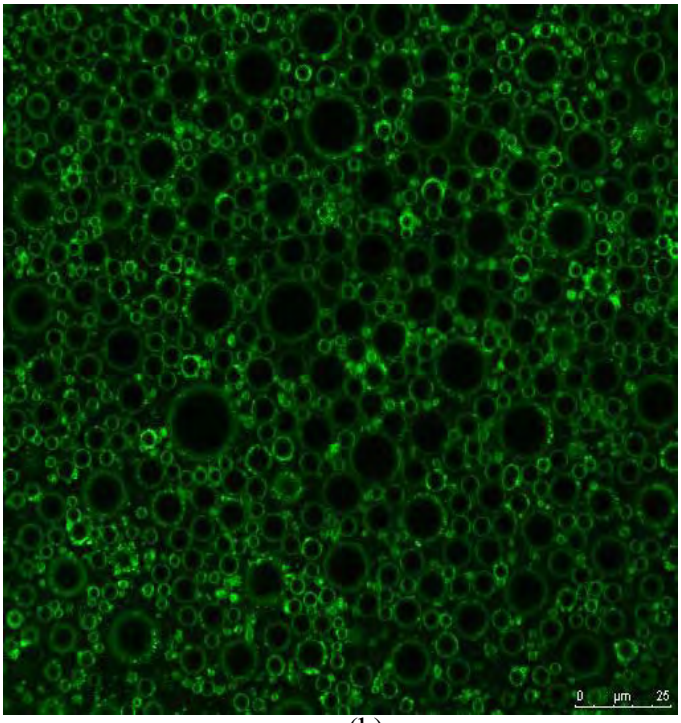

(b)

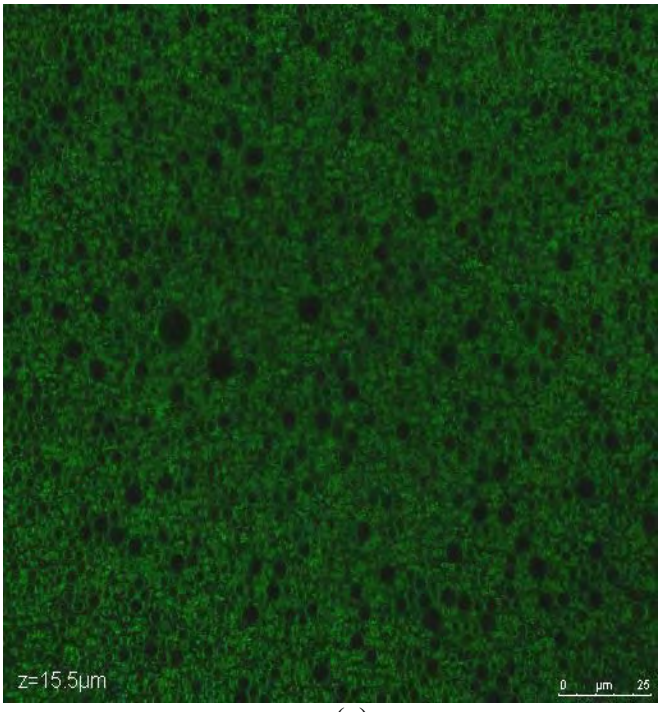

(c)

Figure 6-11. Typical physical appearance and microstructure of H*protein stabilised emulsions. (a), photographs of one month old of 15% emulsions stabilised by 0.4% H*protein B (B_1, B_2) and 0.4% H*protein A (A_1, A_2), made using Silverson ($_1$) and ultrasound ($_2$). (b) and (c) are confocal micrograph of 3 months old of H*protein B stabilised emulsion made with Silverson and ultrasound, respectively.

As indicated above, Table 6-3 shows that the high intensity ultrasound yielded the smallest droplets (d_{32}, 3.6 μm for H*protein A and 2.6 μm for H*protein B) whereas the high shear mixer Silverson gave the biggest oil droplets (d_{32}, 8.4 μm for H*protein A and 7.6 μm for H*protein A). It was apparent that emulsions stabilised by H*proteins B were slightly smaller than those stabilised by H*protein A. The opposite trend was observed for emulsions constructed using a crossflow membrane or a high pressure homogeniser, with the slightly larger oil droplets in the emulsions stabilised by H*protein B than H*protein A.

On the other hand, there was almost no apparent change in droplet size of emulsions made with a Silverson and a membrane over the three months studied. Conversely, and as mentioned in section 6.3, emulsions constructed with the high pressure homogeniser showed a decrease in droplets size with the storage time, especially during the first month of storage. For example, the d_{32} decreases from 4.7 μm to 2.6 μm for H*protein A and from 5.1 μm to 3.4 μm for H*protein B after a month of storage. The size of droplets remained almost unchanged for the last two months of storage. Similar results were observed for some of the emulsions made with ultrasound; i.e. those emulsions stabilised by H*protein A. Two possible mechanisms of how oil droplets could exhibit an apparent decrease in size over time may be considered: (1) there might be oil diffusion from the droplet and solubilisation by non adsorbed protein aggregates in a similar manner to micelles of non-ionic surfactant, Tween 60 (see Chapter 5). At pH 8, H*proteins could be considered to be acting as an ionic surfactant and theoretically there should be an electrostatic repulsion between droplets or any non adsorbed proteins. However there seems to be interaction between them despite the fact that they are negatively charged; (2) or bridging flocculation mediated by the interaction of non adsorbed protein with more than one droplet. This bond in the aqueous phase may be weakened and ruptured with storage, thus releasing smaller droplets. As indicated above,

H*protein oligomers in solution can slowly reverse to monomers when subjected to low temperature for sufficient period of time (Wohlleben *et al.*, 2010). Also a similar pattern has been reported for a non hydrophobins system by Dickinson and Pawlowsky (1997) for BSA-stabilised emulsion containing Iota carrageenan where light scattering measurements indicated a decrease in droplets size with storage time. This was attributed to a gradual flattening of carrageenan and bridging out at the surface of emulsion droplets.

Table 6-3. Effect of emulsification technique upon droplets size of H*protein stabilised O/W emulsions

Storage		Silverson		Ultrasound		High pressure homogeniser		Membrane	
		H*A	H*B	H* A	H* B	H* A	H* B	H*A	H* B
day 0	d_{32}	8.37 ± 0.26	7.64 ± 0.27	3.63 ± 0.16	2.58 ± 0.10	4.70 ± 0.23	5.10 ± 0.04	6.84 ± 0.15	6.99 ± 0.21
	d_{43}	16.17 ± 0.24	14.14 ± 0.35	11.15 ± 0.67	8.14 ± 0.80	7.80 ± 0.17	13.30 ± 0.2	11.93 ± 013	13.19 ± 0.69
	d_{90}	28.19 ± 0.50	25.38 ± 0.83	24.32 ± 1.02	18.21 ± 0.76	14.97 ± 0.49	27.08 ± 0.4	22.33 ± 0.22	24.84 ± 0.89
1 week	d_{32}	8.62 ± 0.14	7.49 ± 0.16	3.0 ± 0.16	2.66 ± 0.43	3.63 ± 0.10	4.35 ± 10	6.34 ± 0.16	6.71 ± 0.25
	d_{43}	16.61 ± 0.53	14.14 ± 0.56	7.99 ± 0.32	8.55 ± 0.93	5.42 ± 0.15	10.62 ± 0.40	11.56 ± 0.31	12.93 ± 0.50
	d_{90}	29.60 ± 0.78	26.38 ± 0.34	18.02 ± 0.60	17.94 ± 0.56	9.85 ± 0.28	21.92 ± 0.88	22.00 ± 0.58	24.51 ± 0.91
1 month	d_{32}	8.54 ± 0.39	7.5 ± 0.21	2.49 ± 0.03	2.65 ± 084	2.62 ± 0.16	3.44 ± 0.15	6.46 ± 0.04	6.70 ± 0.14
	d_{43}	16.29 ± 0.90	14.16 ± 0.37	8.51 ± 1.5	7.35 ± 0.95	3.87 ± 0.13	7.62 ± 1.04	11.63 ± 0.07	13.14 ± 0.17
	d_{90}	29.48 ± 0.21	26.48 ± 0.54	13.86 ± 0.29	17.26 ± 0.95	7.18 ± 0.12	14.9 ± 0.55	21.96 ± 0.11	24.94 ± 0.31
3 months	d_{32}	7.94 ± 0.18	7.05 ± 0.10	2.16 ± 0.56	3.08 ± 0.55	2.90 ± 0.1	3.89 ± 0.18	6.48 ± 0.01	6.10 ± 0.01
	d_{43}	16.26 ± 1.10	13.98 ± 0.34	6.09 ± 0.95	8.70 ± 0.18	4.22 ± 0.08	8.17 ± 0.21	11.66 ± 0.01	11.85 ± 0.02
	d_{90}	28.71 ± 0.95	26.03 ± 0.33	13.15 ± 0.83	18.02 ± 0.39	7.61 ± 0.2	15.96 ± 0.19	21.98 ± 0. 20	22.89 ± 0.50

The slight differences observed between the aggregation behaviour of emulsions made using different emulsification techniques may be explained by the degree of mechanical stresses generated by these methods. This resulted in different states of unfolding of adsorbed and non-adsorbed proteins with previously hidden hydrophobic groups becoming exposed at the protein surface. For example, Demetriades *et al.* (1997) found, by studying the effect of thermal treatment on corn O/W emulsions, stabilised with whey protein, that oil droplet size increased with temperature (65-80°C) but decreased when emulsions were subject to further heating up to 90°C. They explained their findings as the action of both the partially unfolding of proteins at the surface of the droplets at the lower temperatures and an ineffective rearrangement of the protein to fail to direct all nonpolar amino acids towards the oil phase. As a result droplet surfaces would become more hydrophobic and this led to greater propensity for droplet aggregation. In contract, at higher temperatures proteins would be fully unfolded and more flexible to rearrange and shield their hydrophobic groups from the aqueous phase. This would reduce droplets surface hydrophobicity and the succeptibility to droplets aggregation. They also pointed out that, droplets aggregation may occur when around 5% of the surface of droplets became non-polar. Moreover, it has been demonstrated that droplets aggregation is only reinforced by thiol/disulfide cross linking and that determining elements are non covalent interactions between unfolded protein molecules adsorbed on different droplets (Monahan *et al.*, 1996). The emulsions made via high shear rotor stator and membrane formed a very weak flocs that would break down if the emulsion was dispersed in distilled water; for instance in the sample presentation chamber of the "Mastersizer" for particle size determination. This is presumably because less stress was applied to the proteins during emulsion creation. Conversely, high pressure homogeniser is known to cause denaturation and aggregation of proteins as demonstrated in section 5.4, Chapter 5, with whey

protein. This may explain the degree of flocculation observed with emulsions made with the high pressure homogeniser.

The disparity in the behaviour of the emulsion when made using the ultrasound is rather more difficult to explain. It can be imagined that the effects of the protein size are important as H*protein A is almost twice the molecular weight of H*protein B, but a detailed discussion requires specific information on the tertiary structure of H*proteins which, unfortunately is not yet available. Also there is an undeniable strong hydrophobic attraction between hydrophobin molecules and all the results (Figures 6-9 to 12) suggested that H*proteins keep this property once adsorbed at the oil/water interface, to a greater or lesser extent. This is shown by the fact that flocculated droplets were seen even in the very simplified systems at pH 8 where maximum electrostatic repulsion between droplets is expected to occur.

6.7. Influence of emulsification processes upon H*proteins emulsions: oxidative stability

The oxidative stability of the H*Protein stabilised emulsions made using ultrasound and membrane emulsification was studied. For comparison, a Tween 60 stabilised emulsion was also made with different emulsification processes processing. This was investigated in other to find out whether the ultrasound emulsification that produces in one step an O/W emulsion with size distribution closer to that of air filled emulsion is an effective process compared to high pressure homogeniser and membrane emulsification from the oxidative damage standpoint.

To this end 10% OW emulsions stabilised either by 0.4% (w/v) H*Protein A, H*Protein B or by 0.4% Tween 60 at their natural pHs (e.g, emulsifiers were dissolved in distilled water) were made. The droplet sizes for each condition are depicted in Table 6-4. Because of the variation in droplet sizes, oxidation stability data were normalised against the total surface area of droplets exposed to the aqueous phase (see later discussion).

Table 6-4. Mean particle Size (Micrometers) of a 10% OW emulsions prepared with different emulsification processes.

Samples	d_{32}	d_{43}	d_{90}	Span
AS	1.24± 0.07	2.11± 0.03	4.13± 0.03	2.01
BS	1.29± 0.07	2.55± 0.16	5.33± 0.37	2.42
TS	0.46± 0.01	0.95±0.01	2.09± 0.01	2.65
TH	0.72± 0.01	0.99± 0.01	1.71± 0.01	1.45
AM	3.99± 0.06	8.03± 0.06	16.44± 0.09	2.24
BM	5.08± 0.08	11.05± 0.95	21.36± 1.54	2.43

AS, BS and TS refered to emulsions made via a high ultrasound technique and stabilised by H*protein A , H*protein B and Tween 60, respectively. TH is emulsion stabilised by Tween 60 and made via a high pressure homogeniser. AM and BM are emulsions contructed using a cross flow membrane and stabilised a with H*protein A and H*protein B, respectively.

- *Formation of hydroperoxide and secondary oxidation products*

Figure 6-12 depicts the formation of oxidation products in emulsions stored at 40°C and monitored over eight days. Emulsions prepared via membrane emulsification oxidised more rapidly than those produced using ultrasound. This was even more evident when data was normalised against the total surface area. This takes into account the effects of droplet size (Figure 6-13). The membrane system required pressurisation with the laboratory compressed air to work. This may accounts for the higher oxidation rate. However, the formation of lipid hydroperoxides and aldehydes was much greater in emulsions made with ultrasound and

stabilised by H*proteins than in emulsions stabilised by Tween 60. The low oxidative stability observed with proteins stabilised emulsions compared to the anionic, Tween 60 stabilised emulsion could be explained by the initial pH of the emulsion and the charge on the proteins. The rate of lipid oxidation has been found to be considerably higher under alkaline conditions (Memoli *et al.*, 1996). The droplets surface of the emulsions stabilised by H*Proteins are negatively charged due to their initial pH, ≈ 8, (Figure 6-14). This value is far above the PI of theproteins, therefore, they will electrically attract the positively charged prooxidative ions (naturally present in the water phase), thereby accelerating the rate of oxidation. The results here are in good agreement with those of Mei *et al.* (1998; 1999) who showed that a negatively charged SDS-stabilised emulsions is less oxidatively stable than an uncharged polyoxyethylene 10 lauryl ether (Brij) stabilised one. In some cases they reported lipid peroxide concentrations 19-fold greater in SDS sample than that stabilised by Brij.

There was no significant difference in the oxidative stability of Tween 60 stabilised-emulsion made with ultrasound and high pressure homogeniser during the whole of the incubation period, except at day eight where the emulsion made with the homogeniser showed a rapid increase in its lipid peroxides concentration. Although the mean diameter of oil droplets of both emulsions was of the same order of magnitude, the emulsions made with ultrasound showed a wider size distribution and this may explain why their oxidation stability differ in long term. However it is worth mentioning that the effect of droplets size on the oxidative stability of emulsion has yielded ostensibly contradictory results. Nakaya *et al.* (2005) studied the oxidation stability of O/W sytems stabilised by sucrose lauryl ester or decaglycerol lauryl ester. These were made using a membrane filtration technique and it was found that hydroperoxides concentration was lower in emulsion with droplet sizes of 0.81 μm compared to that with droplets sizes of 12.8 μm. They suggested that the lower concentration of

unsaturated triacylglycerols inside smaller oil droplets as well as the suppression of their mobility and the reduction the mobility of hydroperoxides at the oil/water interface by the wedge effect of the emulsifier accounted for the higher oxidation stability shown by emulsion with small droplets size when compared to the bigger droplets ones. On the other hand a higher oxidation rate for the emulsions with small oil droplets (Lethuaut *et al.*, 2002) or no dependence on droplets size on the emulsion deterioration (Osborn and Akoh, 2004) have been reported.

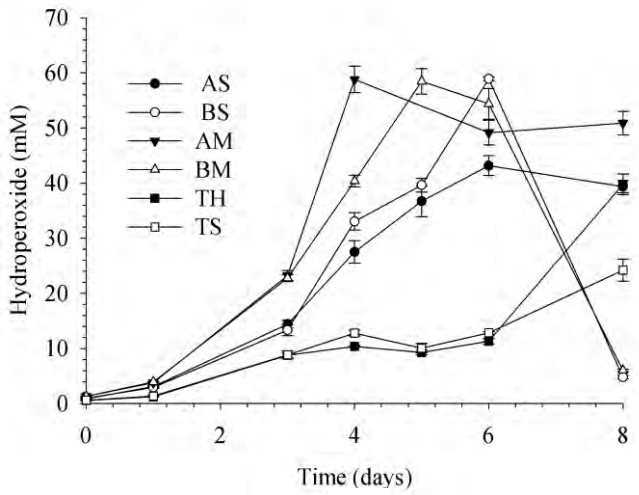

(a)

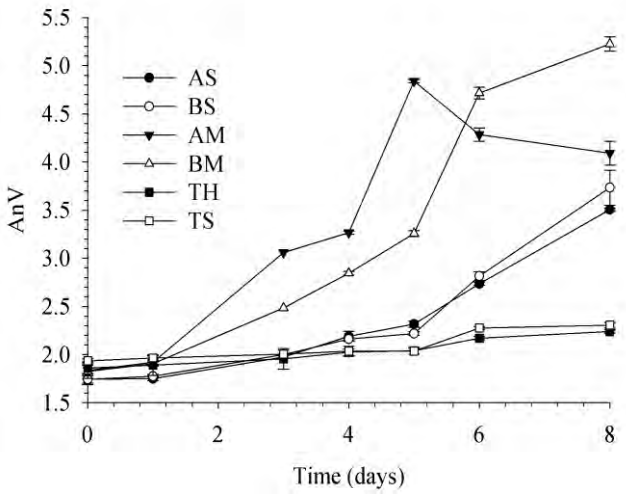

(a)

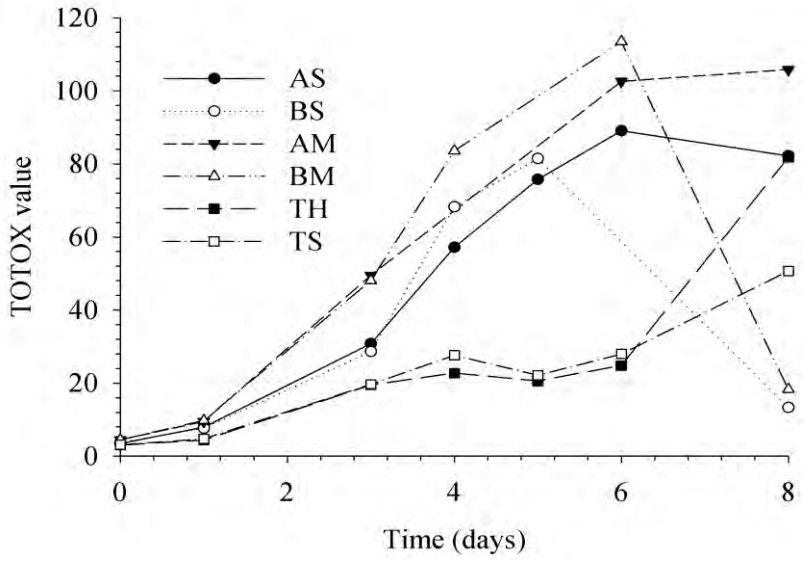

(a)

Figure 6-12. Effect of emulsification processes upon the oxidative stability of 10% O/W during storage at 40 °C. (a) Formation of hydroperoxides (PV); (b) Formation of secondary oxidation product (aldehydes) express as anisidine value (AnV); (c) Totox Value which is 2PV + AnV, calculated using the average value of PV and AnV. AS, BS and TS are emulsions made using an ultrasound technique and stabilised by H*protein A, H*protein B and Tween 60, respectively. TH represents emulsion made with a high pressure homogeniser and stabilised with Tween 60. AM and BM are emulsions prepared with a cross flow membrane and stabilised by H*protein A and H*protein B.

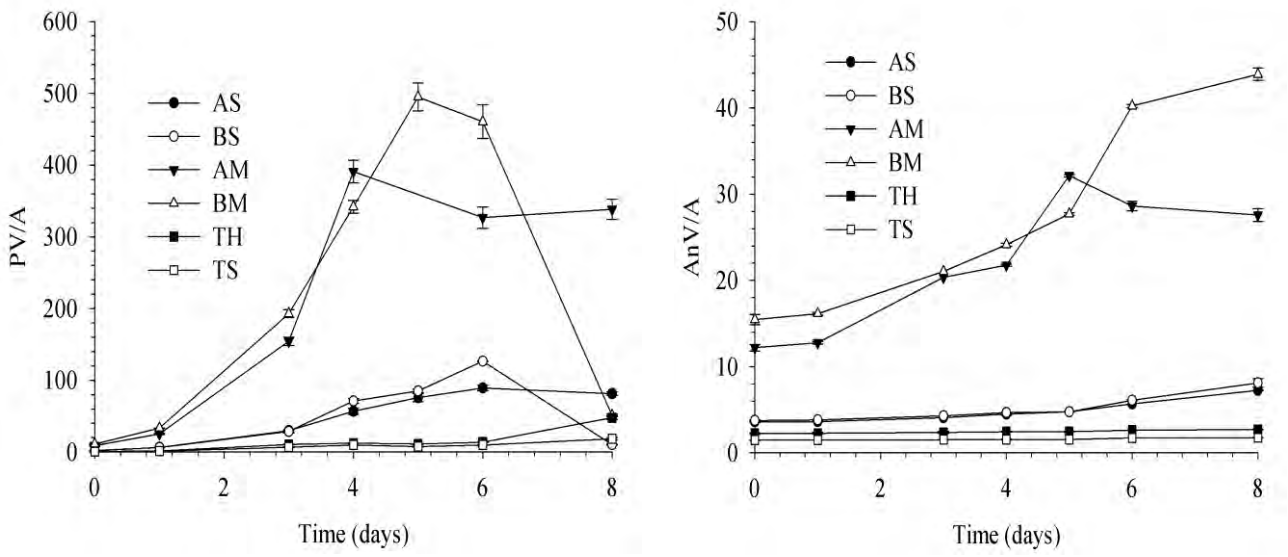

(a) (b)

Figure 6-13. Effect of emulsification processes upon the oxidative stability of 10% O/W during storage at 40 °C. (a) Formation of hydroperoxides normalized to total oil droplets surface area (PV/A); (b) Formation of secondary oxidation product (aldehydes) express as anisidine value and normalised to total oil droplets surface area (AnV/A). AS, BS and TS are emulsions made using an ultrasound technique and stabilised by H*protein A, H*protein B and Tween 60, respectively. TH represents emulsion made with a high pressure homogeniser and stabilised with Tween 60. AM and BM are emulsions prepared with a cross flow membrane and stabilised by H*protein A and H*protein B.

- *Change in pH during oxidation*

Considerable changes were seen in the pH of H*protein stabilised emulsions, compared to those stabilised by Tween 60 stabilised (Figure 6-14). Emulsions stabilised by H*proteins B showed the highest decrease in pH. Indeed, the pHs of freshly prepared H*proteins B stabilised emulsions were 7.4 and 7.8 for the emulsion prepared via membrane emulsification and an ultrasound, respectively.; after 8 days storage these pHs decreased to 3.6 and 4.4. The changes in pH are corroborated with the oxidative stability of these emulsions. H*proteins A stabilised emulsions showed, to some extent a better oxidative stability compared to those stabilised with H*proteins B. H*protein A is a relatively large molecule in comparison to H*protein B and this may have lead to the formation of a thicker interfacial layer for the

emulsion. This increased thickness would contribute to the improvement of the oxidation stability (Hu *et al.*, 2003). The differences between H*protein A stabilised emulsions and those stabilised by H*proteins B, in terms of alteration of pH, may also have been due to the type and number of amino acids available to react with lipid oxidation products resulting in generation of acidic compound as discussed below (see Appendix 5).

Different behaviour, in terms of change in pH was observed with Tween 60 stabilised emulsion and again, this depends on the manufacturing process. The pH of sonochemically produced emulsion increased during the first 3 days (from pH 6.9 to 8) after which time it became fairly constant, though a slight decrease was observed on day 8 (pH 7.3). The emulsion made with the high pressure homogeniser showed the same trend but in an opposite direction with its pH decreasing marginally from 6.9 on day 0 to 6.3 on day 1, remained constant for 7 days before decreasing again on day 8 (pH, 5.7). Dimakou *et al.* (2007) also reported a decrease in pH from 7 to 6 of an O/W emulsion made with high pressure homogenised and stabilised by Tween 20. As mentioned above and in Chapter 5, lipid oxidation might result in a decrease of the pH of an emulsion due to the generation of acidic compounds. N.B. to the best of my knowledge the increase in emulsion pH during oxidation has not been reported.

The most probable mechanism for the acceleration of lipid oxidation in emulsions is the decomposition of lipid hydroperoxides (ROOH) into the more reactive peroxyl (ROO) and alkoxyl (RO) radicals by transition metals or other pro-oxidants (Mn+) e.g. see (Eq. 6-1 and 6-2, McClements and Decker (2000) Jacobsen *et al.* (2008)). These radicals then react with unsaturated lipid (LH) within the droplets or at the oil-water interface and, as a result lipid radicals (L· and LOO·) are generated (see Eq. 6-3 to 6-5). The lipid oxidation chain reaction propagates as these lipid radicals react with other lipids in their immediate vicinity (see Eq. 6-

6), although some lipid radicals may react with other radicals thus terminates the reaction (see Eq. 6-7)

$$M^{n+} + ROOH \rightarrow M^{(n-1)+} + ROO^{\cdot} + H^{+} \quad \text{Eq. 6-1}$$

$$M^{n+} + ROOH \rightarrow M^{(n+1)+} + RO^{\cdot} + OH^{-} \quad \text{Eq. 6-2}$$

$$ROO^{\cdot} + LH \rightarrow ROOH + L^{\cdot} \quad \text{Eq. 6-3}$$

$$RO^{\cdot} + LH \rightarrow ROH + L^{\cdot} \quad \text{Eq. 6-4}$$

$$L^{\cdot} + O_2 \rightarrow LOO^{\cdot} \quad \text{Eq. 6-5}$$

$$LOO^{\cdot} + LH \rightarrow ROOH + L^{\cdot} \quad \text{Eq. 6-6}$$

$$LOO^{\cdot} + LOO^{\cdot} \rightarrow Nonradical\ products \quad \text{Eq. 6-7}$$

Eq. 6-2 could be predominant in the sonochemically prepared emulsion resulting in an increase in pH due to hydroxide ions generated. Moreover hydrogen peroxide is amongst the free radicals produced from ultrasonically irradiating an aqueous solution. This peroxide may react with metal ions commonly present in the water phase and yield a hydroxyl radical (OH) which in turn reacts with fatty acid (LH) (von Sonntag and Scuchmann, 1991).

$$Fe^{2+} + H_2O_2 \rightarrow HO^{\cdot} + OH^{-} \quad \text{Eq. 6-8}$$

$$HO^{\cdot} + LH \rightarrow H_2O + L^{\cdot} \quad \text{Eq. 6-9}$$

$$O_2 \rightarrow LOO^{\cdot} \quad \text{Eq. 6-10}$$

Conversely, because the pH of emulsion made with a high pressure homogeniser decreased over time, reactions illustrated by Eq. 6-1 may prevail. This suggests that the oxidation pathway in an emulsion prepared with ultrasound could differ from that in emulsion made with the high pressure homogeniser.

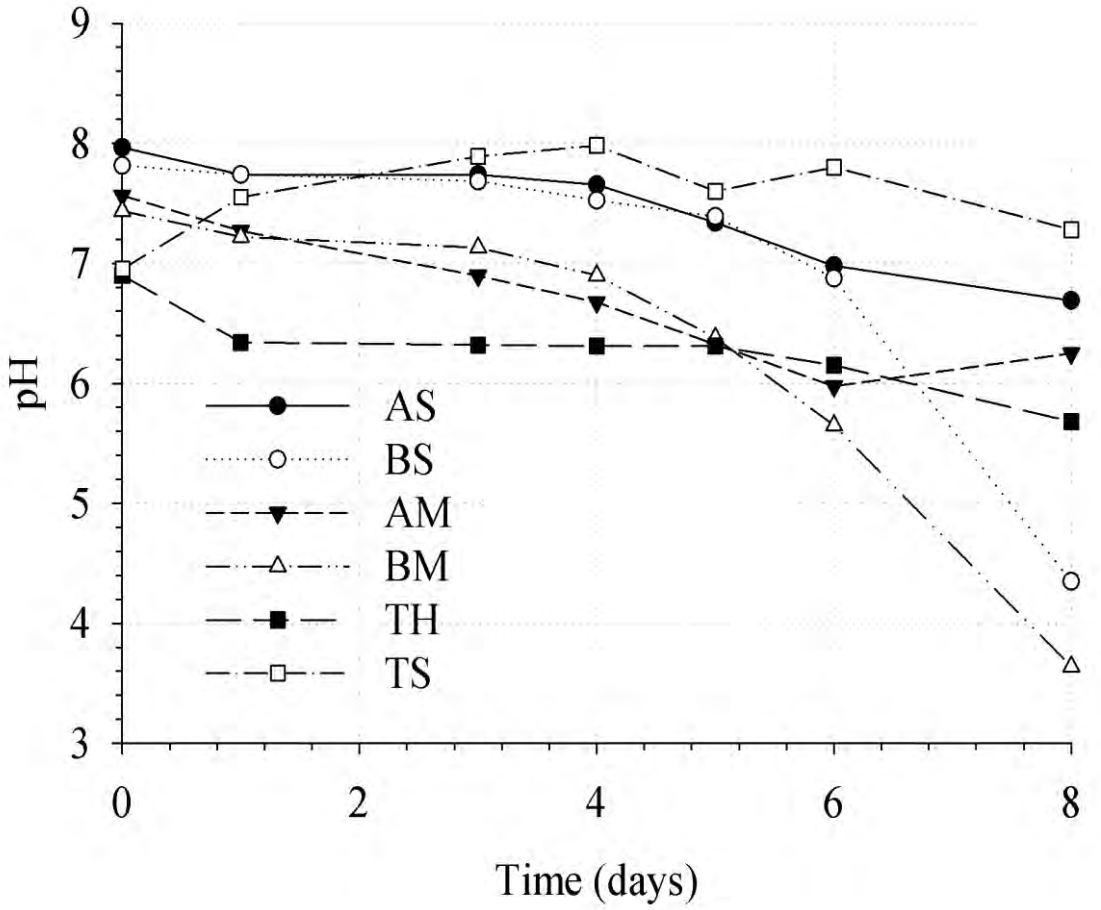

Figure 6-14. pH changing of 10% O/W during storage at 40 °C. AS, BS and TS are emulsions made using an ultrasound technique and stabilised by H*protein A, H*protein B and Tween 60, respectively. TH represents emulsion made with a high pressure homogeniser and stabilised with Tween 60. AM and BM are emulsions prepared with a cross flow membrane and stabilised by H*protein A and H*protein B.

6.8. The formation of H*proteins-lipid oxidations products complexes

A decrease in pH has been seen when emulsions containing hydrophobins (HFBII in Tri-phasic emulsion, Chapter 5 and H*proteins in this chapter) are placed under conditions that allow for the acceleration of lipid oxidation. It was postulated that this decrease in pH was a

consequence of the reaction of lipid oxidation products (hydroperoxides, aldhehydes) with the basic amino acids and the N-terminus amino acid residues of the proteins. In order to verify this hypothesis, H*proteins were incubated with lipid oxidation products, namely Cumene hydroperoxide, Trans, trans-2, 4-decadienal and Trans-2-decenal and modifications were ascertained using fluorescence spectroscopy and liquid chromatography-electrospray tandem mass coupled with mass spectrometry (LC-MS/MS). The results are summarised below and more detailed discussion can be found in Appendix 6.

The results indicated that incubation of the H*protein solutions with lipid oxidation products led to the modification of its intrinsic fluorescence (Figure 6-15), change in the physical appearance and to a decrease in its pH (Figure 6-16). Trypsin digestion and LC-MS/MS analysis showed that, in addition to all amino acids with basic side chains (lysine, histidine, arginine), methionine, tyrosine, phenylalanine and tryptophan were modified by the presence of aldehydes (Figure 9-8, Appendix 6). Moreover 4mg/ml of H*protein B can bind up to 10 mM of aldehyde before reaching saturation (Figure 9-9, Appendix 6).

In conclusion, all the applied techniques have supplemented each other to give clear evidence of the formation of complex hydrophobin-lipid oxidation products, especially aldehydes.

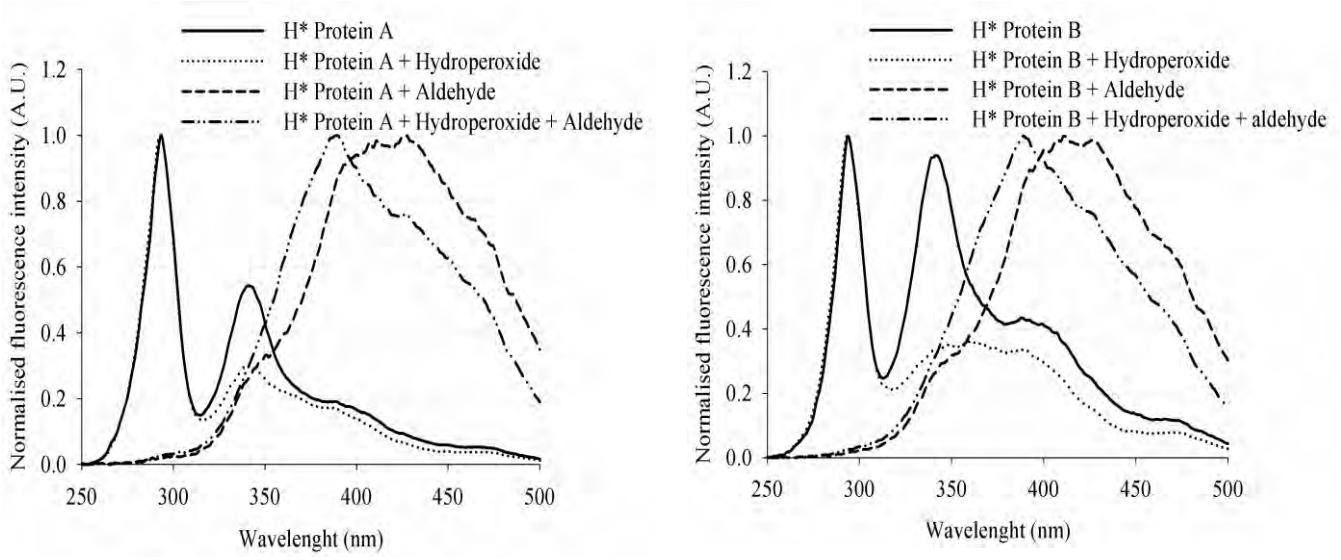

Figure 6-15. Synchronous fluorescence spectra of H* protein A and B (4mg/mL) in absence or in the presence of lipid oxidation products (1mM) recorded at $\Delta\lambda$= 20 nm. Fluorescence intensity normalised to 1.

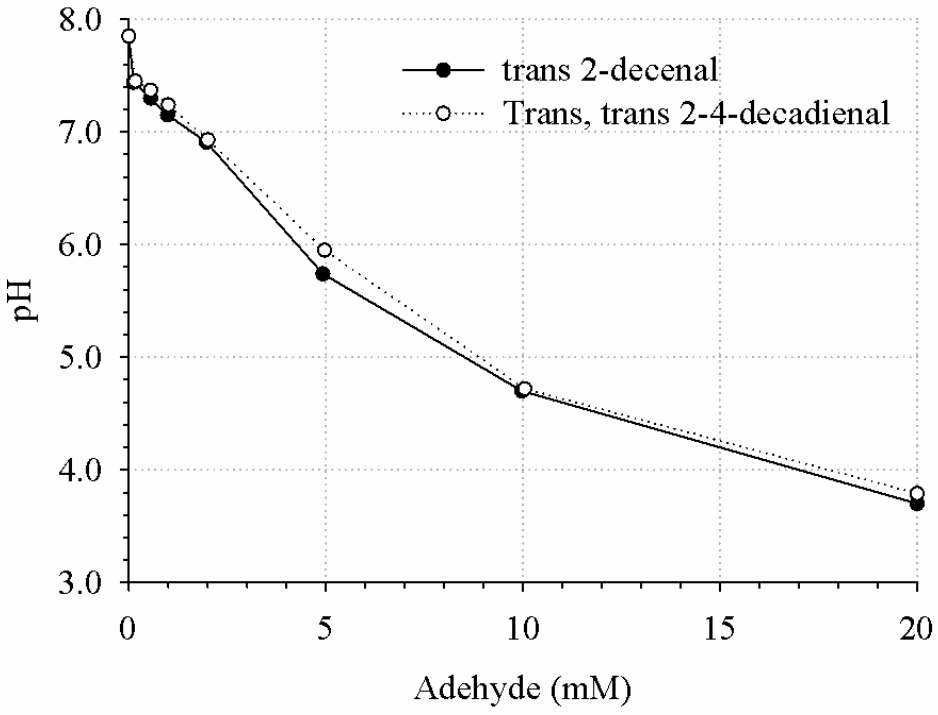

Figure 6-16. Change in pH of H*protein B solution as function of aldehydes concentration.

6.9. Conclusion and remarks

The objectives of this chapter were to ascertain the adsorption behaviour of fusion hydrophobins (H*protein A and H*protein B) at the A/W and O/W interfaces, investigate the effect of pH and emulsification technique upon H*protein stabilised emulsion formation and stability, and to verify the hypothesis of formation of complex hydrophobin-lipid oxidation products as stated in Chapter 5.

It was found that the adsorption behaviour of H*protein B and H*protein A is somewhat comparable to that of other commonly used proteins protein such as milk proteins. H*proteins showed different kinetic behaviour at A/W and O/W interfaces with longer induction period at O/W. This was mainly interpreted in terms of difference in the orientation of proteins at these interfaces. On this basis, a schematic representation of H* proteins at A/W and O/W interfaces has been proposed. However, although the H*protein A is almost twice as large than H*protein B, the adsorption rate of H*protein A was generally higher than that of H*protein B. This was attributed to the higher hydrophobicity of H*protein B. Moreover, the adsorption behaviour of H*proteins was affected by the pH with H*protein B being more sensitive. Upon examining the adsorption kinetics of H*proteins at these interfaces using Hua-Rosen kinetic parameters, it was found that the approach could effectively be used to gain relative information about the hydrophobicity of proteins.

The effect of H*proteins upon emulsion formation and stability was investigated by making emulsion stabilised by H*protein at their natural pH (pH 8) and at pH 6, using a high pressure homogeniser whereas the effect of emulsification technique was ascertained with H*protein at their natural pH. Results showed no apparent difference between H*protein A stabilised emulsions and H*protein B stabilised emulsions at pH 6. Emulsions prepared at pH 6 tend to

flocculate more than that at pH 8 and this was explained by the reduction of electrostatic repulsion as the H*proteins PI is approached which strengthened the interaction between droplets as well as between droplets and any non adsorbed proteins. H*proteins stabilised emulsions could be made using any conventional emulsification method. However dissimilarity was found in the microstructure, the degree of flocculation of these emulsions depending on the method used for their construction. There is naturally a strong hydrophobic attraction between hydrophobin molecules and whatever the method used for the preparation of emulsion, the general trend suggested that H*proteins somewhat keep this property once adsorbed at the oil/water interface. On the other hand the effect emulsification method on the oxidative stability yielded inconclusive results because the membrane emulsification system was pressurised with air. However the results from the emulsion made with Tween 60 suggested that ultrasound emulsification does not cause significant oxidative damage compared to the high pressure homogeniser, and that the emulsion oxidation pathway may be different depending on the method used for its production.

The investigations into complex formation between hydrophobins and lipid oxidation products, using H*proteins as a model system has led to the conclusion that, lipid oxidation products interact with hydrophobins and this involves phenylamine and all basic amino acids. This ability of hydrophobin to bind lipid oxidation products (hydroperoxides and aldehydes) may result in quenching the propagation of free radical chain reactions and prevent/reduce flavour deterioration induced by lipid peroxidation by-products.

CHAPTER 7

ALTERNATIVE FOOD GRADE PROTEINS FOR THE PRODUCTION OF AIR FILLED EMULSIONS

7.1. Introduction

Hydrophobin HFBII (from *Trichoderma reesei*) molecules can pack together closely enough at an interface, in similar way to particles, and make a strong interfacial film with an exceptional high surface shear viscosity and rigidity. These exceptional properties have not been reported so far for any other protein. As a result micron sized air cells stabilised with hydrophobins are highly resistant to coalescence and disproportionation for substantial lengths of time and will resist oil destabilisation (Chapters 4 and 5). However, hydrophobins are rare and currently very expensive due to current industrial non-availability. This chapter deals with the use of alternative food grade proteins such as bovine serum albumin and egg albumen (egg white proteins), for the construction of air cells with a stability comparable to that of hydrophobin stabilised air cells. Firstly the effects of different parameters such as pH, protein concentration and production temperature will be presented. Secondly, the stability of the air cells when challenged by different environmental stresses is discussed. Special emphasis to those relevant to product processing such as high temperature/pressure treatment, mixing and pumping will be given. In the last section of this chapter, the tribological behaviour, by extension the mouth-feel of the suspension of the air cells is examined.

Part of data presented in this chapter has been patented and published in two journals. All these can be found in the CD, Appendix 1 (US patent application 20110287150; Tchuenbou-Magaia *et al.* (2011); Tchuenbou-Magaia and Cox (2011)).

7.2. Effect of production conditions upon air filled emulsion generation

Suspensions of air cells (AFEs) stabilised by the alternative proteins (with reference to hydrophobins) were constructed using a similar sonochemical method to that used for the construction of hydrophobin stabilised air cells (see Chapters 3 and 5). That is by ultrasonic irradiating a protein solution while sparging with oxygen or air. However, it is worth reiterating that the mechanism responsible for the formation and the stability of air cells stabilised by these alternative proteins differ from that of hydrophobins. It relies on a combination of two acoustic phenomena: emulsification and thermal/chemical cross-linking. Firstly, ultrasonic emulsification creates the microscopic dispersion of air cells in a protein solution to form the shape of the microsphere shell (i.e. acoustic templating via cavitation); secondly, superoxides generated by sonolysis of water in the presence of oxygen catalyses the formation of inter-protein disulphide bonds that cross-links the protein shell; thereby imparting the stability necessary for maintaining the microsphere shell's architecture over time (Grinstaff and Suslick, 1991; Suslick *et al.*, 1994). However, work presented here highlights that the sonochemical production of these air cells may involve a more complex mechanism than first postulated. Although the initial screening involved several cysteine rich proteins (Zein, soy proteins, whey proteins) as presented in the resulting patent, detailed study were carried out with bovine serum albumin and egg white proteins chosen as model proteins. Figure 7-1 is a typical confocal micrograph of these emulsions.

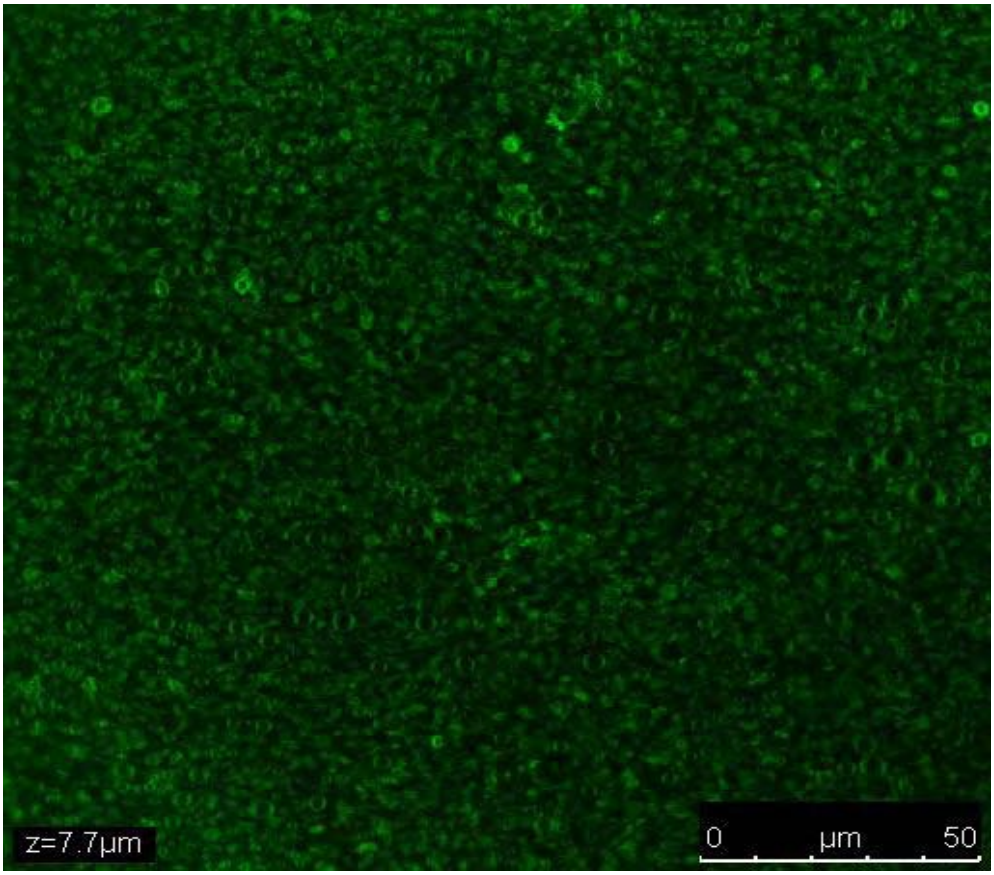

Figure 7-1. Confocal scanning laser micrograph of air filled emulsion stabilised by BSA (30% air by volume). 4 ml of AFE were mixed with 20 µl of 0.01% rhodamine B and 100 µl of the mixture (placed on a microscope slide and covered with a CoverWell imaging chamber) observed with 63X lens. Air cells can be seen with dark area (air) encapsulated inside a protein coat (green area).

The turbidity of the AFE was used as a rapid method to assess production. This net turbidity was correlated to air cells population as determined with a Coulter Counter, using BSA as a model system (Figure 7-2). The correlation coefficient was 0.969 for 95% confidence interval. It is worth noting that protein aggregates and debris could contribute to the increase of the turbidity of AFE and turbidity measurements were verified with microscopic observation.

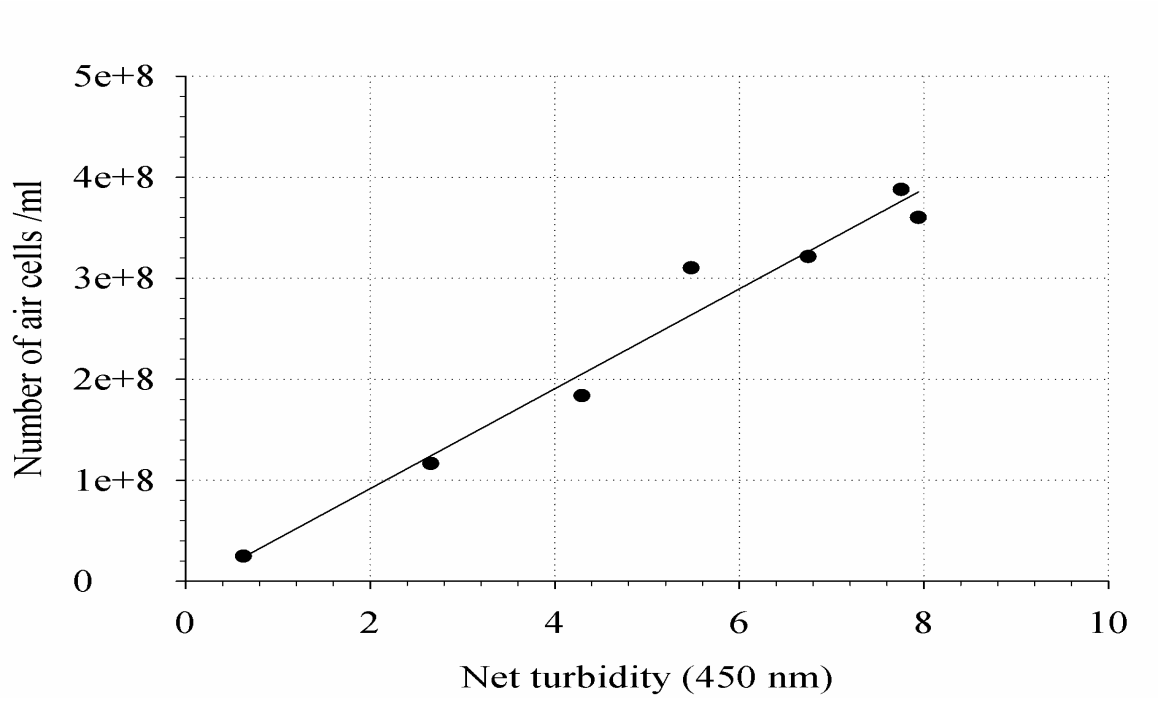

Figure 7-2. Linear regression curve showing the relationship between the number of air cells counted with a Coulter counter and the net turbidity of BSA-AFE expressed as the difference between the turbidity of AFE and that of the protein solution used for its production ($R^2 = 0.969$ at 95 % confidence interval).

The generation of air cells was found to depend not only on the position of the ultrasound horn to the solution but was also influenced by the pH and the concentration of the protein solution, the production temperature and by any pre-treatment to the protein prior the production of air cells.

7.2.1. Effect of the ultrasonic processor horn type and position upon AFEs production

The position of the ultrasound horn is a decisive factor for the production of AFEs. It had to be placed precisely at the interface between the air and the protein solution. Indeed, few or no

air cells were formed when the probe was placed inside the protein solution, but protein debris instead (Figure 7-3). Likewise, AFEs was not obtained with an ultrasonic processor, US70W/ 20 kHz fitted with two millimetre diameter horn (Figure 7-3a). Nothing was observed with a light microscope when using this slender horn (MS 72) at low amplitude (lower than 40%) and increasing the amplitude to 70 % resulted in generation of protein debris and aggregates, similar to the conditions when the 13 mm probe was placed deep inside the protein solution. These results may partially be explained by the quantity of energy transferred into the system as ultrasonic irradiation of a water solution with the horn at different position yielded different estimated energy input (Figure 7-4). The intensity is inversely proportional to the horn area and if the horn area decreases, then the intensity increases. Therefore, it may be speculated that the ultrasound power (which is proportional to the square of the amplitude) and the ultrasound intensity (the rate at which energy passes through the unit area) play an important role in the AFE formation.

It has been suggested in the case of an O/W emulsion that acoustic emulsification involves the disruption of the O/W interface, that is, the ultrasonic waves push along the O/W interface leading to the formation and ejection of large droplets into the water phase. These large droplets are then broken up into tiny emulsified droplets when in contact with the transient cavitation regions (Li and Fogler, 1978; Cucheval and Chow, 2008). Interestingly, Cucheval and Chow (2008) found that emulsion can only be produced when the O/W interface is in the transient cavitation rich region, directly below the probe tip. This corroborates with what observed here and evidence the role of the initial ultrasonic emulsification step in the formation of AFEs (see Table 2-1, Chapter 2).

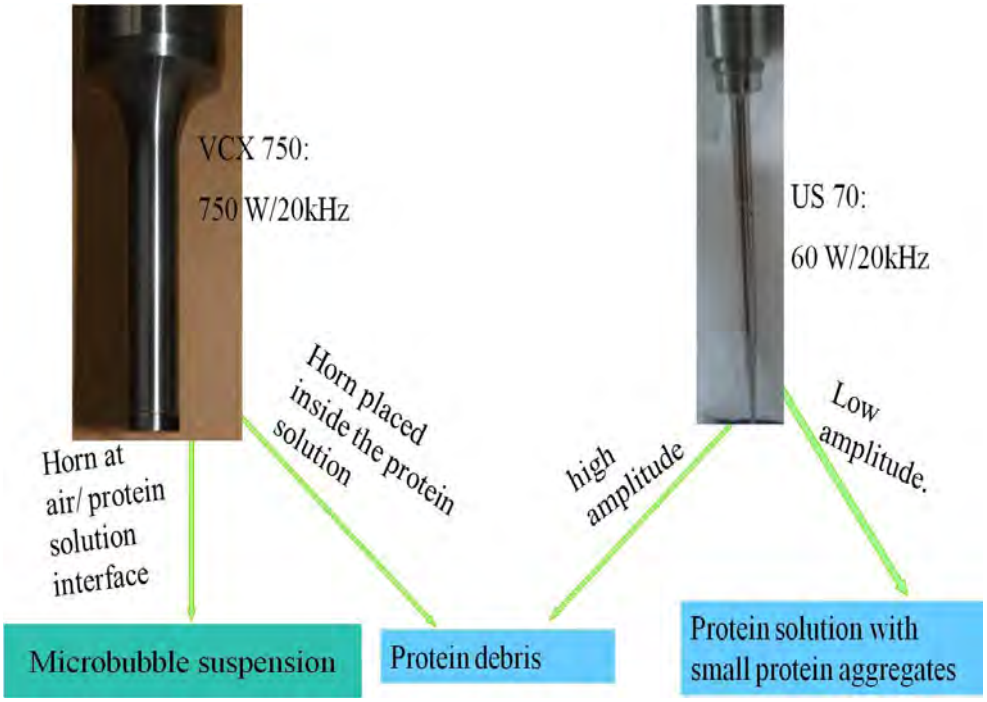

(a)

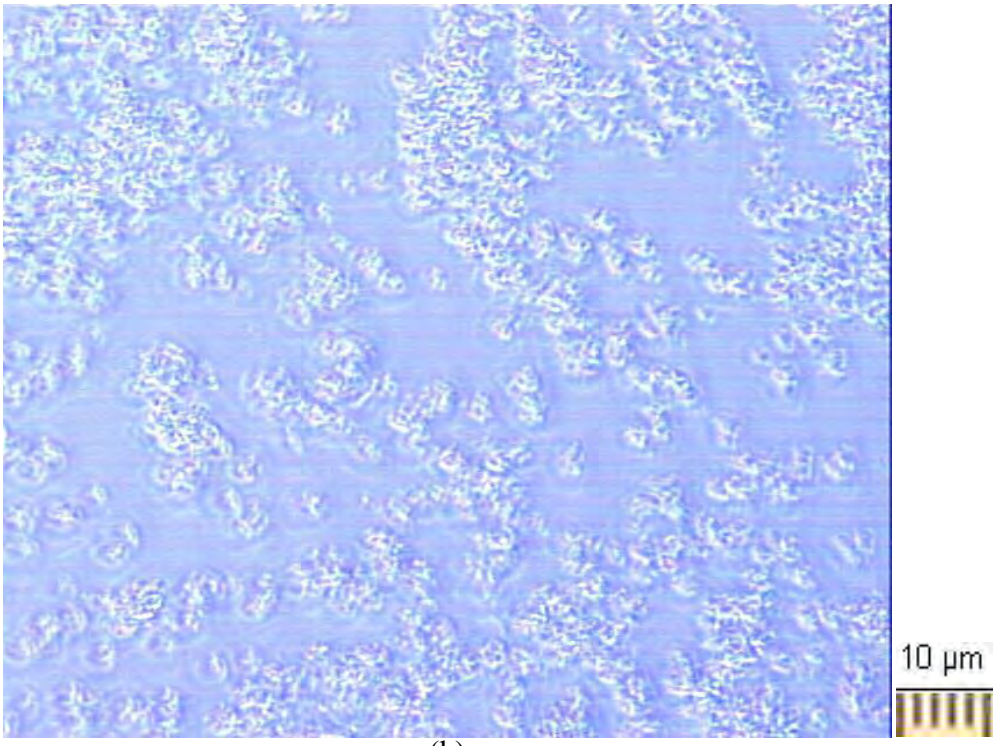

(b)

Figure 7-3. Effect of the ultrasonic processor horn type and position on the AFEs formation. Type of horn used and their effect, (b) typical protein debris and aggregates obtained when a wrong horn was used or the sonicator tip was not placed at the air/protein solution interface.

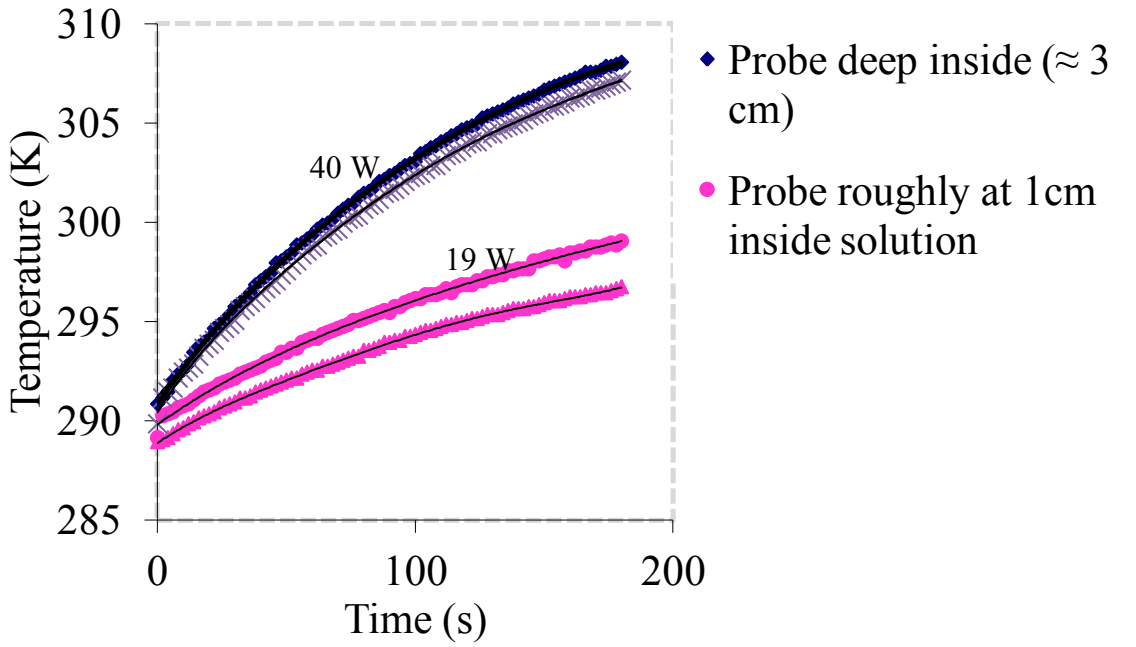

Figure 7-4. Effect of the position of the horn on the energy input during sonication.
For clarity reason, only two replicate examples of the same experiment are shown . The energy transferred into the solution was calculated through $Q = mCp.\Delta T/\Delta t$ (see Chapter 3). The measurement assumes that all ultrasound energy that propagates in the liquid is converted into heat and the loss of energy by thermal exchange at the liquid–liquid interface and at the walls of the vessel is neglected.

7.2.2. Effect of pH/ionic strength and temperature

An attempt was made to construct AFEs with BSA (BSA-AFEs) and EWP (EWP-AFEs) at pH ranging from 3 to 9. The concentration of the protein solution was kept constant, 5% (w/v). Figure 7-5 is a typical graph of the net turbidity of AFE as function of the pH. It can be seen that, for BSA, the yield was maximum at pH 5 and decreased at pHs either side of this pH. It was not possible to make BSA-AFE at pH 3 and 9 as confirmed by light microscopy. Three explanations may be given for these results: (1) a decrease in the rate of adsorption with increasing protein net charge (Wierenga *et al.*, 2005); (2) a change in the secondary and tertiary structures of BSA at extreme pH which reduces its binding capacity to an interface (3)

or the combination of (1) and (2). Around the protein P*I* values, the electrical repulsive force at an interface is minimised or eliminated. This favours the adsorption of proteins and formation of additional layers. Moreover it has been reported that BSA exists in several isoforms depending on the pH, with an increase in its diameter from 10 nm at pH 2.0 to 11, 13 nm and 22 at pH 3.5, 5.0 and 7.0, respectively. The native form with a globular shape is predominant in the pH range 4.5 and 7.0 (Gryboś *et al.*, 2004). BSA conformational changes as function of pH as reflected by the increase in its diameter may correlate with the ability of the protein to form AFEs; an optimal BSA diameter might exist, but this is to be investigated, along with elucidating the exact mechanism.

In contrast to Suslick and co-workers (1994) who initially sonochemically produced BSA stabilised microbubbles at pH 7 (for imaging), no air cells were produced with aqueous BSA in 0.2M sodium phosphate buffer at pH 7 in the experimental conditions using in this work. When the buffer concentration was reduced to 0.01M, it was possible to produce air cells but the phase volume was lower than that observed at pH 5 and at protein natural pH which was around pH 5. This implies that, ionic strength might be among the factors that influence BSA-AFE formation. King *et al.* (1999) have shown by studying the reactivity of the cysteine of silver hake parvalbumin with DTNB that the reactivity of cysteine is buffer species dependent with a substantial change in the kinetic profiles with buffers of different ionic character.

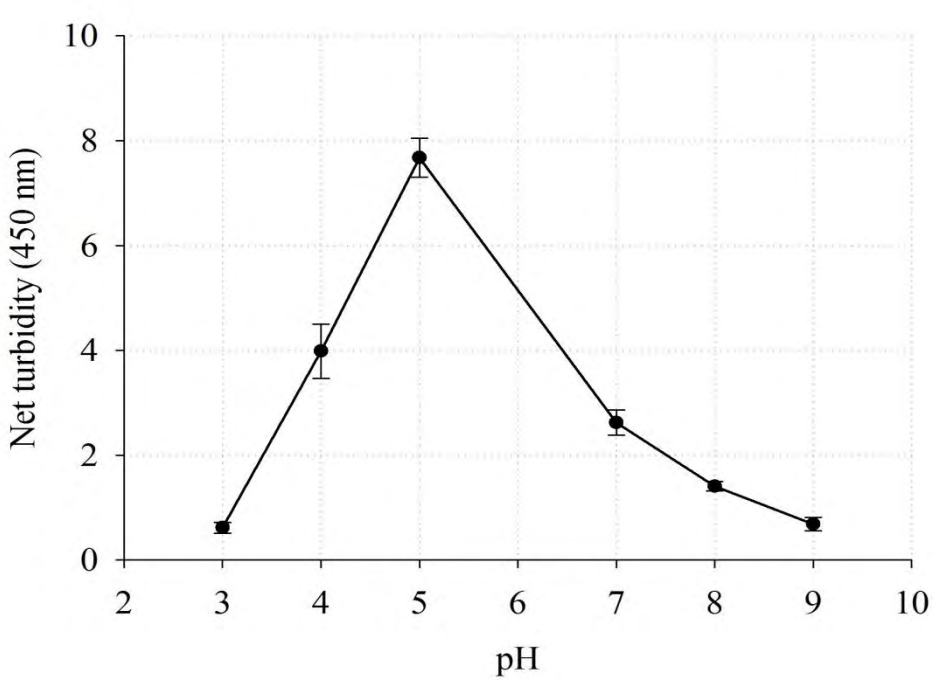

Figure 7-5. Effect of pH upon BSA-AFE yield. Turbidity measured for 2 days old sample.

Likewise EWP-AFE made at pH above 4 was physically unstable (i.e. phase separated) especially when formed at temperature higher than 50°C. This phenomenon was more pronounced at pH between 4.5 and 6. When EWP-AFE was constructed under these conditions, samples phase separated into three layers. The middle phase, made up mainly of water, separated the bottom layer constituted of larger protein aggregates entrapping a small number of bubbles and the top layer with relatively small aggregates without air cells. The formation of protein aggregates could be due to the deprotonated carboxycilic acid providing a salting out effect, which was enhanced by the rise of temperature upon sonication. Egg albumin consists of more than 12 proteins and the five major proteins based on dry mass are: Ovalbumin (54 %; PI, 4.5), Ovotransferrin (13 %; PI, 6.1), Ovomucoid, (11 %; PI, 3.9), Ovoglobulins (8 %; PI, 5.5) and Lysozyme (3.5%; PI, 10.7) (Klostermeyer *et al.*, 2000; Campbell *et al.*, 2003). Acidic amino acid residues, aspartic and glutamic acid, are negatively

charged above a pH of 4.0-4.5 (de Jongh, 2007) and at pHs higher than those pHs all the carboxylic acid groups are deprotonated. These carboxylate anions would increase the dissipation of water from the solvation layer around proteins, thereby promoting protein aggregation. For example, Avivi and Gedanken (2002) were able to produce microspheres sonochemically with a poly(glutamic acid) protein only at pHs lower than 4.5 which is close to the pKa (≈ 4) of the side chain carboxyl groups of glutamic acid residues. In the case of egg albumin, the presence of several proteins with different PI may lead to stronger attraction or repulsion forces between some of the proteins, leading to phase separation.

The greatest yield of air cells was obtained at pH 5 for BSA (Figure 7-5). The size of air cells increased slightly as the pH of their production moved away from the PI. CascaoPereira *et al.* (2003) who investigated the structural conformation of BSA at a single air/water interface over a range of pHs, reported that the BSA conformation in solution are the origin of the difference in A/W surface coverage and that the absorption at the air-water interface was high around BSA isoelectric point (where protein structure are most compact and stable) as well as pH 7. Their finding is in agreement with those of Martin-Rodriguez *et al.* (1994) who reported a maximum adsorption of BSA to hydrophobic latex at pH 5, again close to BSA PI.

As discussed above, because EWP contains several proteins with different denaturation temperatures and isoelectric points, the optimum air cells generation pH lies between pH 3 and 4 depending on the production temperature (Figure 7-6 and 7-7). EWP-AFE constructed at high temperature (60°C and 70°C) yielded larger air cells compared to those produced at 50°C (Figure 7-6d and e). Also, Figure 7-6 and Table 7-1 show that incubation of Egg albumen before sonication at 50°C resulted in a high yield of smaller air cells. However this treatment seems to have an optimum duration (around 50 min). A longer incubation time (100

mins) showed a detrimental effect on the stability of air cells. A study carried out by MEng students under my supervision (the results are not presented in this thesis) showed a similar trend, but to a lesser extent, when EWP powder was heat-treated at 50°C for 3 days before dissolution. However, AFE made with heat-treated BSA at 40°C (about 20°C below its denaturation temperature, even for only one day) was less stable than that made with non treated protein. Also, the highest yield of microbubbles was obtained at pH 5.5 and not at pH 5.0, as seen with the untreated protein. These results confirm the complexity and intriguing effect of partial protein denaturation (e.g., by temperature treatment) on the protein surface activities and emulsions formation/stability, as discussed in Chapter 2, section 2.2.2.

On the other hand, Table 7-1 and Figure 7-8 show that AFEs stabilised with BSA or EWP had a lower volume fraction of air (20-30 %) than those those stabilised with hydrophobins (40 %). In contrast to the hydrophobin system where there were no significant changes in the air volume fraction (as inferred from monitoring the height of AFE in a graduated tube over time) over 48 days, AFEs stabilised with these alternative proteins showed a decrease in their intial air volume fraction which reached an asymptote at about 10 % after two days storage. These results may be linked to the apparent critical bubble size (around 3 μm) above which air cells stabilised with BSA or EWP become less stable to environmental stresses (see later discussion, section 7.3).

Table 7-1. Air phase volume as function of pH and the production temperature.

Protein	**Air phase volume (%)**
BSA, pH 5.0, 50°C	32 ± 5
EWP, pH, 3.8, 50°C	24 ± 4
EWP, pH, 3.8, pre-incubation at 50°C for 50 min	30 ± 3
EWP, pH, 3.0 50°C	25 ± 5
EWP, pH, 3.0, 70°C	27 ± 3

The air phase volume was measured 2.5 hours after the production of AFEs in order to allow all the larger unstable bubbles to disappear.

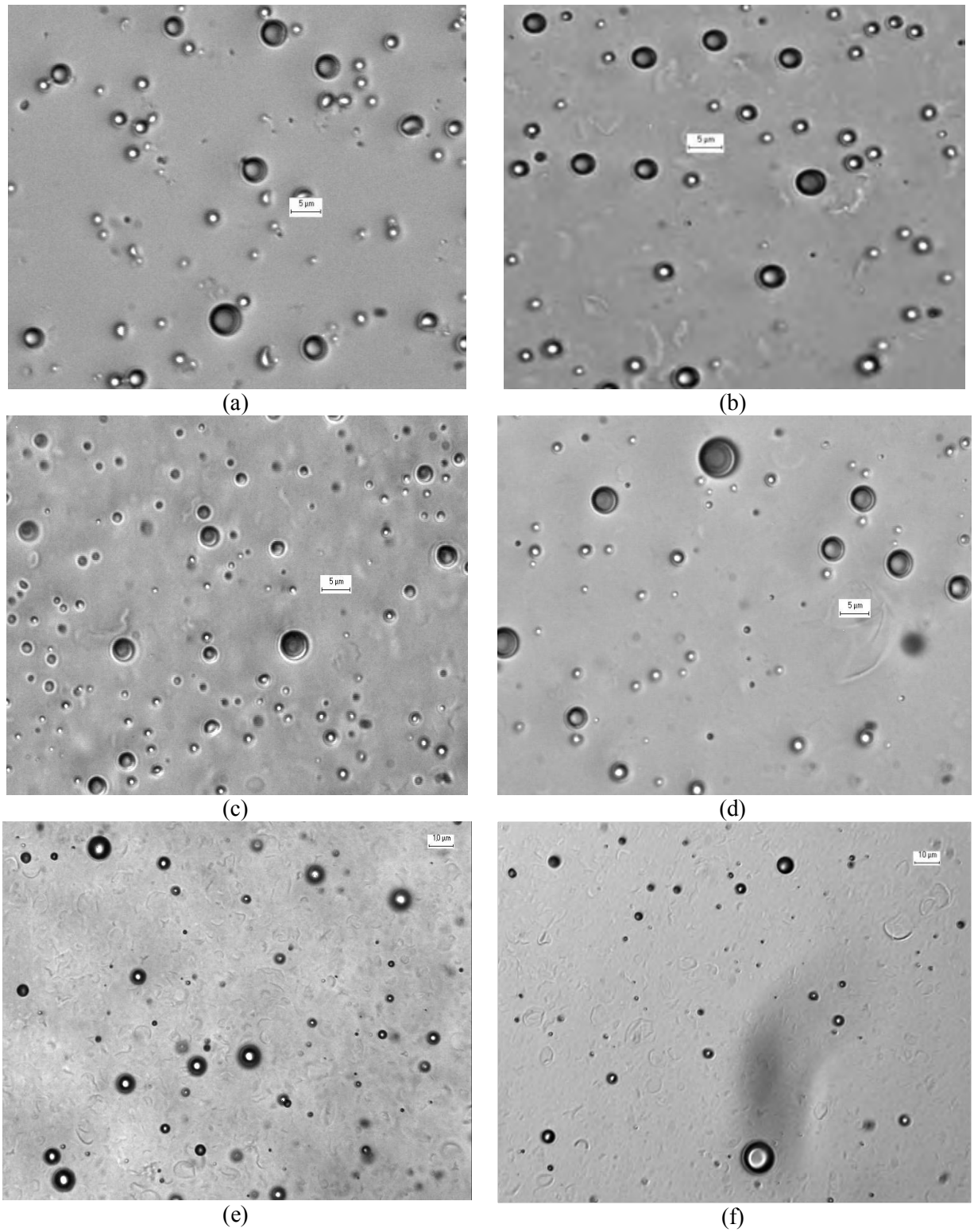

Figure 7-6. Micrographs of AFEs. AFEs made with alternative proteins: (a) BSA-AFE, pH5, 2 days; (b) EWP-AFE, pH3.8 2 days; (c) EWP-AFE, pH3.8, pre-incubation 50 mim, 2 days; (d) EWP-AFE, pH3, 50°C, 2days ; (e) EWP-AFE, pH3, 70°C, 2 days (f) EWP-AFE, pH3, 70°C, 47 days. The estimated air volume fraction is about 10%.

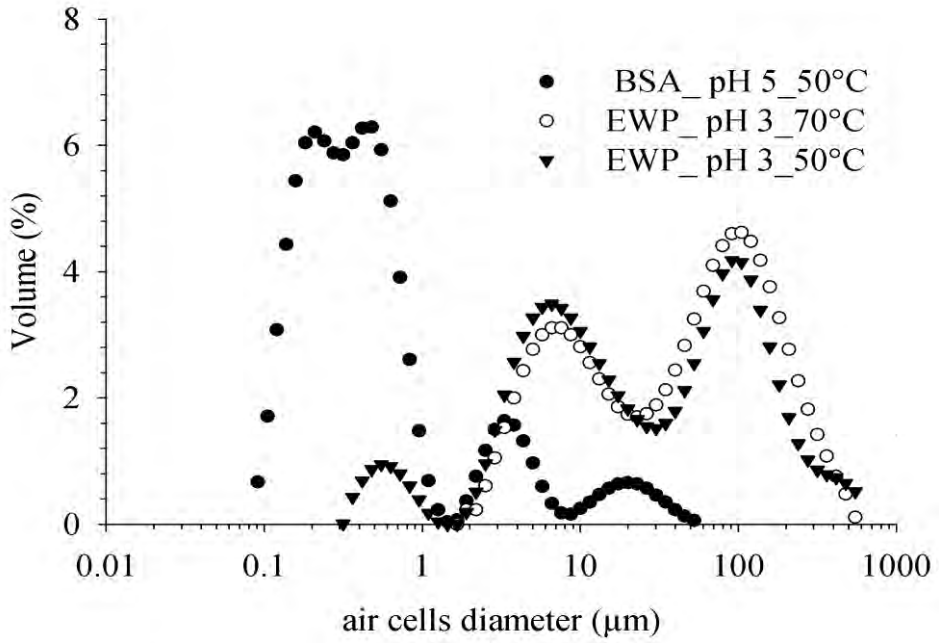

Figure 7-7. Comparison of air cells volume distribution for AFEs made with BSA and EWP (2 days old sample).

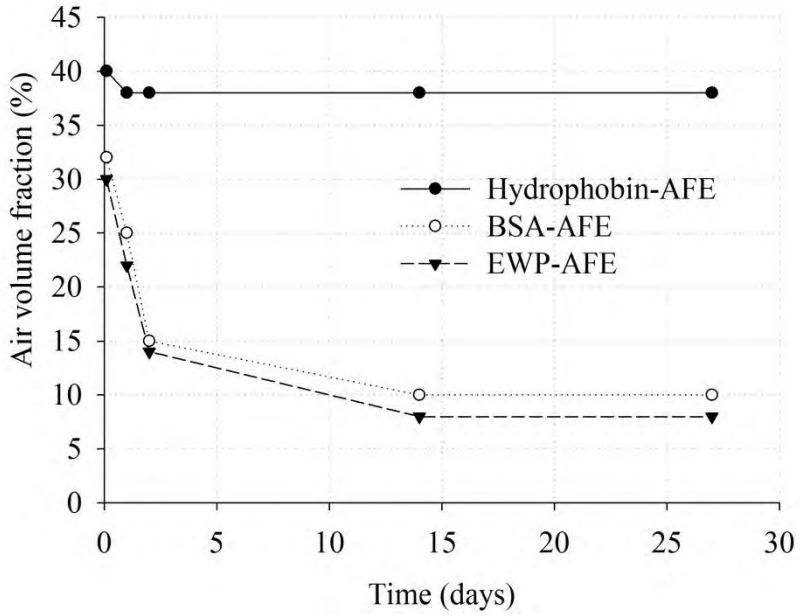

Figure 7-8. Typical air phase volume as function of time for AFEs made with BSA and EWP.
For comparison purpose, a time-course of air volume fraction in AFE stabilised by hydrophobin is also presented.

7.2.3. Effect of protein concentration

Figure 7-9 and Figure 7-10 show that the production yield of AFEs made with EWP was directly proportional to the protein concentration. This is slightly different to BSA-AFE where air cells population tended to become asymptotic at around 4% and 5%. This could be explained by the net concentration of EWP available for the adsorption at air-water interface. Damodaran *et al.* (1998) has demonstrated that the composition of the mixed protein film depends on the ionic strength of the bulk. This was achieved by studying the competitive absorption of five major egg white proteins (ovalbumin, ovotransferrin, ovomucoid, and ovoglobulins and lysozyme) from a bulk mixture (at concentration ration similar to that found in egg white) to the air-water interface, Moreover they reported that ovalbumin and ovoglobulins arrived first at the interface and the late-arriving proteins (ovotransferrin, ovomucoid and lysozyme) could not displace the adsorbed proteins. Also, and as expected the concentration of the protein determine the long term stability of the AFE. Figure 7-10 shows typical micrographs of AFEs made with different protein concentration and stored at 8°C and only few air cells can be seen at 2% protein after 14 days storage. This may be interpreted by the fact that higher bulk protein concentrations favour a high concentration of the protein at the interface and as consequence more reactive groups, all within the time scale necessary for the interfacial chemical reactions to take place.

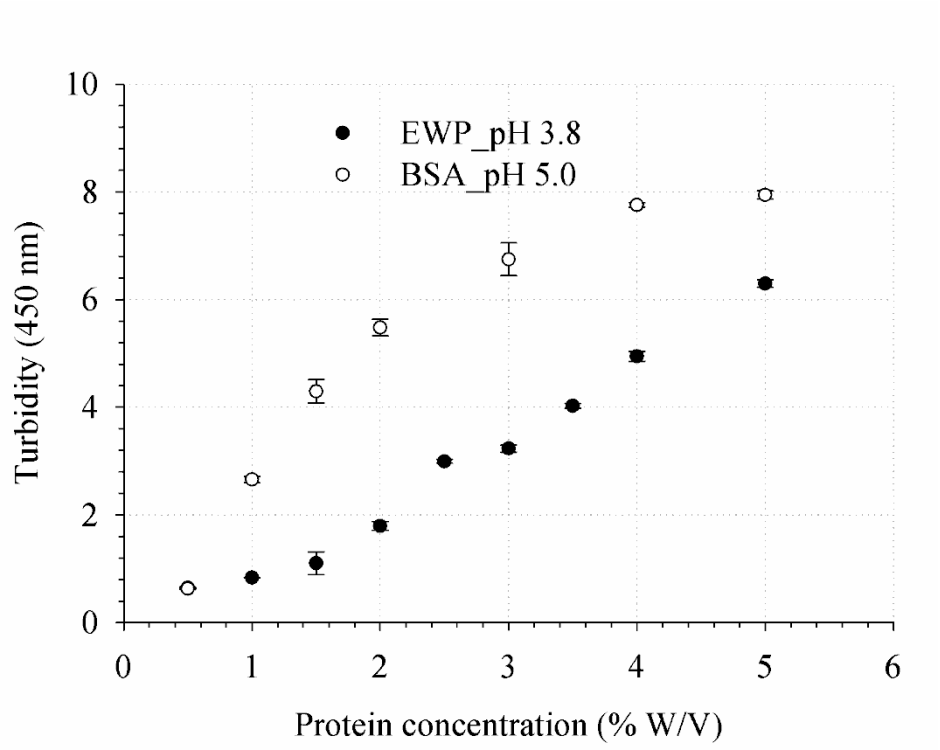

Figure 7-9. Effect of protein concentration upon AFEs production yield.

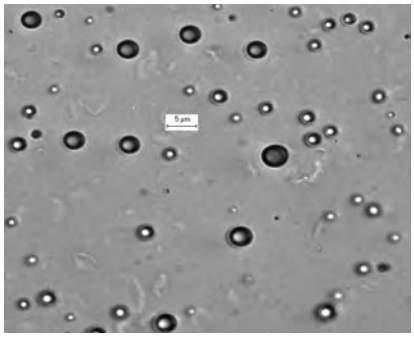

5 % (a)

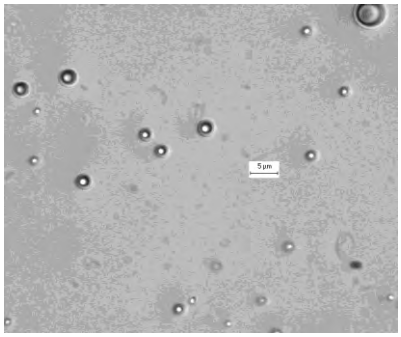

3 % (a)

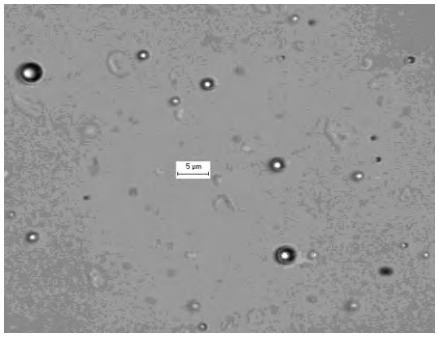

2.5 % (a)

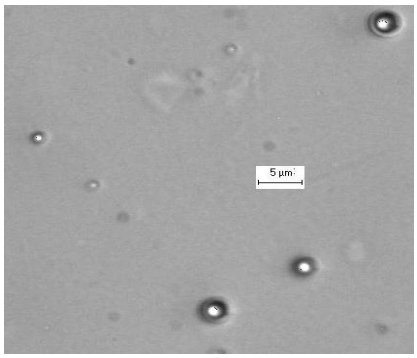

2.0 % (a)

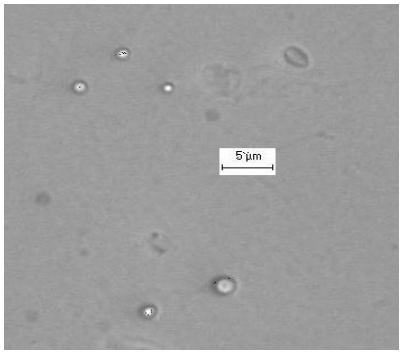

1.5 % (a)

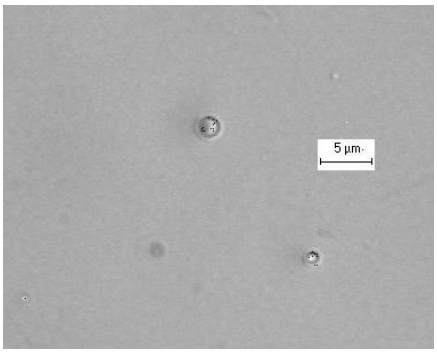

0.5 % (a)

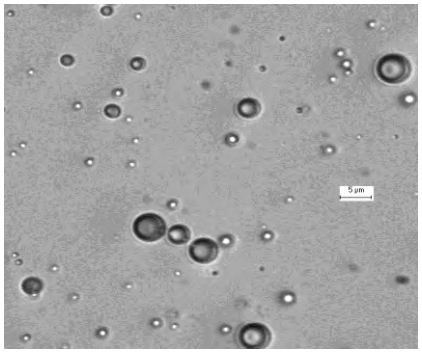

5 % (b)

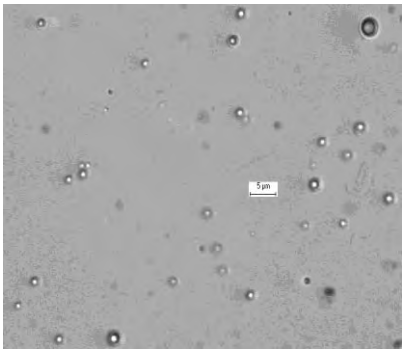

3 % (b)

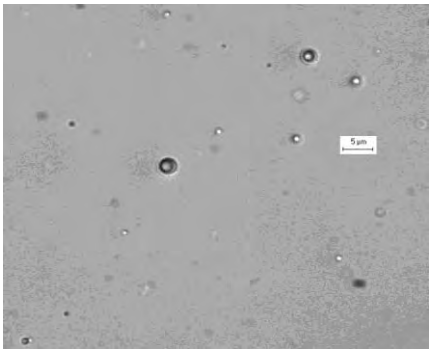

2.5 % (b)

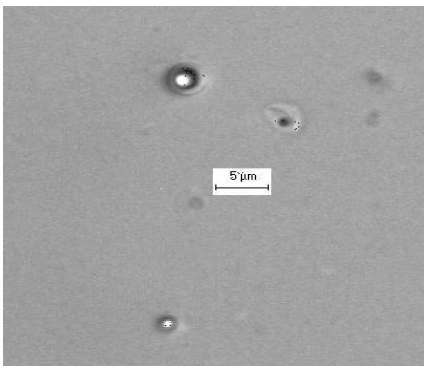

2 % (b)

Figure 7-10. Representative micrographs showing the effect of protein concentration upon AFEs production yield and stability. Case of EWP-AFE, pH 3.8 made at 50°C. (a) 2-day old (b); 14 day old storage at 8° C. No bubbles were observed in 0.5 % -1.5% samples after 14 days.

It is worth mentioning though that some variability between proteins was observed. Indeed air filled emulsion could be produced using two type of BSA, fraction V and BSA obtained via heat shock fractionation process. However, the same protein type when purchased from the same supplier but from a different batches did not allow for the construction of air filled emulsion using the production conditions described above, or where it was possible to form AFEs, poor stability was observed. This is not the first time such variability has been observed. Discrepancy in surface properties of different batches of commercial "pure" globular proteins has also been reported (Dickinson and Pawlowsky, 1997). Although some hypotheses can be put forward based upon published work, the actual reasons for these observations are uncertain and deserve a systematic investigation; as suggested in the follow up section of this thesis.

The probable hypotheses of the loss of BSA functionality are a loss of molecular flexibility, dimerisation of the protein owing to its production conditions and storage history or the presence of trace of metal ion bound to the protein. For example, it has been demonstrated that cadmium affects the adsorption of BSA at the air/aqueous phase interface and that at low concentration of cadmium, less than 10^{-8} M, the cation interact with two negatively charged site on two different BSA molecules, leading to a more structured BSA-dimer with lower diffusion and adsorption rate (Graham *et al.*, 1981). Because cavitation only provides a short-lived (millisecond timescales), air/water interface used as a template for BSA layer formation, less proteins may be present at the interface to allow protein cross-linking or the bridging ion may prevent rapid conformation change and multilayer protein adsorption needed for BSA-AFE formation and stability (see next section). Also, an interesting work by Suzawa and Shirahama (1991) which compares a commercially available protein (native) and a heat denatured BSA showed that the native BSA contained, in addition to BSA monomer, 8 % of

BSA dimers and a very small amount of trimers; whereas the heat-denatured one consisted of 11 % native monomers, 66 % modified monomers, 20% dimers formed mainly by intermolecular SH/S-S exchange reaction (i.e., modified monomer (SH) + modified monomer (S-S)) and 3 % trimers. The modified monomers were formed by intramolecular SH/S-S exchange reaction. Considering these findings, and with in mind the work of Grinstaff and Suslick (1991), which demonstrates that air-filled proteinaceous microbubbles could only be formed only from proteins that have cysteine residues, it is plausible to hypothesise that a loss of BSA flexibility and/or dimerisation with involvement of the unique sulphidryl group present in BSA account for the reduced ability of the protein for the production of AFE.

7.3. AFEs stability to environmental stress

The main purpose of assessing the effect of environmental stresses upon AFEs stabilised by these bulk proteins was to find out if air cells within these AFEs are sufficiently resilient (as those stabilised by hydrophobins) to allow further processing, for example, to concentrate the air cells and for industrial production.

7.3.1. Stability to centrifugal force and shear stress

AFEs were centrifuged at different speeds at room temperature in order to obtain higher air cells in the upper phase. These concentrated air cells were then used to make triphasic A/O/W emulsions under identical conditions to those used in the case of hydrophobin stabilised samples (7 min shear with a Silverson mixing). The air cells were stable to the gravitational force at around 1000 rpm (≈ 200g) for 3 min. Therefore, the centrifugation of AFEs at this speed enabled bubbles to be concentrated at the upper layer (Figure 7-11a) and to separate

protein debris at the bottom layer (Figure 7-11c). Further increase in the centrifuge speed led to the destruction of air cells (estimated by the increase in the proteins debris in bottom layer). Air cells within BSA-AFE were completely destroyed when centrifuged at 4000 rpm (3255g) for 10 min (Figure 7-12a) and only protein debris (bottom layer) and a transparent liquid (upper layer) remained. However, and surprisingly, the stability of air cells to centrifugal force was improved remarkably when they were present in more viscous formulation. Indeed, in the above conditions (4000 rpm/10 min) air cells survived centrifugation (see Figure 12b-f and below discussion).

An air based triphasic A/O/W emulsion, model salad dressings (BSA-MSD) made by diluting and mixing the concentrated BSA-AFE with an O/W emulsion was tested. Four layers were observed after centrifugation, each with distinct air cells size distributions and are summarised in Table 7-2. This indicates that the presence of mixed compounds improved the stability of air cells possibly because of the increase in the viscosity of the bulk which has slowed down the momentum of air cells collision and destruction. However, bubble size distributions in each of these layers were in the inverse order to what would have been expected. As a general rule larger bubbles are more buoyant than smaller ones, which should mean larger air cells in the upper phases. Although the reason behind these conflicting data is not clear, one of the reasonably sound arguments to put forward is the colloidosome behaviour of air cells. Smaller air cells have large surface area which may allow them to sit better (than larger ones) at the surface of oil larger droplets (Figure 7-12). This association would allow them to be entrained, i.e. upward, during the centrifugation. This hypothesis is in line with the suggestion from Chapter 5; i.e. a possible pickering-like stabilisation of hydrophobin stabilised air cells by smaller oil droplets, and vice versa.

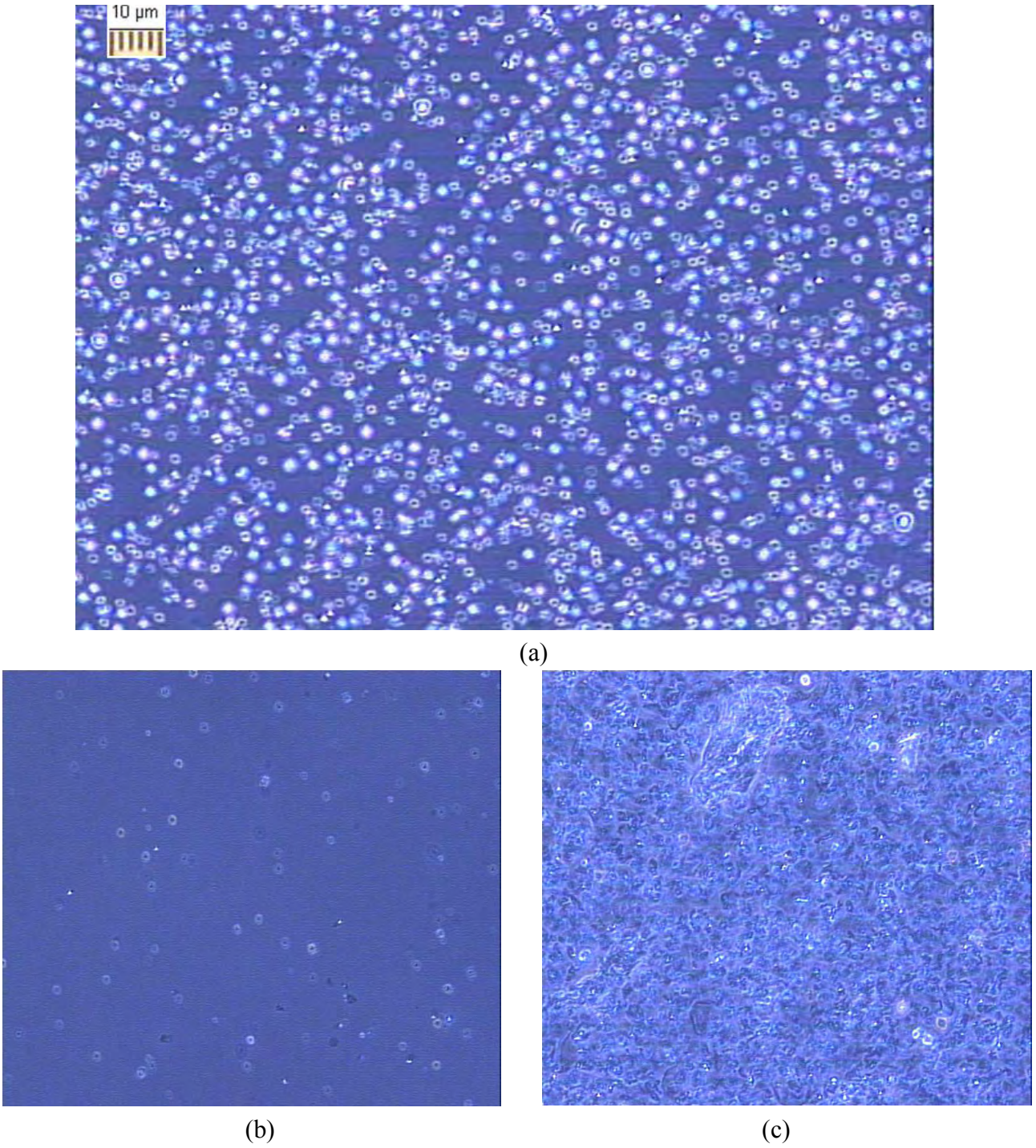

Figure 7-11. Light micrographs of layers obtained after concentration of BSA-AFE by centrifugation. The centrifugation was performed at 1000 rpm for 3 min. (a) is the upper layer rich in air cells, approximately 60% air by volume, (b) the middle layer and (c) the bottom layer rich in protein debris.

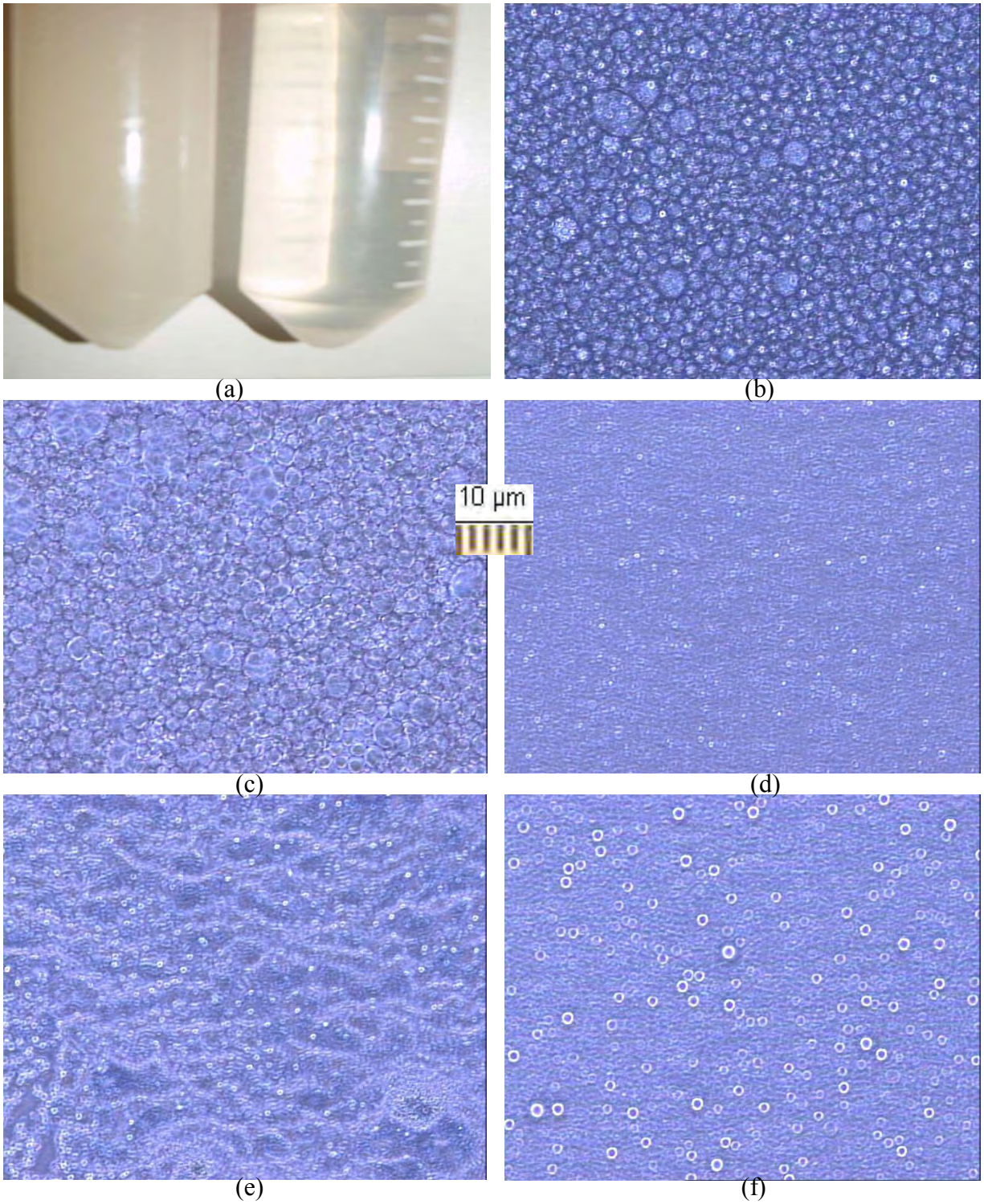

Figure 7-12. Effect of high speed centrifugation upon BSA-AFE and the subsequent triphasic emulsion model salad dressings (20% air and 30% oil by volume).
(a) is the picture of the BSA-AFE before and after centrifugation; (b) micrograph of a one day old BSA-AFE based triphasic emulsion model dressing (BSA-MSD) and (c), (d) (e) and (f) are different layers (from top to the bottom) obtained after centrifugation of BSA-MS. Refer to table 2 for the charactersistic of each layer.

Table 7-2. Different layers with distinct bubbles size distribution after centrifugation of BSA-MSD at 4000 rpm/10min (from top to bottom of the centrifuge tube).

Layers after centrifugation	Characteristic of the layer	Code in Figure 7-7
The upper layer	Mainly formed by oil droplets	(c)
The layer below the upper	Smaller bubbles	(d)
The above the bottom layer	Bubbles with mean size	(e)
The bottom layer	Larger bubbles	(f)

The layout of the air cells and oil droplets within the triphasic A/O/W emulsion has been identified so far by the difference in their original particle sizes. In order to confirm the microstructure of the triphasic A/O/W emulsion, samples were examined via confocal microscopy. This was performed with a simplified formulation of a BSA-AFE based triphasic A/O/W emulsion, and was made with an equal volume of BSA-AFE and an O/W emulsion stabilised with Tween 60 with just water and oil. The triphasic emulsion (Figure 7-13c) was simultaneously stained with Nile blue and Nile red individually dissolved in pure ethanol. Nile blue coloured any phases rich in protein (air cells and non adsorbed proteins (Figure 7-13a) whereas Nile red stained the oil phase (Figure 7-12b). Figure 7-13a also confirms the interaction between air cells (via their protein shell, strong blue) and non- adsorbed proteins (light blue), leading to a network-like structure. This image illustrates and explains the weak gel-like behaviour of the triphasic emulsion as seen in Chapter 5 via the rheology results and the stability to creaming of the triphasic emulsions.

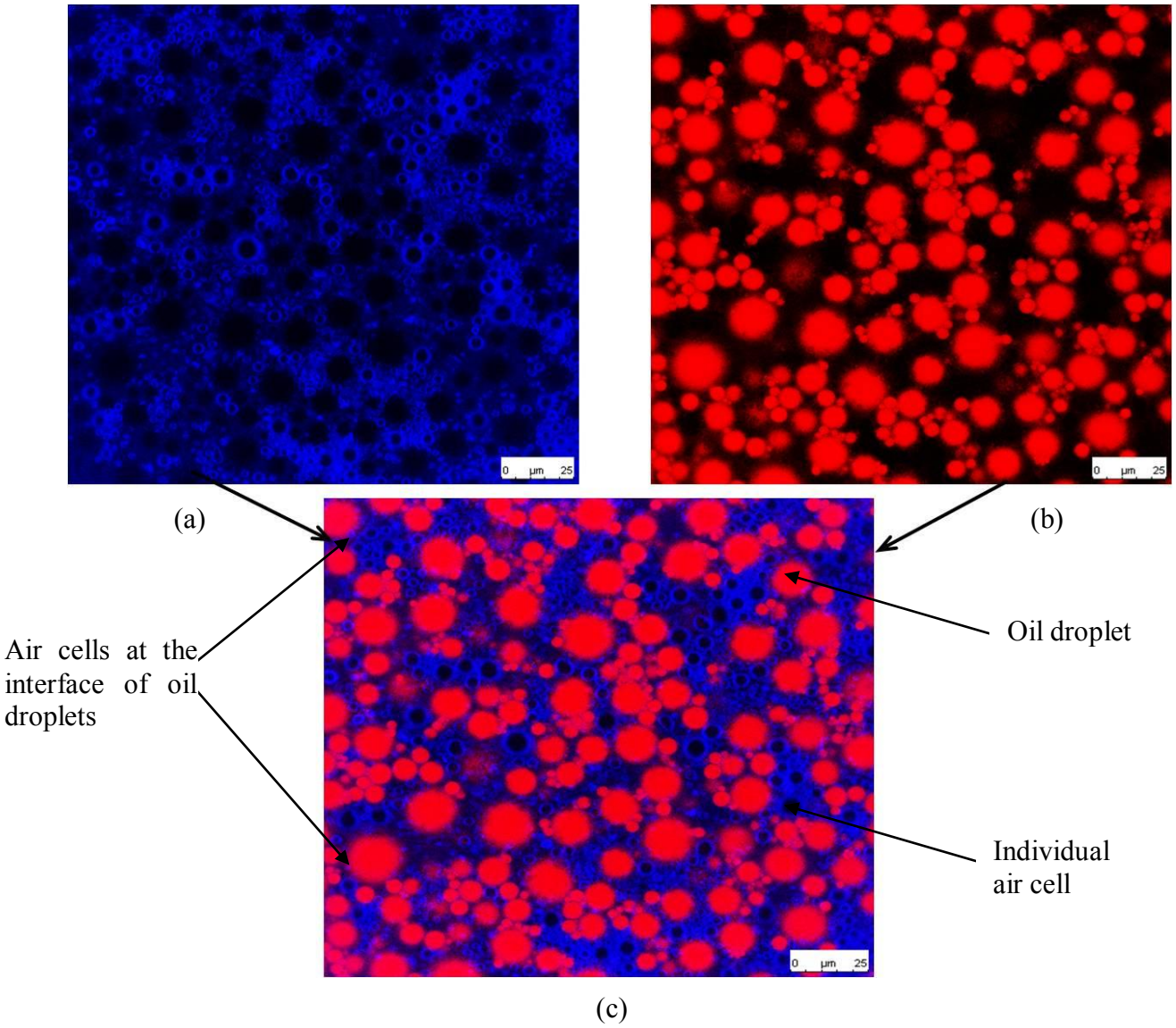

Figure 7-13. Typical microstructure of the triphasic air based A/O/W emulsion.
The emulsion was simultaneously stained with Nile blue which stains proteins and allow observation of the distribution of air cells, black with blue protein coat (a) and Nile red which stains oil droplets red (b). (a) and (b) were then merged using the built in microscope software to give (c),the whole microstructure of the triphasic emulsion (20 % air and 10% oil by volume).

7.3.2. Stability of AFEs to high temperature/pressure and mild vacuum

Many product processing steps involve relatively high pressure (e.g. pumping) and temperature treatment (e.g. pasteurilisation and sterilisation). BSA-AFE and EWP-AFE were subjected to a vacuum and sterilisation (121°C / 15 min, 1 Bar). Figure 7-14 shows that larger air cells (≈ bigger than 3 µm) were completely destroyed when EWP-AFE was treated for 3 h under a laboratory water ring vacuum system. This treatment showed little effect on the bubbles size distribution for BSA-AFE with approximately 90% of air cells falling within 0.1-3 µm (Tchuenbou-Magaia et al., 2009b).

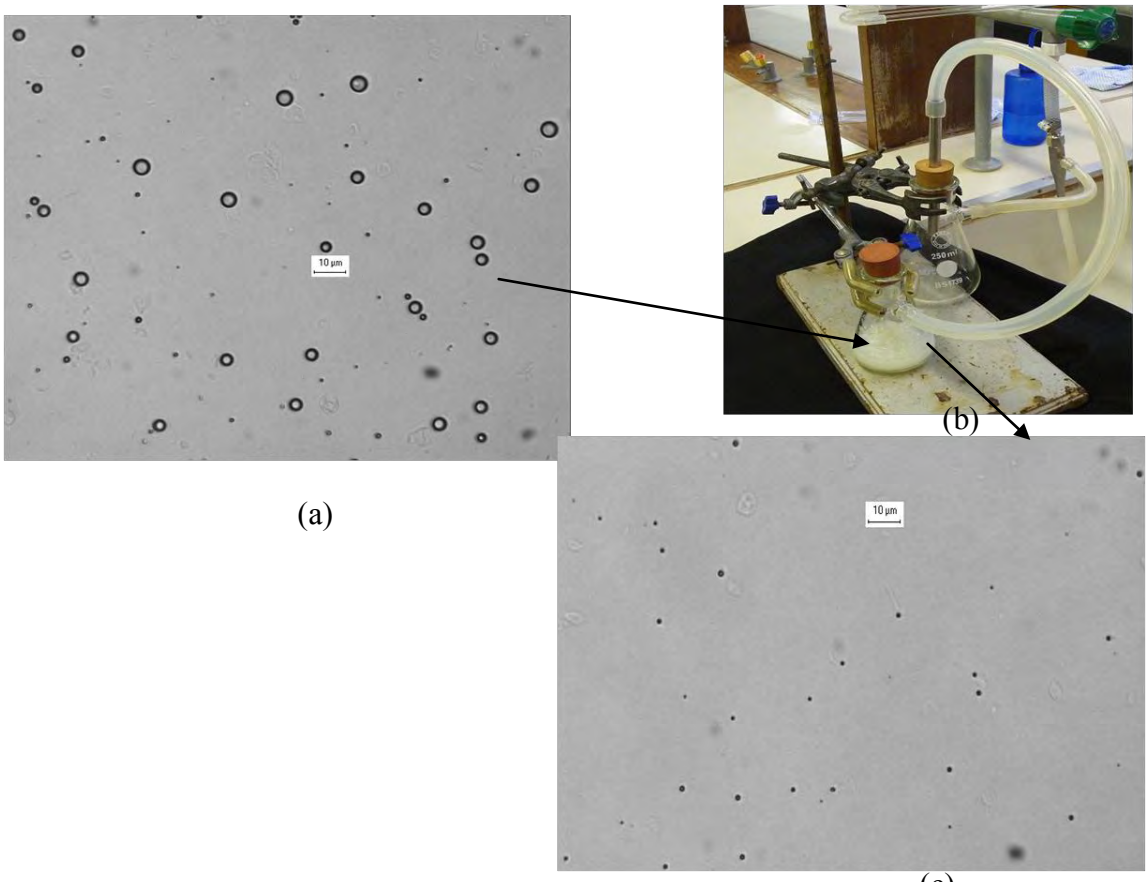

Figure 7-14. Effect of vacuum treatment upon AFE made with alternative proteins: Case of EWP-AFE. EWP-AFE, pH 3.8 made at 50°C (a) was subjected to a vacuum treatment (b) for 3 hours and only smaller air cells (≤ 3µm) survived (c).

Similar results were obtained after BSA-AFE and EWP-AFE underwent a complete sterilisation cycle (121°C/15 min, 1 Bar). AFEs under these conditions became gel-like due to the gelation of non adsorbed proteins but with the smaller surviving air cells entrapped within the gel matrix. Interestingly, EWP-AFEs initially prepared at 70°C formed a transparent soft gel that exuded water just after being removed from the autoclave. Conversely, EWP-AFEs constructed at 50°C formed an opaque gel but less opaque than that of BSA-AFE (Figure 7-15a). Moreover, the BSA gels were grainy and harder with a lower penetration distance when compared to EWP-AFEs constructed at the same temperature (Tchuenbou-Magaia et al., 2011). These results suggest a novel route for the production of a range of aerated protein gels with different properties.

Air cells in the AFEs made with EWP at 50°C withstood this treatment better than those of EWP-AFEs made at 70°C. Here again, the effect of the reduction of the motion of air cells (by increasing the viscosity or by gelation of the system) upon their stability is apparent. It can be postulated that high sonication temperature (70°C) may have led to a partial loss of egg white protein flexibility. This would result in a reduction of the EWP-AFE to withstand any further pressure changes; but also the very soft gel-like product formed during the treatment may have played a role. The later point was confirmed by subjecting a diluted EWP-AFE to the same treatment following by a microscope observation, which indeed revealed no air cells.

Figure 7-15b-f are micrographs of heat treated EWP-AFEs obtained with ESEM and the standard SEM techniques. Samples for the ESEM was removed from the container and processed as is (close to the original, native state) whereas the high vacuum mode samples were air-dried (by leaving them overnight or for 2 days in a fume cupboard) and coated with gold. A slightly larger range of size can be seen in the ESEM micrographs (Figure 7-15b and

(Figure 7-15e) compared to the conventional high vacuum SEM micrographs (Figure 7-15c) and (Figure 7-15f); 0.5-7 µm compared to 0.5- 3 µm. These results demonstrate the possible existence of a threshold size of air cells (around 3µm) above which air cells within AFEs are less stable to environmental stresses. Talu *et al.* (2008) observed that monodispersed microbubbles produced by flow-focusing and stabilised with a mixture of phospholipid derivates grew and underwent Ostwald ripening if their initial size were 12 µm but remain monodispersed when they were initially 2 µm.

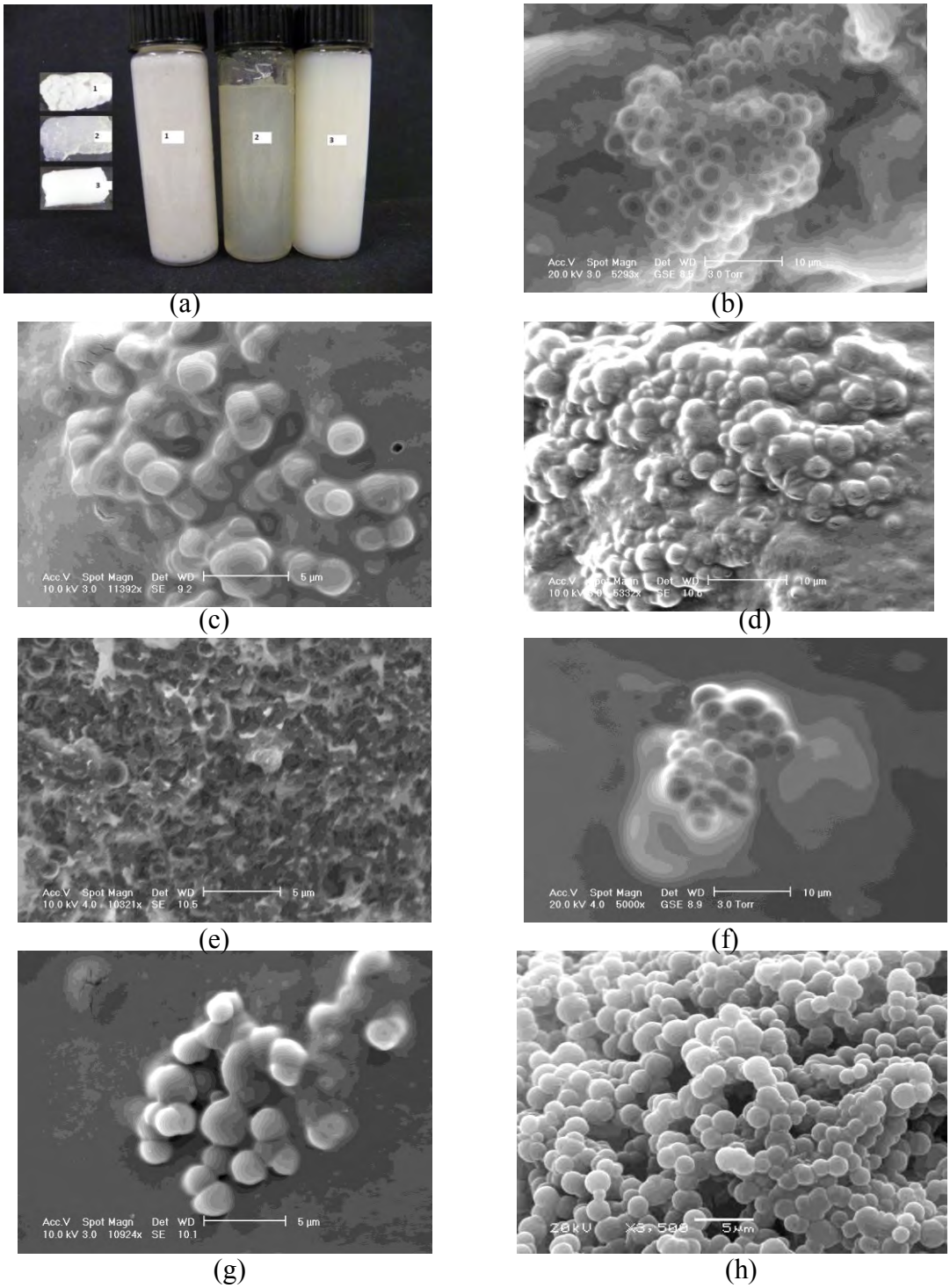

Figure 7-15. Stability of air cells to heat treatment under sterilisation conditions (121°C/15 min, 1 Bar).
Photograph of gel-like AFEs (a) and typical scanning electron micrographs: EWP-AFE made at 50 °C and 70°C ((b) and (f), wet sample (Wet-SEM) for 50°C and 70°C respectively); (c), (d), (e) and (g) are dried samples observed under high vacuum SEM: (c) and (g), samples made at 50 °C and 70°C and dried overnight; (d), samples made at 50 °C and dried 2 days and (e) is the cross section of (d). BSA-AFE made at 50 °C, high vacuum SEM (h). These SEM images showed that bubbles within the protein gel have kept their size and shape especially for samples made at 50 °C.

AFEs stabilised with alternative proteins also resiste lipid destabilisation (Figure 7-12 and Figure 7-16). Indeed a triphasic emulsion system, made by blending BSA- AFEs and an O/W emulsion stabilised with Tween 60 was again, stable to coalescence and Oswald ripening for considerable time (Figure 7-16). Small air cells and larger oil droplets are visible after 2 months storage at room temperature. This indicates that air cells with alternative proteins coat are equally stable as those coated by hydrophobins. Regardless of the chemical and physical effects of cavitation that promote the hydrophobic interactions and cross-linking between superoxide radicals and protein cysteine group, the protein concentration must also be high enough to allow a rapid absorption of protein at the interface and to give surface coverage. Based on results presented here, the stability exhibited by AFEs constructed by alternative proteins could be explained by the high packing density of the protein at the air water interface forming a robust "cage-like" structure around air cells.

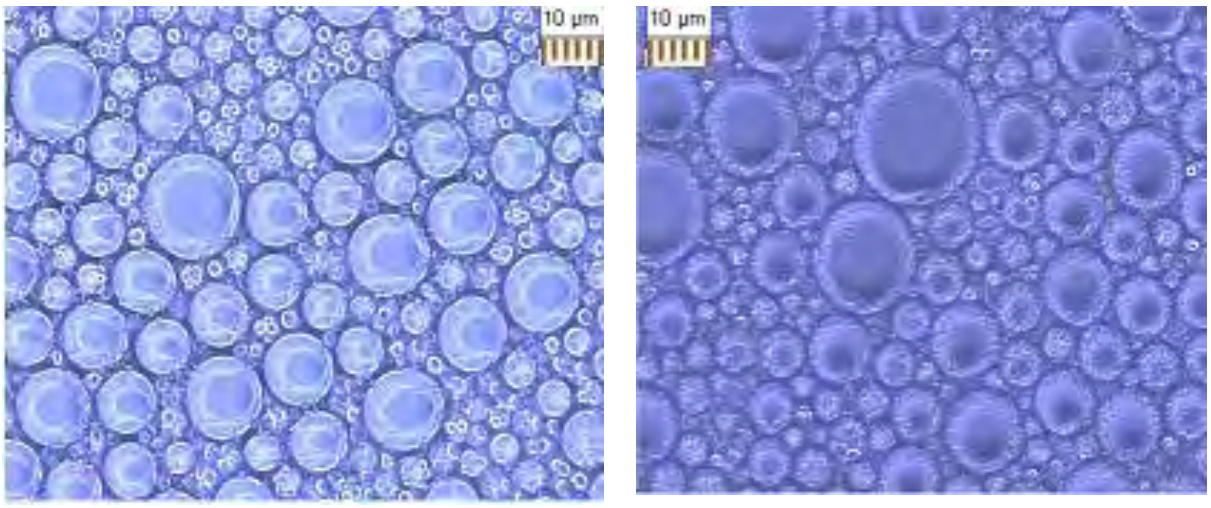

(a) (b)

Figure 7-16. Typical phase contrast micrographs of air filled triphasic emulsions (20% air, 20% oil and 60% water) showing small air cells coated with BSA among larger oil droplets stabilised with Tween 60 and dispersed in water. (a) and (b) are samples stored at room temperature for 4 days and 2 months, respectively.

7.4. Probing the contribution of AFEs to product mouth-feel

It was suggested in Chapter 5 (section 5-3) that the triphasic A/O/W emulsions made with hydrophobins could have similar, if not better lubrication properties (mouth-feel) than the standard oil water emulsions. This section aims to provide a better understanding of the mechanism by which air cells contribute to this and, thus to the perceived indulgence. Here again, the rheology and tribology of AFEs containing approximately 10% air, by volume, are used to evaluate the potential contribution of AFEs to the mouth-feel.

Figure 7-17 is the log-log plot for the viscosity of a BSA-AFE, an EWP-AFE and their parent protein solutions. The "up" and "down" viscosity curves of the BSA-AFE and protein solution used for its preparation are almost identical. In contrast, EWP based samples showed a hysteresis loop, which was more pronounced for EWP-AFE with respect to EWP alone. This time-dependent behaviour was also explored by recording an increase in the viscosity when samples were sheared at 10 s^{-1} for 10 min. It has been shown that the viscosity of food stuff affects the in-mouth friction, only when the viscosity is greater than 100 mPa s (de Wijk and Prinz, 2005; van Aken, 2010b). Above this 100 mPa s limit and at 10 s^{-1}, the friction should decrease with an increase in the viscosity of products (de Wijk and Prinz, 2005). All the samples here showed a viscosity lower than 100 mPa s at 10 s^{-1}, and thus, their viscosity should not contribute to their lubrication properties (see later discussion).

The viscosity of BSA-AFE and its parent protein solution at 10.4 s^{-1} were 21 mPa.s and 15 mPa.s, respectively. EWP-AFE showed slightly lower viscosity than its protein solution, for the ascending curves. The viscosity at 10.4 s^{-1} was 34 mPa.s (ramp up) and 87 mPa.s (ramp down) for EWP-AFE and 46 mPa.s (ramp up) and 71 mPa.s (ramp down) for EWP solution. The increase in the viscosity of EWP-AFE for the downward curve was attributed to a shear

induced structural formation from the growth of fibrillar aggregates composed from non absorbed proteins. Another possible explanation is the interaction between the fibrils and air cells via their shells resulting in a network build up (see Figure 7-18a-b).

Although the sonication conditions are relatively mild (3 min irradiation with the probe at the interface of air-liquid) compared to those reported to degrade/ depolymerise macromolecules (Kanwal *et al.*, 2000; Tsaih and Chen, 2003; Liu *et al.*, 2006) the low viscosity observed with EWP-AFE could theoritically be ascribed to the breakdown of weak hydrogen bonds and van der Waals interactions between the different proteins by ultrasound induced shear or thermolysis. These authors did point out that not only does the degradation depend on the acoustic intensity but also on the size and the viscoelastic response of a polymer; small molecules resist the sonication stress better than high molecular weight ones. This is due to a shorter relaxation time and there should be a minimum size after which no degradation occurs. EWP consists of different proteins, which at high temperatures can interact and form large polymers. Conversely, the BSA used in this study was relatively pure and does not form large aggregates. Also BSA is relatively stable up to 60°C (Su *et al.*, 2008). In addition, no significant differences have been observed between the dichroic spectra for BSA in solution and for BSA in air-filled microspheres (Suslick *et al.*, 1994). Therefore, the shear induced formation of large aggregates in of EWP based samples could have an implication on their lubricational properties.

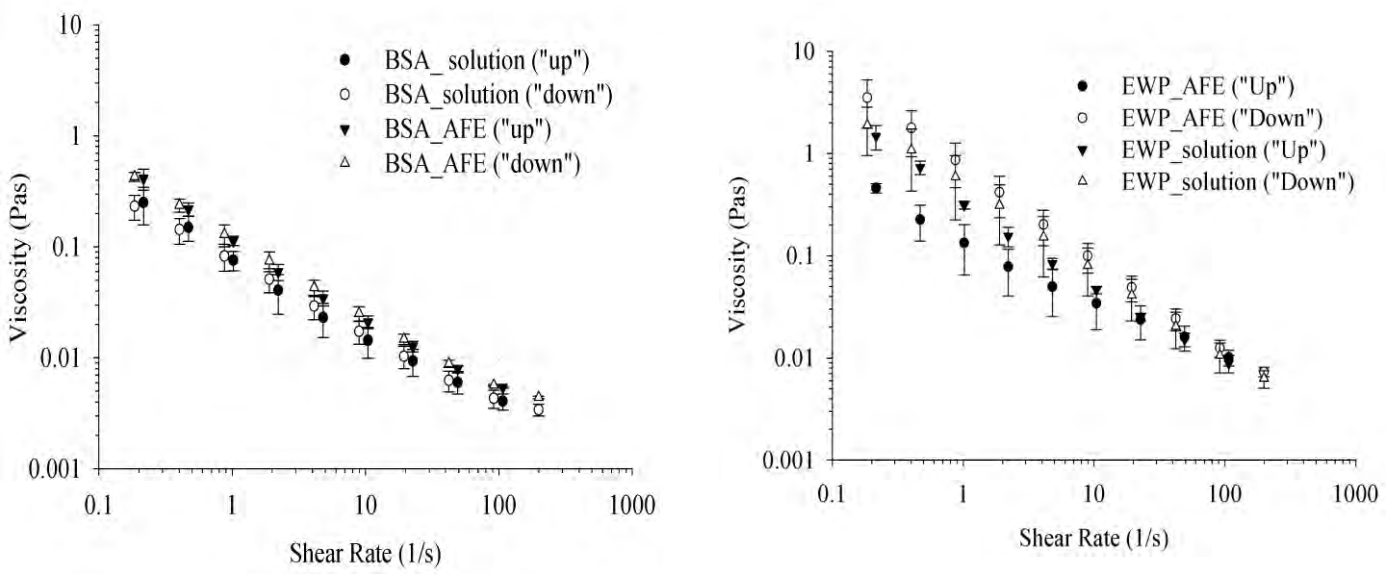

Figure 7-17. Log Log plots of viscosity as function of shear rate for proteins solution and AFEs made at 50°C using BSA, pH 5.0 (a) and EWP, pH 3.8.

Figure 7-19 is the friction against entrainment speed curves for AFE and their parent protein solutions. BSA-AFE showed a relatively lower friction coefficient than the protein solution used for its production. There is an inverse relation between lubricational properties of food and the sensorially perceived creaminess and fattiness (Malone *et al.*, 2003; de Wijk and Prinz, 2005; Dresselhuis *et al.*, 2007b) thus, this result indicates a possible contribution from the air cells to reduce the friction and probably to improve the sensory properties of the food, such as creaminess and other fat related attributes. However, friction curves of EWP-AFE and its parent protein solution are virtually identical. The dissimilarity in BSA and EWP based samples could not be due to difference in their viscosities, because these are lower than the viscosity limit below which viscosity has no appreciable effect upon the friction (100 mPa.s at 10 s^{-1}), but could be explained by properties intrinsic to each of the proteins.

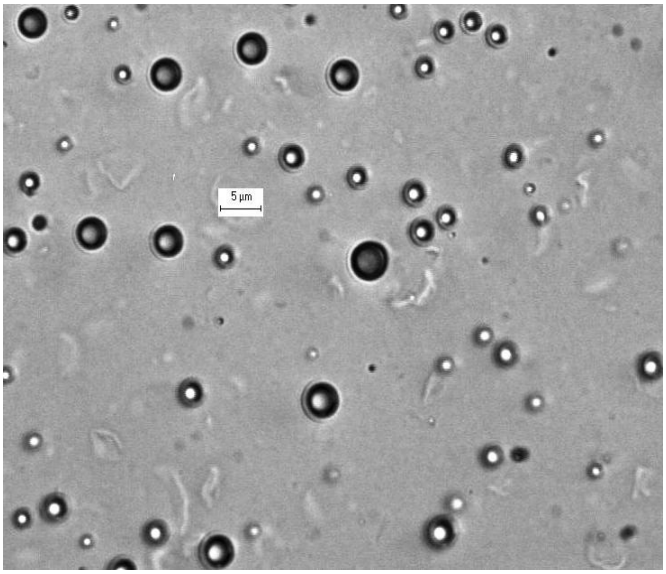

(a)

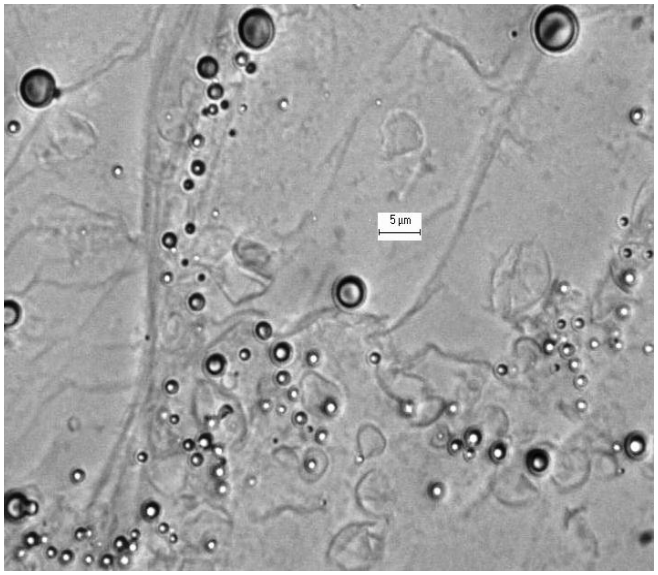

(b)

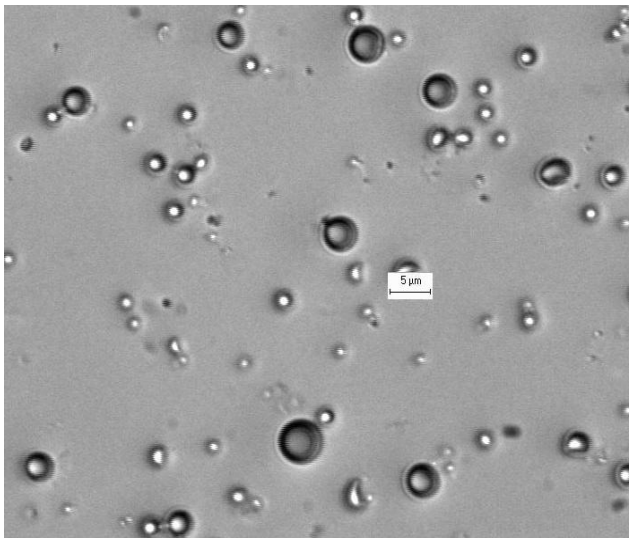

(c)

Figure 7-18. Brightfield micrographs of EWP-AFE (10% air by volume) showing the growth of non adsorbed protein network as induced by shear. The shear rate was systematically increased and decreased between 0.1 s-1 and 200 s-1. (a) Before rheology measurement, air cells and small fibrillar shape of proteins aggregate can be seen; (b) after rheology test, air cells are entrapped within long fibrils of protein networks. For comparison purpose a micrograph of a BSA-AFE (10% air by volume) before rheology test is also presented (c).

It is becoming recognised that the texture perception (friction in the mouth) is not only affected by the size and concentration but also by other properties such as hardness and shape, where hard or sharp particles are more easily detected (by increasing the friction) than softer

or more rounded particles (Tyle, 1993; de Wijk and Prinz, 2005; Engelen *et al.*, 2005). Although the effects of protein aggregates are complicated to interpret and contradictory results are reported in the literature (Chojnicka *et al.*, 2008), it may be postulated that the presence of mixture of fibrillar non-absorbed proteins, air cells, protein aggregates with different sizes and shapes (as illustrated by Figure 7-18b) would increase the friction of EWP-AFE which would be perceived as heterogeneous product in mouth. Therefore, because the friction curves of EWP-AFE and its parent protein solution are virtually identical it is hypothesised that the potential contribution of air cells to the reduction of the friction was counterbalanced by the presence of the aforementioned fibrillar and aggregated proteins which would have had an equal but inverse effect upon the tribological response.

It has been demonstrated that boundary friction predominates for systems with low viscosity such those studied here (van Aken, 2010b). The boundary friction is the friction obtained in the boundary regime where surfaces are in full contact and the friction depends on the tribo-pair's surface asperities and the presence of any coat or adsorbed matter. This implies that the ability of samples to adsorb/interact with the tribo-pair may also be important for the observed lubrication of these samples. A close scrutiny of the friction curve of BSA-AFE and EWP-AFE (Figure 7-19) shows slightly lower boundary friction for EWP-AFE, indicating that EWP may tend to adsorb more on the tribo-pair surfaces. However, when considering that in this regime, the friction does not significantly change with the increase in the entrainment speed, the boundary friction is longer for EWP-AFE and EWP solution (up to entrainment speed of about 40 mm/s) when compared to BSA-AFE. In the case of BSA based samples, the mixed lubrication regime (where the lubricant film partially separates the tribo-pair and the friction decreases) started at much lower entrainment speeds (almost at the start of the measurement). This suggests that BSA based samples are more readily entrained into the

contact zone between the ball and disc when compared to EWP. Because BSA-AFE showed relatively lower friction coefficient compared to its parent protein solution, it is likely that it is the air cells which are contributing to the lubrication; probably by entering the contact zone. Moreover air cells might interact with the tribo-pair via their protein shells, as it is recognised that microbubbles with their large surface area are capable of effectively adsorbing onto particles or molecules (Xu *et al.*, 2008). Also albumin-stabilised microbubbles have proved to adhere to endothelial cells of blood vessels (Tsutsui *et al.*, 2004) and this may involve non covalent interactions such as electrostatic and Van der Waals interactions, hydrogen bonds and hydrophobic force. Such interactions may be taking place here.

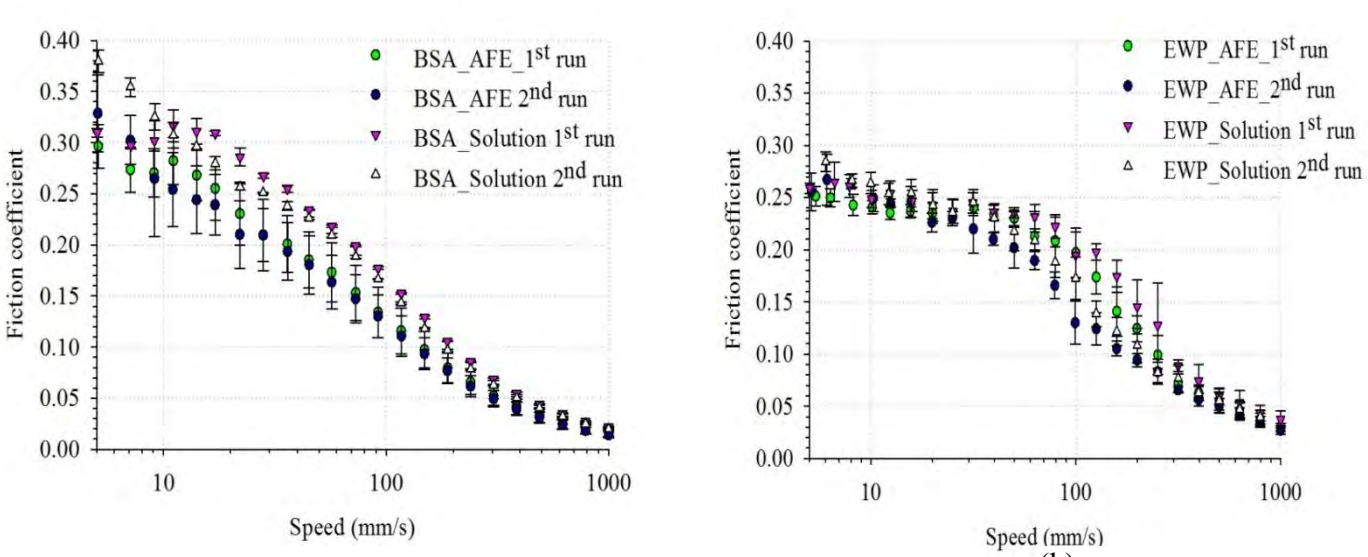

Figure 7-19. Comparison between the tribological behaviour of AFEs (containing approximately 10% air by volume) and protein solutions used for their preparation.
(a) is BSA-AFE and BSA solution; (b) corresponds to EWP-AFE and EWP solution.

In summary, and by considering the two model systems of AFEs, a direct conclusion regarding the contribution of AFE, and thus air cells, to the reduction of the friction and to the mouth-feel could not be drawn. AFEs made with BSA (BSA-AFE) or with EWP (EWP-AFE) showed diverse tribological behaviour. There was a lowering of the friction coefficient for BSA-AFE when compared to the parent BSA solution and no apparent difference between EWP-AFE and its parent solution. Protein aggregates (with different size and shape) formed upon shearing were attributed to the absence of the apparent lubricative properties of EWP-AFE. Also their interaction with air cells may result in a network that may have prevented air cells from entering the contact zone as illustrated by Figure 7-20b. It was apparent that at this low air phase (10 % air by volume) the molecular properties of the protein used for the construction of AFE played a crucial role.

It is hypothesised that AFEs may contribute to lower the friction through the adsorption of air cells on the surfaces via its protein's shell or air cells can be entrained into the narrow gap between the tribo-pair, by extension tongue-palate, if their size is below the critical boundary's film thickness, as depicted in Figure 7-20.

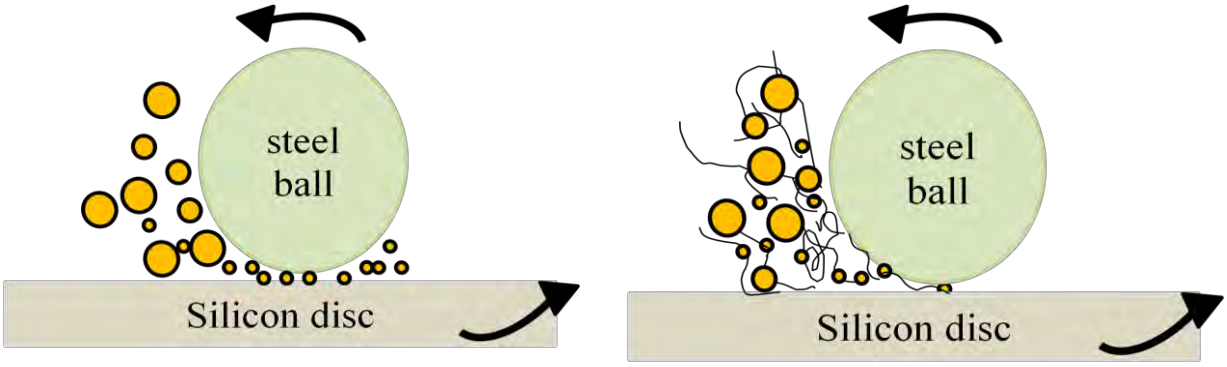

Figure 7-20. Schematic of the mechanism by which AFEs may contribute to lower the friction and to the mouth-feel.
(a) is the scenario where small air cells can freely entrained the contact zone (e.g. BSA-AFE). (b) The entry of air cells into the contact zone is hampered by non.adsorbed proteins which formed a network within which air cells are entrapped and partially accumulated at the inlet of the contact zone (e.g EWP-AFE).

7.5. Conclusion and remarks

Suspensions of micron-sized air cells (majority around 0.5-10 μm) coated and stabilised by commonly used cysteine rich proteins with Bovine Serum Albumin (BSA) and Egg Albumen (EWP) been used as model systems has been constructed using a sonochemical method similar to that used for hydrophobin stabilised air filled emulsions. These systems, AFEs made with BSA (BSA-AFE) and with EWP (EWP-AFE) were used to assess the contribution of air cell to the lubricational properties of food, thus to the mouth-feel.

It was found that air cells stabilised by these alternative proteins could be as stable as those stabilised by hydrophobins. However, the stable air volume fraction was low for AFEs stabilised by these proteins, approximately 10%, as compared to 30-40% for hydrophobin stabilised system. The production of AFEs by alternative proteins requires a protein pre-treatment, a sufficient protein concentration and the manufacturing conditions/process to be controlled. It appears that the temperature and the pH of the protein determined the yield and the stability of air cells, the optimum pH being at the protein's PI. Also, there seemed to exist a critical air cells size of about 2-3 μm, above which air cells are less stable to environmental stress. It is hypothesised that a coagulation process may have been superimposed on the protein adsorption leading to the formation of a multilayered structure cage-like around air cells, leading to a reduction or suppression of gas diffusion among air cells.

A tribological study of BSA-AFE and EWP-AFE showed that molecular properties of the protein used for the construction of AFE played a crucial part in the determination of lubricational properties of AFEs. This study allowed for a suggestion of the mechanism by which air cells may contribute to lower the friction and to the improvement of the sensory attributes of products.

CHAPTER 8

CONCLUSIONS AND FUTURE WORK

8.1. Conclusion

An attempt has been made to construct air cells in a similar size range of the oil droplets found in emulsion based foods. The air cells were in the range of 0.5-100 µm with the majority between 0.5-10 µm. This was achieved with a sonochemical technique using either hydrophobin rich extracts, obtained via submerged fermentation and extraction, or other common cysteine rich proteins. Suspensions of these air cells, Air Filled Emulsions (AFEs), were then used to construct model air based low fat and calorie food products. These triphasic emulsion systems (A/O/W) are intimately mixed oil droplets and air cells in a water continuous phase. The work here has been focussed around four main objectives:

- production and extraction of hydrophobins from edible mushrooms and *Trichoderma reesei* (Chapter 4);
- construction of AFEs using the extracted hydrophobins and evaluation of the use of hydrophobin stabilised AFEs as ingredients for the reduction of fat content of high fat emulsion based products (Chapter 5);
- evaluation of the surface activity and emulsifying capability of recombinantly produced Class I hydrophobins and comparison to other commonly available proteins (Chapter 6);
- investigation into the use of bulk food grade proteins for the production of AFEs with reference to hydrophobins (Chapter 7).

8.1.1. Production and extraction of hydrophobins

Hydrophobins could be extracted from edible mushrooms and submerged cultures of mycelium and broth of *Trichoderma reesei*. Edible mushrooms yielded very low concentration of Class I hydrophobin and the separation method was technically tedious. In contrast, reasonable amounts of Class II hydrophobin rich extract were easily obtained from submerged cultures of *Trichoderma reesei*. These extracts could significantly lower the water surface tension and spontaneously form robust elastic membranes at interfaces, in the same way as pure HFBII.

8.1.2. Construction of suspensions of air cells (AFEs) using hydrophobins rich extract and evaluation of their use as ingredients for fat reduction in emulsion based products

Micron sized air cells stabilised by hydrophobin protein (HFBII) were constructed through a sonochemical process, using the hydrophbin rich extract obtained from a culture broth of *Trichoderma reesei*. These suspensions of air cells, AFEs, showed excellent stability ascribed to the natural robustness of the hydrophobin film reinforced by the formation of multi-layer protein coats. The formation of multi-layer interfaces is novel for HFBII and was attributed to the "hot spot" phenomena of cavitation which promote interaction between hydrophobin molecules. This allows air cells to resist both disproportionation and ripening over a substantial period of time and oil destabilisation, and to survive high shear processing steps. As a result, AFEs were successfully incorporated into triphasic A/O/W emulsions model

dressings. All indications are that this air based formulation could have similar if not better oral properties than the standard O/W emulsion versions; i.e.:

- The triphasic emulsion was stable for months with regard to the particle size and, this was attributed to the combination of a strong hydrophobin film and a possible existence of a thin film, pseudoemulsion, between oil droplets and air cells. This acts as a kinetic barrier to droplet entering the air/water interface. Also it was postulated that the presence of oil droplets and thickener may contribute to the increase in the apparent thickness of the air cell shells, leading to further decrease in Oswald ripening.

- The triphasic A/O/W emulsion showed good stability against creaming (Chapter 5) when compared to an O/W emulsion. This was due to an interaction between the air cells, possibly via their protein shells or other components of the system, resulting in a weak network structure.

- The triphasic A/O/W emulsion showed premature lipid oxidation when compared to the standard O/W emulsion. However the ability of hydrophobins to complex lipid oxidation products leads to the eventual quenching of the propagation of the free radical chain reactions and may have prevented/reduced further flavour deterioration (Chapters 5 and 6). A schematic design showing how the triphasic A/O/W emulsion could be manipulated through adaptation of the pH and/or the oil droplets size in order to reduce oxidation rate of the system was suggested (Figure 5-12).

- Rheological and tribological results suggested that the triphasic A/O/W emulsions could be manipulated to be similar to the standard O/W emulsions in terms of

lubrication behaviour and sensory perception. Mechanisms by which air cells might contribute to lower the friction were proposed.

In essence, it appears that a careful design of the final microstructure of products should help in optimising the stability and the quality of commercially relevant triphasic emulsions.

8.1.3. Evaluation of the surface activity and emulsifying capability of large scale recombinantly produced hydrophobins

Two industrially produced fusion hydrophobins, H*protein A and H*protein B, were characterised in terms of their adsorption behaviour at air/water and oil/water interfaces and were compared to other commonly available proteins. The results showed that:

- The adsorption behaviour of H*protein B and H*protein A was somewhat comparable to that of other commonly used proteins such as milk proteins. H*proteins showed different kinetic behaviour at A/W and O/W interfaces, with longer induction period at O/W. This was interpreted as difference in the orientation of the proteins at these interfaces. From this data, a schematic representation of H* proteins at A/W and O/W interfaces has been proposed (Figure 6-7).

- The adsorption rate of H*protein A was generally higher than that of H*protein B, though H*protein A is almost twice the size of H*protein B. This was attributed to the higher hydrophobicity of H*protein B and was determined by examining the adsorption kinetics of H*proteins at interfaces using Hua-Rosen's kinetic parameters.

The investigation effect of H*proteins upon emulsion formation and stability at different pHs showed that H*proteins-stabilised emulsion could be made using any conventional emulsification method. However, the general trend suggested that H*proteins somewhat keep the natural ability of hydrophobin molecules to attract each other, leading to droplets flocculation and/or weak network formation, whatever the method used for the preparation of emulsion.

8.1.4. Investigation into the use of bulk cysteine rich proteins for the construction of AFEs

Suspensions of micron-sized air cells (the majority around 0.5-10 μm) coated and stabilised by commonly used cysteine rich proteins with Bovine Serum Albumin (BSA) and egg albumen (EWP) being used as model systems, has been constructed using a sonochemical method similar to that used for hydrophobin stabilised air filled emulsions. These systems, AFEs made with BSA (BSA-AFE) and with EWP (EWP-AFE) were used to assess the contribution of air cells to the lubrication properties of food and thus, mouth-feel.

It was found that air cells stabilised by these alternative proteins could be as stable as those stabilised by hydrophobins. However, the stable air volume fraction was low for AFEs stabilised by these proteins, approximately 10%, as compared to 30-40% for hydrophobin stabilised system. The production of AFEs by alternative proteins requires a protein pre-treatment, a sufficient protein concentration and the manufacturing conditions/process to be controlled.

A critical air cells size of about 2-3 μm above which air cells are stable to environmental stress was apparent. A tribological study of BSA-AFE and EWP-AFE showed that molecular properties of the protein used for the construction of AFE played a crucial part in the determination of lubrication properties of AFEs. This study allowed for a suggestion of the mechanism by which air cells may contribute to lower the friction and to the improvement of the sensory attributes of products (Figure 7-20).

8.2. Future work

This work has triggered many questions and hypotheses. Further work in the area presented below might help answering these questions:

Hydrophobins were used as a tool to construct AFEs; therefore, limited work was done regarding their production and purification. However, the information gained in chapter 4, by monitoring pH, nutrient concentration during the fungal growth could be exploited to optimise natural production of hydrophobins via fermentation, along with polished step purification. Also, although hydrophobins rich extract showed strong surface properties that are characteristic of hydrophobins, the identification of the protein by peptide mass fingerprinting was inconclusive and deserves further investigation.

In Chapter 5 it was demonstrated that stable suspensions of hydrophobin stabilised air cells can be constructed but the kinetics and the final morphology of the hydrophobin layers still need to be determined. Moreover, it was postulated that oil droplets size, the ratio AFE/OW emulsions for the formulation of the triphasic A/O/W emulsions may also play a crucial role for the stability of these products. Likewise, a schematic representation of how the triphasic

A/O/W emulsion could be manipulated trough adaption of the pH and the oil droplets size in order to reduce oxidation rate of such system was proposed. A more systematic approach work may be undertaken in these areas.

The tribological behaviour of the triphasic A/O/W emulsion based prototype salad dressing (Chapter 5) was limited to one single air phase volume. Tribological measurement of AFEs (Chapter 7) yielded different results for BSA-AFE and EWP-AFE indicating that the very nature of the protein may play a crucial role. It would therefore be interesting to study the effect of air phase volume, air cells size and surface charge. Additionally, oral processing involves interaction of food material with saliva which may change its lubrication properties. This was overlooked in the present explorative work and suggested to be considered in the studies to follow. Also, it would be interesting to explore the effect of AFEs and air phase volume on nutrient bioavailability and the flavour release from these novel air based triphasisc A/O/W systems.

Small size air cells (e.g., less than 3 μm) have large surface area, thus might adsorb at the surface of larger particles. This effect was discussed in Chapters 5 and 7, and a more systematic study of the pickering stabilisation of larger air cells by smaller ones may allow for the increase in the air phase volume of AFEs and subsequent products.

The emphasis has been given here to the application of AFEs in the food area. However microbubbles also have the potential to be used in many other fields such as environmental sciences and biomedical, for example, for molecule delivery, and work could be done in order to extend the use of air AFEs in these areas.

Scope for further investigation with large scale recombinantly produced hydrophobins, H*proteins (Chapter 6) might be the measurement of surface coverage, layer thickness, conformational changes, using a combination of more advanced methods such as Ellipsometry, neutron reflectometry, attenuated total internal reflectance infrared and circular dichroism spectroscopy. This may also be extended to H*proteins mixed system (H*protein other hydrophobins or H*protein A B and H*Protein small surfactant). These studies, along with dynamic surface tension would not only provide some insights into adsorption mechanism of H*proteins at A/W and O/W, but would also help in the understanding of their colloidal behaviour (e.g. structural re-arrangements upon adsorption, positive cooperative effects and surface aggregation) which has direct implication on product formulation.

Time did not allow for a full rheological study of emulsion made with H*proteins. This would constitute a useful extension of this work as it would help in extending the understanding of the physical properties H*protein stabilised emulsions.

In chapter 7, processing conditions such as pH, concentration and temperature were the only ones considered. It would be interesting to explore a formulation engineering approached by considering proteins and other ingredients such as sugars, particles and/or hydrocolloids or compounds, for example, L-cysteine. For instance, it is well documented the reaction between sugar and proteins (e.g. Maillard reaction) and the possibility of sugar to stabilise globular proteins against thermal unfolding, strengthen protein-protein interactions and accelerate protein diffusion towards the interface; both phenomena may lead to more interfacial reactions. Also, proteins could be treated with high intensity ultrasound prior AFEs production, as this physical treatment has been shown to increase protein surface hydrophobicity without altering its sulphidryl content.

Processing parameters such as ultrasound power, diameter of the ultrasound horn, the air sparger diameter and air flow rate might affect AFE formation. This deserves a systematic study. The combination of processing and formulation engineering approaches may help in extending/improving air cells formation and stability, and more importantly, may improve the air phase volume which is, so far, relatively low. In addition, it would be interesting to explore the production of AFEs using standard emulsification methods that generate uniform air cells follow by a crosslinking of the protein shell by food grade crosslinking agents such a transglutaminase and Genipin.

It was observed towards the final stage of this thesis that there is a great variation between supplied proteins and the BSA in particular, when purchased from the same supplier but different batches would not allow for the construction of air filled emulsion using the same production conditions. It was hypothesised a loss of BSA flexibility and/or dimerisation with involvement of the unique sulphidryl group of the protein. A study involving protein physico-chemical and structural characterisations and their influence on AFEs formation and stability would provide considerable insight and fundamental understanding of the mechanisms taking place.

CHAPTER 9

APPENDIX

9.1. Publications referred to, in this thesis, as appendix 1 (CD included at the back of this thesis).

9.2. Physicochemical properties of some hydrophobins and other cysteine-rich proteins

Table 9-1. Comparison of some hydrophobins physicochemical properties and other cysteine-rich proteins

Protein	Source	MW (kDa)	S-S bonds	SH-groups	PI	T_d °C	Surface tension (mN/m)	Reference
Class I Hydrophobins								
ABH3	*Agaricus bisporus* (common white button mushroom)	9.2	8	0	4.5	-	37	Lugones *et al.* (1998)
POH1	*Pleurotus ostreatus* (oyster mushroom)	11.0	8	0	4.68	-	40	Peñas *et al.* (2004)
POH2	*Pleurotus ostreatus* (oyster mushroom)	8.3	8	0	4.81	-	40	Ma *et al.* (2007)
SC3	*Schizophyllum commune*	13.6	8	0		-	24; 29*	*Corvis *et al.* (2006); (Askolin, 2006)
H*Protein A	[a]Recombinant protein	47	-	-	4.9	-	40-45	Data from this thesis
H*Protein B	[a]Recombinant protein	19	-	-	4.9	-	40-45	Data from this thesis
Class II Hydrophobins								
HFBI	*Trichoderma reesei*	7.5	8	0	5.7	> 90; > 80*	37	Askolin, (2006) ; *Torkkel et al. (2002)
HFBII	*Trichoderma reesei*	7.2	8	0	6.5* ; 4.8	> 80	28-30	* Basheva et al (2011); Cox *et al.* (2007) ; Askolin,(2006)
Other proteins				-				
BSA	Bovine	67	1	17	4.9	65	50*	Tripp *et al.* (1995)
Ovalbumin	Egg white	45	4	1	4.5-4.7	71.5	45	Campbell *et al*. (2003)
Ovotransferrin	Egg white	787.7	0	15	6.5	57.3	46*	Campbell *et al*. (2003); *Tripp *et al.* (1995)
Lysozime	Egg white	14.4	0	4	10.7	70	43*	Tripp *et al.* (1995)

The isoelectric point (PI) of hydrophobins tend s to coincide with the external pH of hyphal membrane which would facilitate self assembly of hydrophobin monomers (Ma *et al.*, 2007).

9.3. Detailed calculation of the amount of Tween 60 required for a complete coverage of droplet surface.

The quantity of Tween 60 needed for droplet interfaces to be fully saturated with surfactant was estimated because Tween 60 in the aqueous solution forms micelle at concentration above 0.03% (Zhong *et al.*, 2008) and the composition of the micelle has an influence on the the emulsion properties and stability. The reasoning was as follows:

- *Calculation of the surface area corresponding to one molecule of Tween 60 (ST).*

It was assumed that only the hydrophilic head-group ($C_{47}H_{91}O_{26}$, Figure 3.6) occupied the oil/water interface as the hydrophobic tail would be at the interior of the droplet and that the surface area of one molecule is the sum of surfaces of atoms that make up the molecule.

$$S_T = S_C + S_H + S_O \qquad Eq.9-1$$

Where S_c, S_H, S_O are the surface occupied by all atoms of carbon, hydrogen and oxygen and S_x equal to $n \times 4\pi r_x^2$ (n and r_x are the number and the radius of a given atom x, respectively). The atomic diameter of C, H and O is 1.82E-10 m, 1.58E-10 m and 1.30E-10 m, respectively (Sargent-Welch, 1979). S_T as estimated with the above equation is 1.341E-17 m^2/mol

- *Calculation of the total O/W interfacial area (A).*

$$\text{Total surface area} = \text{Number of droplets} \times sur face\ of\ the\ droplet \qquad Eq.\ 9-2$$

$$\text{Number of droplets} = \frac{\text{Volume of oil } (\emptyset) \times \text{total volume}}{\text{Volume of droplets}} \qquad Eq.9-3$$

$$Volume\ of\ the\ oil\ droplet\ = \frac{4}{3}\ \pi(\frac{D_{32}}{2})^3 \qquad Eq.\ 9-4$$

$$Surface\ \ of\ the\ oil\ droplet\ = 4\pi\ (\frac{D_{32}}{2})^2 \qquad Eq.\ 9-5$$

Replacing in equations (3.4) in (3.3), (3.3) and (3.5) in (3.2):

$$\text{Total surface area} = \frac{6 \times \emptyset \times \text{Total volume}}{\mathrm{D_{32}}} \qquad Eq.\ 9-6$$

D_{32} is the Sauter diameter or the surface diameter. For a droplet of 0.7 µm and a total volume of emulsion of 200 cm^3, A is equal to 342.857 m^2.

The quantity of Tween 60 (Q_T) needed to cover this interface was estimated using the following equation:

$$\mathrm{Q_T} = \frac{\mathrm{A} \times \text{Molecular weight of Tween 60}}{\mathrm{S_T} \times \text{Avogadro's number}} \qquad Eq.\ 9-7$$

From equation (3.7) and considering 6.022E+23 mol^{-1} for Avogadro's number and 1311.67 g/mol for the molecular weight of Tween 60, approximately 0.03 g of Tween 60 is need for 100 mL of emulsion with 20% oil and 0.7 µm of Sauter diameter.

The interior region of the micelle, containing hydrophobic groups is of radius approximately equal to the length of the fully extended hydrophobic chain.

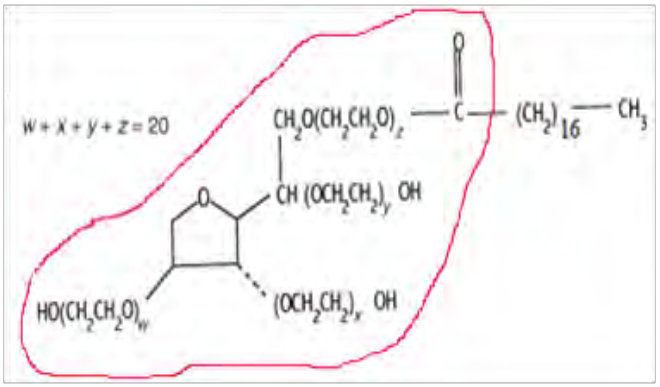

Figure 9-1. Structural formula of Tween 60 (Hait and Moulik, 2001). The head-group is circled and separated from the hydrophobic part by the red line.

9.4. Could the combination of low temperature and surfactant affect the stability of H*protein stabilised emulsions?

It is believed that large agglomarates of H*proteins in solution can reversed into tetramers and monomer if exposed to the cool temperature or surfactant (Wohlleben *et al.*, 2010). In order to investigate whether the same phenomenon could occur with H*proteins adsorbed at the interface, sunflower oil-water emulsions (10% wt/wt) stabilised with H*proteins were made and incubated with different amount of Tween 20 and store at 8°C for a week, followed by confocal microscopy observation and droplet size measurement.

The different amounts of Tween 20 required were calculated in order to produce a range of Tween 20/protein molar ratio (R) from 0 to 32. A range of Tween 20 was dissolved in distilled water. Emulsions were made using a membrane emulsification method as decrisbed in chapter 3. 1 mL of of each Tween 20 solution and 20 µL of rhodamine B solution (0.01% (wt/wt)) were added to 4 mL of freshly made emulsions and mixed with a laboratory vortex

for 10 s. The emulsions were stored at ≈ 5°C for a week and remove from the cold store just before analysis.

Figure 9-2 and 9-3 show no apparent change in the microstructure and droplet size of the emulsions for R, up to 16. However, the Mastersizer results showed a slight decrease in droplet size at a surfactant/protein ratio of 32. This might be explained by high concentration a direct substitution of protein by Tween 20, a reduction of the interaction between droplets or displacement of weakly adsorbed proteins, leading to a reduction of the thickness of the protein surrounding the droplets, when Tween 20 is present at high concentration. Nevertheless, the microscopy image still showed droplet coated with the protein.

It must be admitted that the resolution of the confocal microscopy is low when compared to that of AFM that could have been used to see in great details the interface or the analysis of the protein concentration in the aqueous phase could have provided more information. However, I believe that confocal results are sufficient to answer the question presented at the beginning of this section. And therefore, the present results suggest that H*proteins are unlikely to dissociate by small molecule surfactant, once they assemble at the interface.

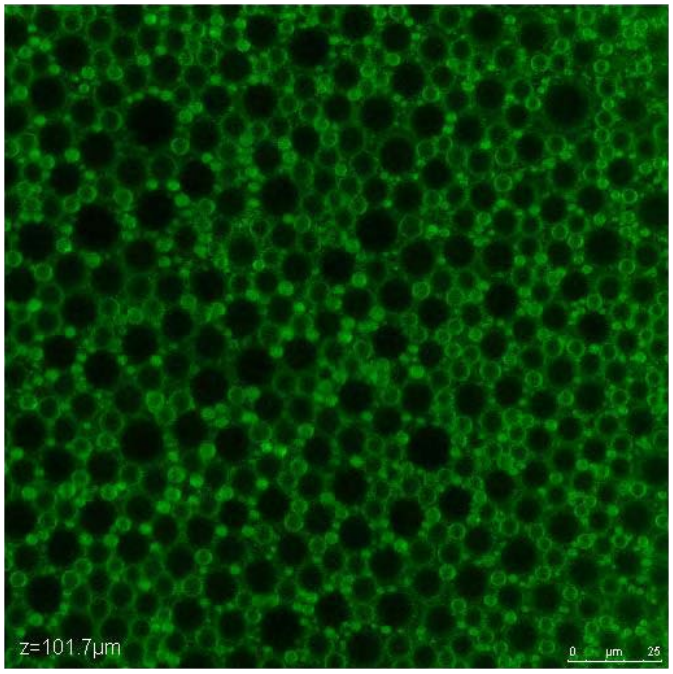

R=0

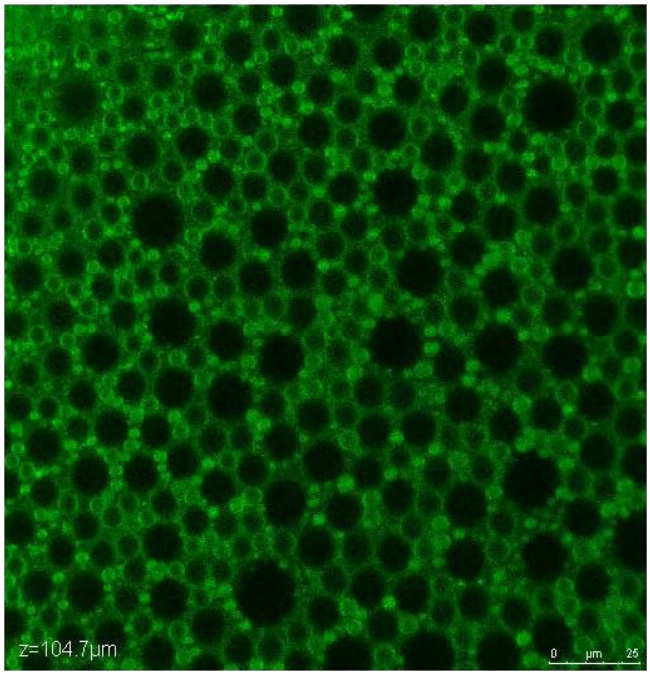

R=4

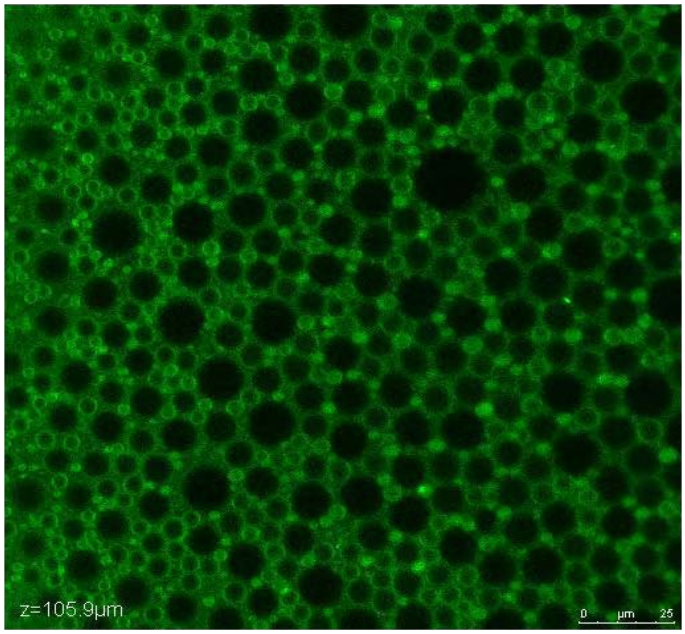

R=8

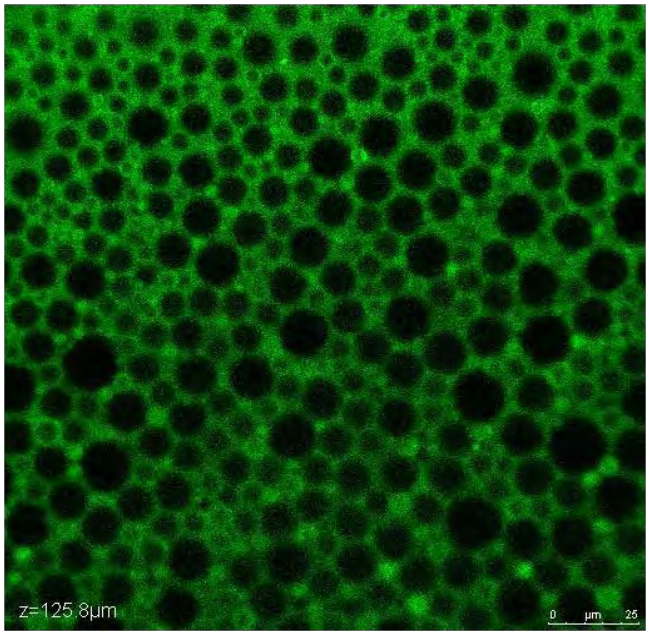

R=32

Figure 9-2. Typical confocal images of 10% sunflower oil-in-water emulsions stabilised by H*proteins as function of the Tween20-to-protein molar ratio R. The image shown here is for H*protein stabilised emulsion made with a crossflow membrane. Images for H*protein A stabilised emulsions were similar

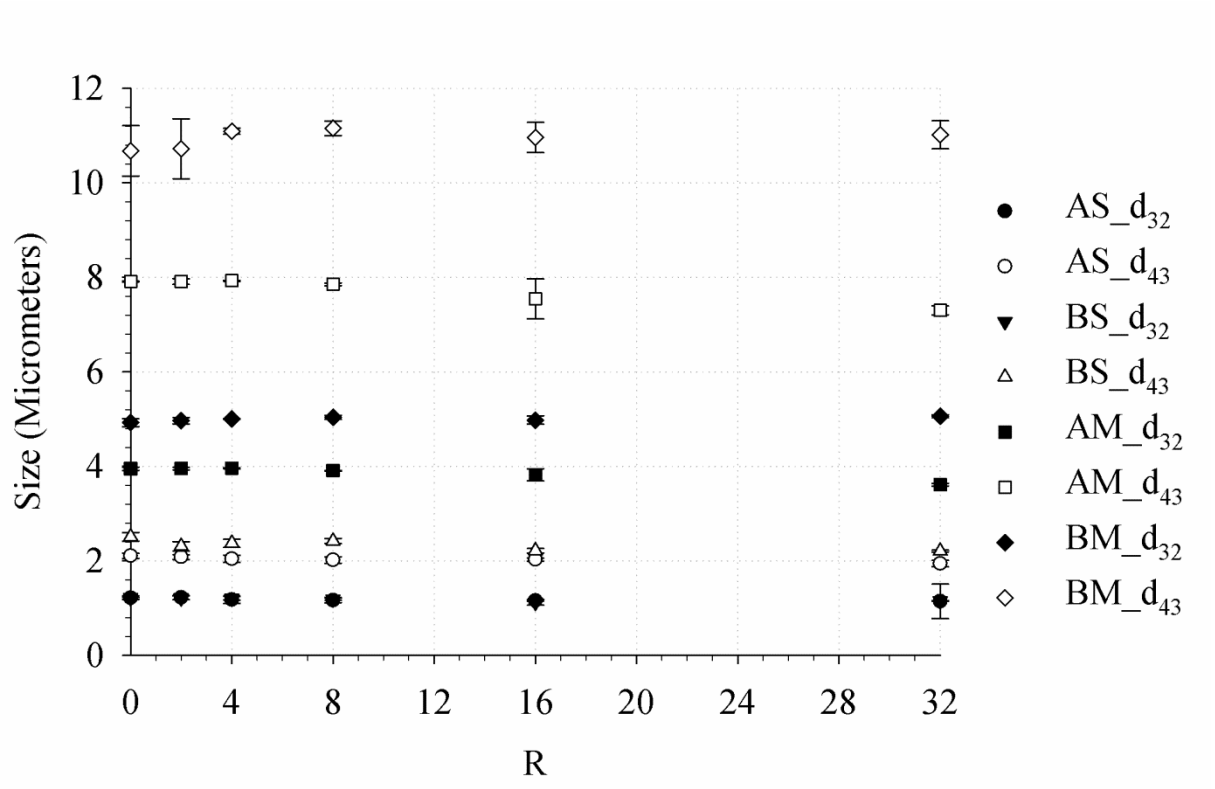

Figure 9-3. Droplet size of 10% sunflower oil-in-water emulsions prepared using a high intensity ultrasound and a cross flow membrane as function of the Tween20-to-protein molar ratio R. AS and AM are emulsions stabilised by H*protein A while BS and BM are those stabilised by H*protein and made with an ultrasound and membrane, respectively.

9.5. Amino acid sequence and secondary structure of H*proteins

The amino acid sequences of H*protein A and H*protein B (Figure 9-4) was obtained from Guzmann *et al.* (2009). These sequences were run through a secondary sequence prediction server, the PSIPRED (http://bioinf.cs.ucl.ac.uk/psipred/), which generated the secondary structure of H*protens (http://bioinf.cs.ucl.ac.uk/psipred/result/131974). The predicted secondary structure shows that H*protein A contains 16 alpha helices and 7 beta sheets, whereas H*protein B have only 4 alpha helices and 4 beta sheets in their structure (see below).

H*protein A

MAQTGTERVKRGMAEMQKGGVIMNVINAEQAKIAEEAGAVAVMALERVPADIRAA
GGVARMADPTIVEEVMNAVSIPVMAKARIGHIVEARVLEAMGVDYIDESEVLTPADE
EFHLNKNEYTVPFVCGCRDLGEATRRIAEGASMLRTKGEPGTGAIVEAVRHMRKVN
AQVRKVVAMSEDELMTEALNLGAPYELLLQIKKDGKLPVVNFAAGGVATPADAAL
MMQLGADGVFVGSGIFKSDNPAKFAKAIVEATTHFTDYKLIAELSKELGTAMKGIEIS
ALLPEQRMQERGWRSIEGRMRFIVSLLAFTAAATATALPASAAKNAKLATSAAFAKQ
AEGTTCNVGSIACCNSPAETNNDSLLSGLLGAGLLNGLSGNTGSACAKASLIDQLGLL
ALVDHTEEGPVCKNIVACCPEGTTNCVAVDNAGAGTKAEGSHHHHHH

H*protein B

MAQTGTERVKRGMAEMQKGGVIMDVINAEQAKIAEEAGAVIEGRMRFIVSLLAFTA
AATATALRASAAKNAKLATSAAFAKQAEGTTCNVGSIACCNSPAETNNDSLLSGLLG
AGLLNGLSGNTGSACAKASLIDQLGLLALVDHTEEGPVCKNIVACCPEGTTNCVAVD
NAGAGTKAEGSHHHHHH

Figure 9-4. Amino acid sequences of H*protein A and H*protein B (Guzmann *et al.*, 2009).

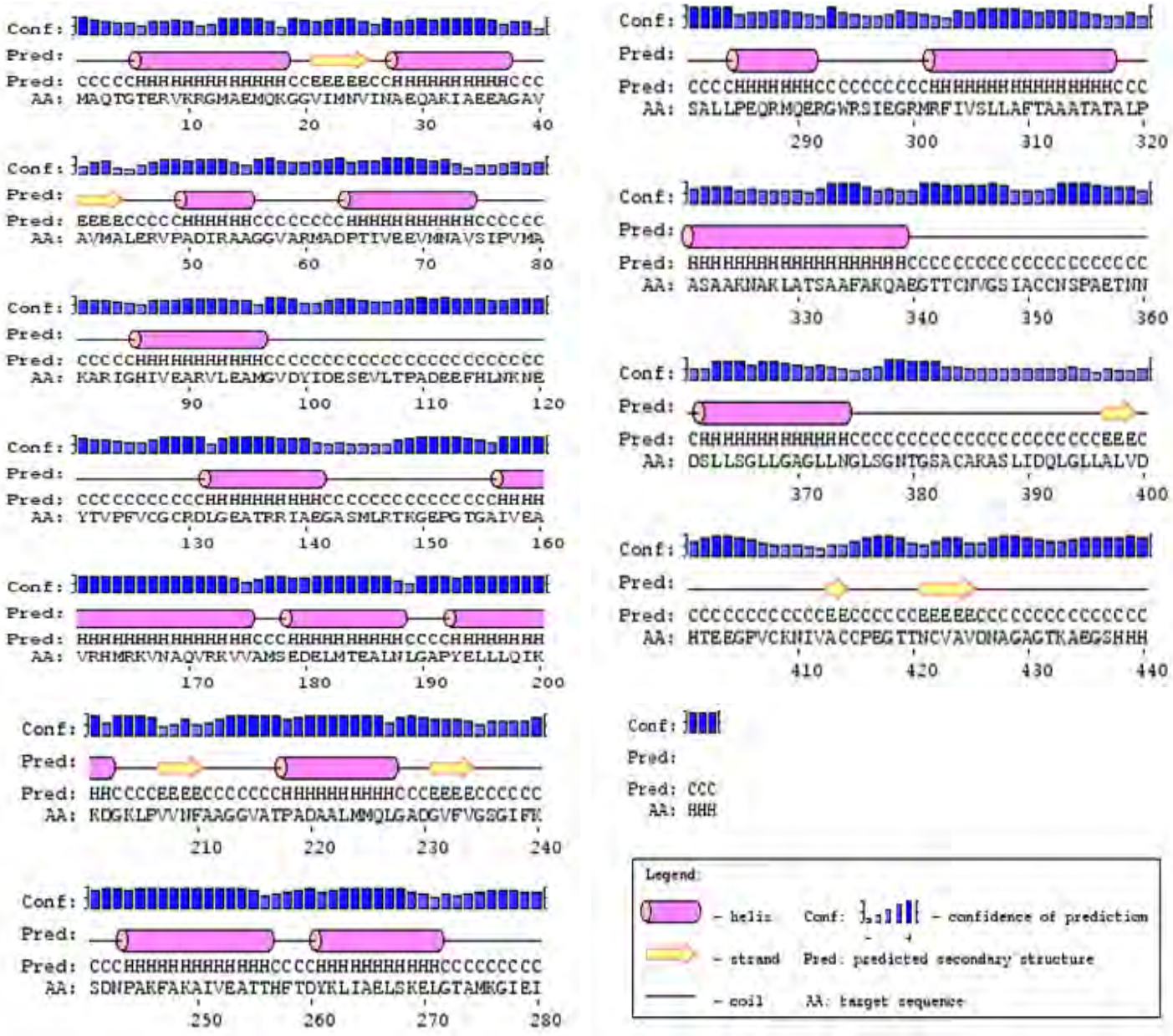

Figure 9-5. Secondary structure of H*protein A

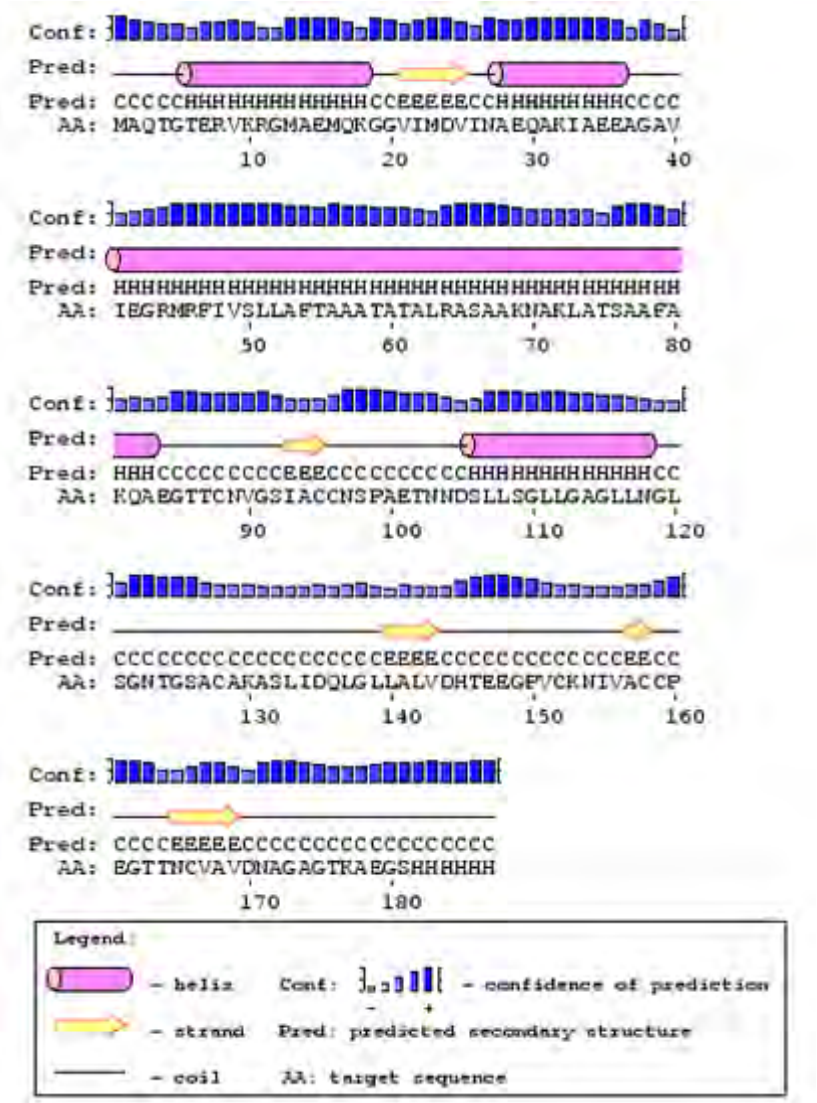

Figure 9-6. Secondary structure of H*protein B

9.6. Evidence of the formation of complex hydrophobin-lipid oxidation products

Material and methods

Two genetically modified hydrophobins supplied by BASF (Germany), H*protein A and H*protein B, were used as a model hydrophobin to investigate whether hydrophobins form complexes with lipid oxidation products. 10 mL aqueous solution of 4 mg/mL of each protein were mixed with standard lipid oxidation products (i.e. either with cumen hydroperoxide, trans, trans-2, 4-decadienal, trans-2-decenal or their mixture). The final concentration of hydroperoxide or each aldehyde was 1 mM. In certain experiments a range of concentrations of aldhehydes (from 0.1 mM to 20 mM) were used. These were mixed by means of a vortex mixer for one minute and the mixtures were then incubated at 40°C for 45h. Except for the buffering capacity of the protein itself, no attempt was made to control the pH of samples. The temperature and protein concentration were chosen in order to be consistent with the conditions used for the study of lipid oxidation in emulsions. Blanks consisting of only protein solutions were also examined under the same reaction conditions.

Changes of protein fluorescence and appearance of new fluorophores due to lipid oxidation products were measured at room temperature using a Perkin-Elmer LS 50B and a non fluorescent cell (CXA-110-005J, Fisher, UK). Synchronous fluorescence spectra were collected by simultaneously scanning the excitation (slit, 5 nm) and the emission (slit, 5 nm) from 250 to 500 nm in 2 nm steps and with 20 nm intervals. Synchronous fluorescence spectroscopy (the excitation and emission monochromators are scanned simultaneously in

such a manner that a constant wavelength interval is kept between emission and excitation wavelength). This method was chosen because it has an advantage over conventional fluorescence spectroscopy (single-wavelength fluorescence measurement) as it can provide information about several compounds present in a mixture in a single run; it reduces spectral overlaps, by narrowing spectral bands, and simplifies spectra by using a suitable wavelength interval (Patra and Mishra, 2002). Also intrinsic tryptophan fluorescence spectroscopy was used to probe the local structural changes in the vicinity of the tryptophan residues. Emission spectra (slit 5 nm) for tryptophanyl residues of the proteins were recorded from 300 to 500 nm with an increment of 2 nm. The excitation wavelength was set at 290 nm (slit 2.5 nm). The scan speed was 400 nm/min). The sample was diluted 2 folds before fluorescence measurement.

In order to identify amino acids involved in formation of hydrophobin-lipid oxidation compound complexes samples were tripsin digested, analysed using a liquid chromatography-electrospray tandem mass coupled with mass spectrometry (LC-MS/MS) and searched against a database compiled by the National Centre for Biotechnology Information (NCBInr). This was performed as follows:

(1) Liquid trypsin digestion

Trypsin digestion was performed using 10 µL of samples (containing 0.7 mg of protein/mL) mixed with 40 µL of 100 mM ammonium bicarbonate (pH 8). Then, 50 µL of 10 mM dithiothreitol (DTT) were added and samples were incubated at 56°C for 30 mins. Samples were then cooled to room temperature and cysteines alkylated by addition of 50 µl of 50mM iodoacetamide followed by incubation at room temperature in the dark for 30 mins. 25 µl of

trypsin gold (Promega, UK, 6 ng/μL) was subsequently added to the samples, which were then incubated at 37°C overnight.

(2) Desalt samples

The samples were desalted using millipore C18 ZipTips. Tips were prepared by pre-wetting in 100% acetonitrile and rinsed in 2x10 μL 0.1% trifluoroacetic acid. Samples were repeat pipetted throughout the volume of the samples five times. The tip was then washed with three times with 10 μl of 0.1% trifluoroacetic acid to remove excess salts before elution of peptides with 10 μL of a mixture of 50% acetonitrile, 0.1% trifluoroacetic acid and water. Samples were dried to remove the acetonitrile, and then re-suspended in an aqueous 0.1% formic acid solution. All chemicals were purchased from Sigma (UK), Fisher Scientific (UK) and J.T. Baker (USA).

(3) LC-MS/MS Experiment

UltiMate® 3000 HPLC series (Dionex, USA) was used for peptide concentration and separation. Samples were trapped on uPrecolumn Cartridge, Acclaim PepMap 100 C18, 5 um, 100A 300um i.d. x 5mm (Dionex, USA) and separated in Nano Series™ Standard Columns 75 μm i.d. x 15 cm, packed with C18 PepMap100, 3 μm, 100Å (Dionex, USA). The gradient used was from 3.2% to 44% solvent B (0.1% formic acid in acetonitrile) for 30 min. Peptides were eluted directly (~ 300 nL min-1) via a Triversa Nanomate nanospray source (Advion Biosciences, NY) into a LTQ Orbitrap Velos ETD mass spectrometer (ThermoFisher Scientific, Germany). The data-dependent scanning acquisition was controlled by Xcalibur 2.7 software. The mass spectrometer alternated between a full FT-MS scan (m/z 380 – 1600) and subsequent collision-induced dissociation (CID) MS/MS scans of the 20 most abundant ions. Survey scans were acquired in the Orbitrap with a resolution of 100 000 at m/z 400 and

automatic gain control (AGC) 1x106. Precursor ions were isolated and subjected to CID in the linear ion trap with AGC 1x105. Collision activation for the experiment was performed in the linear trap using helium gas at normalized collision energy to precursor m/z of 35% and activation Q 0.25. The width of the precursor isolation window was 2 m/z and only multiply-charged precursor ions were selected for MS/MS.

The MS and MS/MS scans were searched against NCBInr database using the SEQUEST algorithm (ThermoFisher Scientific, Germany). Variable modifications were deamidation (N and Q), oxidation (M) and phosphorylation (S, T and Y). The precursor mass tolerance was 5 ppm and the MS/MS mass tolerance was 0.8 Da. Two missed cleavage was allowed and were accepted as a real hit protein with at least two high confidence peptides.

Results

The results indicated that incubation of the H*protein solutions with lipid oxidation products led to the modification of its intrinsic fluorescence, change in the physical appearance and decrease of its pH.

Synchronous spectra of the H* proteins and lipid oxidation products mixtures were relatively broad, especially when aldehyde was present in the mixture (Figure 9-7). These spectra are most likely to be the sum of several spectra from different fluorescent compounds. Indeed synchronous spectra recorded from 250 to 500 nm showed two bands with a shoulder more pronounced for H*protein B. The maximum emissions of these bands were 293.5 nm and 341 nm for H* protein A and at 294 nm and 341.5 nm for H* protein B. Addition of cumene hydroperoxide, trans, trans-2, 4-decadienal and trans-2-decenal caused a decrease in fluorescence intensity of the second band in both proteins. This band may be assigned to aromatic amino acids especially tryptophan residues (Meynier *et al.*, 2004). However this

assignment may only be true for H*protein A since this protein contains 9 phenylalanine, 4 tyrosine and 1 tryptophan residues (Subkowski *et al.*, 2010). Conversely, because H* protein B has only 3 phenylalanine residues and no tyrosine and tryptophan residues, further studies are needed to confirm the assignment of this fluorescent band. Otherwise this may indicate the presence of contaminating proteins. Nevertheless the decrease in the fluorescence intensity does indicate the probable interaction of cumene hydroperoxide and the H*proteins (Geng *et al.*, 2010).

The intrinsic tryptophan fluorescence spectra also showed only a small shift for both proteins when incubated with cumene hydroperoxide whereas the tryptophan band completely disappeared in the presence of aldehydes. The presence of aldehydes resulted in a single broad single emission peak with maximum wavelength towards 411 nm and 427 nm (trans, trans-2, 4-decadienal) and 389 nm and 389 nm (cumene hydroperoxide, trans, trans-2, 4-decadienal trans-2-Decenal) for H* protein A and H* proteins B, respectively. These results are in line with those reported in the literature for fluorophore molecules generated by the binding of lipid peroxidation by-products to proteins, peptides or amino acids (Fukuzawa *et al.*, 1985; Yamaki *et al.*, 1992; Yin, 1996; Meynier *et al.*, 2004; Veberg *et al.*, 2006). In addition to the formation of complexes of lipid oxidation products and proteins, the accumulation and, or the polymerisation of the fluorophore monomers may have resulted in the quenching/shift of the intrinsic fluorescence of the proteins. It has been suggested that an occurrence of quenching-related fluorescence shifts when high concentrations of fluorophores or mixed fluorophores are analysed. The net result of this is that the fluorophores cannot exhibit their original, individual fluorescence maxima, typically observed at low concentrations (Yin, 1996). Some authors have reported a red shift from 400- 490 nm to 500-600 nm whereas others found the a shift of the fluorescence maxima to shorter wavelengths (Yin, 1996). This may partially

account for the blue shift observed when H* proteins were incubated with a mixture of cumene hydroperoxide, trans, trans-2, 4-decadienal and trans-2-decenal compared to the

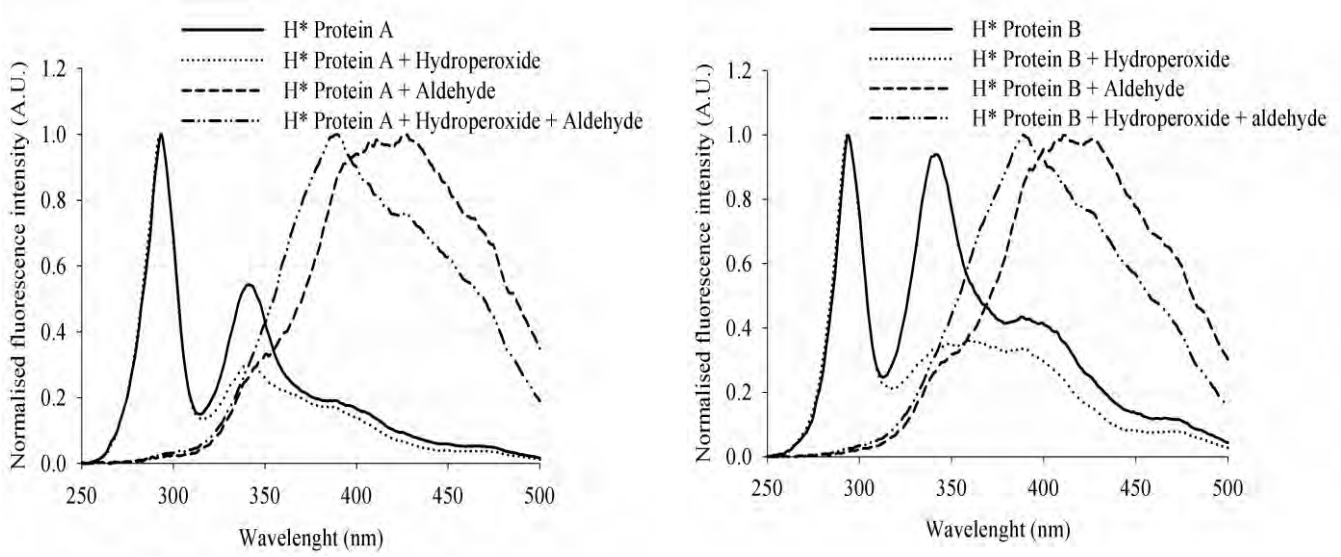

spectra of protein and trans, trans 2, 4-decadienal or protein and cumene hydroperoxide.

Figure 9-7. Synchronous fluorescence spectra of H* protein A and B (4mg/mL) in absence or in the presence of lipid oxidation products (1mM) recorded at $\Delta\lambda$= 20 nm. Fluorescence intensity normalised to 1.

Trypsin digestion and LC-MS/MS analysis showed that, in addition to all amino acids with basic side chains (lysine, histidine, arginine), methionine, tyrosine, phenylalanine and tryptophan were modified by the presence of aldehydes. Figure 9-8 is typical spectra of non modified and modified peptides. This indicates that covalent interaction is involved in the protein modification by lipid peroxidation by-products. These findings are in good agreement with covalent Michael adduct reactions between nucleophile amino acids (lysine, histidine, arginine, methionine and tyrosine) and lipid peroxidation by-products (Leaver *et al.*, 1999; Doorn and Petersen, 2002, 2003). Similarly, it has been demonstrated by

incubating tryptophan, triptophan-containing peptides and lysozyme with hydrogen peroxide that the oxidative attack of the tryptophan occurs first at the pyrrole ring and secondly on the phenyl moiety with the concomitant generation of fluorescent and non fluorescent compounds (Simat and Steinhart, 1998). Since phenylalanine were modified, it can also be speculated that lipid peroxidation product also react via its phenyl side group. However it is conceivable that aldehydes can also react with primary amines through condensation reaction to form Schiff bases.

The results presented above suggest that aldehydes interacts more with proteins than does cumene hydroperoxide and this was also observed through a greater decrease in pH when proteins were incubated with aldehydes. This phenomenon was most pronounced with H*protein B probably because this protein contains lower amino acids with basic side chains (8 lysine, 4 arginine and 7 histidine residues) as compared to H*protein A (24 lysine, 19 arginine and 11 histidine residues).

In order to draw final conclusions about the implications of lipid oxidation products affinity and the protection of polyunsaturated fatty acid against oxidation and off flavour masking, H*protein B solution (4mg/mL) was incubated with different concentrations of trans, trans-2, 4-decadienal or trans-2-decenal (0.1 mM to 20 mM). Not only did the pH of the proteins solution decreases with the increase of the aldehyde concentration (Figure 9-9) but also high concentration (more than 2 mM) resulted in protein precipitation. Although other possibilities such as a decrease of the pH close to the protein isoelectric point are not excluded, it is suggested that aldehydes interact with the protein and causes their cross-linking, and aggregation. Explicitly, it was found that 4mg/ml of H*protein B can bind up to 10 mM of aldehyde before reaching saturation (Figure 9-9).

In conclusion, all the applied techniques have supplemented each other to give clear evidence of the formation of complexes of hydrophobin-lipid oxidation products, especially aldehydes. Moreover the hypothesis postulated in chapters 5 and 6 the decrease in pH of the triphasic A/O/W system and O/W emulsions stabilised by hydrophobins was in part due to the interaction between lipid oxidation products and the proteins.

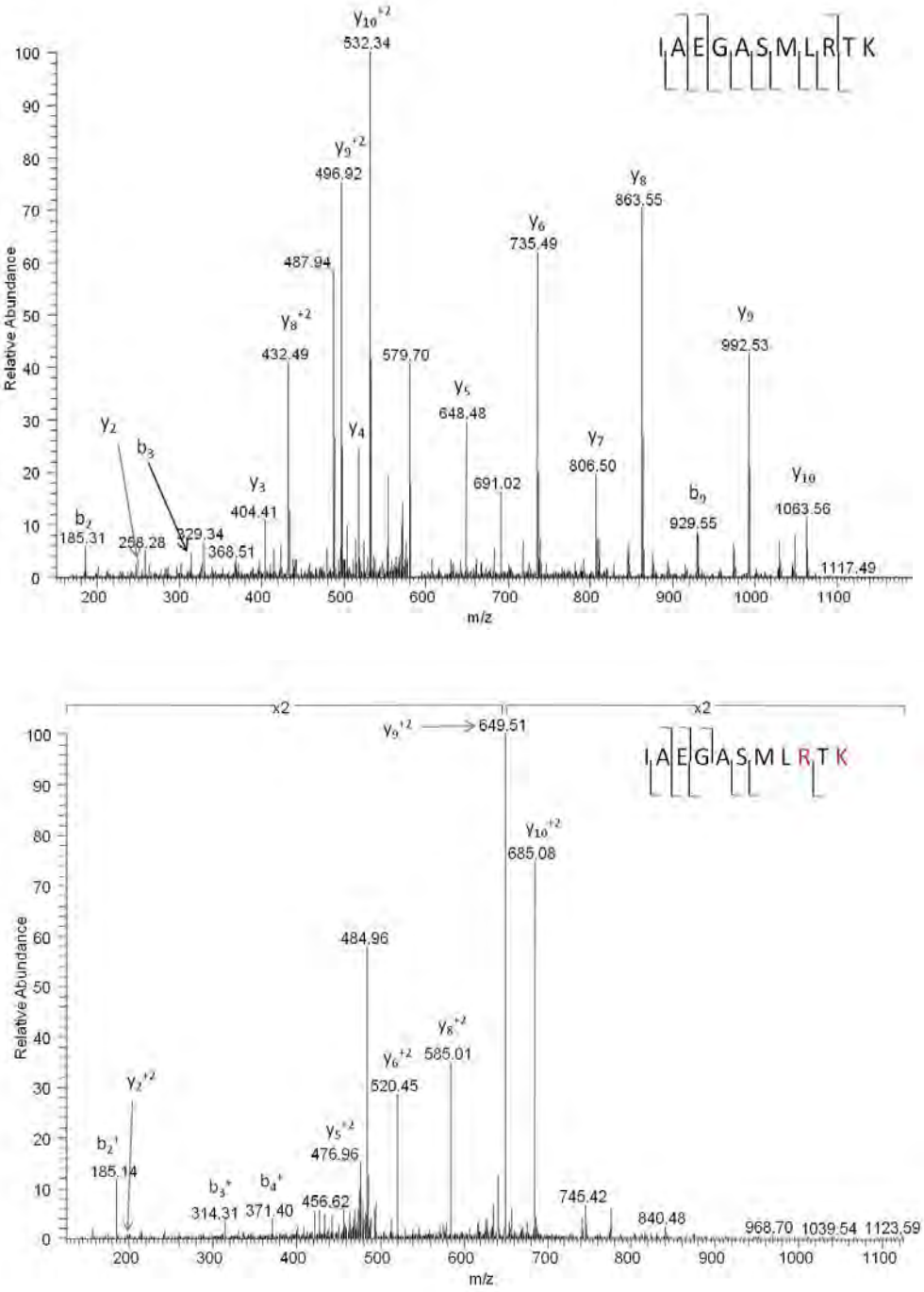

Figure 9-8. Example of collision-induced dissociation (CID) mass spectra of a non modified peptide (a) and a modified peptide by trans,trans-2, 4-decadienal in the arginine (R) and and lysine (K) sites. The calculated mass difference is presented in table 2.

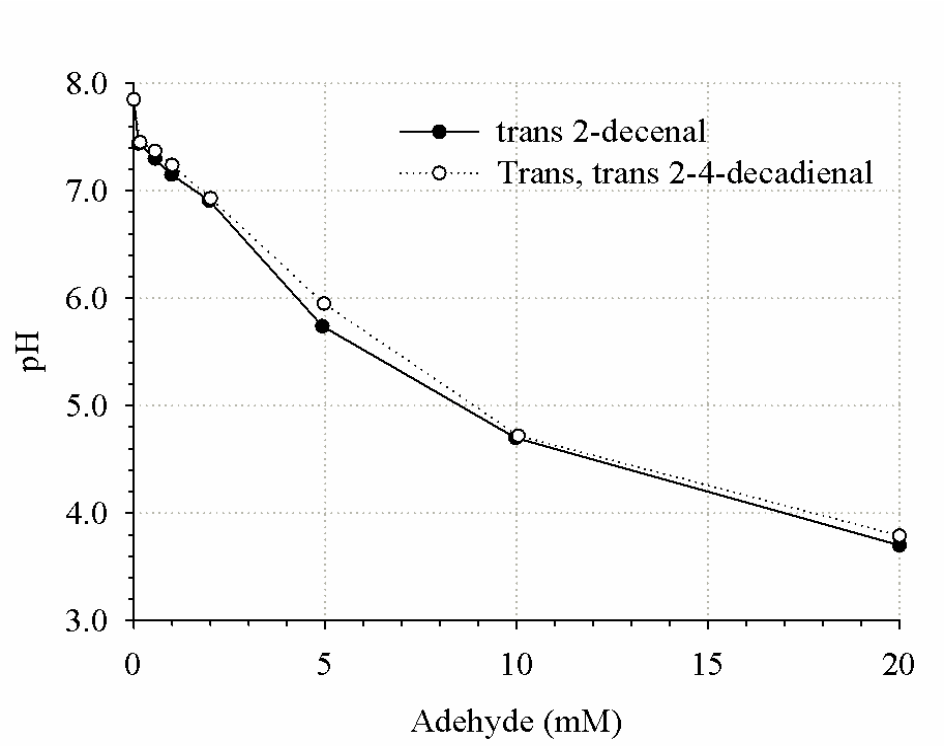

Figure 9-9. Change in pH of H*protein B solution as function of aldehydes concentration.

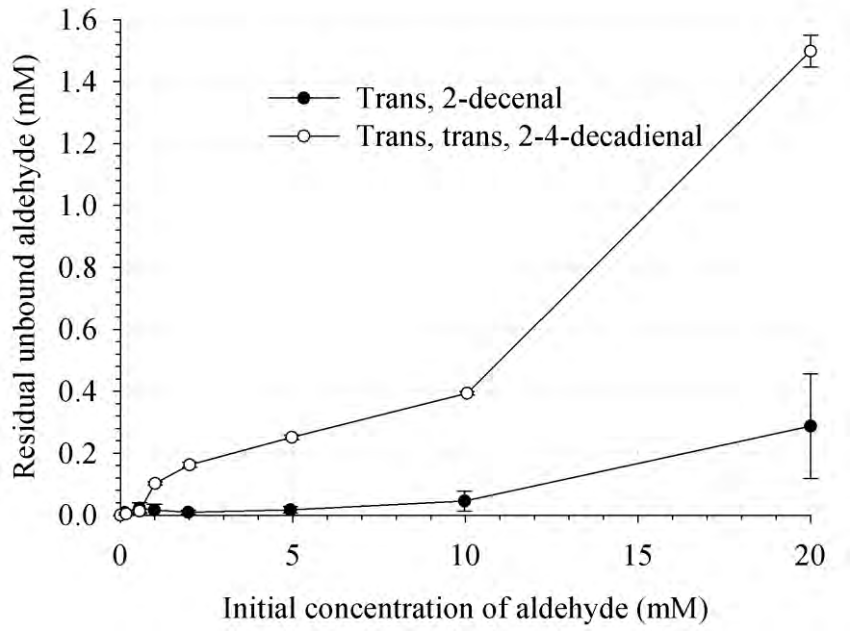

Figure 9-9. Residual unbound aldehydes with proteins as function of the initial concentration of aldehydes incubated with 0.4% of H*protein B solution (40°C/45h). Aldehydes were extracted with isooctane and analysed using P-anisidine method.

REFERENCES

Abismaïl, B., Canselier, J. P., Wilhelm, A. M., Delmas, H. & Gourdon, C. 1999. Emulsification by ultrasound: drop size distribution and stability. *Ultrasonics Sonochemistry,* 6**,** 75-83.

Aguilera, J. M. 2005. Why food microstructure? *Journal of Food Engineering,* 67**,** 3-11.

Akhtar, M., Murray, B. S. & Dickinson, E. 2006. Perception of creaminess of model oil-in-water dairy emulsions: Influence of the shear-thinning nature of a viscosity-controlling hydrocolloid. *Food Hydrocolloids,* 20**,** 839-847.

Alahverdjieva, V. S., Grigoriev, D. O., Fainerman, V. B., Aksenenko, E. V., Miller, R. & Mohwald, H. 2008. Competitive Adsorption from Mixed Hen Egg-White Lysozyme/Surfactant Solutions at the Air−Water Interface Studied by Tensiometry, Ellipsometry, and Surface Dilational Rheology. *The Journal of Physical Chemistry B,* 112**,** 2136-2143.

Aldred, D. L., Cox, A. R. & Stoyanov, S. D. 2007. *Aerated products with reduced creaming*. United Stated patent application 11/524977.

Allen, K. E., Dickinson, E. & Murray, B. 2006. Acidified sodium caseinate emulsion foams containing liquid fat: A comparison with whipped cream. *LWT - Food Science and Technology,* 39**,** 225-234.

Arnaudov, L., Denkov, N. D., Surcheva, I., Durbut, P., Broze, G. & Mehreteab, A. 2001. Effect of Oily Additives on Foamability and Foam Stability. 1. Role of Interfacial Properties. *Langmuir,* 17**,** 6999-7010.

Ashokkumar, M. 2006. Sonochemical preparation of colloids. *In:* SOMASUNDARAN, P. (ed.) *Encyclopedia of Surface and Colloid Science.* Second edition ed. London: Taylor & Francis.

Askolin, S. 2006. *Characterisation of Trichoderma reesei hydrophobins HFBI and HFBII.* Thesis, Helsinki University of Technology.

Askolin, S., Linder, M., Scholtmeijer, K., Tenkanen, M., Penttila, M., De Vocht, M. L. & Wosten, H. a. B. 2006. Interaction and Comparison of a Class I Hydrophobin from Schizophyllum commune and Class II Hydrophobins from Trichoderma reesei. *Biomacromolecules,* 7**,** 1295-1301.

Askolin, S., Nakari-Setala, T. & Tenkanen, M. 2001. Overproduction, purification, and characterization of the Trichoderma reesei hydrophobin HFBI. *Applied Microbiology and Biotechnology,* 57**,** 124-130.

Aveyard, R., Binks, B. P., Fletcher, P. D. I., Peck, T.-G. & Garrett, P. R. 1993. Entry and spreading of alkane drops at the air/surfactant solution interface in relation to foam

and soap film stability. *Journal of the Chemical Society, Faraday Transactions,* 89**,** 4313-4321.

Aveyard, R., Binks, B. P., Fletcher, P. D. I., Peck, T. G. & Rutherford, C. E. 1994. Aspects of aqueous foam stability in the presence of hydrocarbon oils and solid particles. *Advances in Colloid and Interface Science,* 48**,** 93-120.

Aveyard, R. & Clint, J. H. 1996. Foam and thin film breakdown processes. *Current Opinion in Colloid & Interface Science,* 1**,** 764-770.

Avivi, S. & Gedanken, A. 2002. S-S bonds are not required for the sonochemical formation of proteinaceous microspheres: the case of streptavidin. *Biochemical Journal,* 366**,** 705-707.

Bailey, M., Askolin, S., Horhammer, H, N., Tenkanen, M., Linder, M., Penttila, M. & Nakari-Setala, T. 2002. Process technological effects of deletion and amplification of hydrophobins I and II in transformants of Trichoderma reesei. *Applied Microbiology and Biotechnology,* 58**,** 721-727.

Basheva, E. S., Ganchev, D., Denkov, N. D., Kasuga, K., Satoh, N. & Tsujii, K. 1999. Role of Betaine as Foam Booster in the Presence of Silicone Oil Drops. *Langmuir,* 16**,** 1000-1013.

Basheva, E. S., Gurkov, T. D., Christov, N. C. & Campbell, B. 2006. Interactions in oil/water/oil films stabilized by β-lactoglobulin; role of the surface charge. *Colloids and Surfaces A: Physicochemical and Engineering Aspects,* 282-283**,** 99-108.

Basheva, E. S., Kralchevsky, P. A., Christov, N. C., Danov, K. D., Stoyanov, S. D., Blijdenstein, T. B. J., Kim, H.-J., Pelan, E. G. & Lips, A. 2011a. Unique Properties of Bubbles and Foam Films Stabilized by HFBII Hydrophobin. *Langmuir,* 27**,** 2382-2392.

Basheva, E. S., Kralchevsky, P. A., Danov, K. D., Stoyanov, S. D., Blijdenstein, T. B. J., Pelan, E. G. & Lips, A. 2011b. Self-Assembled Bilayers from the Protein HFBII Hydrophobin: Nature of the Adhesion Energy. *Langmuir,* 27**,** 4481-4488.

Baszkin, A., Boissonnade, M. M., Kamyshny, A. & Magdassi, S. 2001. Native and Hydrophobically Modified Human Immunoglobulin G at the Air/Water Interface: Sequential and Competitive Adsorption. *Journal of Colloid and Interface Science,* 239**,** 1-9.

Behrend, O., Ax, K. & Schubert, H. 2000. Influence of continuous phase viscosity on emulsification by ultrasound. *Ultrasonics Sonochemistry,* 7**,** 77-85.

Behrend, O. & Schubert, H. 2001. Influence of hydrostatic pressure and gas content on continuous ultrasound emulsification. *Ultrasonics Sonochemistry,* 8**,** 271-276.

Benjamins, J., Vingerhoeds, M. H., Zoet, F. D., De Hoog, E. H. A. & Van Aken, G. A. 2009. Partial coalescence as a tool to control sensory perception of emulsions. *Food Hydrocolloids,* 23**,** 102-115.

Beverung, C. J., Radke, C. J. & Blanch, H. W. 1999. Protein adsorption at the oil/water interface: characterization of adsorption kinetics by dynamic interfacial tension measurements. *Biophysical Chemistry,* 81**,** 59-80.

Bilewicz, R., Witomski, J., Van Der Heyden, A., Tagu, D., Palin, B. & Rogalska, E. 2001. Modification of Electrodes with Self-Assembled Hydrophobin Layers. *The Journal of Physical Chemistry B,* 105**,** 9772-9777.

Binks, B. P. & Dong, J. 1998. Mixing of silicone oils with monolayers of nonionic surfactant at the air/water surface. *Journal of the Chemical Society, Faraday Transactions,* 94**,** 401-410.

Blakemore, W. R. & Harpell, A. R. 2010. Carrageenan. *In:* IMESON, A. (ed.) *Food Stabilisers, Thickeners and Gelling Agents.* Sussex, UK: Blackwell Publishing Ltd.

Blijdenstein, T. B. J., De Groot, P. W. N. & Stoyanov, S. D. 2010. On the link between foam coarsening and surface rheology: why hydrophobins are so different. *Soft Matter,* 6**,** 1799-1808.

Boode, K., Walstra, P. & De Groot-Mostert, A. E. A. 1993. Partial coalescence in oil-in-water emulsions 2. Influence of the properties of the fat. *Colloids and Surfaces A: Physicochemical and Engineering Aspects,* 81**,** 139-151.

Bradford, M. 1976. A rapid and sensitive method for the quantification of microgram quantities of protein using the principle of protein dye binding. *Anal.Biochem.,* 72**,** 248-253.

Braun, D. B. & Rosen, M. R. 2000. *Reology modifiers handbook: Practical Use and Application,* New York, USA, William Andrew Publishing.

Calonje, M., Bernardo, D., Novaes-Ledieu, M. & Mendoza, C. G. 2002. Properties of a hydrophobin isolated from the mycoparasitic fungus Verticillium fungicola *Canadian Journal of Microbiology,* 48**,** 1030-1034.

Campbell, G. M., Webb, C., Pondiella, S. S. & Niranjan, K. 1999. *Bubbles in food*, American Association of Cereal Chemists.

Campbell, L., Raikos, V. & Euston, S. R. 2003. Modification of functional properties of egg-white proteins. *Food / Nahrung,* 47**,** 369-376.

Cascaopereira, L. G., Theodoly, O., Blanch, H. W. & Radke, C. J. 2003. Dilatational Rheology of BSA Conformers at the Air/Water Interface. *Langmuir,* 19**,** 2349-2356.

Castro, M. J. L., Kovensky, J. & Fernández Cirelli, A. 2002. New Family of Nonionic Gemini Surfactants. Determination and Analysis of Interfacial Properties. *Langmuir,* 18**,** 2477-2482.

Chanamai, R. & Mcclements, D. J. 2000a. Dependence of creaming and rheology of monodisperse oil-in-water emulsions on droplet size and concentration. *Colloids and Surfaces A: Physicochemical and Engineering Aspects,* 172**,** 79-86.

Chanamai, R. & Mcclements, D. J. 2000b. Impact of Weighting Agents and Sucrose on Gravitational Separation of Beverage Emulsions. *Journal of Agricultural and Food Chemistry,* 48**,** 5561-5565.

Choe, E. & Min, D. B. 2006. Mechanisms and factors for edible oil oxidation. *comprehensive reviews in Food Science and Food Safety,* 5**,** 169-186.

Chojnicka, A., De Jong, S., De Kruif, C. G. & Visschers, R. W. 2008. Lubrication Properties of Protein Aggregate Dispersions in a Soft Contact. *Journal of Agricultural and Food Chemistry,* 56**,** 1274-1282.

Chowdhury, P. & Viraraghavan, T. 2009. Sonochemical degradation of chlorinated organic compounds, phenolic compounds and organic dyes – A review. *Science of The Total Environment,* 407**,** 2474-2492.

Christov, N. C., Denkov, N. D., Kralchevsky, P. A., Broze, G. & Mehreteab, A. 2002. Kinetics of Triglyceride Solubilization by Micellar Solutions of Nonionic Surfactant and Triblock Copolymer. 1. Empty and Swollen Micelles. *Langmuir,* 18**,** 7880-7886.

Ciron, C. I. E., Gee, V. L., Kelly, A. L. & Auty, M. a. E. 2012. Modifying the microstructure of low-fat yoghurt by microfluidisation of milk at different pressures to enhance rheological and sensory properties. *Food Chemistry,* 130**,** 510-519.

Collén, A., Persson, J., Linder, M., Nakari-Setälä, T., Penttilä, M., Tjerneld, F. & Sivars, U. 2002. A novel two-step extraction method with detergent/polymer systems for primary recovery of the fusion protein endoglucanase I-hydrophobin I. *Biochimica et Biophysica Acta (BBA) - General Subjects,* 1569**,** 139-150.

Corvis, Y., Brezesinski, G., Rink, R., Walcarius, A., Van Der Heyden, A., Mutelet, F. & Rogalska, E. 2006. Analytical Investigation of the Interactions between SC3 Hydrophobin and Lipid Layers: Elaborating of Nanostructured Matrixes for Immobilizing Redox Systems. *Analytical Chemistry,* 78**,** 4850-4864.

Coupland, J. N. & McClements, D. J. 1996. Lipid oxidation in food emulsions. *Trends in Food Science & Technology,* 7**,** 83-91.

Cravotto, G. & Cintas, P. 2012. Introduction to sonochemistry: a historical and conceptual overview. *In:* CHEN, D., SHARMA, S. K. & MUDHOO, A. (eds.) *Handbook on application of ultrasound:sonochemistry for sustanaibility.* Boc Rota, US: RCR Press.

Cox, A. R., Aldred, D. L. & Russell, A. B. 2009. Exceptional stability of food foams using class II hydrophobin HFBII. *Food Hydrocolloids,* 23**,** 366-376.

Cox, A. R., Cagnol, F., Russell, A. B. & Izzard, M. J. 2007. Surface Properties of Class II Hydrophobins from Trichoderma reesei and Influence on Bubble Stability. *Langmuir,* 23**,** 7995-8002.

Cox, P. W. & Hooley, P. 2009. Hydrophobins: New prospects for biotechnology. *Fungal Biology Reviews,* 23**,** 40-47.

Cucheval, A. & Chow, R. C. Y. 2008. A study on the emulsification of oil by power ultrasound. *Ultrasonics Sonochemistry,* 15**,** 916-920.

Dadras, S., Torkamany, M. J. & Sbbaghzadeh, J. 2012. Ultrasound-assisted synthesis of nanomaterials. *In:* CHEN, D., SHARMA, S. K. & MUDHOO, A. (eds.) *Handbook on applications of ultrasound: sonochemistry for sustainability.* Boca Raton, US: CRC Press.

Damodaran, S. 2005. Protein Stabilization of Emulsions and Foams. *Journal of Food Science,* 70**,** R54-R66.

Damodaran, S., Anand, K. & Razumovsky, L. 1998. Competitive Adsorption of Egg White Proteins at the Airâ˚Water Interface: Direct Evidence for Electrostatic Complex Formation between Lysozyme and Other Egg Proteins at the Interface. *Journal of Agricultural and Food Chemistry,* 46**,** 872-876.

De Hoog, E. H. A., Prinz, J. F., Huntjens, L., Dresselhuis, D. M. & Van Aken, G. A. 2006. Lubrication of Oral Surfaces by Food Emulsions: the Importance of Surface Characteristics. *Journal of Food Science,* 71**,** E337-E341.

De Jongh, H. H. J. 2007. Proteins in food microstructure formation. *In:* MCCLEMENTS, D. J. (ed.) *Understanding and controlling the microstructure of complex foods.* Cambridge, England: Woodhead Publishing Limited

De Vicente, J., Stokes, J. R. & Spikes, H. A. 2005. Lubrication properties of non-adsorbing polymer solutions in soft elastohydrodynamic (EHD) contacts. *Tribology International,* 38**,** 515-526.

De Vocht, M. L., Wosten, H. A. B. & Wessels, J. G. H. 2005. *Method of purifying a hydrophobin present in a hydrophobin-containing solution*.

De Vries, O. M. H., Fekkes, M. P., Wosten, H. a. B. & Wessels, J. G. H. 1993. Insoluble hydrophobin complexes in the walls of Schizophyllum commune and other filamentous fungi. *Archives of Microbiology,* 159**,** 330-335.

De Wijk, R. A. & Prinz, J. F. 2005. The role of friction in perceived oral texture. *Food Quality and Preference,* 16**,** 121-129.

De Wijk, R. A. & Prinz, J. F. 2006. Mechanisms underlyng the role of friction in oral texture. *Journal of Texture Studies,* 37**,** 413-427.

De Wijk, R. A., Prinz, J. F. & Janssen, A. M. 2006. Explaining perceived oral texture of starch-based custard desserts from standard and novel instrumental tests. *Food Hydrocolloids,* 20**,** 24-34.

Deleu, M., Paquot, M., Razafindralambo, H., Popineau, Y., Budziekiewicz, H., Jaques, P. & Thonart, P. 1999. Structure, interfacial properties, and functional qualities in foams and emulsions of surfactin, a lipopeptide from bacillus subtilis. *In:* DICKINSON, E. & RODRÍGUEZ PATINO, J. M. (eds.) *Food Emulsions and Foams:Interfaces,interactions and stability*. Cambridge, UK: Royal Society of Chemistry.

Demetriades, K., Coupland, J. N. & Mcclements, D. J. 1997. Physicochemical Properties of Whey Protein-Stabilized Emulsions as affected by Heating and Ionic Strength. *Journal of Food Science,* 62**,** 462-467.

Denkov, N. D. 1999. Mechanisms of Action of Mixed Solid−Liquid Antifoams. 2. Stability of Oil Bridges in Foam Films. *Langmuir,* 15**,** 8530-8542.

Denkov, N. D. 2004. Mechanisms of Foam Destruction by Oil-Based Antifoams. *Langmuir,* 20**,** 9463-9505.

Depree, J. A. & Savage, G. P. 2001. Physical and flavour stability of mayonnaise. *Trends in Food Science & Technology,* 12**,** 157-163.

Dickinson, E. 1986. Mixed proteinaceous emulsifiers: review of competitive protein adsorption and the relationship to food colloid stabilization. *Food Hydrocolloids,* 1**,** 3-23.

Dickinson, E. 1989. A model of a concentrated dispersion exhibiting bridging flocculation and depletion flocculation. *Journal of Colloid and Interface Science,* 132**,** 274-278.

Dickinson, E. 2003. Hydrocolloids at interfaces and the influence on the properties of dispersed systems. *Food Hydrocolloids,* 17**,** 25-39.

Dickinson, E. 2010. Food emulsions and foams: Stabilization by particles. *Current Opinion in Colloid & Interface Science,* 15**,** 40-49.

Dickinson, E., Ettelaie, R., Kostakis, T. & Murray, B. S. 2004. Factors Controlling the Formation and Stability of Air Bubbles Stabilized by Partially Hydrophobic Silica Nanoparticles. *Langmuir,* 20**,** 8517-8525.

Dickinson, E. & Golding, M. 1997. Depletion flocculation of emulsions containing unadsorbed sodium caseinate. *Food Hydrocolloids,* 11**,** 13-18.

Dickinson, E., Goller, M. I. & Wedlock, D. J. 1993. Creaming and rheology of emulsions containing polysaccharide and non-ionic or anionic surfactants. *Colloids and Surfaces A: Physicochemical and Engineering Aspects,* 75**,** 195-201.

Dickinson, E. & Matsumura, Y. 1994. Proteins at liquid interfaces: Role of the molten globule state. *Colloids and Surfaces B: Biointerfaces,* 3**,** 1-17.

Dickinson, E. & Pawlowsky, K. 1997. Effect of ,ι-Carrageenan on Flocculation, Creaming, and Rheology of a Protein-Stabilized Emulsion. *Journal of Agricultural and Food Chemistry,* 45**,** 3799-3806.

Dickinson, E., Pogson, D. J., Robson, E. W. & Stainsby, G. 1985. Time-dependent surface pressures of adsorbed films of caseinate + gelatin at the oil-water interface. *Colloids and Surfaces,* 14**,** 135-141.

Dickinson, E., Ritzoulis, C., Yamamoto, Y. & Logan, H. 1999. Ostwald ripening of protein-stabilized emulsions: effect of transglutaminase crosslinking. *Colloids and Surfaces B: Biointerfaces,* 12**,** 139-146.

Dimakou, C., Kiokias, S., Tsaprouni, I. & Oreopoulou, V. 2007. Effect of Processing and Storage Parameters on the Oxidative Deterioration of Oil-in-Water Emulsions. *Food Biophysics,* 2**,** 38-45.

Dolatowski, Z. J., Stadnik, J., D., S. & 2007. Applications of ultrasound in food technology. *Acta Sci.Pol., Technol. Aliment. ,* 6**,** 88-99.

Doorn, J. A. & Petersen, D. R. 2002. Covalent Modification of Amino Acid Nucleophiles by the Lipid Peroxidation Products 4-Hydroxy-2-nonenal and 4-Oxo-2-nonenal†. *Chemical Research in Toxicology,* 15**,** 1445-1450.

Doorn, J. A. & Petersen, D. R. 2003. Covalent adduction of nucleophilic amino acids by 4-hydroxynonenal and 4-oxononenal. *Chemico-Biological Interactions,* 143-144**,** 93-100.

Dresselhuis, D., Klok, H., Stuart, M., De Vries, R., Van Aken, G. & De Hoog, E. 2007a. Tribology of o/w Emulsions Under Mouth-like Conditions: Determinants of Friction. *Food Biophysics,* 2**,** 158-171.

Dresselhuis, D. M., De Hoog, E. H. A., Cohen Stuart, M. A. & Van Aken, G. A. 2007b. Tribology as a tool to study emulsion behaviour in the mouth. *In:* DICKINSON, E. & LESER, M. E. (eds.) *Food Colloids: Self-Assembly and Material Science.* RSC.

Dutta, A., Chengara, A., Nikolov, A. D., Wasan, D. T., Chen, K. & Campbell, B. 2004. Texture and stability of aerated food emulsions--effects of buoyancy and Ostwald ripening. *Journal of Food Engineering,* 62**,** 169-175.

Dynesen, J. & Nielsen, J. 2003. Surface Hydrophobicity of Aspergillus nidulans Conidiospores and Its Role in Pellet Formation. *Biotechnology Progress,* 19**,** 1049-1052.

Elias, R. J., Mcclements, D. J. & Decker, E. A. 2005. Antioxidant Activity of Cysteine, Tryptophan, and Methionine Residues in Continuous Phase +Ý-Lactoglobulin in Oil-in-Water Emulsions. *Journal of Agricultural and Food Chemistry,* 53**,** 10248-10253.

Elwell, M. W., Roberts, R. F. & Coupland, J. N. 2004. Effect of homogenization and surfactant type on the exchange of oil between emulsion droplets. *Food Hydrocolloids,* 18**,** 413-418.

Engelen, L., De Wijk, R. A., Van Der Bilt, A., Prinz, J. F., Janssen, A. M. & Bosman, F. 2005. Relating particles and texture perception. *Physiology & Behavior,* 86**,** 111-117.

Exerowa, D. & Kruglyakov, P. M. 1998. *Foam and Foam Films: Theory, Experiment, Application,* Amsterdam, Elsevier Science B.V.

Fainerman, V. B., Vollhardt, D. & Emrich, G. 2001. Dynamics and Phase Transition in Adsorbed Monolayers of Sodium Dodecyl Sulfate/Dodecanol Mixtures. *The Journal of Physical Chemistry B,* 105**,** 4324-4330.

Ferreira, S. M. P., Duarte, A. P., Queiroz, J. A. & Dominguez, J. M. 2009. Influence of buffer systems on Trichoderma reesei Rut C-30 morphology and cellulase production. *Electronic Journal of Biotechnology,* 12**,** 1-9.

Foegeding, E. A., Luck, P. J. & Davis, J. P. 2006. Factors determining the physical properties of protein foams. *Food Hydrocolloids,* 20**,** 284-292.

Folch, J., Lees, M. & Stanley, G. H. S. 1957. A sample method for the isolation and purification of total lipids from animal tissues. *Journal of Biological Chemistry,* 226**,** 497-509.

Frøst, M. B. & Janhøj, T. 2007. Understanding creaminess. *International Dairy Journal,* 17**,** 1298-1311.

Fukuzawa, K., Kishikawa, K., Tokumura, A., Tsukatani, H. & Shibuya, M. 1985. Fluorescent pigments by covalent binding of lipid peroxidation by-products to protein and amino acids. *Lipids,* 20**,** 854-861.

Gao, T. & Rosen, M. J. 1995. Dynamic Surface Tension of Aqueous Surfactant Solutions: 7. Physical Significance of Dynamic Parameters and the Induction Period. *Journal of Colloid and Interface Science,* 172**,** 242-248.

Gardner, H. W. 1979. Lipid hydroperoxide reactivity with proteins and amino acids: a review. *Journal of Agricultural and Food Chemistry,* 27**,** 220-229.

Garrec, D. A. & Norton, I. T. 2012. The influence of hydrocolloid hydrodynamics on lubrication. *Food Hydrocolloids,* 26**,** 389-397.

Geng, F., Zheng, L., Yu, L., Li, G. & Tung, C. 2010. Interaction of bovine serum albumin and long-chain imidazolium ionic liquid measured by fluorescence spectra and surface tension. *Process Biochemistry,* 45**,** 306-311.

Goff, H. D. & Vega, C. 2007. Structured-engineered of ice-cream and foam-based foods. *In:* MCCLEMENTS, D. J. (ed.) *Understanding and controlling the microstructure of complex foods.* Cambridge, England: Woodhead Publishing Limited.

Golding, M. & Pelan, E. 2008. Application of emulsifiers to reduce fat and enhance nutritional quality. *In:* HASENHUETTL, G. L. & HARTEL, R. W. (eds.) *Food emulsifiers and their applications.* second edition ed. New York: Springer.

Graham, D. E., Birch, H. S. & Mckechnie, M. T. 1981. Heavy methal interactions with adsorbing proteins. *In:* TADROS, T. F. (ed.) *Internatinal symposium on the effect of polymers on dispersion properties.* University College, London: Society of Chemical Industry, Colloid and Surface Chemistry Group and Pure and Applied Macromolecular Chemistry Group.

Graham, D. E. & Phillips, M. C. 1979. Proteins at liquid interfaces: Kinetics of adsorption and surface denaturation. *Journal of Colloid and Interface Science,* 70**,** 403-414.

Grinstaff, M. W. & Suslick, K. S. 1991. Air-Filled Proteinaceous Microbubbles: Synthesis of an Echo-Contrast Agent. *Proceedings of the National Academy of Sciences,* 88**,** 7708-7710.

Gryboś, J., Marszałek, M., Lekka, M., Heinrich, F. & Tröger, W. 2004. PAC Studies of BSA Conformational Changes. *Hyperfine Interactions,* 159**,** 323-329.

Guzey, D. & Mcclements, D. J. 2006. Formation, stability and properties of multilayer emulsions for application in the food industry. *Advances in Colloid and Interface Science,* 128-130**,** 227-248.

Haahr, A. M. & Jacobsen, C. 2008. Emulsifier type, metal chelation and pH affect oxidative stability of n -3-enriched emulsions *Eur.J.Lipid Sci.Technol,* 110**,** 949-961.

Haas Jimoh Akanbi, M., Post, E., Meter-Arkema, A., Rink, R., Robillard, G. T., Wang, X., Wösten, H. a. B. & Scholtmeijer, K. 2010. Use of hydrophobins in formulation of water insoluble drugs for oral administration. *Colloids and Surfaces B: Biointerfaces,* 75**,** 526-531.

Hait, S. & Moulik, S. 2001. Determination of critical micelle concentration (CMC) of nonionic surfactants by donor-acceptor interaction with Iodine and correlation of CMC with hydrophile-lipophile balance and other parameters of the surfactants. *Journal of Surfactants and Detergents,* 4**,** 303-309.

Hakanpaa, J., Paananen, A., Askolin, S., Nakari-Setala, T., Parkkinen, T., Penttila, M., Linder, M. B. & Rouvinen, J. 2004. Atomic Resolution Structure of the HFBII Hydrophobin, a Self-assembling Amphiphile. *Journal of Biological Chemistry,* 279**,** 534-539.

Hakanpää, J., Szilvay, G. R., Kaljunen, H., Maksimainen, M., Linder, M. & Rouvinen, J. 2006. Two crystal structures of Trichoderma reesei hydrophobin HFBI-The structure of a protein amphiphile with and without detergent interaction. *Protein Science,* 15**,** 2129-2140.

Hattori, T., Kimura, K., Seyrek, E. & Dubin, P. L. 2001. Binding of Bovine Serum Albumin to Heparin Determined by Turbidimetric Titration and Frontal Analysis Continuous Capillary Electrophoresis. *Analytical Biochemistry,* 295**,** 158-167.

Hektor, H. J. & Scholtmeijer, K. 2005. Hydrophobins: proteins with potential. *Current Opinion in Biotechnology,* 16**,** 434-439.

Hiemenz, P. C. & Rajagopalan, R. 1997. *Principles of Colloid and Surface Chemistry* New York, Taylor & Francis.

Heuer, E. a. K. 2009. *Formulation and stability of model food foam microstructures.* Engineering doctorate Thesis, The University of Birmingham.

Hiller, B. & Lorenzen, P. C. 2007. Surface Hydrophobicity of Physicochemically and Enzymatically Treated Milk Proteins in Relation to Techno-functional Properties. *Journal of Agricultural and Food Chemistry,* 56**,** 461-468.

Horowitz, B. Z. 1997. Bromism from Excessive Cola Consumption. *Clinical Toxicology,* 35**,** 315-320.

Hotrum, N. E., Cohen Stuart, M. A., Van Vliet, T. & Van Aken, G. A. 2003. Flow and Fracture Phenomena in Adsorbed Protein Layers at the Air/Water Interface in Connection with Spreading Oil Droplets. *Langmuir,* 19**,** 10210-10216.

Hotrum, N. E., Cohen Stuart, M. A., Van Vliet, T. & Van Aken, G. A. 2004. Spreading of partially crystallized oil droplets on an air/water interface. *Colloids and Surfaces A: Physicochemical and Engineering Aspects,* 240**,** 83-92.

Hotrum, N. E., Stuart, M. a. C., Vliet, T. V., Avino, S. F. & Van Aken, G. A. 2005. Elucidating the relationship between the spreading coefficient, surface-mediated partial coalescence and the whipping time of artificial cream. *Colloids and Surfaces A: Physicochemical and Engineering Aspects,* 260**,** 71-78.

Houmadi, S., Ciuchi, F., De Santo, M. P., De Stefano, L., Rea, I., Giardina, P., Armenante, A., Lacaze, E. & Giocondo, M. 2008. Langmuir−Blodgett Film of Hydrophobin Protein from Pleurotus ostreatus at the Air−Water Interface. *Langmuir,* 24**,** 12953-12957.

Hu, M., Mcclements, D. J. & Decker, E. A. 2003. Lipid Oxidation in Corn Oil-in-Water Emulsions Stabilized by Casein, Whey Protein Isolate, and Soy Protein Isolate. *Journal of Agricultural and Food Chemistry,* 51**,** 1696-1700.

Hua, X. Y. & Rosen, M. J. 1991. Dynamic surface tension of aqueous surfactant solutions : 3. Some effects of molecular structure and environment. *Journal of Colloid and Interface Science,* 141**,** 180-190.

Ibba, M., Taylor, S. J. C., Weedon, C. M. & Mantle, P. G. 1987. Submerged Fermentation of Penicillium paxilli Biosynthesizing Paxilline, a Process Inhibited by Calcium-induced Sporulation. *Journal of General Microbiology,* 133**,** 3109-3119.

Ilmen, M., Saloheimo, A., Onnela, M. L. & Penttila, M. E. 1997. Regulation of cellulase gene expression in the filamentous fungus Trichoderma reesei. *Applied and Environmental Microbiology,* 63**,** 1298-1306.

Imeson, A. 2010. *Food Stabilisers, Thickeners and Gelling Agents,* Oxford, John Wiley & Sons.

Ivanov, I. B., Danov, K. D. & Kralchevsky, P. A. 1999. Flocculation and coalescence of micron-size emulsion droplets. *Colloids and Surfaces A: Physicochemical and Engineering Aspects,* 152**,** 161-182.

Jacobsen, C., Let, M. B., Nielsen, N. S. & Meyer, A. S. 2008. Antioxidant strategies for preventing oxidative flavour deterioration of foods enriched with n-3 polyunsaturated lipids: a comparative evaluation. *Trends in Food Science & Technology,* 19**,** 76-93.

Jakubczyk, E. & Niranjan, K. 2006. Transient development of whipped cream properties. *Journal of Food Engineering,* 77**,** 79-83.

Jensen, B. G., Andersen, M. R., Pedersen, M. H., Frisvad, J. C. & Søndergaardens, I. 2010. Hydrophobins from Aspergillus species cannot be clearly divided into two classes BioMed Central,, 3**,** 344.

Johns, M. L. 2009. NMR studies of emulsions. *Current Opinion in Colloid & Interface Science,* 14**,** 178-183.

Kallio, J. M., Linder, M. B. & Rouvinen, J. 2007. Crystal Structures of Hydrophobin HFBII in the Presence of Detergent Implicate the Formation of Fibrils and Monolayer Films. *Journal of Biological Chemistry,* 282**,** 28733-28739.

Kanwal, F., Liggat, J. J. & Pethrick, R. A. 2000. Ultrasonic degradation of polystyrene solutions. *Polymer Degradation and Stability,* 68**,** 445-449.

Kargar, M., Spyropoulos, F. & Norton, I. T. 2011. The effect of interfacial microstructure on the lipid oxidation stability of oil-in-water emulsions. *Journal of Colloid and Interface Science,* 357**,** 527-533.

Kaszuba, M., Corbett, J., Watson, M. F. & Jones, A. 2010. High-concentration zeta potential measurements using light-scattering techniques. *Philos Transact A Math Phys Eng Sci. ,* 368**,** 12.

Kato, A. & Nakai, S. 1980. Hydrophobicity determined by a fluorescence probe method and its correlation with surface properties of proteins. *Biochim Biophys Acta* 624**,** 13-20.

Kato, A., Tsutsui, N., Matsudomi, N., Kobayashi, K. & Nakai, S. 1981. Effects of Partial Denaturation on Surface Properties of Ovalbumin and Lysozyme. *Agricultural and Biological Chemistry* 45**,** 2755-2760.

Katsuda, M. S., Mcclements, D. J., Miglioranza, L. H. S. & Decker, E. A. 2008. Physical and Oxidative Stability of Fish Oil-in-Water Emulsions Stabilized with beta-Lactoglobulin and Pectin. *Journal of Agricultural and Food Chemistry,* 56**,** 5926-5931.

Kawakami, M., Ward, L. & Doi, H. 2000. Mechanisms of tubulin modification by phosphatidylcholine hydroperoxides. *Lipids,* 35**,** 205-211.

Kazmierczak, P., Kim, D. H., Turina, M. & Van Alfen, N. K. 2005. A Hydrophobin of the Chestnut Blight Fungus, Cryphonectria parasitica, Is Required for Stromal Pustule Eruption. *Eukaryotic Cell,* 4**,** 931-936.

Kentish, S., Wooster, T. J., Ashokkumar, M., Balachandran, S., Mawson, R. & Simons, L. 2008. The use of ultrasonics for nanoemulsion preparation. *Innovative Food Science & Emerging Technologies,* 9**,** 170-175.

Keogh, M. K., Lainé, K. I. & O'connor, J. F. 1996. RHEOLOGY OF SODIUM CASEINATE-CARRAGEENAN MIXTURES. *Journal of Texture Studies,* 26**,** 635-652.

Keszler, A., Kriska, T. & Nemeth, A. 2000. Mechanism of Volatile Compound Production during Storage of Sunflower Oil. *Journal of Agricultural and Food Chemistry,* 48**,** 5981-5985.

Kilcast, D. & Clegg, S. 2002. Sensory perception of creaminess and its relationship with food structure. *Food Quality and Preference,* 13**,** 609-623.

Kim, D. A., Cornec, M. & Narsimhan, G. 2005. Effect of thermal treatment on interfacial properties of β-lactoglobulin. *Journal of Colloid and Interface Science,* 285**,** 100-109.

King, N. M., Elkins, K. M. & Nelson, D. J. 1999. Reactivity of the invariant cysteine of silver hake parvalbumin (Isoform B) with dithionitrobenzoate (DTNB) and the effect of differing buffer species on reactivity. *Journal of Inorganic Biochemistry,* 76**,** 175-185.

Kiokias, S., Reszka, A. A. & Bot, A. 2004. The use of static light scattering and pulsed-field gradient NMR to measure droplet sizes in heat-treated acidified protein-stabilised oil-in-water emulsion gels. *International Dairy Journal,* 14**,** 287-295.

Kisko, K., Szilvay, G. R., Vainio, U., Linder, M. B. & Serimaa, R. 2008. Interactions of Hydrophobin Proteins in Solution Studied by Small-Angle X-Ray Scattering. *Biophysical Journal,* 94**,** 198-206.

Kisko, K., Szilvay, G. R., Vuorimaa, E., Lemmetyinen, H., Linder, M. B., Torkkeli, M. & Seimaa, R. 2007. Self-assembled films of hydrophobin protein HFBIII from Trichoderma reesei *J.Appl.Cryst,* 40**,** s355-s360.

Klijn, J. E., Stuart, Scarzello, M., Wagenaar, A. & Engberts, J. B. F. N. 2007. pH-Dependent Phase Behavior of Carbohydrate-Based Gemini Surfactants. The Effects of Carbohydrate Stereochemistry, Head Group Hydrophilicity, and Nature of the Spacer. *The Journal of Physical Chemistry B,* 111**,** 5204-5211.

Kloek, W., Van Vliet, T. & Meinders, M. 2001. Effect of Bulk and Interfacial Rheological Properties on Bubble Dissolution. *Journal of Colloid and Interface Science,* 237**,** 158-166.

Klostermeyer, H., Schmandke, H., Soeder, C. J., Schreiber, W., Oehlenschläger, J., Scholtyssek, S., Kobald, M., Sander, A., Eilers, E. & Von Kries, E. 2000. Proteins. *Ullmann's Encyclopedia of Industrial Chemistry.* Wiley-VCH Verlag GmbH & Co. KGaA.

Kniemeyer, O., Lessing, F., Scheibner, O., Hertweck, C. & Brakhage, A. 2006. Optimisation of a 2-D gel electrophoresis protocol for the human-pathogenic fungus *Aspergillus fumigatus*. *Current Genetics,* 49**,** 178-189.

Koczo, K., Lobo, L. A. & Wasan, D. T. 1992. Effect of oil on foam stability: Aqueous foams stabilized by emulsions. *Journal of Colloid and Interface Science,* 150**,** 492-506.

Kubow, S. 1992. Routes of formation and toxic consequences of lipid oxidation products in foods. *Free Radical Biology and Medicine,* 12**,** 63-81.

Kubow, S. 1993. Lipid oxidation products in food and atherogenesis. *Nutrition Reviews,* 51**,** 33-40.

Laemmli, U. K. 1970. Cleavage of Structural Proteins during the Assembly of the Head of Bacteriophage T4. *Nature,* 227**,** 680-685.

Lau, C. K. & Dickinson, E. 2005. Instability and structural change in an aerated system containing egg albumen and invert sugar. *Food Hydrocolloids,* 19**,** 111-121.

Leaver, J., Law, A. J. R. & Brechany, E. Y. 1999. Covalent Modification of Emulsified [beta]-Casein Resulting from Lipid Peroxidation. *Journal of Colloid and Interface Science,* 210**,** 207-214.

Lethuaut, L., Metro, F. O. & Genot, C. 2002. Effect of droplet size on lipid oxidation rates of oil-in-water emulsions stabilized by protein. *Journal of the American Oil Chemists' Society,* 79**,** 425-430.

Li, M. K. & Fogler, H. S. 1978. Acoustic emulsification. Part 2. Breakup of the large primary oil droplets in a water medium. *Journal of Fluid Mechanics,* 88**,** 513-528.

Li, S. & Li, Y. S. 1991. FTIR spectra of matrix isolated complexes between sulfur compounds. *Spectrochimica Acta Part A: Molecular Spectroscopy,* 47**,** 201-209.

Li, Y. S. & Li, S. 1994. FTIR spectra of $HSCH_2CH_2SH$, CH_3SCH_2SH, and CH_3SSCH_3 in argon and nitrogen matrices. *Spectrochimica Acta Part A: Molecular Spectroscopy,* 50**,** 509-519.

Lin, S. Y., Mckeigue, K. & Maldarelli, C. 1991. Diffusion-limited interpretation of the induction period in the relaxation in surface tension due to the adsorption of straight chain, small polar group surfactants: theory and experiment. *Langmuir,* 7**,** 1055-1066.

Littlejohn, K. A., Hooley, P. & Cox, P. W. 2011. Bioinformatics predicts diverse Aspergillus hydrophobins with novel properties. *Food Hydrocolloids*.

Liu, H., Bao, J., Du, Y., Zhou, X. & Kennedy, J. F. 2006. Effect of ultrasonic treatment on the biochemphysical properties of chitosan. *Carbohydrate Polymers,* 64**,** 553-559.

Lobo, L. & Wasan, D. T. 1993. Mechanisms of aqueous foam stability in the presence of emulsified non-aqueous-phase liquids: structure and stability of the pseudoemulsion film. *Langmuir,* 9**,** 1668-1677.

Lugones, L. G., Wos, H. a. B. & Wessels, J. G. H. 1998. A hydrophobin (ABH3) specifically secreted by vegetatively growing hyphae of Agaricus bisporus (common white button mushroom). *Microbiology,* 144**,** 2345-2353.

Lumsdon, S. O., Green, J. & Stieglitz, B. 2005. Adsorption of hydrophobin proteins at hydrophobic and hydrophilic interfaces. *Colloids and Surfaces B: Biointerfaces,* 44**,** 172-178.

Ma, A., Shan, L., Wang, N., Zheng, L., Chen, L. & Xie, B. 2007. Characterization of a Pleurotus ostreatus fruiting body-specific hydrophobin gene, Po.hyd. *Journal of Basic Microbiology,* 47**,** 317-324.

Macarron, R., Acebal, C., Castillon, M. P., Dominguez, J. M., Mata, S., Pettersson, G., Tomme, P. & Claeyssens, M. 1993. Mode of action of the endoglucanase III from Trichoderma reesei *Biochemical Journal,* 289**,** 867-873.

Macritchie, F. 1978. Proteins at Interfaces. *In:* C.B. ANFINSEN, J. T. E. & FREDERIC, M. R. (eds.) *Advances in Protein Chemistry.* Academic Press.

Madras, G. & Chattopadhyay, S. 2001. Effect of solvent on the ultrasonic degradation of poly(vinyl acetate). *Polymer Degradation and Stability,* 71**,** 273-278.

Maduko, C., Park, Y. & Akoh, C. 2008. Characterization and Oxidative Stability of Structured Lipids: Infant Milk Fat Analog. *Journal of the American Oil Chemists' Society,* 85**,** 197-204.

Malone, M. E., Appelqvist, I. a. M. & Norton, I. T. 2003. Oral behaviour of food hydrocolloids and emulsions. Part 1. Lubrication and deposition considerations. *Food Hydrocolloids,* 17**,** 763-773.

Manoj, P., Watson, A. D., Hibberd, D. J., Fillery-Travis, A. J. & Robins, M. M. 1998. II. Steady-State Rheological Investigations. *Journal of Colloid and Interface Science,* 207**,** 294-302.

Manzi, P., Aguzzi, A. & Pizzoferrato, L. 2001. Nutritional value of mushrooms widely consumed in Italy. *Food Chemistry,* 73**,** 321-325.

Margulis, M. A. 1995. *Sonochemistry and cavitation* Luxembourg, Gordon and Breach Scientific Publishers.

Martin-Rodriguez, A., Cabrerizo-Vilchez, M. A. & Hidalgo-Alvarez, R. 1994. A comparative study on the electrokinetic behavior of bovine serum albumin molecules adsorbed onto different polymer colloids. *Colloids and Surfaces A: Physicochemical and Engineering Aspects,* 92**,** 113-119.

Martin, G. G., Cannon, G. C. & Mccormick, C. L. 2000. Sc3p Hydrophobin Organization in Aqueous Media and Assembly onto Surfaces As Mediated by the Associated Polysaccharide Schizophyllan. *Biomacromolecules,* 1**,** 49-60.

Matsudomi, N., Kato, A. & Kobayashi, K. 1982. Conformation and Surface Properties of Deamidated Gluten. *Agricultural and Biological Chemistry* 46 1583-1586.

McClements, D. J. 2005. Food Emulsions; Priciples, Practices, and Techniques. New York.

McClements, D. J. & Coupland, J. N. 1996. Theory of droplet size distribution measurements in emulsions using ultrasonic spectroscopy. *Colloids and Surfaces A: Physicochemical and Engineering Aspects,* 117**,** 161-170.

McClements, D. J. & Decker, E. A. 2000. Lipid oxidation in Oil-in-Water emulsions: Impact of molecular environment on chemical reactions in heterogeneous food systems. *Journal of Food Science,* 65**,** 1270-1282.

McClements, D. J., Dungan, S. R., German, J. B. & Kinsella, J. E. 1993. Factors which affect oil exchange between oil-in-water emulsion droplets stabilized by whey protein isolate: Protein concentration, droplet size and ethanol. *Colloids and Surfaces A: Physicochemical and Engineering Aspects,* 81**,** 203-210.

Mei, L., McClements, D. J. & Decker, E. A. 1999. Lipid Oxidation in Emulsions As Affected by Charge Status of Antioxidants and Emulsion Droplets. *Journal of Agricultural and Food Chemistry,* 47**,** 2267-2273.

Mei, L., McClements, D. J., Wu, J. & Decker, E. A. 1998. Iron-catalyzed lipid oxidation in emulsion as affected by surfactant, pH and NaCl. *Food Chemistry,* 61**,** 307-312.

Memoli, A., Palermiti, L. G., Travagli, V. & Alhaique, F. 1996. Studies of Differently Induced Peroxidation Phenomena in Lecithins. *Journal of Agricultural and Food Chemistry,* 44**,** 2814-2817.

Mewis, J. & Wagner, N. J. 2009. Thixotropy. *Advances in Colloid and Interface Science,* 147-148**,** 214-227.

Meynier, A., Rampon, V., Dalgalarrondo, M. & Genot, C. 2004. Hexanal and t-2-hexenal form covalent bonds with whey proteins and sodium caseinate in aqueous solution. *International Dairy Journal,* 14**,** 681-690.

Mikus, M., Hatvani, L., Neuhof, T., Komon-Zelazowska, M., Dieckmann, R., Schwecke, T., Druzhinina, I. S., Von Dohren, H. & Kubicek, C. P. 2009a. Differential Regulation and Posttranslational Processing of the Class II Hydrophobin Genes from the Biocontrol Fungus Hypocrea atroviridis. *Applied and Environmental Microbiology,* 75**,** 3222-3229.

Mikus, M., Hatvani, L., Neuhof, T., Komon-Zelazowska, M., Dieckmann, R., Schwecke, T., Druzhinina, I. S., Von Dohren, H. & Kubicek, C. P. 2009b. Differential Regulation and Posttranslational Processing of the Class II Hydrophobin Genes from the Biocontrol Fungus Hypocrea atroviridis. *Appl. Environ. Microbiol.,* 75**,** 3222-3229.

Miñones Conde, J. & Rodríguez Patino, J. M. 2007. The effect of enzymatic treatment of a sunflower protein isolate on the rate of adsorption at the air-water interface. *Journal of Food Engineering,* 78**,** 1001-1009.

Monahan, F. J., McClements, D. J. & German, J. B. 1996. Disulfide-mediated Polymerization Reactions and Physical Properties of Heated WPI-stabilized Emulsions. *Journal of Food Science,* 61**,** 504-509.

Monsanto, S. S. 2000. Xanthan Gum. *In:* PHILLIPS, G. O. & WILLIAMS, P. A. (eds.) *Handbook of hydrocolloids.* Cambridge, England: Woodhead Publishing limited.

Moro, A., Gatti, C. & Delorenzi, N. 2001. Hydrophobicity of Whey Protein Concentrates Measured by Fluorescence Quenching and Its Relation with Surface Functional Properties. *Journal of Agricultural and Food Chemistry,* 49**,** 4784-4789.

Muik, B., Lendl, B., Molina-Díaz, A. & Ayora-Cañada, M. J. 2005. Direct monitoring of lipid oxidation in edible oils by Fourier transform Raman spectroscopy. *Chemistry and Physics of Lipids,* 134**,** 173-182.

Murray, B. S. 1997. Equilibrium and dynamic surface pressure-area measurements on protein films at air-water and oil-water interfaces. *Colloids and Surfaces A: Physicochemical and Engineering Aspects,* 125**,** 73-83.

Murray, B. S., Dickinson, E. & Wang, Y. 2009. Bubble stability in the presence of oil-in-water emulsion droplets: Influence of surface shear versus dilatational rheology. *Food Hydrocolloids,* 23**,** 1198-1208.

Nakari-Setala, T., Aro, N., Ilmen, M., Munoz, G., Kalkkinen, N. & Penttila, M. 1997. Differential Expression of the Vegetative and Spore-Bound Hydrophobins of Trichoderma Reesei Cloning and Characterization of the Hfb2 Gene. *Eur.J.Biochem.,* 248**,** 415-423.

Nakari-Setälä, T., Aro, N., Ilmén, M., Muñoz, G., Kalkkinen, N. & Penttilä, M. 1997. Differential Expression of the Vegetative and Spore-Bound Hydrophobins of Trichoderma Reesei Cloning and Characterization of the Hfb2 Gene. *European Journal of Biochemistry,* 248**,** 415-423.

Nakari-Setälä, T., Aro, N., Kalkkinen, N., Alatalo, E. & Penttilä, M. 1996. Genetic and Biochemical Characterization of the Trichoderma Reesei Hydrophobin HFBI. *European Journal of Biochemistry,* 235**,** 248-255.

Nakaya, K., Ushio, H., Matsukawa, S., Shimizu, M. & Ohshima, T. 2005. Effects of droplet size on the oxidative stability of oil-in-water emulsions. *Lipids,* 40**,** 501-507.

Neethling, S. J., Morris, G. & Garrett, P. R. 2011. Modeling Oil Droplets in Plateau Borders. *Langmuir,* 27**,** 9738-9747.

Neuhof, T., Dieckmann, R., Druzhinina, I. S., Kubicek, C. P., Nakari-Setälä, T., Penttilä, M. & Von Döhren, H. 2007. Direct identification of hydrophobins and their processing in Trichoderma using intact-cell MALDI-TOF MS. *FEBS Journal,* 274**,** 841-852.

Nielsen, N. S., Yang, T., Xu, X. & Jacobsen, C. 2006. Production and oxidative stability of a human milk fat substitute produced from lard by enzyme technology in a pilot packed-bed reactor. *Food Chemistry,* 94**,** 53-60.

Nikolov, A. D. & Wasan, D. T. 1989. Ordered micelle structuring in thin films formed from anionic surfactant solutions: I. Experimental. *Journal of Colloid and Interface Science,* 133**,** 1-12.

Noskov, B. A. 2002. Kinetics of adsorption from micellar solutions. *Advances in Colloid and Interface Science,* 95**,** 237-293.

Nuchi, C. D., Hernandez, P., Mcclements, D. J. & Decker, E. A. 2002. Ability of Lipid Hydroperoxides To Partition into Surfactant Micelles and Alter Lipid Oxidation Rates in Emulsions. *Journal of Agricultural and Food Chemistry,* 50**,** 5445-5449.

Orthoefer, F. 2008. Applications of emulsifiers in baked foods. *In:* HASENHUETTL, G. L. & HARTEL, R. W. (eds.) *Food emulsifiers and their applications.* Second edition ed. New York: Springer.

Osborn, H. T. & Akoh, C. C. 2004. Effect of emulsifier type, droplet size, and oil concentration on lipid oxidation in structured lipid-based oil-in-water emulsions. *Food Chemistry,* 84**,** 451-456.

Patra, D. & Mishra, A. K. 2002. Recent developments in multi-component synchronous fluorescence scan analysis. *TrAC Trends in Analytical Chemistry,* 21**,** 787-798.

Peñas, M. M., Aranguren, J., Ramírez, L. & Pisabarro, A. G. 2004. Structure of gene coding for the fruit body-specific hydrophobin Fbh1 of the edible basidiomycete Pleurotus ostreatus. *Mycologia,* 96**,** 75-82.

Peñas, M. M., Asgeirsdottir, S. A., Lasa, I., Culianez-Macia, F. A., Pisabarro, A. G., Wessels, J. G. H. & Ramirez, L. 1998. Identification, Characterization, and In Situ Detection of a Fruit-Body-Specific Hydrophobin of Pleurotus ostreatus. *Appl. Environ. Microbiol.,* 64**,** 4028-4034.

Peñas, M. M., Rust, B., Larraya, L. M., Ramirez, L. & Pisabarro, A. G. 2002. Differentially Regulated, Vegetative-Mycelium-Specific Hydrophobins of the Edible Basidiomycete Pleurotus ostreatus. *Appl. Environ. Microbiol.,* 68**,** 3891-3898.

Phillips, G. O. & Williams, P. A. 2000. Introduction to food hydrocolloids. *In:* PHILLIPS, G. O. & WILLIAMS, P. A. (eds.) *Handbook of hydrocolloids.* Cambridge: Woodhead Publishing Limited.

Podhipleux, N., Krisdhasima, V. & Mcguire, J. 1996. Molecular charge effects on protein behavior at hydrophobic and hydrophilic solid surfaces. *Food Hydrocolloids,* 10**,** 285-293.

Pourkomailian, B. 2000. Sauces and dressings. *In:* KILCAST, D. & SUBRAMANIAM, P. (eds.) *The stability and shelf-life of food.* Cambridge: Woodhead Publishing Limited.

Princen, H. M. & Goddard, E. D. 1972. The effect of mineral oil on the surface properties of binary surfactant systems. *Journal of Colloid and Interface Science,* 38**,** 523-534.

Princen, H. M. & Kiss, A. D. 1989. Rheology of foams and highly concentrated emulsions : IV. An experimental study of the shear viscosity and yield stress of concentrated emulsions. *Journal of Colloid and Interface Science,* 128**,** 176-187.

Ranc, H., Servais, C., Chauvy, P. F., Debaud, S. & Mischler, S. 2006. Effect of surface structure on frictional behaviour of a tongue/palate tribological system. *Tribology International,* 39**,** 1518-1526.

Reddy, S. R. & Fogler, H. S. 1981. Emulsion Stability: Determination from Turbidity. *Journal of Colloid and Interface Science,* 79**,** 101-104.

Richardson, R. K., Morris, E. R., Ross-Murphy, S. B., Taylor, L. J. & Dea, I. C. M. 1989. Characterization of the perceived texture of thickened systems by dynamic viscosity measurements. *Food Hydrocolloids,* 3**,** 175-191.

Robins, M. M. 2000. Emulsions -creaming phenomena. *Current Opinion in Colloid & Interface Science,* 5**,** 265-272.

Robins, M. M., Watson, A. D. & Wilde, P. J. 2002. Emulsions--creaming and rheology. *Current Opinion in Colloid & Interface Science,* 7**,** 419-425.

Rodríguez Niño, M. R., Sánchez, C. C., Ruíz-Henestrosa, V. P. & Patino, J. M. R. 2005. Milk and soy protein films at the air-water interface. *Food Hydrocolloids,* 19**,** 417-428.

Rogalska, E., Bilewicz, R., Brigaud, T., Moujahid, C. E., Foulard, G., Portella, C. & Stébé, M.-J. 2000. Formation and properties of Langmuir and Gibbs monolayers: a comparative study using hydrogenated and partially fluorinated amphiphilic derivatives of mannitol. *Chemistry and Physics of Lipids,* 105**,** 71-91.

Rosen, M. J. 2004. *Surfactants and Interfacial Phenomena,* New Jersey, John Wiley & Sons, Inc.

Rosen, M. J. & Gao, T. 1995. Dynamic Surface Tension of Aqueous Surfactant Solutions: 5. Mixtures of Different Charge Type Surfactants. *Journal of Colloid and Interface Science,* 173**,** 42-48.

Ross, S. 1950. The Inhibition of Foaming. II. A Mechanism for the Rupture of Liquid Films by Anti-foaming Agents. *The Journal of Physical and Colloid Chemistry,* 54**,** 429-436.

Sargent-Welch 1979. Atomic diameter computed using quantum mechanical calculations, Periodic Chart of the Atoms *In:* CO, S.-W. S. (ed.). Skokie, IL: Sargent-Welch Scientific.

Scholtmeijer, K., De Vocht, M. L., Rink, R., Robillard, G. T. & Wosten, H. a. B. 2009. Assembly of the Fungal SC3 Hydrophobin into Functional Amyloid Fibrils Depends on Its Concentration and Is Promoted by Cell Wall Polysaccharides. *Journal of Biological Chemistry,* 284**,** 26309-26314.

Schröder, V., Behrend, O. & Schubert, H. 1998. Effect of Dynamic Interfacial Tension on the Emulsification Process Using Microporous, Ceramic Membranes. *Journal of Colloid and Interface Science,* 202**,** 334-340.

Shahidi, F. 1998. Indicators for evaluation of lipid oxidation and off-flavor development in food. *In:* CONTIS, E. T. (ed.) *Developments in Food Science Food Flavors: Formation, Analysis and Packaging Influences, Proceedings of the 9th International Flavor Conference The George Charalambous Memorial Symposium.* Elsevier.

Sherman, P. 1983. Rheological properties of emulsions. *In:* BECHER, P. (ed.) *Encyclopedia of emulsion technology.* New York: Dekker,Marcel.

Shevchenko, A., Wilm, M., Vorm, O. & Mann, M. 1996. Mass Spectrometric Sequencing of Proteins from Silver-Stained Polyacrylamide Gels. *Analytical Chemistry,* 68**,** 850-858.

Siepen, J. A., Keevil, E.-J., Knight, D. & Hubbard, S. J. 2006. Prediction of Missed Cleavage Sites in Tryptic Peptides Aids Protein Identification in Proteomics. *Journal of Proteome Research,* 6**,** 399-408.

Simat, T. J. & Steinhart, H. 1998. Oxidation of Free Tryptophan and Tryptophan Residues in Peptides and Proteins. *Journal of Agricultural and Food Chemistry,* 46**,** 490-498.

Smullin, C., Wetterau, F. & Olsanski, V. 1971. The determination of polysorbate 60 in foods. *Journal of the American Oil Chemists' Society,* 48**,** 18-20.

Smyth, C., Kudryashov, E., O'driscoll, B. & Buckin, V. 2004. High-resolution ultrasonic spectroscopy for analysis of industrial emulsions and suspensions. *Journal of the Association for Laboratory Automation,* 9**,** 87-90.

Song, K. B. & Damodaran, S. 1991. Influence of electrostatic forces on the adsorption of succinylated .beta.-lactoglobulin at the air-water interface. *Langmuir,* 7**,** 2737-2742.

Sorensen, A. D., Baron, C. P., Let, M. B., Brüggemann, D. A., Pedersen, L. R. L. & Jacobsen, C. 2007. Homogenization Conditions Affect the Oxidative Stability of Fish Oil Enriched Milk Emulsions: Oxidation Linked to Changes in Protein Composition at the Oil-Water Interface. Journal of Agricultural and Food Chemistry, 55, 1781-1789.

Stajich, J. E., Wilke, S. K., Ahrén, D., Au, C. H., Birren, B. W., Borodovsky, M., Burns, C., Canbäck, B., Casselton, L. A., Cheng, C. K., Deng, J., Dietrich, F. S., Fargo, D. C., Farman, M. L., Gathman, A. C., Goldberg, J., Guigó, R., Hoegger, P. J., Hooker, J. B., Huggins, A., James, T. Y., Kamada, T., Kilaru, S., Kodira, C., Kües, U., Kupfer, D., Kwan, H. S., Lomsadze, A., Li, W., Lilly, W. W., Ma, L.-J., Mackey, A. J., Manning, G., Martin, F., Muraguchi, H., Natvig, D. O., Palmerini, H., Ramesh, M. A., Rehmeyer, C. J., Roe, B. A., Shenoy, N., Stanke, M., Ter-Hovhannisyan, V., Tunlid, A., Velagapudi, R., Vision, T. J., Zeng, Q., Zolan, M. E. & Pukkila, P. J. 2010. Insights into evolution of multicellular fungi from the assembled chromosomes of the mushroom Coprinopsis cinerea (Coprinus cinereus). *Proceedings of the National Academy of Sciences,* 107**,** 11889-11894.

Stapelfeldt, H. & Skibsted, L. H. 1994. Modification of beta-lactoglobulin by aliphatic aldehydes in aqueous solution. *Journal of Dairy Research,* 61**,** 209-219.

Stringer, M. A. & Timberlake, W. E. 1995. dewA encodes a fungal hydrophobin component of the Aspergillus spore wall. *Molecular Microbiology,* 16**,** 33-44.

Stroud, P. A., Goodwin, J. S., Butko, P., Cannon, G. C. & Mccormick, C. L. 2003. Experimental Evidence for Multiple Assembled States of Sc3 from Schizophyllum commune. *Biomacromolecules,* 4**,** 956-967.

Subkowski, T., Karos, M., Barg, H. & Bollschweiler, C. 2010. *Use of hydrophobin polypeptides as penetration enhancers*. US patent application US 20100240774A1.

Sunde, M., Kwan, A. H. Y., Templeton, M. D., Beever, R. E. & Mackay, J. P. 2008. Structural analysis of hydrophobins. *Micron,* 39**,** 773-784.

Suslick, K. S., Didenko, Y., Fang, M. M., Hyeon, T., Kolbeck, K., Mcnamara Iii, W. B., Mdleleni, M. M. & Wong, M. 1999. Acoustic cavitation and its chemical consequences. *Philosophical Transactions of the Royal Society A: Mathematical, Physical and Engineering Sciences,* 357**,** 335-353.

Suslick, K. S., Grinstaff, M. W., Kompany, E. & Wong, M. 1994. Characterization of sonochemiclly prepared proteinaceous microspheres. *Ultrasonics Sonochemistry,* 1**,** S65-S68.

Suzawa, T. & Shirahama, H. 1991. Adsorption of plasma proteins onto polymer latices. *Advances in Colloid and Interface Science,* 35**,** 139-172.

Sworn, G. 2010. Xanthan Gum. *In:* IMESON, A. (ed.) *Food Stabilisers, Thickeners and Gelling Agents.* Sussex, UK: Blackwell Publishing Ltd.

Szilvay, G. R., Kisko, K., Serimaa, R. & Linder, M. B. 2007. The relation between solution association and surface activity of the hydrophobin HFBI from Trichoderma reesei. *FEBS Letters,* 581**,** 2721-2726.

Tadros, T. F. 1996. Correlation of viscoelastic properties of stable and flocculated suspensions with their interparticle interactions. *Advances in Colloid and Interface Science,* 68**,** 97-200.

Takai, S. & Richards, W. 1978. Cerato-ulmin, a Wilting Toxin of Ceratocystis ulmi: Isolation and some Properties of Cerato-ulmin from the Culture of C. ulmi. *Journal of Phytopathology,* 91**,** 129-146.

Talu, E., Hettiarachchi, K., Powell, R. L., Lee, A. P., Dayton, P. A. & Longo, M. L. 2008. Maintaining Monodispersity in a Microbubble Population Formed by Flow-Focusing. *Langmuir,* 24**,** 1745-1749.

Tchuenbou-Magaia, F. L., Al-Rifai, N., Ishak, N. E. M., Norton, I. T. & Cox, P. W. 2011. Suspensions of air cells with cysteine-rich protein coats: Air-filled emulsions. *Journal of Cellular Plastics,* 47**,** 217-232.

Tchuenbou-Magaia, F. L. & Cox, P. W. 2011. Tribological study of suspensions of cysteine-rich proteins stabilised microbubbles and subsequent triphasic AO/W emulsions *Journal of Texture Studies*, 42**,** 185–196

Tchuenbou-Magaia, F. L., Norton, I. T. & Cox, P. W. 2009a. Hydrophobins stabilised air-filled emulsions for the food industry. *Food Hydrocolloids,* 23**,** 1877-1885.

Tchuenbou-Magaia, F. L., Norton, I. T. & Cox, P. W. 2009b. Novel air based ingredient for the food industry. *In:* 2nd International Conference on biofoams, 2009.

Tchuenbou-Magaia, F. L., Norton, I. T. & Cox, P. W. 2010. Microbubbles with protein coats for healthy food: Air filled emulsions. *In:* WILLIAMS, P. A. & PHILLIPS, G. O. (eds.) *Gums and Stabilisers for the Food Industry 15.* Cambridge: RSC.

Torkkeli, M., Serimaa, R., Ikkala, O. & Linder, M. 2002. Aggregation and self-assembly of hydrophobins from Trichoderma reesei: low-resolution structural models. *Biophysical Journal,* 83**,** 2240-2247.

Trembley, M. L., Ringli, C. & Honegger, R. 2002. Hydrophobins DGH1, DGH2, and DGH3 in the Lichen-Forming Basidiomycete Dictyonema glabratum. *Fungal Genetics and Biology,* 35**,** 247-259.

Tripp, B. C., Magda, J. J. & Andrade, J. D. 1995. Adsorption of Globular Proteins at the Air/Water Interface as Measured via Dynamic Surface Tension: Concentration Dependence, Mass-Transfer Considerations, and Adsorption Kinetics. *Journal of Colloid and Interface Science,* 173**,** 16-27.

Tsaih, M. L. & Chen, R. H. 2003. Effect of degree of deacetylation of chitosan on the kinetics of ultrasonic degradation of chitosan. *Journal of Applied Polymer Science,* 90**,** 3526-3531.

Tsutsui, J., Xie, F. & Porter, R. 2004. The use of microbubbles to target drug delivery. *Cardiovascular Ultrasound,* 2**,** 23.

Tyle, P. 1993. Effect of size, shape and hardness of particles in suspension on oral texture and palatability. *Acta Psychologica,* 84**,** 111-118.

Valo, H. K., Laaksonen, P. I. H., Peltonen, L. J., Linder, M. B., Hirvonen, J. T. & Laaksonen, T. J. 2010. Multifunctional Hydrophobin: Toward Functional Coatings for Drug Nanoparticles. *ACS Nano,* 4**,** 1750-1758.

Van Aken, G. A. Year. Modelling textural perception by the tongue: implications for designing a smooth and creamy mouthfeel of liquids and soft solids. *In:* Food oral processing physics, physiology and psychology of eating, 2010a Leeds, UK,.non published

Van Aken, G. A. 2010b. Modelling texture perception by soft epithelial surfaces. *Soft Matter,* 6**,** 826-834.

Van Aken, G. A. & De Hoog, E. H. A. 2009. Oral processing and perception of food emulsions: the relevance for fat reduction in food. *In:* MCCLEMENTS, D. J. & DECKER, E. A. (eds.) *Designing functional foods: measuring and controlling food structure breakdown and nutrient adsorption.* Cambridge: Woodhead.

Van Ruth, S. M., Roozen, J. P., Posthumus, M. A. & Jansen, F. J. 1999. Volatile Composition of Sunflower Oil-in-Water Emulsions during Initial Lipid Oxidation: Influence of pH. *Journal of Agricultural and Food Chemistry,* 47**,** 4365-4369.

Van Wetter, M. A., Wösten, H. a. B., Sietsma, J. H. & Wessels, J. G. H. 2000. Hydrophobin Gene Expression Affects Hyphal Wall Composition in Schizophyllum commune. *Fungal Genetics and Biology,* 31**,** 99-104.

Veberg, A., Vogt, G. & Wold, J. P. 2006. Fluorescence in aldehyde model systems related to lipid oxidation. *LWT - Food Science and Technology,* 39**,** 562-570.

Vermeer, A. W. P. 2006. Conformation of adsorbed proteins. *In:* SOMASUNDARAN, P. (ed.) *Encyclopedia of Surface and Colloid Science.* second edition ed. London: Taylor & Francis.

Vijayalakshmi, S. P. & Madras, G. 2004. Effect of temperature on the ultrasonic degradation of polyacrylamide and poly(ethylene oxide). *Polymer Degradation and Stability,* 84**,** 341-344.

Von Sonntag, C. & Scuchmann, H.-P. 1991. The eluicidation of peroxyl radical reactions in aqueous solution with the help of radation-chemical methods. *Angew.Chem.Int.Ed.Engl.,* 30**,** 1229-1253.

Walstra, P. 1993. Principles of emulsion formation. *Chemical Engineering Science,* 48**,** 333-349.

Walther, A. & Muller, A. H. E. 2008. Janus particles. *Soft Matter,* 4**,** 663-668.

Wang, X., Graveland-Bikker, J. F., De Kruif, C. G. & Robillard, G. T. 2004. Oligomerization of hydrophobin SC3 in solution: From soluble state to self-assembly. *Protein Science,* 13**,** 810-821.

Wang, Z., Lienemann, M., Qiau, M. & Linder, M. B. 2010. Mechanisms of Protein Adhesion on Surface Films of Hydrophobin. *Langmuir,* 26**,** 8491-8496.

Waraho, T., Mcclements, D. J. & Decker, E. A. 2011. Mechanisms of lipid oxidation in food dispersions. *Trends in Food Science & Technology,* 22**,** 3-13.

Wasan, D. T., Koczo, K. & Nikolov, A. D. 1995. Interfacial characterization of food systems. *In:* ANILKUMAR, G. G. (ed.) *Characterization of Food.* Amsterdam: Elsevier Science B.V.

Wessels, J. G. H. 1994. Developmental Regulation of Fungal Cell Wall Formation. *Annual Review of Phytopathology,* 32**,** 413-437.

Wessels, J. G. H., De Vries, O. M. H., Asgeirsdottir, S. A. & Schuren, F. H. J. 1991. Hydrophobin Genes Involved in Formation of Aerial Hyphae and Fruit Bodies in Schizophyllum. *THE PLANT CELL,* 3**,** 793-799.

WHO. 2010. *Obesity and overweight* [Online]. World Health, Organisation. Available: http://www.who.int/dietphysicalactivity/publications/facts/obesity/en/ [Accessed 20/09/210 2010].

Wierenga, P. A., Meinders, M. B. J., Egmond, M. R., Voragen, A. G. J. & Dejongh, H. H. J. 2005. Quantitative Description of the Relation between Protein Net Charge and Protein Adsorption to Air-Water Interfaces. *Journal of Physical Chemistry B,* 109**,** 16946-16952.

Wierenga, P. A., Meinders, M. B. J., Egmond, M. R., Voragen, F. a. G. J. & De Jongh, H. H. J. 2003. Protein Exposed Hydrophobicity Reduces the Kinetic Barrier for Adsorption of Ovalbumin to the Air-Water Interface. *Langmuir,* 19**,** 8964-8970.

Wildmoser, H., Scheiwiller, J. & Windhab, E. J. 2004. Impact of disperse microstructure on rheology and quality aspects of ice cream. *Lebensmittel-Wissenschaft und-Technologie,* 37**,** 881-891.

Wohlleben, W., Subkowski, T., Bollschweiler, C., Von Vacano, B., Liu, Y., Schrepp, W. & Baus, U. 2010. Recombinantly produced hydrophobins from fungal analogues as highly surface-active performance proteins. *European Biophysics Journal,* 39**,** 457-468.

Wosten, H. a. B. 2001. Hydrophobins: Multipurpose Proteins. *Annual Review of Microbiology,* 55**,** 625-646.

Wosten, H. a. B. & De Vocht, M. L. 2000. Hydrophobins, the fungal coat unravelled. *Biochimica et Biophysica Acta (BBA) - Reviews on Biomembranes,* 1469**,** 79-86.

Wosten, H. a. B., De Vries, O. M. H. & Wessels, J. G. H. 1993. Interfacial Self-Assembly of a Fungal Hydrophobin into a Hydrophobic Rodlet Layer. *The plant cell,* 5**,** 1567-1574.

Wu, Y., He, K., Ludtke, S. J. & Huang, H. W. 1995. X-ray diffraction study of lipid bilayer membranes interacting with amphiphilic helical peptides: diphytanoyl phosphatidylcholine with alamethicin at low concentrations. *Biophysical Journal,* 68**,** 2361-2369.

Wüstneck, R., Krägel, J., Miller, R., Fainerman, V. B., Wilde, P. J., Sarker, D. K. & Clark, D. C. 1996. Dynamic surface tension and adsorption properties of [beta]-casein and [beta]-lactoglobulin. *Food Hydrocolloids,* 10**,** 395-405.

Xu, Q., Nakajima, M., Ichikawa, S., Nakamura, N. & Shiina, T. 2008. A comparative study of microbubble generation by mechanical agitation and sonication. *Innovative Food Science & Emerging Technologies,* 9**,** 489-494.

Yamaki, S., Kato, T. & Kikugawa, K. 1992. Characteristics of fluorescence formed by the reaction of proteins with unsaturated aldehydes, possible degradation products of lipid radicals *Chemical and Pharmaceutical Bulletin,* 40**,** 2138.

Yin, D. 1996. Biochemical basis of lipofuscin, ceroid, and age pigment-like fluorophores. *Free Radical Biology and Medicine,* 21**,** 871-888.

Yoshimura, T., Ishihara, K. & Esumi, K. 2005. Sugar-Based Gemini Surfactants with Peptide BondsSynthesis, Adsorption, Micellization, and Biodegradability. *Langmuir,* 21**,** 10409-10415.

Yu, L., Zhang, B., Szilvay, G. R., Sun, R., Janis, J., Wang, Z., Feng, S., Xu, H., Linder, M. B. & Qiao, M. 2008. Protein HGFI from the edible mushroom Grifola frondosa is a novel 8 kDa class I hydrophobin that forms rodlets in compressed monolayers. *Microbiology,* 154**,** 1677-1685.

Yuyama, H., Watanabe, T., Ma, G. H., Nagai, M. & Omi, S. 2000. Preparation and analysis of uniform emulsion droplets using SPG membrane emulsification technique. *Colloids and Surfaces A: Physicochemical and Engineering Aspects,* 168**,** 159-174.

Zana, R. 1996. Gemini (dimeric) surfactants. *Current Opinion in Colloid & Interface Science,* 1**,** 566-571.

Zana, R. 2002. Dimeric and oligomeric surfactants. Behavior at interfaces and in aqueous solution: a review. *Advances in Colloid and Interface Science,* 97**,** 205-253.

Zangi, R., De Vocht, M. L., Robillard, G. T. & Mark, A. E. 2002. Molecular Dynamics Study of the Folding of Hydrophobin SC3 at a Hydrophilic/Hydrophobic Interface. *Biophysical Journal,* 83**,** 112-124.

Zhang, Q., Lo, C.-M. & Ju, L.-K. 2006. Affinity Foam Fractionation of *Trichoderma* Cellulase. *In:* MCMILLAN, J. D., ADNEY, W. S., MIELENZ, J. R. & KLASSON, K. T. (eds.) *Twenty-Seventh Symposium on Biotechnology for Fuels and Chemicals.* Humana Press.

Zhong, Y., Given, P. S., Olcese, G., Fang, Y. & Gomez, S. 2008. *Use of surfactants to solubilize water-insoluble solids in beverages.* US patent application 10/63542.

Zinoviadou, K. G., Janssen, A. M. & De Jongh, H. H. J. 2008. Tribological properties of neutral polysaccharide solutions under simulated oral conditions. *Journal of Food Science,* 73**,** E88-E94.

Zuniga, R. N. & Aguilera, J. M. 2008. Aerated food gels: fabrication and potential applications. *Trends in Food Science & Technology,* 19**,** 176-187.